Numerical and experimental investigation of novel foundation systems for offshore wind turbines

by

Koohyar Faizi

A thesis submitted to the University of Birmingham

for the degree of DOCTOR OF PHILOSOPHY

Department of Civil Engineering,

School of Engineering

University of Birmingham

January 2020

DEDICATED TO MY BELOVED PARENTS

ABSTRACT

The next generation of offshore wind turbines (OWTs) greatly depend on the development of reliable foundations which will enable the utilisation of generators with larger capacity at greater water depths.

Traditionally, pile foundations have been used to support superstructures in the offshore wind industry. However, recently, suction caissons are being increasingly considered as alternative foundations for supporting offshore renewable structures. The arrangement options for these suction caisson foundations could be a monopod, tripod or quadropod. In general, caisson foundations for offshore wind turbines are subjected to combined loadings of lateral, vertical and overturning moment. The most unfavourable loading condition results in a large overturning moment for monopods, whereas the structural design approach for a tripod must take into account the fact that the most unfavourable conditions involve the possibility of tensile loads in the caissons induced by the overall overturning moment. To guarantee the normal operation of offshore wind turbines (OWTs), the foundations of OWTs are required to resist significant lateral loads and overturning moments generated by wind and currents.

This research presents an innovative type of suction caisson, a "winged suction caisson", as a monopod foundation for offshore wind turbines, which has the ability to provide a larger overturning capacity compared with standard suction caisson designs. In order to assess the behaviour of the winged caissons, a series of laboratory works was conducted under 1-g and centrifuge conditions. The experimental campaign was complemented by detailed numerical studies employing finite element analyses (FEA). The short-term cyclic performance of a winged caisson foundation, installed in sand, was also investigated using a series of small-scale laboratory tests under 1-g condition. Different models with various wing sizes and different soil densities were tested in the laboratory under an overturning loading and the results were

compared with a conventional suction caisson. The moment-rotation performance of the foundation under both monotonic and cyclic loading were examined to assess the potential benefits of adding wings to suction caisson foundations. The results showed that there is a significant increase (up to 75%) in overturning capacity provided by the novel foundation, demonstrating its great potential over standard suction caissons for their use in offshore wind turbine foundations.

It is known that mono-pod caissons, have a limited maximum capacity which prohibits their use in very large foundations particularly when lateral loading governs the design. Multi-pod suction bucket foundations are rapidly expanding as a foundation system for OWTs, therefore, this research has proposed a novel capacity improvement system for a tripod arrangement of suction caissons.

Tripod suction bucket foundations have the potential to increase the bearing capacity and overturning resistance of the foundation for offshore wind turbines. However, existing tripod suction bucket foundations, as utilised for offshore wind turbines, are required to resist significant lateral loads and overturning moments generated by wind and currents with the most optimized foundation dimensions. This research presents an innovative type of tripod bucket foundation, a 'hybrid tripod bucket foundation', for foundations of offshore wind turbines, which has the ability to provide a larger overturning capacity compared with conventional tripod buckets. The proposed foundation consists of a conventional tripod bucket foundation combined with three large circular mats attached to each bucket. Several numerical models of varying geometries were validated with very good agreement against the conducted laboratory tests. The results of experimental and numerical studies performed on the proposed hybrid tripod bucket foundations installed in loose sand, and subjected to overturning moments, are discussed. The experiments were conducted on small-scale models under 1-g conditions in

sand. Different circular mat diameter sizes with various bucket spacing under an overturning loading were considered and the results were compared with a conventional tripod bucket foundation. The results showed that there is a significant increase in overturning capacity provided by the novel foundation.

LIST OF PUBLICATIONS

The results of this research project have been published or submitted for publication in scientific journals, conferences and patent application relevant to the research field and are the author's own work.

Koohyar Faizi, Asaad Faramarzi, Samir Dirar, David Chapman. "Monotonic and Cyclic Lateral Load Tests on Monopod Winged Caisson Foundations in Sand". Proceedings of the Institution of Civil Engineers – Geotechnical Engineering, https://doi.org/10.1680/jgeen.19.00056.

Koohyar Faizi, Asaad Faramarzi, Samir Dirar, David Chapman. Investigating the monotonic behaviour of hybrid tripod suction bucket foundations for offshore wind towers in sand. Applied Ocean Research, Volume 89, August 2019, Pages 176-187.

Koohyar Faizi, Asaad Faramarzi, Samir Dirar, David N Chapman. "Finite Element Modelling of the Performance of Hybrid Foundation Systems for Offshore Wind Turbines". SEG-2018, DOI: 10.1007/978-3-319-99670-7_61.

L. W. Derby, A. Faramarzi, **K. Faizi**, M. Mehravar, O. Harireche. "Finite element modelling of winged suction caissons in clay under uniaxial and combined loading". 2nd International Conference on Natural Hazards & Infrastructure, June 2019, Chania, GREECE.

Faramarzi, Asaad; **Faizi, Koohyar**; Dirar, Samir; Mehravar, Moura; Harireche, Ouahid. "Modelling the seepage flow during caisson installation in a natural seabed". Conference: Proceedings of the 24th UK Conference of the Association for Computational Mechanics in Engineering, At Cardiff University, Cardiff.

Koohyar Faizi, Asaad Faramarzi, Samir Dirar, David Chapman. "Development of an Analytical Model for Predicting the Lateral Bearing Capacity of Suction Caisson Foundations in Cohesionless Soil". (Under review).

Koohyar Faizi, Asaad Faramarzi, Samir Dirar, David Chapman, Alec Marshall, Charles Heron. "Experimental and numerical investigation of winged suction caisson foundations in sand". (In preparation).

Koohyar Faizi, Asaad Faramarzi, Samir Dirar,. "Evaluation of Seepage Flow During Installation of Suction Caisson Foundation In Homogeneous Sand and Sand Overlaying Inclined Clay". (Under review)

UK Patent Application No. 1819844.0 'Caisson' (UoBE ref: ZSR1110).

ACKNOWLEDGEMENTS

I am indebted to my many of my colleagues to support me with this thesis. Most importantly, I sincerely thank my supervisors, Dr Asaad Faramarzi, Dr Samir Dirar and Professor David Chapman, for their generous guidance, advice and constructive suggestions throughout this project.

Furthermore, I have been very privileged to get to know and to collaborate with many other great people who have become friends over the last few years. I learned a lot from them about life, research, how to tackle new problems and how to develop techniques to solve them.

Thanks to the family at University of Birmingham: Civil Engineering laboratory technical staff, Luís Portela, Mohammed Naveed Aslam, and Mark Carter for their assistance during the experiments; the academics for their excellent advice and feedback during my PhD study: Dr Dexter Hunt, and Dr Gurmel Ghataora. I greatly appreciate the support received through the collaborative work undertaken with the University of Nottingham. More specifically, I would like to thank Professor Alec Marshall and his team for their support and for providing me the great opportunity to do the centrifuge tests.

It's my fortune to gratefully acknowledge the support of my friends; Mehran, Aryan, Amin, Arasti, and Naty you were all part of the colourful fabric of daily life, sharing friendship and laughter and helping the time to pass so quickly! Special thanks to all of the researchers who generously gave up precious time to help in the laboratory, as well as all of those who remain unnamed, but not forgotten - Finally, I must thank my real family, especially my father and mother who mean a lot to me, without whose love and inspiration I would never have made it so far.

TABLE OF CONTENTS

LIST OF TABLES

LIST OF FIGURES

LIST OF ABBREVIATIONS AND ACRONYMS

CBF	Composite Bucket Foundation
CD	Consolidated Drained
CSC	Conventional Suction Caisson
D-P	Dracker-Prager
ESA	Embedded Suction Anchor
EU	European Union
Exp.	Experiment
FEM	Finite Element Method
GBF	Gravity Base Foundation
MSC	Modified Suction Caisson
M-C	Mohr-Coulomb
NCG	Nottingham Centre for Geomechanics
OWT	Offshore Wind Turbine
PIV	Particle Image Velocimetry
RP	Rotation Point
SCF	Suction Caisson Foundation
ULS	Ultimate Limit State
WSC	Winged Suction Caisson

NOMENCLATURE

A	Coefficient
C_c	Coefficients of curvature
C_u	Coefficients of uniformity
c'	Cohesion
D	Caisson diameter
Dr	Relative density
D'	Circular mat diameter
d_{50}	Median grain size
E	Young's modulus
E_s	Young's modulus of sand
e	Load eccentricity
e'	Constant horizontal load eccentricity
e_0	Initial void ratio
f_1, f_2, f_3	Constants
G_s	Specific gravity
G'_s	Secant shear modulus
g	Gravity
H	Constant horizontal load
H'	Monotonic horizontal load
H'_u	Ultimate lateral load capacity
h	Wing height
h'	Mid-depth of the soil
K, f	Soil parameters
K_A	Rankin's active earth pressure coefficient

K_p	Rankin's passive earth pressure coefficient
K_0	Earth pressure coefficient
k	Ratio *(e/D)*
L	Embedment length (Skirt length)
$LE3$	Axial strain (FE)
M	Moment
M_{max}	Maximum moment in a load cycle.
M_{min}	Minimum moment in a load cycle.
M_s	Static (monotonic) moment capacity of the caisson
M_u	Ultimate overturning capacity
M_R	Required overturning capacity
M_u^{CSC}	Ultimate overturning capacity of conventional caisson foundation
M_u^{WSC}	Ultimate overturning capacity of winged caisson foundation
N	Scaled factor
n_h	Constant of the horizontal subgrade
P_a	Atmospheric pressure
P_z	Peak soil passive pressure at any depth z
R_e	Effective centrifuge radius
R_{max}	Maximum roughness
R_n	Normalized roughness
S	Bucket spacing
$S11$	Lateral earth pressure in FE model
s, α, β	Shape factors
T	Wing width
t	Wall thickness
t'	Smaller base (the top) in trapezium shape of the wing
V	Vertical load

V_u	Ultimate vertical capacity
W_c	Buoyant weight of the caisson
W_t	Buoyant weight of the tower
W'	Buoyant weight of the soil plug inside the caisson
x	Distance to the point of rotation
y	Capacity improvement
z_m	Depth of point of rotation
β', d	Material parameters in DP
β''	Coefficient
γ_{max}	Maximum dry density
γ_{min}	Minimum dry density
γ_d	Dry density of the soil
γ'	Effective weight of the soil
λ'	Wing efficiency
λ, F	Coefficients
σ'	Stress
σ'_m	Man effective stress
σ_1, S_1	Major principal effective stress
σ_2, S_2	Intermediate principal effective stress
σ_3, S_3	Minor principal effective stress
μ	Coefficient of friction
ε^{pl}	Plastic strain
δ	Interface friction angle
ϕ'	Angle of friction of the soil
$\emptyset'_{\mathrm{peak}}$	Peak angle of friction
θ	Angular rotation of the foundation

ϑ	Poisson's ratio
ξ_b, ξ_c	Independent parameter in cyclic loading
$\overline{\omega}$	Angular velocity
ω	Constant

Chapter 1

1. INTRODUCTION

1.1 Summary

The first chapter of this thesis opens with the background of the renewable energy and general foundations are used for offshore wind turbines. This is followed by the research objectives, and significance of the study. The chapter concludes with the organization of the thesis.

1.2 General background

The increasing global demand for renewable and sustainable energy has appeared to lead a search for alternatives to fossil fuels. Renewable energy, also referred to as green energy, is now starting to replace fossil fuels in various sectors, to help addressing environmental and energy security concerns (Kåberger, 2018). Sustainable energy is defined as energy sources that are not expected to be depleted within a human lifetime; therefore they contribute to the sustainability of all species (Lund, 2014).

Renewable energy is generated from natural energy sources that can be continuously replenished. Wind, solar, geothermal, biomass, and hydropower are examples of renewable resources that play an important role in tackling global warming on a large scale (Owusu and Asumadu-Sarkodie, 2016).

Generating electricity from wind turbines has proven to be a reliable source of producing renewable energy (Thomson and Harrison, 2015). At sea, the wind blows faster and steadier than on land (Musial et al., 2006), therefore offshore wind farms can potentially deliver a higher power per unit area than onshore wind farms. As can be seen from Figure 1.1, which

has been generated by Sharp et al. (2015), an offshore wind turbine has more electricity output (5 MW) compared with an onshore wind turbine (2.5 MW) at a particular wind speed. The Vindeby in Denmark hosted the world's first offshore wind installation in 1991. Despite the fact that offshore wind turbines generate more energy compared with onshore wind turbines, most existing wind farms have been built on land (onshore) (Europe, 2018a), because it is thought to be cheaper compared with offshore wind turbines (Bassi et al., 2012). It is difficult to give an accurate comparison of costs between onshore and offshore foundations since this is primarily dependent on such factors as soil type and water depth, but it is considered that the cost of an offshore foundation will be at least two and a half times the cost of an onshore one. For example, for a 3.6MW onshore wind turbine this may be in the order of circa £400K, while the costs for an offshore will be more than circa £1M (DTI, 2007).

Notwithstanding this cost difference, several countries, such as the UK, have started to invest in offshore wind energy (IRENA, 2018). In 2018 Europe connected 409 new offshore wind turbines to the grid across 18 projects. This brought 2,649 MW of net additional capacity. At the end of 2017, a total of 4149 turbines and a capacity of 15,780 MW (see Figure 1.2) were operating in Europe (Europe, 2018b). By 2020, offshore wind is planned to grow to a total installed capacity of 25 GW in Europe (Europe, 2018b) indicating a great interest to invest in this field at governmental level. The growth of offshore wind turbine sizes and farm capacities is shown in Table 1.2, which gives details of some of these wind farms (Jensen et al., 2018).

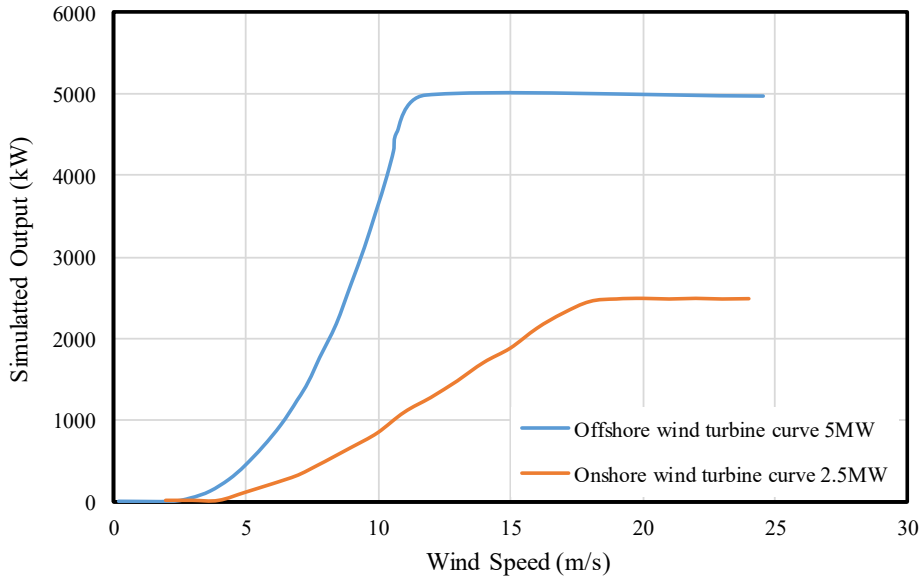

Figure 1.1. Power production from offshore and onshore wind turbines, (after Sharp et al. (2015))

In the UK there are future plans to develop offshore wind farms to make up nearly one-third of its generating capacity in the 2020s (Green and Vasilakos, 2011). Additionally, there is an ambitious target in the UK to increase its offshore wind capacity nearly tenfold by 2050, from its current capacity of 7.9 gigawatts (GW) to 75GW by 2050. The number of wind turbines designed and installed in the UK has increased, with the installation rate predicted to grow to an impressive 2.5 new turbines installed per day by the year 2020, as shown in Figure 1.3. On average, the results of the prediction would give us a correct estimate of the true installation rate in 2017 if the capacity of each wind turbine is 4.6 MW (Table 1.1). Similar, or higher, trends are also being pursued in the Europe Union (EU) and North America (Europe, 2017; Musial et al., 2017).

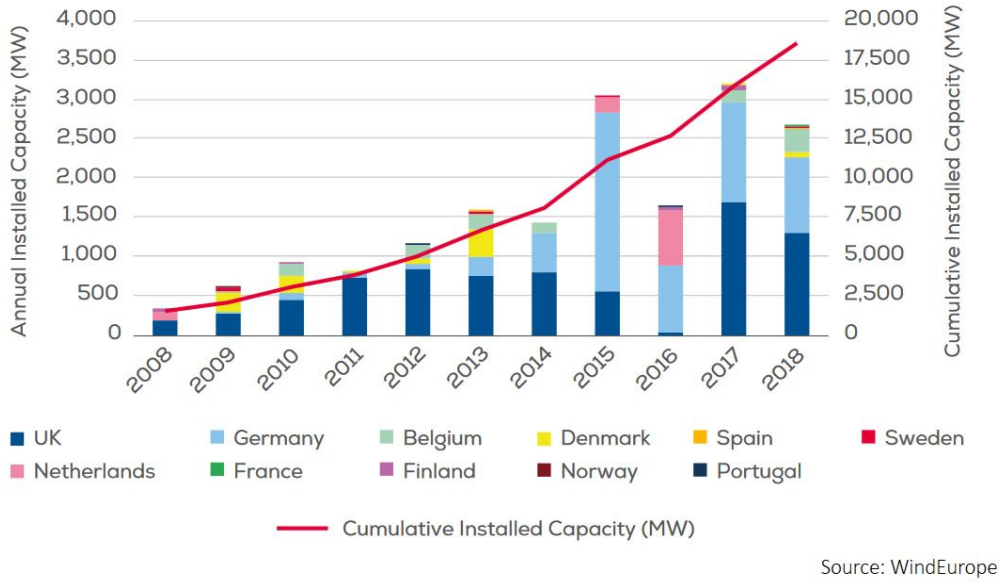

Figure 1.2. Annual offshore wind installations by country and cumulative capacity (MW) (Europe, 2018b)

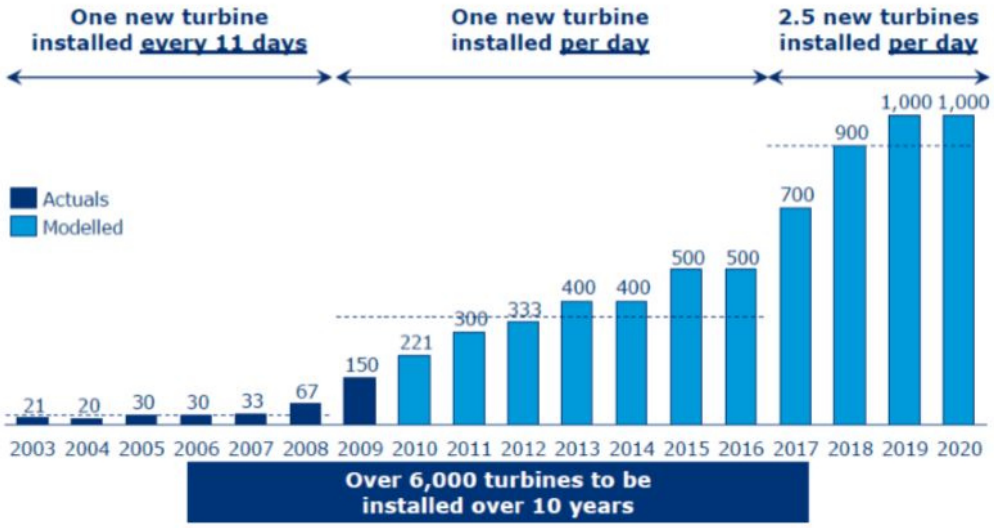

Figure 1.3. Number of wind turbines installed in the UK (Carbon trust analysis, 2010)

Table 1.1. Historic development of total installations (MW) in the United Kingdom (GWEC, 2019)

	New Installations 2017	Total Installations 2017	New Installations 2018	Total Installations 2018
MW, Onshore	2,641	12,412	589	13,001
MW, Offshore	1,715	6,651	1,312	7,963

Table 1.2. Key data on some offshore wind farms (data from 4C Offshore (2018))

Wind farm	**Turbine size: MW**	**Wind farm capacity: MW**	**Water depth: m**	**Location**	**Foundation type**	**Year commissioned**
Norgersund	0·22	0.22	5	Sweden	Platform	1990
Vindeby	0·45	4.95	2-4	Denmark	Concrete gravity base (flat)	1991
Lely	0·5	2	3-4	Netherlands	Monopile	1994
Tuno Knob	0·5	5	4-7	Denmark	Concrete gravity base (flat)	1995
Middelgrunden	2	40	3-6	Denmark	Concrete gravity base (flat)	2001
Nysted	2.3	166	6-9	Denmark	Concrete gravity base (flat)	2003
Beatrice	5	10	45	UK	Jacket	2007
Thornton Bank I	5	30	17-25	Belgium	Concrete gravity base (conical)	2009
Alpha Ventus	5	24	28-30	Germany	Jacket and tripod	2010
Rodsand II	2·3	207	7-12	Denmark	Concrete gravity base (flat)	2010
Ormonde	5	150	17-21	UK	Jacket	2012
Amrumbank West	3.6	302	20-25	Germany	Monopile	2015
Luchterduinen	3	129	18-24	Netherlands	Monopile	2015
Wikinger	5	350	36-40	Germany	Jacket	2017
Aberdeen Bay	8.4	93	20-30	UK	Jacket (suction bucket)	2018
Blyth Demonstrator	8	40	35-40	UK	Concrete gravity base (buoyant)	2018
Borkum Riffgrund II	8	448	25-28	Germany	Concrete gravity base (buoyant)	Under construction

For most offshore projects, the foundations constitute the most important design consideration and often determines the financial viability of the project (Nikitas et al., 2019). Designing foundations for offshore wind turbines (OWTs) is more challenging compared with other types of offshore projects (e.g. oil and gas platforms) as they are susceptible, and possibly more vulnerable structures, to lateral motions (Duan, 2016). Therefore, there are large financial implications associated with the choice of foundation made for OWTs (Bhattacharya, 2014a). In addition, as wind farms move further offshore, the foundations of OWTs have to withstand harsher weather conditions; consequently, they become a potentially more costly part of the design. Typically, the foundations cost 15% to 40% of the whole project for an offshore wind farm (Houlsby, 2000). Several attempts have been made in the past decade to introduce new foundations to support OWTs and reduce the costs imposed on offshore projects (Nguyen-Sy, 2005; Butterfield et al., 2007; Esteban et al., 2015; Wang et al., 2018d). Some of these have been implemented in offshore wind farm projects such as floating foundations, jacket foundations, gravity base foundation, whereas some have remained at a conceptual/research level (Byrne and Houlsby, 2015; Zhu et al., 2014). It might be due to the fact that they are not sufficiently attractive for the market to invest at scale.

The most typical foundations used for offshore structure platforms are divided into four categories (Arshi, 2016);

- Pile foundations used for water depths ranging from 5m to over 120 m (Westgate and DeJong, 2005)
- Gravity base foundations installed in water-depths of up to 25 m
- Suction caissons used in shallow water depths up to 20 m (Houlsby, 2000)
- Floating foundations are also being proposed in water depths greater than 50 m (DNV, 2004a)

Monopiles are the most common foundation type for OWTs, are a foundation in which a single large diameter, hollow steel cylindrical pipe is driven or drilled into the seabed. Alternatively, a foundation could consist of several piles, connected at the top. The piles can be vertical, battered, or a combination of both (Kopp, 2010).

Gravity-base foundations (GBFs) are another common foundation types employed in the offshore wind industry to date (Ref: Gravity-Based Foundations in the Offshore Wind Sector). GBFs have been used for many years in the oil and gas sector. The concept of gravity relies solely on the dead weight of the foundation material (typically concrete), which enables the base to generate the restoring forces required to resist the lateral loads and overturning moments.

The floating support structure consists of a floating platform and a platform anchoring system. The platform has a transition piece to install the tower on top of that (Bento et al., 2019).

Recently, the suction caisson foundation (SCF) has been considered to use for offshore structures as there is a significant potential to reduce the costs of foundations in the offshore wind industry. These structures are made of steel in the shape of inverted 'buckets' and are installed into the seabed via the creation of a pressure difference within the caisson cavity drawing the caisson into the seabed (Harireche et al., 2013; Mehravar et al., 2017; Tran et al., 2007). This method of installation allows for comparatively quick placement and, importantly, removal, therefore making it cheaper and more sustainable than traditional foundations (Lombardi et al., 2011). A typical 5 MW wind tower, including typical dimensions of its component, and supported by a caisson foundation is depicted in Figure 1.4.

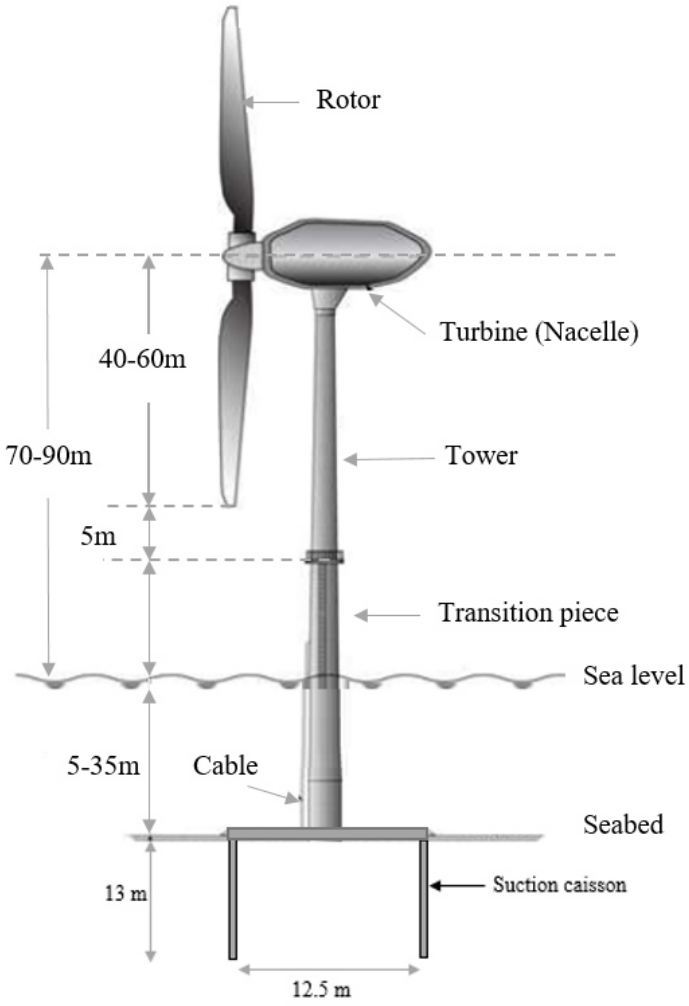

Figure 1.4. Wind turbine system components (after Malhotra (2010))

In general, foundations for offshore wind turbines, including suction caissons, are subjected to various loadings; vertical, horizontal, and moment loads or combinations of all of these. In particular, they experience large overturning moments due to the significant horizontal wind pressures acting high above the foundation level (Gourvenec and Jensen, 2009; Houlsby et al., 2005; Villalobos et al., 2004). Lateral loads or moments are more critical for wind turbine foundations compared to the vertical load (Kim et al., 2016a). The resistance of these foundations to overturning moments is the biggest challenge facing designers (Zhu et al., 2014). There is also a need to enhance the capacity of OWTs when the bearing capacity is not sufficient for conventional suction caissons to be stable due to the overturning moment or when

additional overturning capacity is needed, e.g. taller wind turbines. In addition, the loads induced by the offshore environment, i.e. wind and waves, poses an additional challenge because the OWTs are dynamically sensitive to the cyclic loading (Duan, 2016). Therefore, the resistivity of the suction caisson under cyclic loading should be considered in design and analysis of foundations.

A large penetration to diameter ratio (>1.0) of the bucket (deep penetration) has typically been recommended to obtain satisfactory overturning capacities (Sukumaran et al., 1999). However, because of uncertainties (e.g. geological properties) associated with deep penetration, shallow foundations are generally preferred both from an installation and operation point of view. The shallow soil coring and seabed properties evaluation can result in less cost to the project and time consuming, compared with deep drilling which is required for foundations in greater depths.

Using buckets with large diameters is another solution to increase the capacities. However, aside from fabrication and transportation challenges related to a large structure, as suction buckets are sensitive to structural buckling during the installation process due to the profile characteristics (thin-walled structures) (Bakmar et al., 2009; Welschen, 2015), installation of a very large thin wall bucket involves significant risks of buckling. Large diameter suction buckets therefore require a significant number of stiffeners to prevent skirt buckling during installation. However, any additional stiffeners may adversely impact the installation process (Bienen et al., 2012).

To improve the static and dynamic performance of offshore wind turbine foundations, a series of novel hybrid systems of skirted/caisson foundations have been proposed in recent years (Dimmock et al., 2013; Fu et al., 2014; Kim et al., 2016b; Zhang et al., 2016a; Wang et al., 2018c; Gaudin et al., 2011; Bienen et al., 2012). There is potentially a broad scope to

develop hybrid foundations in order to provide higher resistance against the large lateral forces and overturning moments induced into a wind turbine. Despite the obvious advantages of using these modified systems, there are still some concerns about the practicalities of installation and long-term performance of these foundations for OWT projects.

In addition, single caisson foundations may become uneconomic, as future generations of offshore wind turbines are likely to have taller towers and be located further away from the coast (deep-water wind turbines). Therefore, tripod foundations are more suitable for the heavier wind turbines located in deeper water (Fischer, 2011; Arshad and O'Kelly, 2013b; Houlsby et al., 2005).

In deeper waters, the tripod foundation requires larger caissons with bigger spacing of the buckets to support the OWTs. Although the increased capacity of tripod buckets has been demonstrated by increasing the spacing of the buckets (Stergiou et al., 2015; Kim, 2014), this will impose significant additional costs to the structure of the connecting frames, thereby reducing the cost-effectiveness of tripod foundations. Apart from manufacturing challenges associated with large buckets (González, 2017), the risk of buckling during the installation of a large thin structure (i.e. the buckets) should also be taken in to account. Therefore, development and testing of hybrid/modification systems will help to drive down the cost and the risk of the traditional and established tripod foundations.

This research study presents a modified single suction caisson foundation to address some of the issues associated with the bearing capacity of conventional suction caisson foundations. The proposed innovative type of suction caisson, the "winged suction caisson", for foundations of offshore wind turbines, has the ability to provide a larger overturning capacity compared with simple suction caissons, or can enable the size of the conventional caisson to be optimised by reducing the diameter.

In addition, a novel tripod foundation, taking advantage of combining tripod caissons with circular mats as additional supporting structural elements, is presented. Hereafter, this is referred to as a 'hybrid tripod bucket foundation'. The hybrid tripod bucket foundation aims to provide additional horizontal and moment capacity by optimising the bucket spacing and consequently minimising the construction and installation costs associated with large diameter skirted foundations.

The research was conducted using small-scale laboratory models at 1-g and at true stresses using centrifuge tests and numerical analyses using the finite element method.

ABAQUS, which is a commercially available suite of finite element analysis software (Abaqus, 2013), was employed in this thesis using the high-performance computational cluster BlueBEAR (Birmingham Environment for Academic Research). The cluster was employed to reduce the computational effort associated with the numerical models.

1.3 Aim and objectives

The aim of this study is to evaluate the performance of a series of innovative foundation systems that can be used for offshore wind turbines. Two novel foundation systems are proposed, one to enhance the overturning capacity of monopod suction caisson foundations and a second one to improve the overturning capacity of tripod suction caisson foundations.

The 'winged suction caisson' is proposed as a monopod foundation for offshore wind turbine, which has the ability to provide a larger overturning capacity compared with simple suction caissons. The proposed foundation is a caisson with four wings attached to the main shaft in vertical positions at 90 degrees intervals.

An innovative type of tripod bucket foundation (1/100 scaled models), the 'hybrid tripod bucket foundation', is also proposed for foundations of OWTs in order to provide a larger

overturning capacity compared with conventional tripod buckets. The proposed foundation consists of a conventional tripod bucket foundation combined with three large circular mats attached to the top of each bucket.

The behaviour of these proposed novel foundations, installed in dry sand, were investigated through experimental and numerical modelling using a series of small-scale laboratory tests and finite element (FE) simulations, respectively.

The measurable objectives associated with the proposed study program are as follows:

- Review the main and recent research studies on hybrid/modified foundations for OWTs with a focus on suction caisson foundations.
- Evaluate the performance of winged suction caisson foundation against overturning loading using numerical simulation (finite element analysis) and an experimental study (1-g and centrifuge).
- Develop an analytical solution to estimate the horizontal bearing capacity of the conventional and winged suction caisson foundation installed in sand.
- Investigate the overturning capacity enhancement offered by the hybrid tripod bucket foundation using numerical analysis and a 1-g experimental study.

1.4 Layouts of the thesis

The thesis consists of 6 chapters; a brief description of the contents of each chapter is given in the following paragraphs.

Chapter 2 provides a comprehensive literature review of the hybrid and novel foundations proposed for OWTs. This chapter begins with a discussion about conventional foundations used in OWTs and provides a summary of advantages and disadvantages regarding each foundation.

A historical background of the conventional monopod and tripod suction caissons as well as using hybrid or modified systems for OWTs foundations are covered of the following chapter. The conventional methods proposed for estimating of overturning capacity of the suction caisson foundation in sand are also reviewed in Chapter 2.

All the soil tests preparations, the sample preparation techniques, and loading systems used in this research, are presented in chapter 3. All the numerical methods (i.e. FEM and analytical solutions) conducted for simulating the behaviour of the foundations under the loading (i.e. winged caisson foundations and hybrid tripod caisson foundations in sand) are also covered in this chapter. The principles used to develop the analytical solutions in order to estimate the overturning capacity of conventional and winged caissons are also presented in Chapter 3.

Chapter 4 presents the results of extensive experimental simulations (i.e. 1-g and centrifuge) as well as 3D finite element numerical modelling program to examine the behaviour of the winged caisson foundations with different aspect ratio (embedment depth divided by caisson diameter) under pure overturning moment and various combinations of vertical, horizontal and moment ($V-H-M$) drained loadings. A detailed information about the drained combined loading capacity in the three-dimensional $V-H-M$ load space is also provided. This chapter also aims to present the analytical solutions and the validations were used to predict the bearing capacity of the conventional and winged caisson in sand. The response of the winged caisson foundation under short-term cyclic loading are also discussed in this chapter.

Chapter 5 presents the results of extensive experimental simulations (1-g) as well as 3D finite element numerical modelling program to examine the behaviour of the tripod hybrid

foundation with different circular mats sizes and bucket spacing under pure overturning moment.

Chapter 6 summarizes the main findings of this research and provides recommendations for future studies and research.

It worth nothing that a series of laboratory experiments and numerical simulations was performed to examine the installation behaviour of a suction caisson foundation in sand during the 1st year of this PhD. However, the results and information have been placed in an appendix (Appendix C) because this is not a key aim of the research. Moreover, due to a technical problem, the study concerning the installation was not completed and it was therefore decided to remove the results from the main body of the thesis. Hence, all the numerical methods (i.e. FEM) and experimental work conducted to simulate the suction installation trends, including the results, have been presented in the format of two conference papers.

In addition, a small project in form of a Master's dissertation, based on the foundation concept proposed by the current research (winged caisson), was simultaneously carried out by one of the students at the University of Birmingham. The Master's project focused on studying the behaviour of the winged caisson under torsional loading using finite element modelling. The torsional capacity of the winged caisson foundation was investigated in undrained condition. That work was deemed beyond the scope of the current thesis, as the present study focuses mainly on the overturning capacity of the foundations under drained soil conditions. Hence, the results of the torsional capacity of the winged caisson in undrained soil has only been presented in an appendix (Appendix D).

An overview of the approach and methods adopted in the present research project is shown in Figure 1.5.

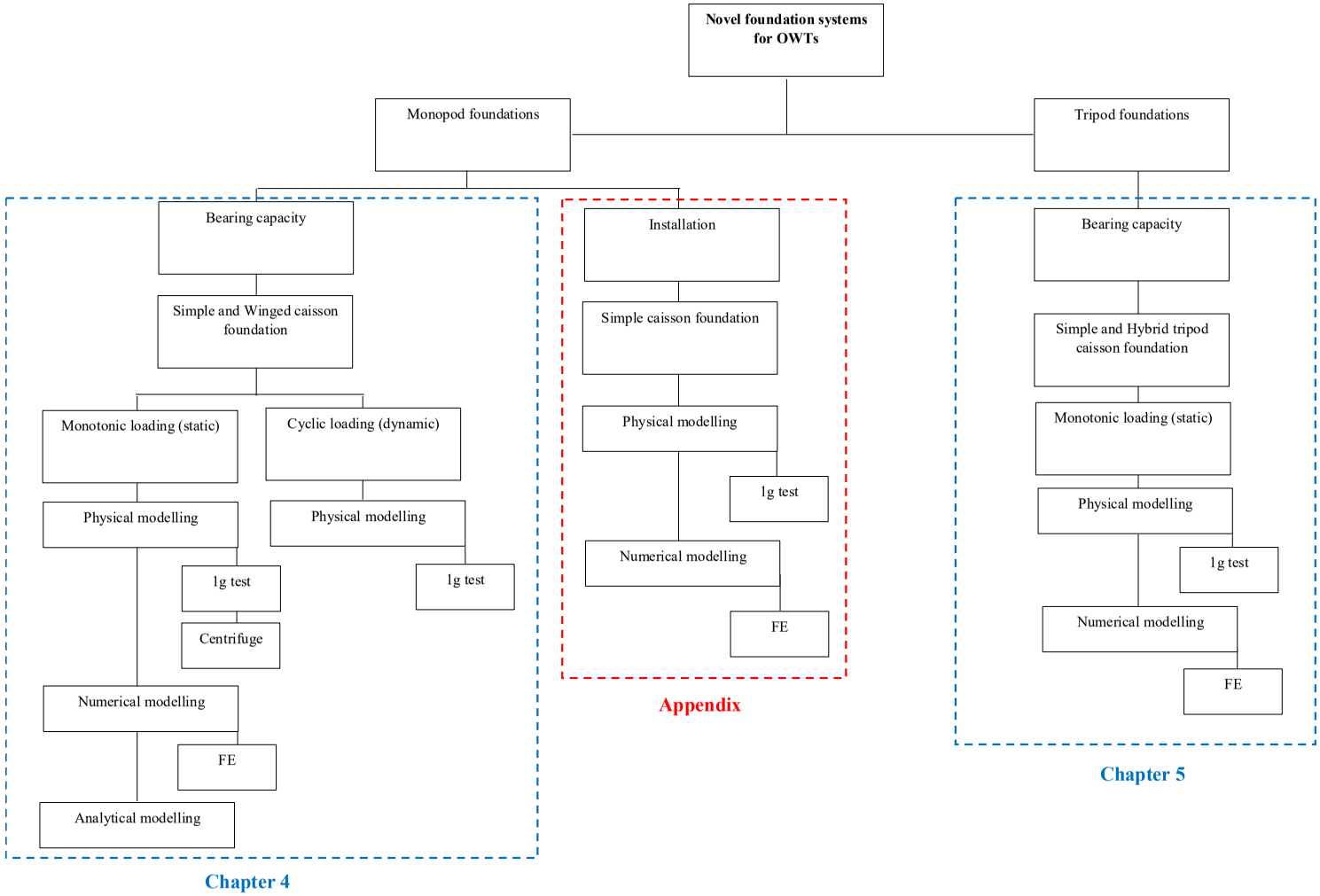

Figure 1.5. The research approach adopted in this project

Chapter 2

2. LITERATURE REVIEW:

2.1 Summary:

This chapter provides a general background of suction caisson foundations and gives an overview of the most common concepts of hybrid/modified foundations proposed for offshore wind-turbine applications. The main findings from the literature review are described, which is leading to identify knowledge gaps.

2.2 Offshore Foundations

Designing foundations for offshore wind turbines (OWTs) is more challenging compared with other types of offshore projects (e.g. oil and gas platforms) as they are typically subjected to a combination of vertical, horizontal and moment loadings due to vertical self-weights of the foundation, horizontal soil pressures, wind load and waves and currents (El-Marassi, 2011). These are dynamically sensitive structures as well due to their slender nature coupled with irregular mass and stiffness distribution (Yu et al., 2015); therefore there are large financial implications attached to the choices of foundation made. In addition, as wind farms move further offshore, the foundations of OWTs have to withstand harsher weather conditions; consequently, they become a potentially more costly part of the design. Typically, the foundations cost 15% to 40% of the whole project for an offshore wind farm (Houlsby, 2000). The designers of foundations for offshore wind turbines (OWT) face the challenges of finding an economical solution for this problem (Nguyen-Sy, 2005). Several attempts have been made in the past decade to introduce new foundations to support OWTs and reduce the costs imposed

on offshore projects (Nguyen-Sy, 2005; Butterfield et al., 2007; Esteban et al., 2015; Wang et al., 2018d).

Figure 2.1, shows the various types of foundations commonly used for different depths of water.

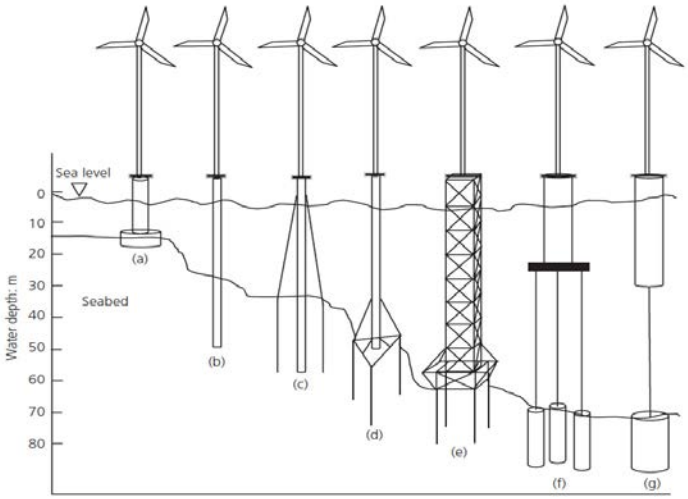

Figure 2.1. Support structure/foundation options for OWTs:
(a) gravity; (b) monopile; (c) monopile with guy wire; (d) tripod;
(e) braced frame; (f) tension leg with suction buckets (ballast stabilised);
(g) suction anchor
(Arshad and O'Kelly, 2013a)

In general, five main types of foundations are considered: piled, gravity bases, mats, spud-can and caissons (Nguyen-Sy, 2005). Some of them are well-known, such as monopiles and gravity base foundations (see Figure 2.1a and b), while others such as suction caissons are relatively new. A monopile is essentially a vertical tubular pile with a diameter in the range of 3-6 m, which is driven or bored into the soil. Gravity base foundations consists of a large base constructed from either concrete or steel which rests on the seabed (Figure 2.1a).

Suction caisson foundation (SCF) is a relatively new design concept used for offshore structures with significant potential to reduce the costs of foundations in the offshore construction industry. These structures are made of steel in the shape of inverted 'buckets' and are installed into the seabed via the creation of pressure difference within the caisson cavity

drawing the caisson into the seabed (Harireche et al., 2013; Mehravar et al., 2017; Tran et al., 2007). Single suction caisson foundations with diameter of 12 m to 18 m and the skirt length from 6 m to 15 m are typically adopted for shallow water (<20 m) whereas the multi-bucket foundations are considered at deeper waters (Fugro Consultants, 2016). Two types of structural configuration of suction caisson foundation: a single large caisson as monopod foundation, and tripod foundations are schematically shown in Figure 2.2.

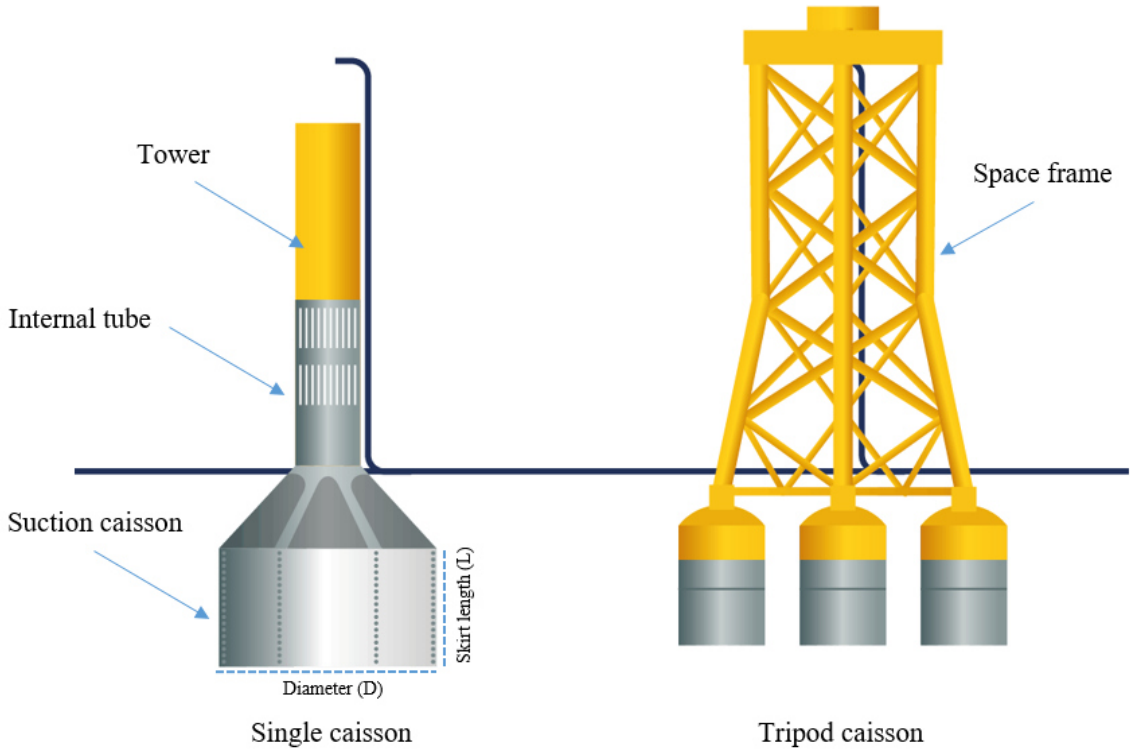

Figure 2.2. Schematic plots of suction caisson foundations in two different configurations of single and tripod caissons

This method of installation allows for comparatively quick placement and, importantly, removal, therefore making it cheaper and more sustainable than traditional foundations (Lombardi et al., 2011). It can take typically around 6-12 hours to install a suction caisson foundation, which is much shorter than the installation time of a conventional foundation, which can last several days (Chatzivasileiou, 2014). Often, the caisson is designed to be used as an

anchor for clay sites, with aspect ratios (skirt length to caisson diameter ratio, L/D) as high as 5 (Houlsby and Byrne, 2005a), whereas lower aspect ratios are appropriate for installation in sand (Villalobos et al., 2004). Suction caisson foundations with a small aspect ratio (i.e. L/D <1.0, also known as skirted foundations), due to the easy installation process, are becoming increasingly viable options for offshore wind turbines (Houlsby et al., 2005).

A list of offshore wind projects with suction bucket foundations is provide in Table 2.1. Europe is home to majority of the projects (i.e., Denmark, Germany, and the UK), whereas there is only one project in the United States, which will be operated in a lake rather than an ocean or sea environment.

Table 2.1. OWT Projects/trials with Suction Bucket Foundation

Project	**Location**	**Water Depth**	**Foundation**		**Soil**	**General Observation**
			Type	**Dimension**		
Frederikshavn	Denmark, 2002	1~4 m	Single Caisson	D=12 m L=6 m	Clay	3.0 MW OWT prototype was installed at a water depth of ~4 m. Instrumented with details presented in Liingaard (2006).
Wilhelmshaven	Germany, 2005	~18 m	Single Caisson	D=16 m L=15 m	Sand	4.5 MW OWT prototype. Some failures were reported during installation: hit by barge during installation and failed due to buckling.
Horns Rev 2 Met Mast	Denmark, 2009	9~17 m	Single Caisson	D=12 m L=6 m	multilayer	With tower height of 38 m, and weight of 165 tones.
Dogger Bank	UK, 2013	~18 m	Single Caisson	D=14 m L=8 m	unknown	Met mast.
Borkum Riffgrund 1	Germany, 2014	~25 m	Tripod	D=8 m L=8 m	Sand	3.6 MW Turbines
Gunsan	Korea, 2016	~20 m	Tripod	D=6 m L=12 m	Sand	3 MW Turbines
Icebreaker	Lake Erie, USA	~20 m	Single Caisson	D=18 m L=12 m	multilayer	Under construction in lake. Six, 3 MW turbines. Icing conditions, but small wave loads due to location (lake).
OWT, trial programme (North sea)	UK, 2014	n.a	Single Caissons	D=8 m L=6 m , D=4 m L=6 m	Varied (mostly clay)	Trials conducted to assess the installation process, water injection impact on soil plug, forces and stress in skirt structure.
Ørsted's Borkum Riffgrund 2	Germany	n.a	Suction bucket jackets	D=8 m L=8 m	multilayer	4.0 MW Turbines
Aberdeen Bay	UK, 2018	19-32 m	Tripod (Jacket*)	D=9.8-10 m L= 7-12.5 m	Loose to medium dense sand	8.4 MW turbine, On average 19 minutes were needed for the self-weight penetration phase and 01:53 h for the suction installation phase, resulting in a total suction operation time of less than 2½ hours on average.

* Space frame structures usually called 'jackets'

2.2.1 Design codes and guidelines:

There are several specific standards dealing with OWT systems. Some of them, such as International Electrotechnical Commission (IEC) 61400-3 (2010) are proposed from the point of view of structural design and they establish design cases and site ambient load specification procedures, introduce a safety factor and give broad indications about structural design procedures (Arroyo et al., 2013). However, detailed specification of foundation design procedures is deliberately referred to other documents, such as the ISO 1990X (Snell and Wisch, 2008) offshore standard series or DNV-OS-J101 (2004b). Generally, the design of OWT foundations is governed by wind and wave loading, which generates large overturning moments combined with low vertical loads. American Petroleum Institute API(2011) and API & ISO19901-4 (2016) are generally recommended for the design of long pipe piles. Recommended practices from the Det Norske Veritas DNV (1992) and DNV (2004a) are generally preferred for the design of gravity base foundations (GBFs). The DNV offshore standard DNV-OS-C502(2010) can be used for offshore concrete structures (i.e. GBFs). Although there is no dedicated design code for suction caisson foundations for OWTs application, however, a series of general guidelines (i.e. DNV, (2016) , Houlsby and Byrne (2004)) are typically used for installation and bearing capacity of the suction caisson foundations.

Generally, there are three major concerns in the design of wind turbine foundations; (i) the foundation stiffness, (ii) the performance under fatigue loading, and (iii) the ultimate capacity. Most of these concerns have been addressed in the recommended codes/standards and guidelines. Depending on the type of foundation, some of the concerns directly affect the design of the foundations, and can be prominent as a result of other issues. One of the biggest concerns with the design of monopiles is their behaviour under very large numbers of cycles in relation

to lateral loads and moments. It is the stiffness degradation and accumulation of foundation deflections occurring under cyclic loading that governs the design of OWTs, rather than ultimate capacity (LeBlanc et al., 2010). For gravity foundations, uplift, overturning, sliding, lateral displacement and settlement are potential failure modes (Malhotra, 2011), whereas in the case of monopod suction caissons overturning moments are the biggest issue (Zhu et al., 2014) due to the lower penetration depth compared with pile foundations.

Therefore, suction caisson foundation system has to be prepared to resist overturning moment generated due to resultant lateral load, arising from wind and water wave action.

2.2.2 Estimation of horizontal capacity of monopod suction caisson in sand

Suction caisson foundations have been widely used as a foundation support system in the offshore oil and gas industries (Colliat et al., 1996). Recently, the suction caisson has also been considered in the design of the OWTs (Zhang et al., 2016c). Despite these attempts, available design experiences of suction caisson foundations for OWTs are still very limited because of insufficient trails and limited existing data obtained from laboratory model tests.

As mentioned earlier, in most cases, lateral and overturning moment are more critical for wind turbine foundations compared to the vertical load (Kim et al., 2016a). To ensure safe operation of the offshore wind turbine, it is necessary to predict the bearing capacity of caisson foundations under the lateral loading (Houlsby, 2016). Existing methods for predicting the lateral-load resistance of suction caisson foundations in sand are mainly based on analytical models developed using data from experiments (Villalobos.F, 2007; Byrne and Houlsby, 2003a) or finite element analysis (Zhu et al., 2014; Achmus et al., 2013).

Finite element (FE) analysis has been used to predict bearing capacity of suction caisson foundations (Bagheri et al., 2017; Ahmed and Hawlader, 2015; Deb and Singh, 2018; Achmus et al., 2013). On the other hand, some researchers have incorporated analytical methods to

evaluate stability of suction caisson foundations (Zhu et al., 2014; Zhang et al., 2010; Byrne and Houlsby, 2003a; Villalobos Jara, 2006).

Villalobos (2006) carried out small-scale laboratory tests on model caisson with aspect ratio of 0.5 and 1.0 in dry sand (loose sand). General loading conditions, including vertical loads were examined. Villalobos (2006) derived moment–horizontal load interaction diagrams for yield state by defining a yield point from the load–deformation curves.

Byrne and Houlsby (2003a) presented a model to predict the capacity of the caisson foundation in sand which is developed based on the experiments that are applicable to low aspect ratio ($L/D < 1.0$) (Byrne et al., 2004).

Zhang et al.(2010) studied the load capacity of caisson foundations and developed a three dimensional limit method based on the upper bound theory for prediction. The method was developed based on the assumption of a fictitious soil layer, having a thickness equals to the vertical distance from the loading point to the surface of the foundation. The unit weight and shear strength of the fictitious soil were neglected. Using a series of centrifuge tests for comparison, they showed that the method can be used to estimate the load capacity of a caisson in sand.

Zhu et al.(2011b) conducted a large-scale experiment at 1-g on model caisson with an internal diameter (D) of 1.0 m and skirt length (L) of 0.5 m installed in silt. To estimate ultimate moment capacity, an analytical model was presented which incorporates the assumption of a common position of the rotation point and dominating resistance forces on the skirt of the caisson. Zhu et al. (2011b) showed that the rotation points of the caisson (L/D = 0.5) at failure were about $0.8L$ in depth and almost right below the centre of the caisson's lid. A failure mode of the caisson foundation under overturning moments was proposed combining the position of the instantaneous rotation point with the distribution of lateral soil pressures. An analytical

model for the ultimate overturning capacity of the caisson foundation was then presented, and its predictions were compared with the test results.

Achmus et al.(2013) investigated the bearing behaviour of single caissons in sand, which are mainly subjected to horizontal forces with varying eccentricities. They presented a hyperbolic method by means of numerical simulation, which enable to predict ultimate horizontal capacity of monopod buckets for OWTs in sand soils.

As mentioned earlier, the most available models to determine ultimate lateral capacity of caisson installed in sandy soil are provided by Byrne and Houlsby (2003a), Villalobos (2006), Zhu et al. (2014), and Achmus et al. (2013). Of these four models, the first two present their works in form of practical equations which can be readily adopted by practitioners for a quick estimation of the capacity. The works by Zhu et al. (2014) and Achmus et al. (2013), however, includes determination of a relatively large number of parameters and involves tedious calculations. Therefore, this thesis will focus on the models presented by Byrne and Houlsby (2003a) and Villalobos (2006) in order to make a comparison between these two models and the equation proposed in the present study. These models are based on best fit equations on results from small-scale laboratory model tests. Below the equations presented by Byrne and Houlsby (2003a) and Villalobos (2006) are explained in details.

For a suction caisson with skirt length to diameter ratios of $\frac{L}{D} < 1.0$, the ultimate lateral load capacity H'_u , with force eccentricity e, is estimated by Byrne and Houlsby (2003a) as:

$$H'_u = \left[\left(f_1 + \frac{f_2}{k}\right)^{-1} (V + f_3 W')\right] \mathrm{D}/e \qquad 2.1$$

where, W' is the buoyant weight of the soil trapped inside the bucket; V is the vertical load on the caisson due to the buoyant self-weight of the foundation; $f_1 = 3.26$, $f_2 = 1.073$, and $f_3 = 0.71$ are achieved by experimental data obtained from small-scale 1-g model tests, k is e/D.

Villalobos (2006) proposed the following equation to estimate the lateral-load capacity of a caisson foundation with $L/D < 1.0$.

$$H'_u = \left[\frac{2R\gamma' K_0}{3}(L^3 - 2{z_m}^3) + F_h L + f(F_v)R\right]/e \quad 2.2$$

where R is the caisson radius, K_0 is the difference between the passive and active lateral earth pressure coefficients $K_0 = K_p - K_A$, e is the force eccentricity, z_m is the depth of point of rotation and:

$$f(F_v) = \frac{(K_A + K_P)[(L - z_m)^2 + {z_m}^2]}{LK(2z_m - L)} F_v \quad 2.3$$

$$F_h = \sigma'_v \tan\phi' \pi R^2 \quad 2.4$$

$$F_v = 2R\gamma' L \tan\delta \, K(2z_m - L) \quad 2.5$$

where σ'_v is vertical effective stress, and K_A and K_P are Rankine active and passive lateral earth pressure coefficients.

The force equilibrium model for embedded caissons has been established in previous studies (Zhu et al., 2014; Yang et al., 2018; Villalobos, 2006) based on the distribution of lateral earth pressure along the skirt. The shapes of the distributed forces are graphically shown in Figure 2.3 for the studies above. In all of these studies earth pressure acting on the skirt included both active and passive pressures. They showed that, the pressure in the active zone (outer skirt, left side in Figure 2.3a, b, and c) increases with depth and reach a maximum pressure in the skirt tip. On the other hand, the maximum pressure in passive zone (outer skirt, right side) is

zero at the ground surface and increases with depth until a maximum is reached at a point on the same level as the rotation point. The lateral soil pressures on the inner skirt are neglected in the studies conducted by Villalobos (2006) (Figure 2.3a) and Zhu et al.(2014) (Figure 2.3b), whereas, the pressure inside the caisson was considered in the study conducted by Yang et al.(2018) (Figure 2.3c).

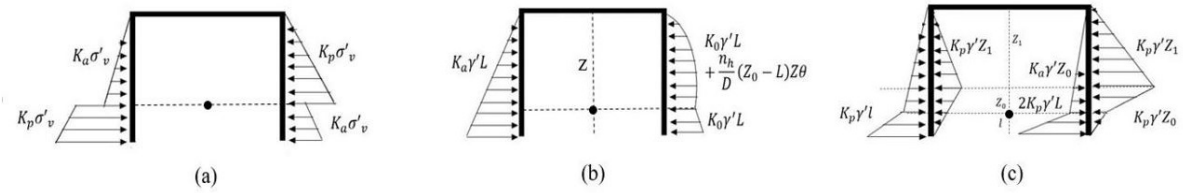

Legend

K_a : Active earth pressure coefficient
K_p : Passive earth pressure coefficient
D : Caisson diameter
L : Length of caisson skirt
γ' : Effective unit weight of soil
n_h : Constant of the horizontal subgrade
θ : Angular rotation of caisson
σ'_v : Vertical effective stress

Figure 2.3. Assumed soil pressure distribution under lateral load: (a) Villalobos (2006); (b) Zhu et al.(2014); (c) Yang et al.(2018)

2.3 Hybrid/modified foundations to support offshore structures

To improve the static and dynamic performance of offshore wind turbine foundations, a series of novel hybrid systems have been proposed in recent years. Some of them are shown schematically in Figure 2.4. A hybrid/modified foundation is a combination of two or more types of foundations (e.g. a combination of a mat and pile foundation) or additional elements (e.g. skirts and wings). Several studies confirmed the effectiveness of the hybrid systems on the bearing capacity of the foundations offered for OWT (Gaudin et al., 2011; Bienen et al., 2012; Dimmock et al., 2013; Fu et al., 2014; Kim et al., 2016b; Zhang et al., 2016a).

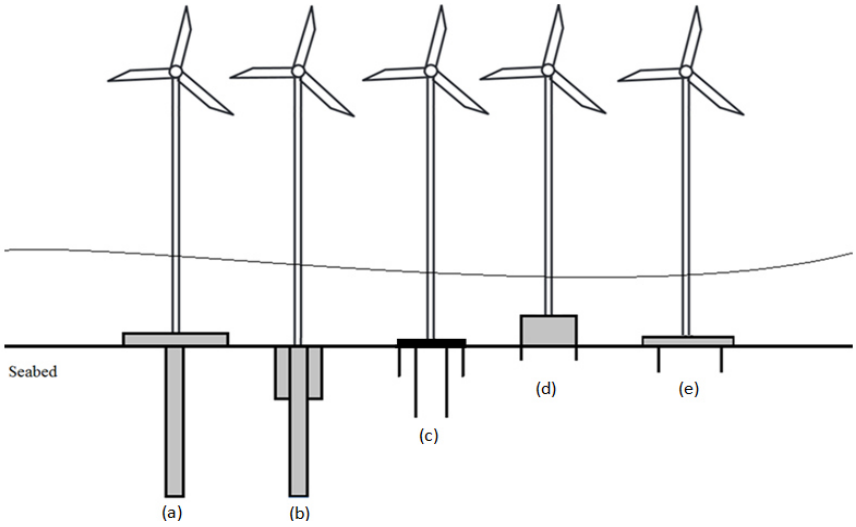

Figure 2.4. Hybrid foundations proposed for OWT (a) monopile with mat; (b) winged pile; (c) double skirted caisson (d) skirted gravity base foundation; (e) caisson with large mat

2.4 Hybrid/modified monopile foundations

The concepts of hybrid/modified monopile foundations, i.e. combining a monopile and footing or monopile and wings have been studied through physical and numerical modelling (Anastasopoulos et al., 2016; Lehane et al., 2014; Dührkop et al., 2010; Dührkop and Grabe, 2009). The winged pile (or finned pile) concept was investigated by means of experimental and numerical simulations under lateral loading to understand the effectiveness of the wings (Nasr, 2013). The effectiveness of the wings in a pile foundation was also investigated by Peng et al. (2010). Peng et al. (2010) showed that the wings can reduce the pile head deflection at a given load level (Figure 2.5). The effectiveness of using circular footing in hybrid system under different loading conditions was also investigated in experimental and numerical studies (Anastasopoulos et al., 2016; Lehane et al., 2014). The role of two modification systems in the enhancement of bearing capacity is shown in a combined graph (Figure 2.5). The buckling of the footing (due to the material and the geometry of the footing) and difficulties that might be encountered during installation due to the placing wings, were reported as concerns in these studies.

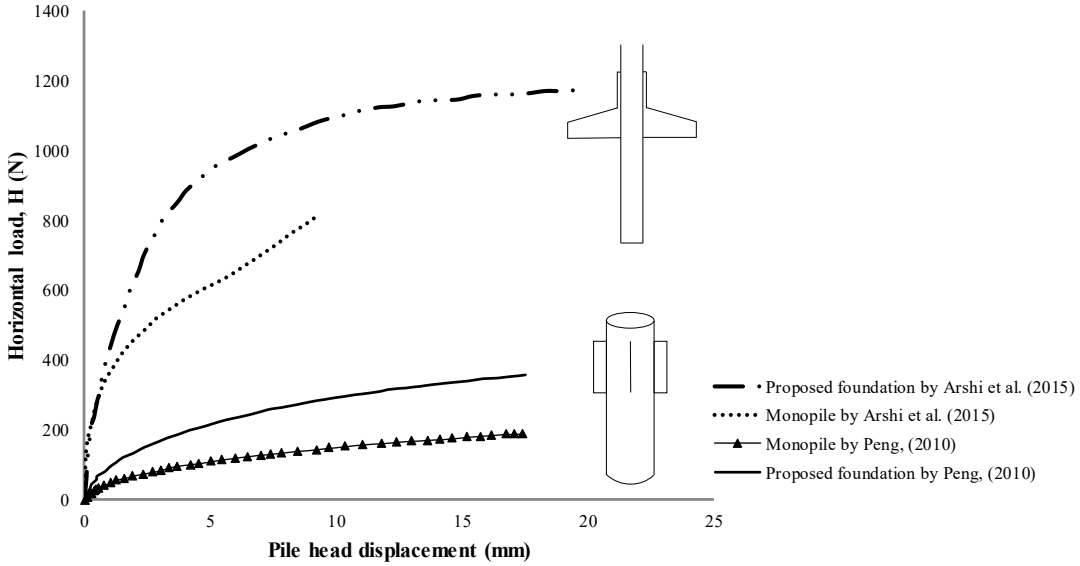

Figure 2.5. Lateral load vs. lateral displacement scale model test results

2.5 Modified gravity base and Spud-can foundations

Gravity base foundations (GBFs) are in fact the second most frequently used foundation types (monopile being the most common) employed in the offshore wind industry to date (LORC, 2013). The gravity type support structure is normally a concrete based structure, which can be constructed with or without small steel or concrete skirts. Nowadays they consist of hollow reinforced and pre-stressed concrete structures, but there are also examples constructed in steel and hybrids of concrete and steel. After transportation to their final location, they are filled with ballast to obtain the full design weight. Although in some standards and guidelines (DNV, 2013), the application of a skirt in gravity base foundations has been recommended, there are few studies regarding the effectiveness of a skirt in such foundations. Skirted foundations are usually circular in shape and as the name suggests, include a skirt at the bottom, usually made of steel, making the base open. The foundations penetrate partially into the seabed by self-weight, improving the bearing area. In these structures, lateral load capacity is improved

by the lateral resistance of the skirt and the moment load capacity rises (Ahmadi and Ghazavi, 2012). Skirts helps to prevent washing away or softening the soil beneath the foundations under the foundation when contact between the soil and the foundation is lost, and hence reduces associated erosion of the soil underneath the foundation (Rasch, 2016). The skirts can also provide an air cushion when being floated into position and suction to reduce the time for consolidation of the soil beneath the GBS (Waters et al., 2007). Swift et al. (2008) concluded that the lateral load capacity could be increased by incorporating shear keys or a perimeter skirt on the base of the GBS, however there has been no robust evidence to confirm this.

Spud-can foundations for offshore structures are large saucer-shaped foundations that can penetrate several tens of metres into soft sediments (Hossain and Randolph, 2009).Figure 2.6 shows a schematic diagram of the spud-can foundation. A potential means of improving their performance is to fit conventional spud-cans with external and internal skirts (Svanø and Tjelta, 1996; Vulpe et al., 2013). To obtain higher embedment depth spud-cans with various geometries and sizes can be used in the field. The effect of the spud-can penetration and its base geometry on the penetration and extraction resistance as used for three-legged jack-up rigs in soft soil was investigated in a series of centrifuge tests conducted by Hossain et al. (2015). However, the effect of base geometry on the lateral capacity was not covered in this study. The overturning moment capacity for skirted spud-can foundations was evaluated in a study conducted by Svano and Tjelta (1996). They concluded that the foundation performance could be significantly improved if spud-can foundations are equipped with skirts (Figure 2.7). However, the application of skirted spud-can foundations has not been approved for OWTs. Since these types of foundation are not designed as a mono pod, therefore there is no economic justification for use in OWTs.

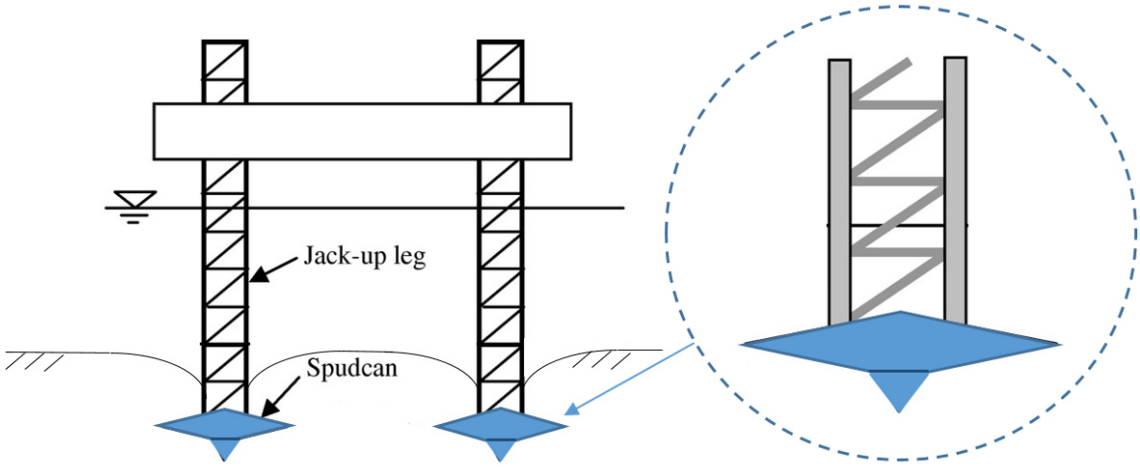

(a)

(b)

Figure 2.6. a) Spud-can foundation, b)Spud-can Equipped with Truss-worked Leg (Emren et al., 2017)

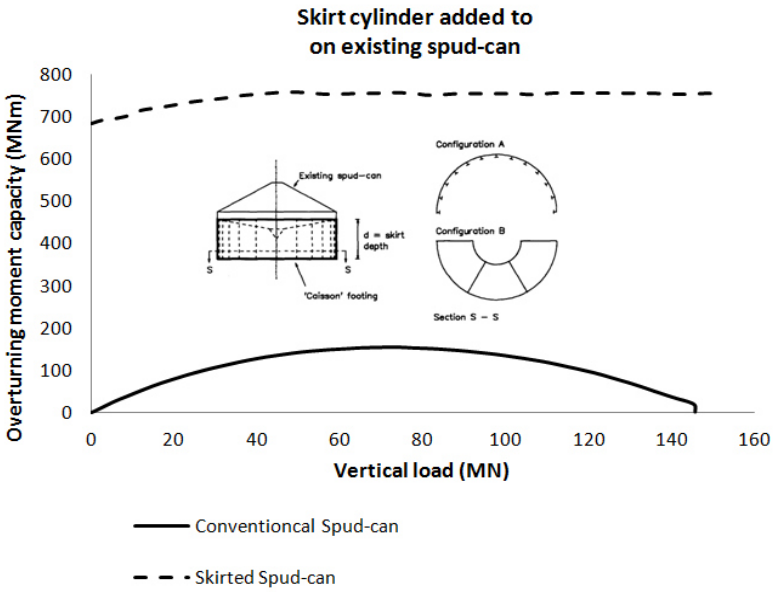

Figure 2.7. Moment fixity of a 21 m diameter skirted spud-can foundation, compared to a conventional spud-can foundation (Svanø and Tjelta, 1996)

2.6 Hybrid/modified suction caisson foundations

As mentioned earlier, the resistance of the suction caisson foundations to overturning moments is the biggest challenge facing designers (Zhu et al., 2014). There is also a need to enhance the bearing capacity of OWTs when the bearing capacity is not sufficient for conventional suction caissons to be stable due to the overturning moment or when additional overturning capacity is needed e.g. taller wind turbines.

To address the ever-increasing demand for capacity enhancement of OWT foundations (Lehane et al., 2010), and in order to improve the static and dynamic performance of OWT foundations, a series of novel hybrid systems of skirted/caisson foundations have been proposed in recent years (Dimmock et al., 2013; Fu et al., 2014; Kim et al., 2016b; Zhang et al., 2016a; Wang et al., 2018c). Gaudin et al. (2011), Bienen et al. (2012), and Cheng et al. (2014) presented a hybrid foundation unit consisting a skirted mat with (an) internal caisson compartment (s). The general concept is shown in Figure 2.8a. A circular skirted foundation equipped with a caisson at its centre was considered in finite element analysis (Figure 2.8b). The ultimate

capacity and the combined capacity of the hybrid foundation system in undrained soil conditions were investigated through numerical and experimental methods. They concluded that using this geometry results in significant changes in the soil failure mechanisms compared to a simple foundation, which importantly leads to increases in horizontal capacity foundation in undrained soil conditions.

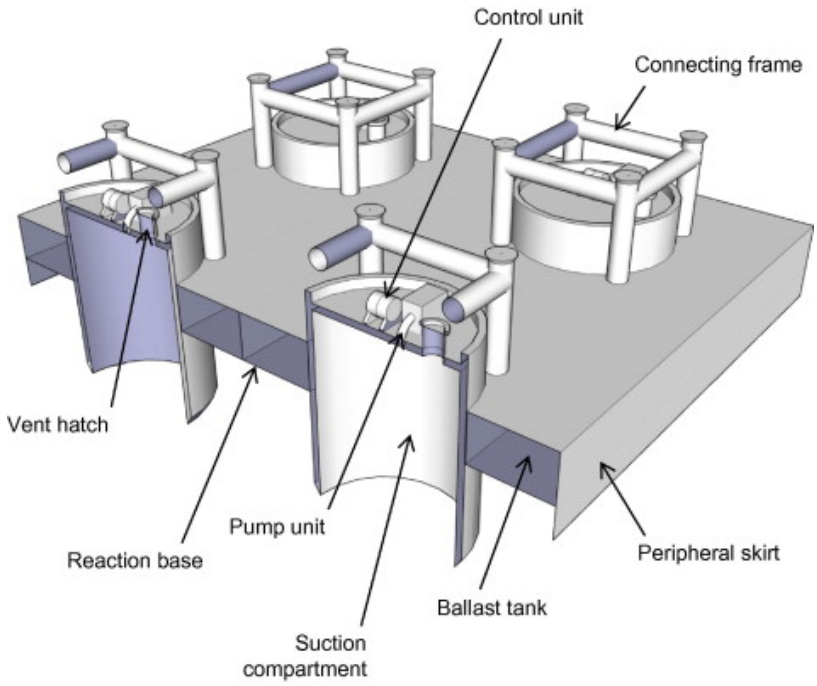

(a)

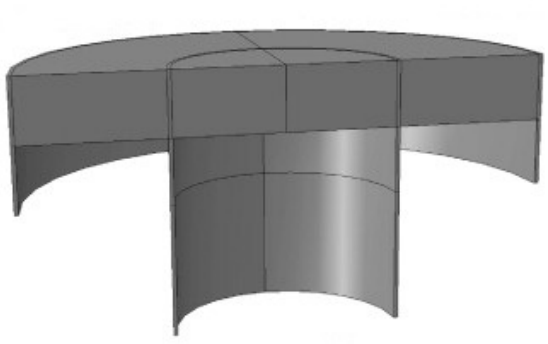

(b)

Figure 2.8. a) Schematic of hybrid foundation concept; b) Model adopted in finite element analysis (Bienen et al., 2012)

Other researchers proposed various hybrid skirted/caisson foundations, sometimes also known as modified foundation, which usually include a conventional suction caisson foundation combined with: internal honeycombs (Figure 2.9a), an external short skirt, (Figure 2.9b) (Li et al., 2015; Li et al., 2014), reinforced with double or multiple skirts (Figure 2.9c) (Wang et al., 2017; Li et al., 2015; Fu et al., 2014; Mana et al., 2012) and combined with a circular or rectangular mat (Figure 2.9d) (Fu et al., 2014; Li et al., 2015). In addition, a new series of composite bucket foundations (CBFs) with different materials (concrete and steel) were examined experimentally and numerically by Tianjin University (Ding et al., 2012; Zhang et al., 2013). The foundations were fabricated from an upturned steel or concrete bucket with honeycomb compartments or circular compartments made of steel added inside the bucket. The CBFs had large diameters and relatively shallow penetration depths.

In line with above, a modified suction caisson (MSC) was presented by Zhang et al. (2016a) with the idea of increasing bearing capacity. The proposed model comprised of an internal part and an external skirt that were connected with a lid (see Figure 2.9b). The concept of the model presented was inspired by the hybrid-skirted foundation proposed by Gaudin et al. (2011), Bienen et al. (2012), and Cheng et al. (2014). Through a series of experiments, they showed that the MSC could increase the lateral bearing capacity and reduce the lateral deflection. The authors concluded that the external skirt embedment length plays an important role in increasing the horizontal and moment bearing capacity of the proposed foundation (Zhang et al., 2016a). A series of hybrid systems comprising a circular mat combined with a single caisson and group suction caisson foundations, which is composed of a square mat, and multi suction caissons have been also studied by Kim et al. (2016b) (Figure 2.9d).

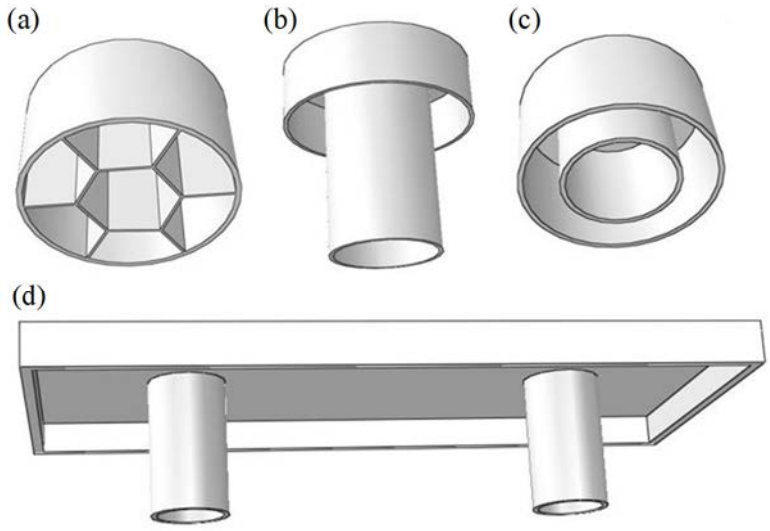

Figure 2.9. Some proposed hybrid foundations concepts on research studies (a) composite bucket foundation (CBF), (b) modified suction caisson (MSC), (c) double skirted caisson foundation, (d) skirted mat with caissons

Suction anchors:

Various types of foundation systems using suction mechanism have been also developed for floating structures in the past years (Larsen, 1989). One of the most popular foundation systems for floating oil and gas production facilities in the open sea is embedded suction anchor (ESA) (Bang et al., 2009). ESA is a type of permanent offshore foundation that is installed using a suction pile. Suction-anchor system has also been considered in construction of the floating offshore wind power foundation system (Na et al., 2013). Offshore anchors are usually subjected to large pull-out forces, which they need to resist.

To increase the capacity against pull-out, a novel suction anchor system has been examined by Bang et al.(2009) and Boonyong et al., 2015. The proposed system consists of three to four wings (vertical flanges) attached along the circumference with equal spacing (Figure 2.10). They showed that, the pull-out capacity increases as the anchor depth and the soil strength increase, and decreases as load inclination angle increases (see Figure 2.11) (Boonyong

et al., 2015; Bang et al., 2009). Although, the mechanism of the suction anchor installation is well described by authors, however, a comparison study has not been provided between the pull-out capacity of the proposed anchor system with and without wings.

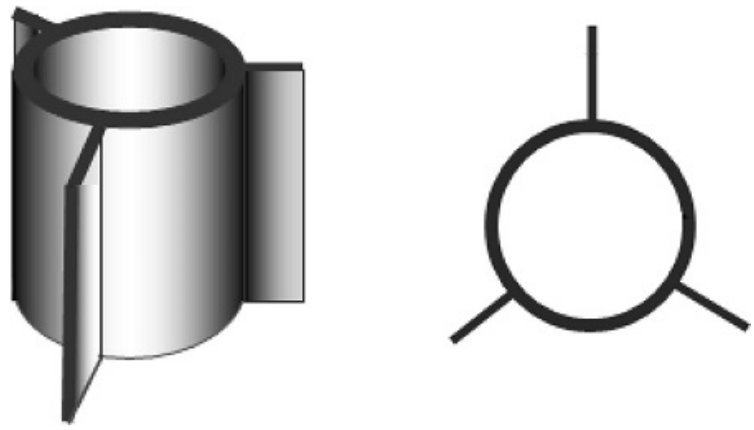

(a)

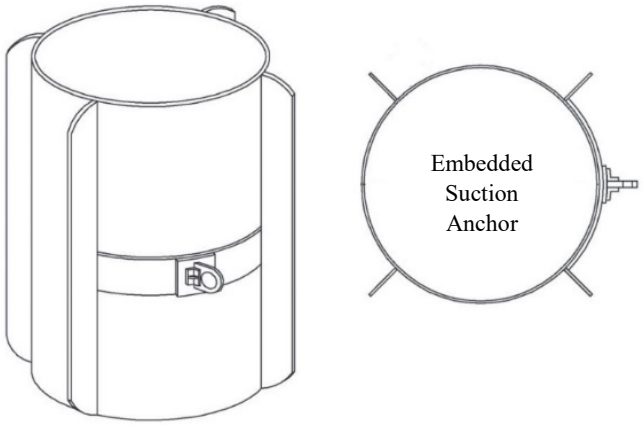

(b)

Figure 2.10. Schematic diagrams of embedded suction anchor; a) three (Bang et al., 2009) b) four wings (Boonyong et al., 2015)

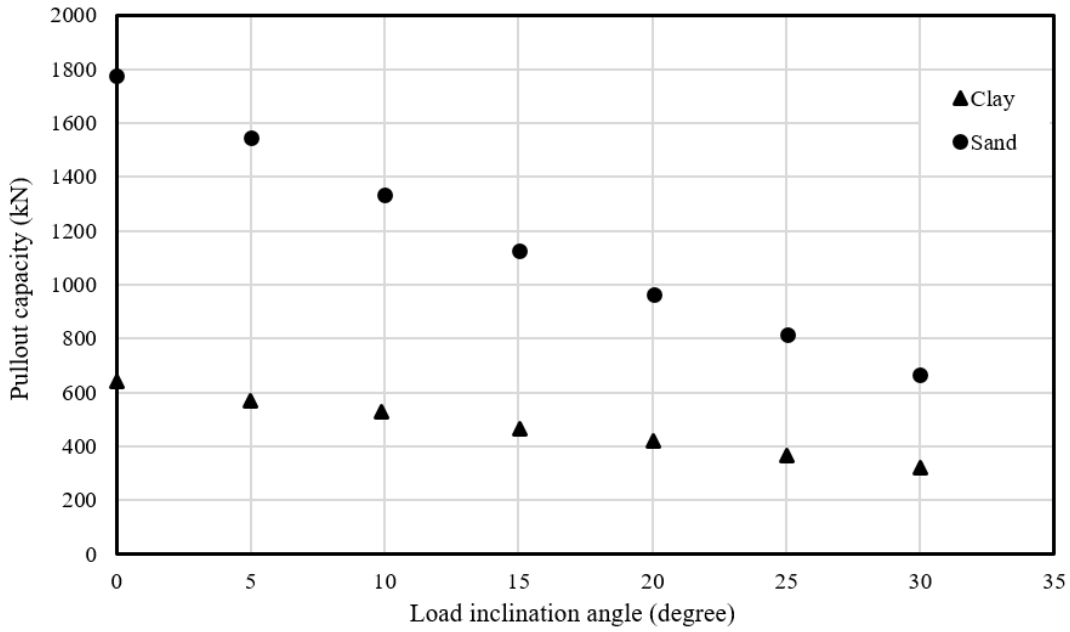

Figure 2.11. Pullout capacity vs. load inclination angle with sand and clay (Boonyong et al., 2015)

The results from the above studies on modified suction caissons, presented the effective performance of the modified system in terms of increased lateral and rotational stiffnesses, which are key factors for foundation of offshore wind turbines, and contribute to increase the factor of safety against excessive lateral displacement.

2.7 Tripod suction caisson foundations

As future generations of offshore wind turbines are likely to have taller towers and be located further away from the coast, the standard monopod foundations may become uneconomic and tripod suction buckets can be more suitable (Houlsby et al., 2005).

Tripod bucket foundations are a standard three-legged structure made of cylindrical bucket foundations. The central steel shaft of the tripod is attached to the turbine tower by tubular space frames. This type of foundation is a popular design due to the smaller diameter buckets, which reduces the probability of structural failure and easier installation, (Cotter, 2010) and provides higher bearing capacity for the foundations of OWTs compared with single leg foundations (Veritas, 2004; Kim and Oh, 2014).

Apart from the shape, the load transfer mechanism from the foundation to the soil is the main difference between the mono and tripod bucket foundations (Kim and Oh, 2014). The large overturning moment can be resisted by a combination of tension and compression on the windward and leeward legs in a tripod foundation, while a single bucket only transfers the loading moment by the individual bucket surface interfaces with surrounding soil (Byrne et al., 2002; Foglia, 2011b). Tripod suction caisson foundations are suitable (cost effective) for OWTs at sites with water depth ranging from 20 to 50 m (Veritas, 2013). In 2014 a prototype tripod bucket foundation was installed at Borkum Riffgrund in Germany, with a 3·6 MW turbine fitted.

Previous studies showed that, tripod caisson foundation exhibits much better capacity resistance under monotonic and cyclic lateral loading in sand compared with the single caisson (Wang et al., 2018a; Kim et al., 2014). Kim et al.(2014) used centrifuge experiments to show that, tripod is more efficient in terms of controlling the rotation angle for the design of a typical wind turbine tower structure. The rotation is acting to rotate the caisson through an angle θ about the origin (centre of the lid of the caisson). Since offshore wind turbine is a sensitive structure to deformation, it is often recommended to adopt the tripod as foundation instead of the monopod (Wang et al., 2018a).

The installation process of the tripod bucket foundation into the seabed is similar to that of the single suction bucket foundation (monopod). The suction caissons are sunk into the soil by pumping out the water trapped in the caisson cavity when they are located on the seabed, allowing the pressure of water outside the cavity to push the foundation in (Jensen et al., 2018).

The bearing capacity of the single suction bucket foundations has been extensively studied in different soil types (Achmus et al., 2013; Kim, 2012; Mehravar et al., 2016; Zhu et al., 2014), whereas only a few studies have examined the behaviour of tripod suction bucket

foundations under lateral loading (Tran and Kim, 2017; Kim, 2014; Gourvenec and Jensen, 2009). Various bucket and soil parameters have a direct influence on the bearing capacity of the tripod bucket foundation, such as the ratio of the bucket spacing to the bucket diameter (S/D), the embedment depth of the bucket (L), the soil–bucket friction angle (δ) and the unit weight (γ) of the soil (Tran and Kim, 2017; Stergiou et al., 2015; Kim et al., 2013).

The combination effects of a multi-bucket structural (bucket group) on the bearing capacity of the caisson foundation in sand was investigated by the study conducted by Jin et al. (2014). The configurations and layout of the multi-bucket structure were investigated through ABAQUS nonlinear finite element analysis program. The calculation and analysis indicated that the bucket group effects have a substantial impact (vary depending upon the spacing conditions) on the bearing capacity of the multi-bucket foundation in sand. Kim et al. (2014) developed a three-dimensional finite element analysis to evaluate the group effect of tripod bucket foundations in clay. Parametric studies were conducted varying the spacing between individual buckets, loading directions, and embedded depth of the bucket foundation. The ratio of bearing capacities of the tripod bucket foundations to that of the single bucket foundations, which was defined as group efficiency factor, were evaluated under different horizontal, moment, and vertical combined loading conditions. The results showed that the horizontal capacity factor increased with increasing the spacing ratio (S/D) and the embedment ratio (L/D), where L is the skirt length and D is the diameter of the bucket. Similar study conducted by Tran et al. (2017) to analyse the bearing capacities of tripod bucket foundations in medium and dense sands by performing a series of 3D finite element analyses. Tran et al. (2017) concluded that the horizontal bearing capacity of a tripod bucket foundation increased with an increase in S/D ratios for foundations in both medium and dense sands. The effect of the foundation diameter and vertical load on the bearing capacities of tripod foundation were

investigated as well. The results showed that the horizontal and moment bearing capacities increased almost linearly with the increase in vertical load.

2.8 Modified tripod caisson foundations

Very few studies have investigated modified tripod caisson foundations supporting OWTs. A novel tripod foundation model attached with double windward caissons with internal skirts was presented by Kim et al. (2014). The reinforced tripod foundation was formed with double windward caissons (Figure 2.12). Another reinforced foundation with two additional skirts with smaller diameters than that of the outside skirt were attached inside the windward side bucket (Figure 2.12). The skirts was added to provide additional skin friction resistance. A series of centrifuge load tests was carried out by Kim et al. (2014) to investigate the monotonic and cyclic behaviours of the novel tripod bucket foundations. The moment-rotation angle curves were compared with the results to those obtained from a test of a simple tripod bucket foundation. Kim et al. (2014), showed that the efficiency of OWTs is higher in terms of controlling the rotation angle using tripod foundation. The rotation angle for the yield moment was only 20% that of the monopod as well as the tripod provides greater stiffness at the elastic range than that of the monopod. This means that the load capacity was successfully enhanced using the proposed foundations due to the increase in the contact area achieved through the doubling of the number of windward buckets as well as the adding of internal skirts in the buckets. However, the use of internal skirts could increase the resistance during the installation stage.

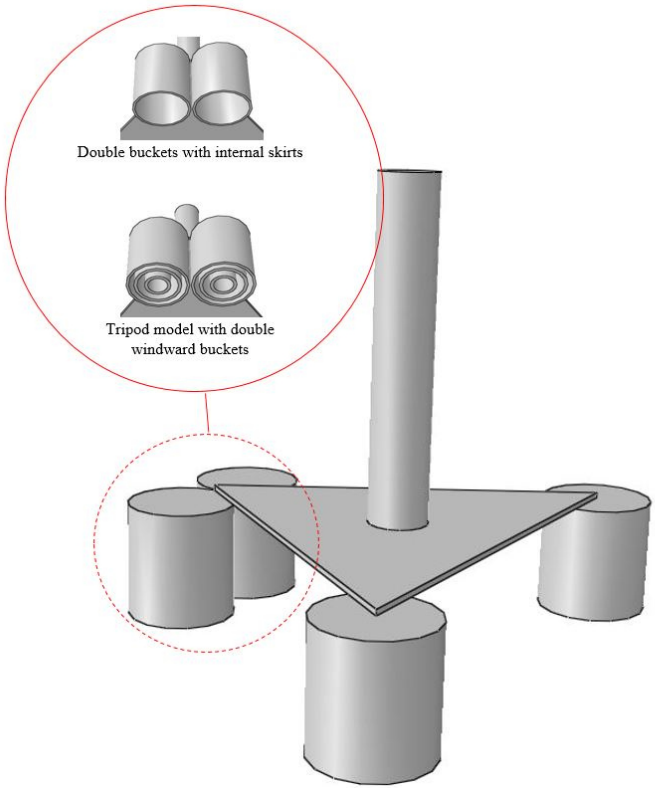

Figure 2.12. Schematics of the reinforced tripod models, Kim et al. (2014)

The studies above demonstrate: the usefulness of modification/hybrid systems to increase the bearing capacity of the foundations used in offshore marine structures, specifically for offshore wind turbines. The advantages and disadvantages of the proposed hybrid/modified foundations are listed in Table 2.2. Table 2.3 gives a short overview of studies on various hybrid/modified systems and assessing the potential impacts on the bearing capacity of offshore foundations. Most of them are proposed for OWT applications.

Despite such promising results, the feasibility of the hybrid/modified suction caisson foundation is challenged by several factors. Construction, transportation, and installation of such a large and heavy foundation can be costly. In addition, given the complexity and challenges associated with uncertainty of offshore projects, finding novel and practical ways to increase the capacity of the foundation of offshore wind turbines, whilst ensuring material

efficiency and sustainability during installation, is vital. Therefore, further investigations on hybrid/modified caisson systems are required before they can be adopted as a cost-effective solution by designers and end users. This project addresses some of the issues associated with the horizontal and overturning capacity of suction caisson foundations by proposing innovative designs for single and tripod caisson foundations. The suitability of the proposed solutions is investigated using experiments on scaled physical models and computational modelling.

Table 2.2. Advantages and disadvantages of the most common types of hybrid/modified foundations

Hybrid/ modified foundation with a base of:	**Advantages**	**Disadvantages**
Monopile	- Installation in different types of soil (versatile) - A shorter pile length can be used - Improved lateral bearing capacity compared to the original foundation	- Driving resistance is increased in proportion to the area of the wings - Very expensive installation - Difficult to remove
Gravity base	- Self-installing - Cheaper installation cost - Improve bearing capacity - Decrease the risks of scouring - Improve settlement	- Relatively expensive transportation cost - Issues relating to the composite connection between concrete and steel
Spud-can	- Self-installing - Relatively inexpensive installation - Reduces the risks of scouring - Improve settlement (lower settlement compared to the original type of foundation)	- Normally used for jackets (single foundations not approved) - Application for OWT has not been proved - Relatively expensive transportation costs - Issues relating to the composite connection between the concrete and steel
Suction caisson	- Cheaper installation cost - Fastest offshore installation - Lightweight foundation - Improved bearing capacity - Easy removal - Noise free (no impact on marine life)	- Installation in stiff layers - Increases the cost of installation in the case of adding a skirt - Capacity loss as a result of footing detachment
Mat/ raft	- Lightweight foundation - Improved bearing capacity (if combined with other conventional foundations e.g. pile) - Decreases the risks of scouring (if combined with other foundations) - Spreading of applied load over a large area assists in the reduction of generated contact stress beneath the raft foundation.	- Issues relating to the composite connection between concrete and steel - Heavy installation tools required to penetrate skirt deeper - Capacity loss as a result of footing detachment

Table 2.3. Summary of research on hybrid/modified foundations for offshore structures

		Type of foundation						Test type					Loading				Type of soil	
Reference	**Year**	Monopile	Gravity base	Spudcan	Caisson	Mat/Raft	**Modified (or combined) with**	Filed trial (OWT)	Filed trial (Platform)	1-g	Centrifuge	Numerical modelling	Horizontal	Vertical	Combined	Cyclic/seismic	Sand	Clay
Svanø et al.	1996			■			Skirt		■						■		■	
Eide et al.	1996			■			Skirt		■						■			
Karunakaran et al.	1998			■			Skirt		■							■		
Swift et al.	2008		■				Skirt		■								■	■
Peng et al.	2010	■					Wings					■		■			■	
Gaudin et al.	2011					■	Suction caisson				■							■
Bienen et al.	2012					■	Suction piles					■			■			■
Bienen et al.	2012	■					Wings				■				■	■		
Arshi and Stone et al.	2012	■					Footing			■					■		■	
Dimmock et al.	2013					■	Short piles					■			■			■
Mana et al.	2013					■	Skirt					■			■			■
Vulpe et al.	2013			■			Skirt					■			■			■
Li et al.	2014				■		Circular footing/Additional skirt			■			■				■	
Lehan et al.	2014						Footing				■	■			■		■	
Kim et al.	2014				■		Monopod and tripod with double skirt				■		■				■	
Kim et al.	2015				■		Suction piles/Circular footing				■		■	■			■	
Hossain et al.	2015			■			Skirt				■			■				■
Anastasopoulos and Theofilou	2016	■					Circular footing					■			■	■		■
Zhang et al.	2016				■		Additional skirt			■					■		■	
Murphy et al.	2016	■					Wings	■					■				■	
Choo et al.	2016		■				Piles					■			■			■
Abdelkader et al.	2018	■					Ripped plate					■			■		■	
Yang et al.	2019	■					Friction wheel				■		■				■	

Chapter 3

3. METHODOLOGY:

3.1 Summary:

As identified in Chapter 2, structurally modified/enhanced caisson foundations can potentially offer great advantage with respect to their over-turning capacity which is an essential characteristic of foundations that support off-shore wind turbines. However, the proposed solutions in the literature suffer from various limitations ranging from excessive costs involved in their constructions/installations to practical limitations in their use. Therefore, this research project offers two novel, yet practical, postulated cost-effective solutions to overcome the problems associated with the available solutions for foundations of offshore wind turbines. In this chapter, details regarding to the experimental and numerical methods were used to evaluate the behaviour of the two novel foundations, 'winged caisson foundation' and 'hybrid caisson tripod foundation' proposed for use in OWTs, are described. As mentioned earlier (in Chapter 1), both of the foundations studied in this research emphasise the importance of hybrid/modified systems to enhance the bearing capacity of the conventional foundations applicable for OWTs.

Physical modelling tests (1-g) and numerical simulation (finite element method) were used to investigate the behaviour of winged caisson foundations under drained monotonic and combined loading in loose and medium dense sand are described in this chapter. Different aspect ratios, wing sizes, load's orientations, and number of wings used in this project are also investigated. Furthermore, two centrifuge modelling tests related to a simple caisson and a winged suction caisson used to investigate the behaviour of winged caisson under real stress

soil conditions are specified. Analytical expressions for the ultimate lateral capacity of the conventional and winged caissons are then presented. In addition, details of the laboratory physical models used to examine the capacity of the winged caissons under short-term cyclic loading are presented.

In addition, the physical modelling tests (1-g) and numerical simulation (finite element method), as well as geometric configuration of foundation structures (i.e. aspect ratio, bucket spacing and circular mat sizes) were used to investigate the behaviour of hybrid tripod bucket foundations installed in drained loose sand are expressed.

3.2 Winged suction caisson foundation

This section describes the experimental and numerical methods that were used to investigate the monotonic and cyclic behaviours of the winged caisson foundations in sand.

The proposed foundation is a caisson with four wings attached to the main shaft in vertical positions at 90 degrees intervals (see Figure 3.1a and Figure 3.1b). Environmental loads (i.e. wind and current loads) act on the wind tower through different load directions and are transformed into an overturning moment to be resisted by the foundation (Malhotra, 2011; Ogunjuyigbe et al., 2017). Similar to any design problems, the loading combinations that represent the worst-case scenario should be considered. As such, four wings were selected in this proposed foundation as this configuration should ensure a complete resistance against all loading scenarios, due to the symmetrical geometry of 90 degrees of the wings. The effectiveness of four wings in the comparison of three wings was approved using FEM. The results is presented in section 4.1.3.4.

As shown in chapter 2, additional structural elements have been considered in the past for monopile foundations to improve their pull-out and horizontal capacity. For example, wings

were attached along the length of embedded suction anchors to enhance pull-out capacity (Na et al., 2013; Boonyong et al., 2015). However, their use on skirted foundations to improve overturning capacity has not been considered before.

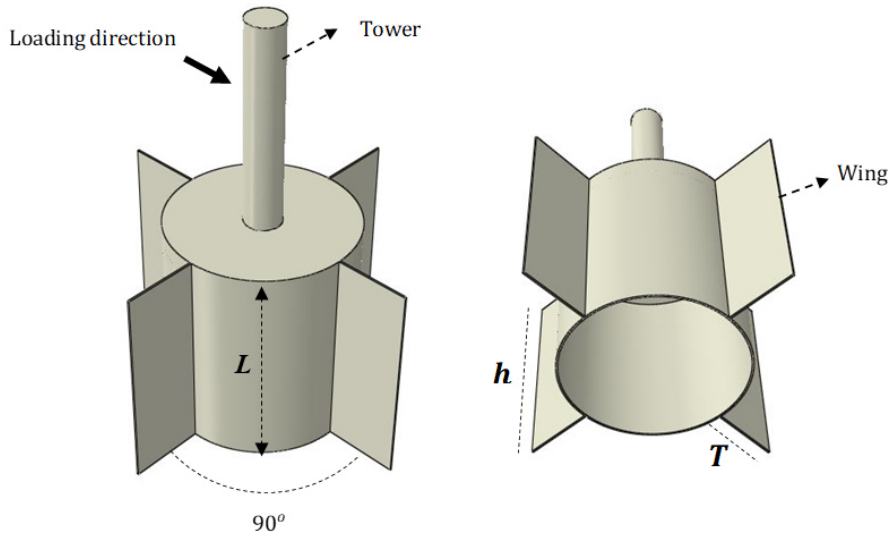

(a)

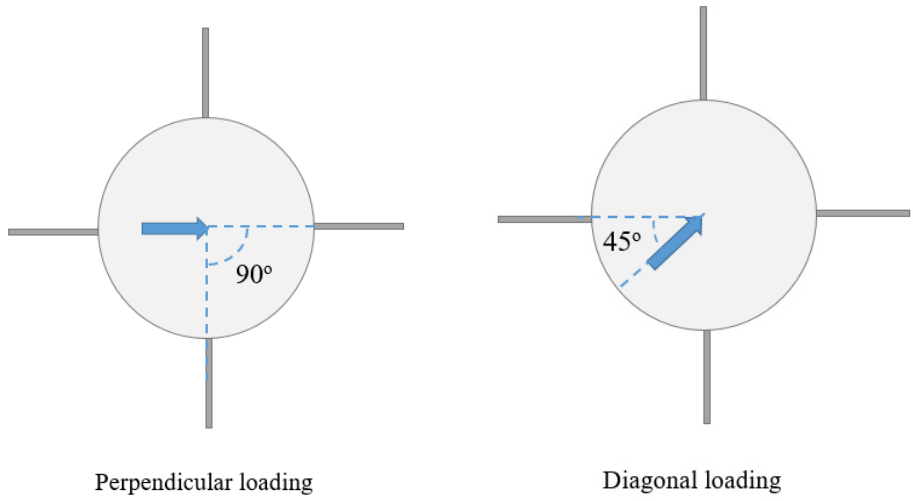

(b)

Figure 3.1. a) A schematic of the proposed winged suction caisson; (T, wing width; h, wing height, L, skirt height); b) Cross-section of the winged caisson

The monotonic behaviour of the winged caisson foundations in sand was investigated in this research using experimental tests and numerical simulation. The experiments were conducted on scaled models ($1/70^{th}$) under 1-g conditions. Different sizes of wing were evaluated with respect to their effect on the overturning resistance of the suction caisson. Furthermore, the impact of different caisson aspect ratios (length to diameter) in two different soil densities are examined. In addition, the behaviour of the conventional and winged caissons installed in loose sand under combined loading were examined. In this study, simple suction caissons are referred to as "conventional suction caissons", i.e. with no attachments to or alteration from the original inverted steel bucket.

The results of the experiments are used to develop, and validate, finite element (FE) models of the proposed system in order to understand the mechanisms associated with the proposed wings in caisson foundations. Since full-scale experimental tests of the proposed foundation are expensive and time consuming, the validated FE models are extended to predict the behaviour of full-scale winged foundations and the winged caisson with different geometries under overturning loadings. In practical applications, lateral load may act in any direction, hence it is essential to consider the performance of wings under different lateral load's orientation. In this project, a series of FE models are conducted in order to investigate the effect of lateral load's orientation on the overturning capacity of the winged caissons in dry loose sand. A winged caisson with $L/D = 1.0$ is applied in perpendicular and diagonal to the wings.

The response of the winged caisson foundations under cyclic loading was also studied experimentally under 1-g controlled condition.

3.2.1 Experimental investigation (Monotonic/static loading)

The following section contains a description of the test setup, including the laminar test chamber, used for the monotonic and cyclic load tests carried out in the geotechnical laboratory at the University of Birmingham.

To investigate the overturning capacity of winged suction caissons in sand, three contributing factors were considered: wing width (T), caisson length (L) and the relative density of the sand. Three wing widths (T) were investigated: $0.2D$, $0.3D$, and $0.4D$ of the caisson diameter (D). In addition, three embedment length to caisson diameter ratios (L/D) of 0.5, 1.0, and 1.5 were studied. All tests were carried out in dry sand conditions, replicating a fully drained case. The water column above the seabed has been omitted for simplification. For reference, three tests were conducted on conventional suction caissons. Of the total foundation models two conventional and winged caissons with $L/D = 1.0$ were selected in order to study the capacity under combined (vertical – horizontal – moment) loading. Silica Redhill sand was used with two different relative densities (Dr) of 23-25% and 48-50%. These values corresponded to loose and medium dense soil, which are representative of sand density in the North Sea (Cotter, 2010).

3.2.1.1 Description of the models and the soil

The foundation models built for this study are shown in Figure 3.2. The external diameter (D) of all the caissons shafts was 75 mm. A factor of 70 was chosen to scale the dimensions of the caissons based on the available size of the test rig, and limitations of the available loading system. The caisson specimens were fabricated from a smooth stainless steel tube with a wall thickness (t) of 1.2 mm (the wings also had the same thickness). In order to apply the load, a tubular tower, with a total height (e) of 220 mm, and a diameter of 25 mm was connected to a cap (thickness 5mm) on the top surface of the caissons. The winged models, were positioned such that two wings were perpendicular to the lateral loading direction and two

wings were along the loading direction (see Figure 3.1). Further details of the loading arrangement and test set up are provided in section 3.2.1.2.

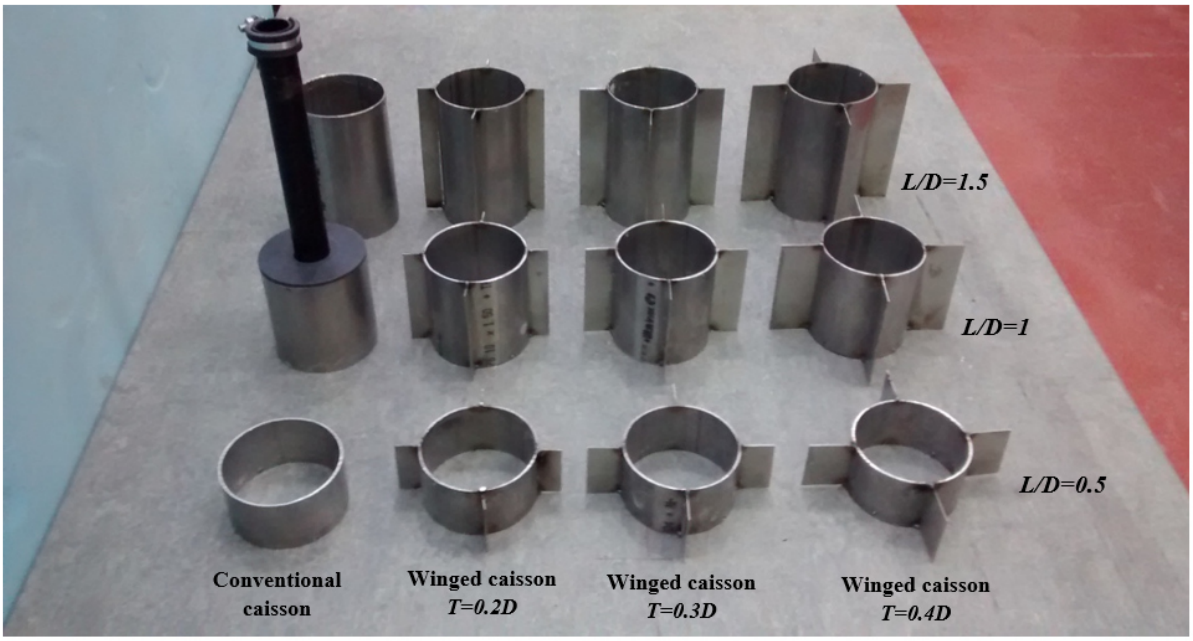

Figure 3.2. Foundation models used in the experiments, with different aspect ratios and wing sizes (the loading 'tower' is also shown attached to one of the conventional caissons)

One of the important parameters in the bearing capacity of the foundation, is the surface roughness of the caisson, which in turn increases the friction resistance (Sudagar et al., 2013). A normalised roughness (R_n) were defined by Uesugi and Kishida (1986) to evaluate surface characteristics $R_n = R_{max}/d_{50}$, where R_{max} is the maximum roughness (the height between the highest and lowest point of the surface profile). According to Villalobos (2006), a smooth, intermediate and rough interface correspond to $R_n < 0.02$, $0.02 \leq R_n \leq 0.5$, and $R_n > 0.5$, respectively. For the caisson models used in this study, the maximum roughness was $R_{max} = 1.23\mu m$. Hence, an R_n value of 0.01 was assumed in this study, which corresponds to a smooth interface between the sand and the model caissons.

All the information about the models and tests are summarised in Table 3.1; in this table conventional suction caissons and winged caissons are denoted CSC and WSC, respectively. The particle size distribution of the Redhill 110 silica sand is shown in Figure 3.3. The main reason for using fine sand particles and a smooth surface for the models is to minimize the scale effect between the model caisson surface roughness and the sand particles. Scaling the soil particle dimensions is normally used to relate the results of a model test in a reduced scale (Cuéllar, 2011). The use of the prototype-size sand for the model tests may inevitably induce some undesirable forces whenever localized failure or shear bands appear (Cuéllar, 2011; Kuhn, 2005). Several studies have shown that the influence of these shear-zones on the overall response of the foundation may be neglected if the applied loads lie well below the failure limit (Hettler, 1981) or if the ratio of foundation diameter to the median grain size (D/d_{50}) is greater than 30 (or in some references: greater than 60) (Ovesen, 1979; Franke and Muth, 1985; Verdure et al., 2003). In the present investigation, a sand with fine particles was used to reasonably meet the above scaling law ($\frac{D}{d_{50}} = 625$). A commercially available sand, Redhill-110 used during the experiments. To save time and money on unnecessary testing, the properties of the sand used in this study (Table 3.2) were obtained from the study conducted by Kelly et al.(2004) and Villalobos et al. (2005; 2006).

Table 3.1. Model caisson testing series undertaken in the experiments

Model	Length (L) mm	Aspect ratio (L/D)	Wing width (T)	Wing height (h) mm	Relative density (Dr %)	Loading system	Type of study	Applied gravity
CSC1	75	1.0	-	-	23-25,48-50	Pure moment/combined**	Exp./Num.	1g/70g
CSC2	37.5	0.5	-	-	23-25	Pure moment	Exp./Num.	1g
CSC3	112.5	1.5	-	-	23-25	Pure moment	Exp./Num.	1g
WSC1	75	1.0	(0.2D)	75	23-25,48-50	Pure moment/combined	Exp./Num.	1g
WSC2	75	1.0	(0.3D)	75	23-25,48-50	Pure moment/combined	Exp./Num.	1g
WSC3	75	1.0	(0.4D)	75	23-25,48-50	Pure moment/combined	Exp./Num.	1g/70g
WSC4	37.5	0.5	(0.2D)	37.5	23-25	Pure moment	Exp.	1g
WSC5	37.5	0.5	(0.3D)	37.5	23-25	Pure moment	Exp.	1g
WSC6	37.5	0.5	(0.4D)	37.5	23-25	Pure moment	Exp./Num.	1g
WSC7	112.5	1.5	(0.2D)	112.5	23-25	Pure moment	Exp.	1g
WSC8	112.5	1.5	(0.3D)	112.5	23-25	Pure moment	Exp.	1g
WSC9	112.5	1.5	(0.4D)	112.5	23-25	Pure moment	Exp./Num.	1g
WSC10	75	1.0	(0.4D)	0.75L (from the top)	23-25	Pure moment	Num.	1g
WSC11	75	1.0	(0.4D)	0.5L (from the top)	23-25	Pure moment	Num.	1g

*Num.: Numerical

EXP.: Experimental

** combined: Vertical (V), Horizontal (H), and Overturning moment (M)

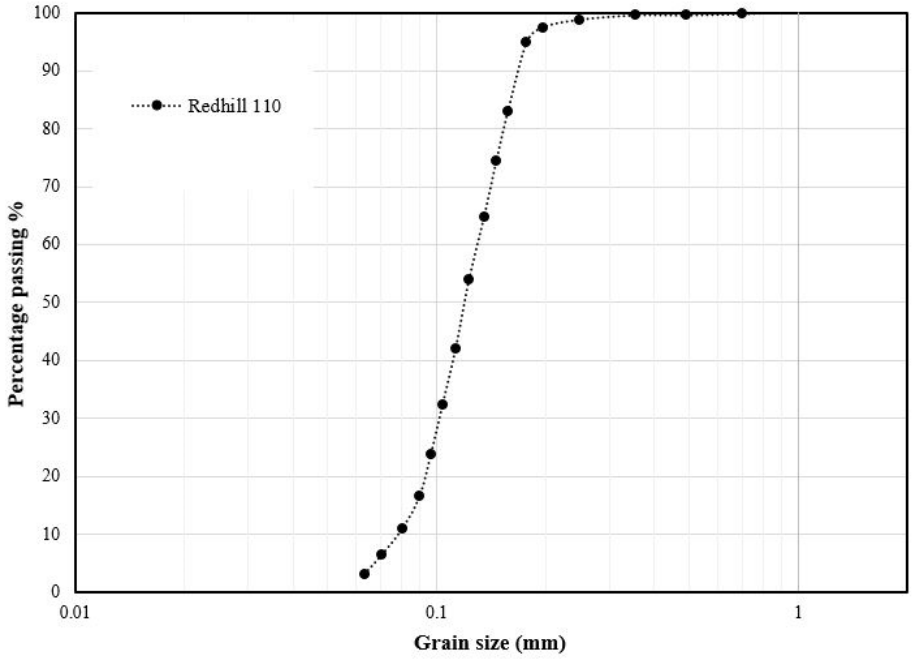

Figure 3.3. Particle size distribution curve for Redhill 110

Table 3.2. Physical properties of sand used in the model tests, Redhill 110

Properties	Value
$d_{10}, d_{30}, d_{50}, d_{60}$ (mm)	0.08, 0.10, 0.12, 0.13
Coefficients of uniformity (C_u), and curvature (C_c)	1.63, 0.96
Specific gravity (G_s)	2.65
Minimum dry density, γ_{min} (kN/m3)	12.76
Maximum dry density, γ_{max} (kN/m3)	16.80
Angle of friction of the soil,ϕ'	36º
Permeability (m/s)	3.8×10^{-4}

Figure 3.4 shows the expression for the peak friction angle proposed for triaxial and plane strain conditions for the silica sand Redhill 110, where the dashed lines correspond to plane strain and solid curves to triaxial strain conditions (Villalobos J, 2006). The internal friction angle value of the sand was extracted from the figure in order to use in FE modelling.

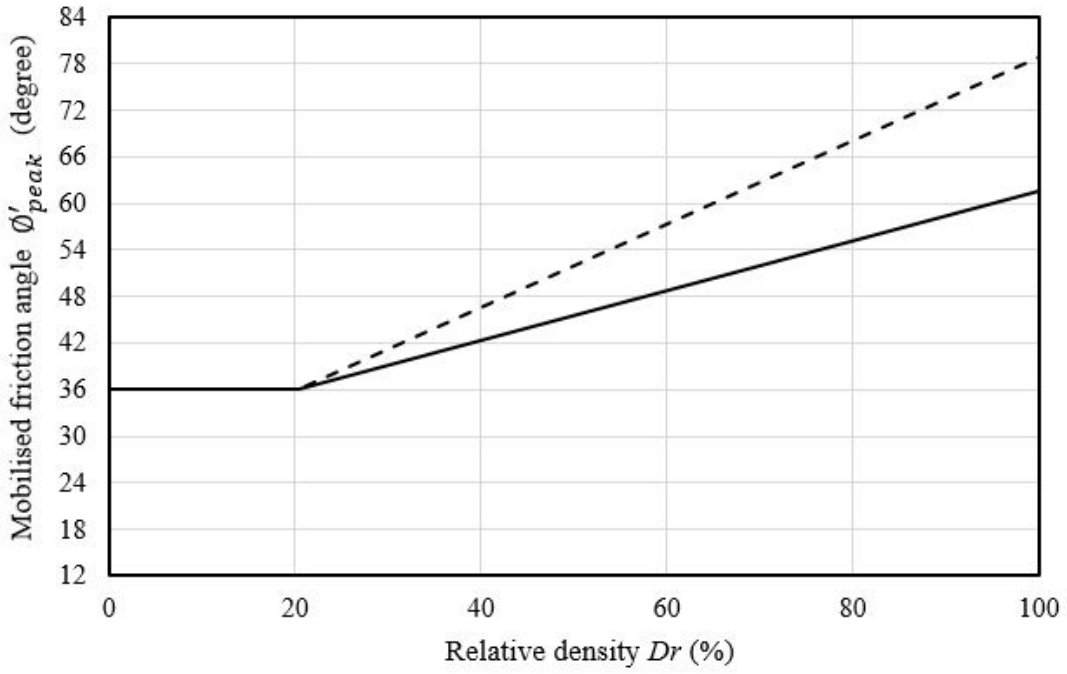

Figure 3.4. Variation of peak angles of shearing resistance $\emptyset'_{\text{peak}}$, with relative density Dr, for Redhill 110 sand tested; solid curves for triaxial conditions and dashed curves for plane strain (Villalobos J, 2006)

3.2.1.2 Test rig preparation and loading system

Tests were conducted in a strong cylindrical container made of thin-wall acrylic glass. The container had an inner diameter of 550 mm with a thickness of 30 mm ($D_o - D_i$) and a height of 600 mm filled with Redhill 110 sand. A 100 mm thick layer of gravel was placed uniformly at the base of the tank to provide a stiff layer underneath the sand layer. The sand layer was prepared by a pluviation method to achieve the targeted density. The amount of dry soil was placed by adding sand to funnel. Once the funnel was in-place over the area to be filled, the soil flew slowly into the test cylinder through a funnel, where a constant drop height of

about 10 cm (between the funnel outlet and the current sand surface) was maintained. Consistent relative densities (Dr) can be maintained using this drop height and it helps to minimized sand segregation during pluviation.

The density of the in-situ sand sample is verified using density tubes which are placed throughout the test container and pluviation method via a funnel with a 1.0 cm opening. The tubes are carefully located to ensure they will not be disturbed by the model installation (Figure 3.5). After installing the caisson model in sand and a load test has been carried out, the tubes were carefully removed. Once removed from the test container, the tubes are levelled off and weighed. With the volume and weight of the empty tubes known, the density, γ of the sand in each tube during the test can be established. The sample densities are presented in terms of relative density using the sand properties and equation Eq. (3.1).

$$Dr = \frac{\frac{1}{(\gamma_d)_{min}} - \frac{1}{\gamma_d}}{\frac{1}{(\gamma_d)_{min}} - \frac{1}{(\gamma_d)_{max}}} \qquad 3.1$$

where γ_{min}, γ_{max} and γ_d are the maximum, minimum and current unit weights, respectively.

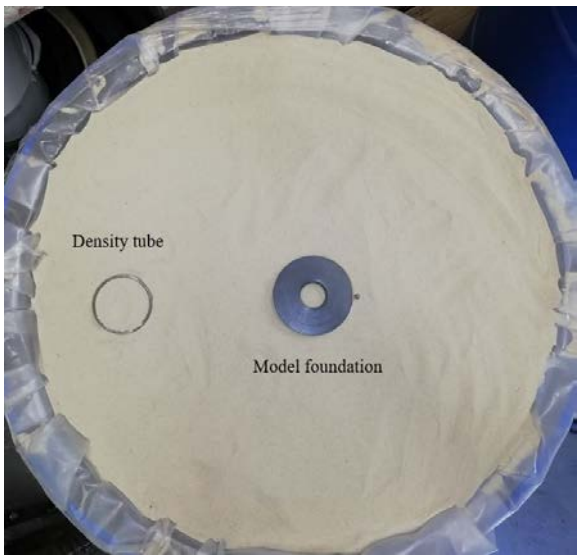

Figure 3.5. Plan view of the sand density preparation

The sand layer was prepared by a pluviation method to achieve the targeted density (23–25%). Soil was slowly poured through a funnel with an opening of 20 mm over the area to fill the test container. A constant drop height of 50 mm (between the funnel outlet and the surface of sand) was maintained during the filling process. For the experiments with medium relative density (Dr=48–50%), the sand was poured into the test container in layers 50 mm thick and compacted by a vibrator compactor to the desired unit weights and heights. Once the sand surface was prepared, the model caissons were placed and sand was poured around the instruments to secure them and minimize further disturbance. The model caissons were installed in dry sand by pushing rather than by suction. The pushing process was carried out very gently to avoid any major disruption to the soil density. Previous studies showed that the caissons installed by suction provides lower moment capacity than caissons installed by pushing (Villalobos, 2006), however, pushing installation was used in the laboratory owing to simplicity. The models were installed into the soil at a rate of 0.1mm/s until the lid made complete contact with the soil. A installation rate of 0.1mm/s was used by Kelly et al.(2006) for the identical soil in a saturated condition.

For all the models, to create a moment M, a horizontal load H' was applied using an electric actuator at a height above the cap of the caisson.

As the overturning capacity is controlled by horizontal load so that it represents a selected ratio of the moment load $M/(H'D)$. The ratio of $M/(H'D)$ varies between 0.5 and 2 for offshore wind turbine projects (Byrne et al., 2003b). However, bigger ratios have been considered in the former studies (Foglia et al., 2015; Zhu et al., 2011a). Recently, the lateral load eccentricity, $M/(H'D)$ ranges of 5-15 is also considered in new design methods for offshore wind applications (Byrne et al., 2015). An eccentricity ratio (i.e. $M/(H'D)$) equal to 2.9 was used in this study, which corresponds to tall wind turbine towers (>100 m). A load cell

was attached in the actuator for measuring the interaction force. The rotation of the foundation was recorded by an inclinometer sensor placed on the top of the tower (as shown in Figure 3.6).

For the ease of overturning load application, horizontal force (H) is applied separately at the caisson lid level using a pulley and weight system as shown in Figure 3.6. This allows us to avoid moving the position of the top horizontal force.

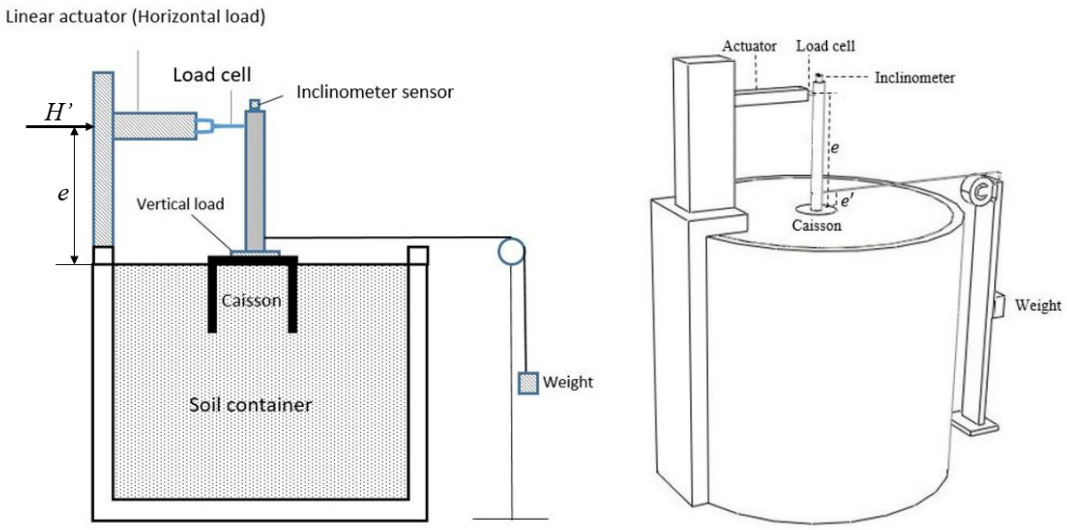

(a) Schematic of the experimental setup

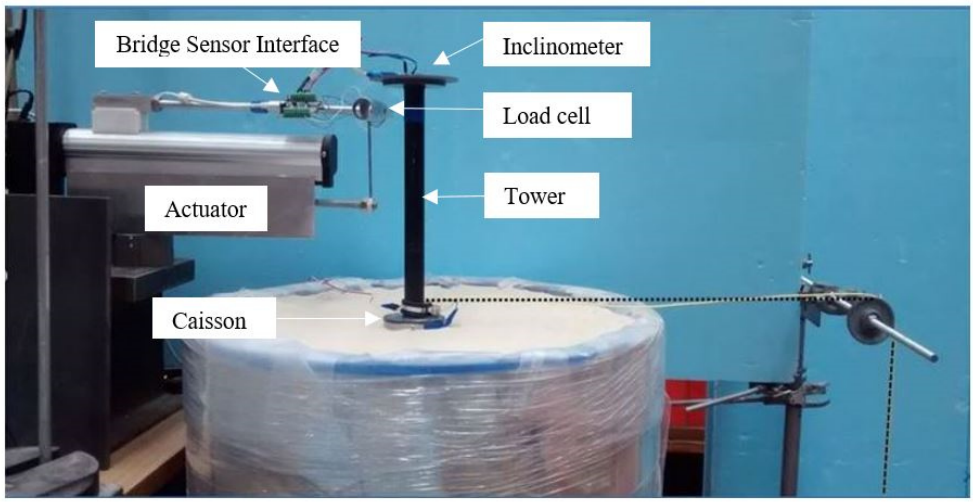

(b) Photograph of the experimental setup

Figure 3.6. Loading system and experimental setup: (a) schematic of the experimental setup; (b) photograph of the monotonic loading rig and experimental setup

The tests were carried out under dry soil conditions to explore the drained response of the model foundation with a loading rate of 0.1mm/s. To set up the combined loading system, a steel frame with frictionless pulleys was fixed to the test rig. A rope connected to the foundation head at one end and on a hanger at the other end was used to apply a constant horizontal load (H) (Figure 3.6). Constant vertical loads, in addition to the self-weight of the foundation model, were added on the top of the foundations to mimic the structural dead weight (V) (Byrne and Houlsby, 2004). The horizontal load at the top of the caisson (H) as well as the vertical dead load (V) were kept constant but, a horizontal load at the top of the tower (H') was gradually applied. It is important to keep the testing condition consistent, especially the relative densities of the sand for all the models, in order to make the results as comparable as possible (Bang et al., 2011). Therefore, prior to each test, the test chamber was emptied and refilled with the pluviation system.

A description of the apparatus with technical specifications are provided in Appendix A.

3.2.1.3 Centrifuge test

Geotechnical centrifuge modelling provides the condition of scaling down a full-scale prototype model to a small-scale centrifuge model, with replication of in-situ stress field.

In recent years, centrifuge testing has played an important role, which is an advanced physical modelling technique for measuring and recording geotechnical problems. It provides physical data for validating analytical and numerical methods (Ng, 2014), also noted that it is necessary to perform soil tests in the centrifuge, which provides the analogous stress field for boundary value problems. Thus, this is also adopted in the present study to investigate the behaviour of the winged caisson foundations.

In this research, the centrifuge tests were carried out with the objectives as follows:

1. To improve the testing methodology for the winged suction caisson modelling within the geotechnical centrifuge;

2. To investigate the overturning capacity with variation of soil conditions;

A total of 2 tests were performed at 70 g (i.e., acceleration scaling factor N = 70) using the University of Nottingham Centre for Geomechanics centrifuge, as listed in Table 3.3, which provides details on caisson load condition, geometry, and configuration.

The foundation models built for the centrifuge test are shown in Figure 3.7. The external diameter (D) of all the caissons shafts was 75 mm. A factor of 70 was chosen to scale the dimensions of the caissons based on the available size of the test rig, and limitations of the available loading system. The caisson specimens were fabricated from a smooth stainless steel tube with a wall thickness (t) of 1.5 mm (the wings also had the same thickness). In order to apply the load, a rectangular steel bar (tower), with a total height of 220 mm, and dimension of 25 x 25 mm was connected to a cap (thickness 5mm) on the top surface of the caissons. Similar to 1-g models, the winged models, were positioned such that two wings were perpendicular to the lateral loading direction and two wings were along the loading direction.

Horizontal forces applied on the tower utilising a linear actuator. Two laser beams were used for measuring displacement of the tower during lateral loading. The centrifuge test set-up is shown in Figure 3.8.

Table 3.3. Details of the model test (centrifuge test)

Test ID	Length (L) mm	Diameter (D) mm	Wing width (T)	Wing height mm	Relative density (Dr %)
G1	75	75	-	-	50
G2	75	75	0.4D	75 mm	50

Figure 3.7. Foundation models used in the centrifuge

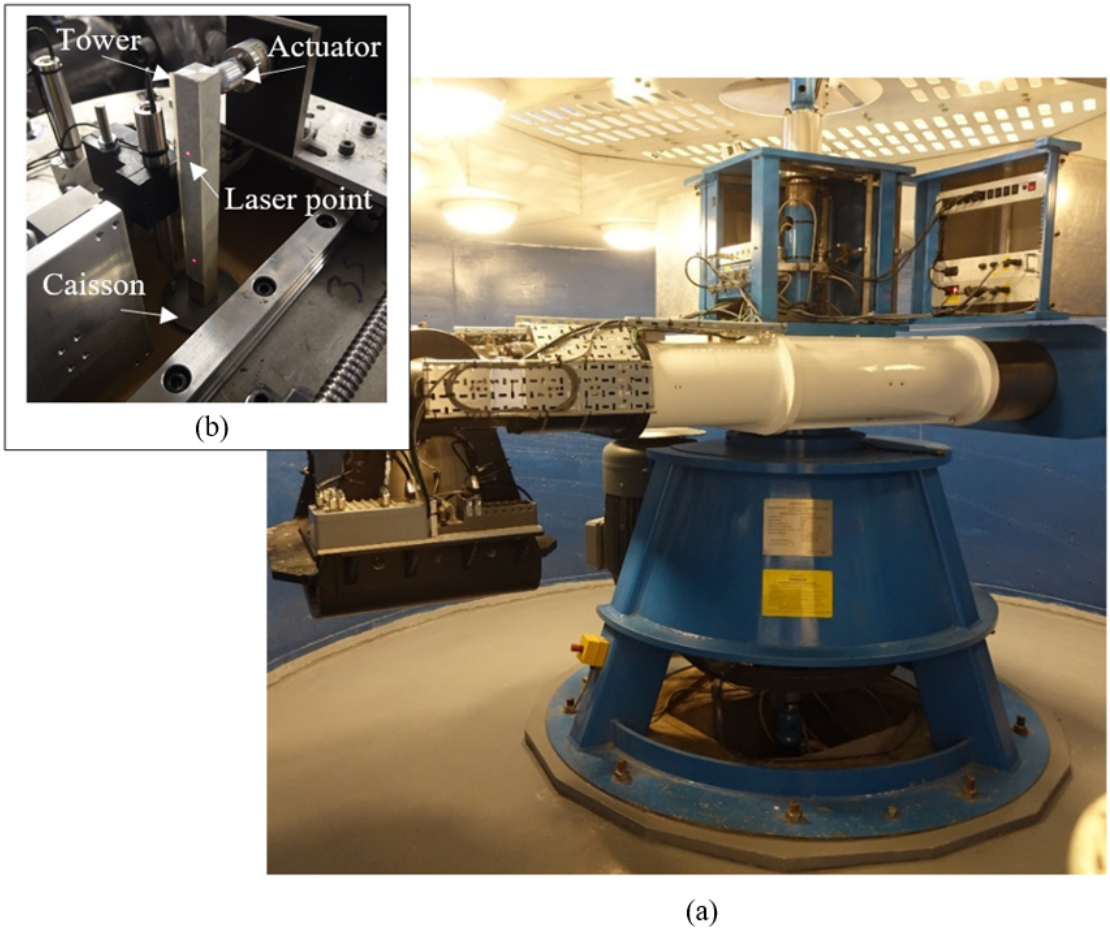

Figure 3.8. a) Overview of NCG geotechnical centrifuge chamber; b) Centrifuge set up test

Silica sand of HST95 with relative density of 50% was used in centrifuge tests. Particle size distribution for the Silica sand of HST95 is shown in Figure 3.9. A summary of the sand properties are shown in Table 3.4.

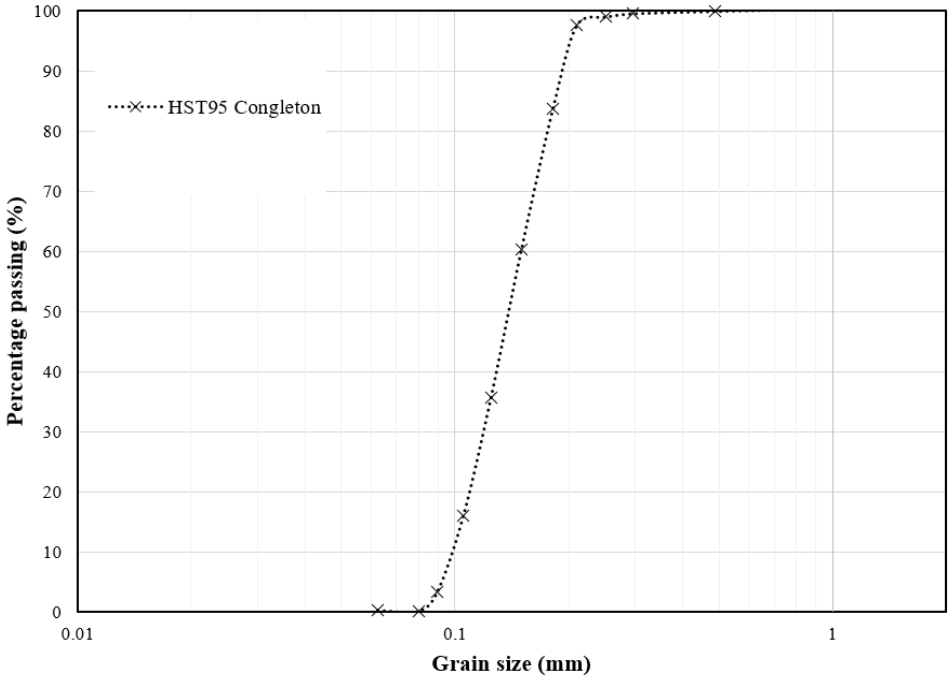

Figure 3.9. Particle size distribution curve for HST95

Table 3.4. Physical properties of sand used in the centrifuge tests (Liang et al., 2015)

Properties	HST95
d_{10}, d_{30}, d_{60} (mm)	0.1, 0.12, 0.14
Coefficients of uniformity (C_u) and curvature (C_c)	1.4, 0.96
Specific gravity, G_s	2.63
Minimum dry density, γ_{min} (kN/m^3)	14.34
Maximum dry density, γ_{max} (kN/m^3)	17.60
Angle of friction of the soil, ϕ'	32º

The centrifuge with swinging platform, and a payload capacity of 500 kg at a nominal radius of 1.70 m can be spun up to 100 g. The Nottingham Centre for Geomechanics (NCG) geotechnical centrifuge, manufactured by Broadbent G-Max, is a 50g-T machine, with 2.0 m platform radius.

The centrifuge container, made from steel, with inner diameter of 500 mm and depth of 500 mm. Specification of the NCG geotechnical centrifuge and the components are given in Table 3.5 and Figure 3.10.

Table 3.5. Specification of the NCG geotechnical centrifuge (Ellis et al., 2006)

Platform radius	2.0m
Assumed effective radius of payload	1.7m
Maximum size of payload	0.8m wide (vertical in flight)
Maximum payload	0.6m wide (circumferential in flight)
	0.9m high (radial in flight)
	850kgm (500kg at 1.7m) up to 100g
Maximum acceleration	150g (at 1.7m)
Motor	75kW three phase induction motor

A number of scaling criteria is applied for the physical model to represent the prototype. For the basic scaling law of centrifuge modelling, the uniform acceleration field is assumed to apply to the model by selecting an effective centrifuge radius R_e which will minimise the scaling errors due to the nonlinear stress distribution and the difficulty of representing sufficient detail. Thus, the inertial acceleration field of N times earth gravity (g, ≈ 9.8m/s2) is provided in accordance with Equation (3.2).

$$N = \frac{\bar{\omega}^2 R_e}{g} \qquad 3.2$$

where $\bar{\omega}$ is angular velocity, rad/s.

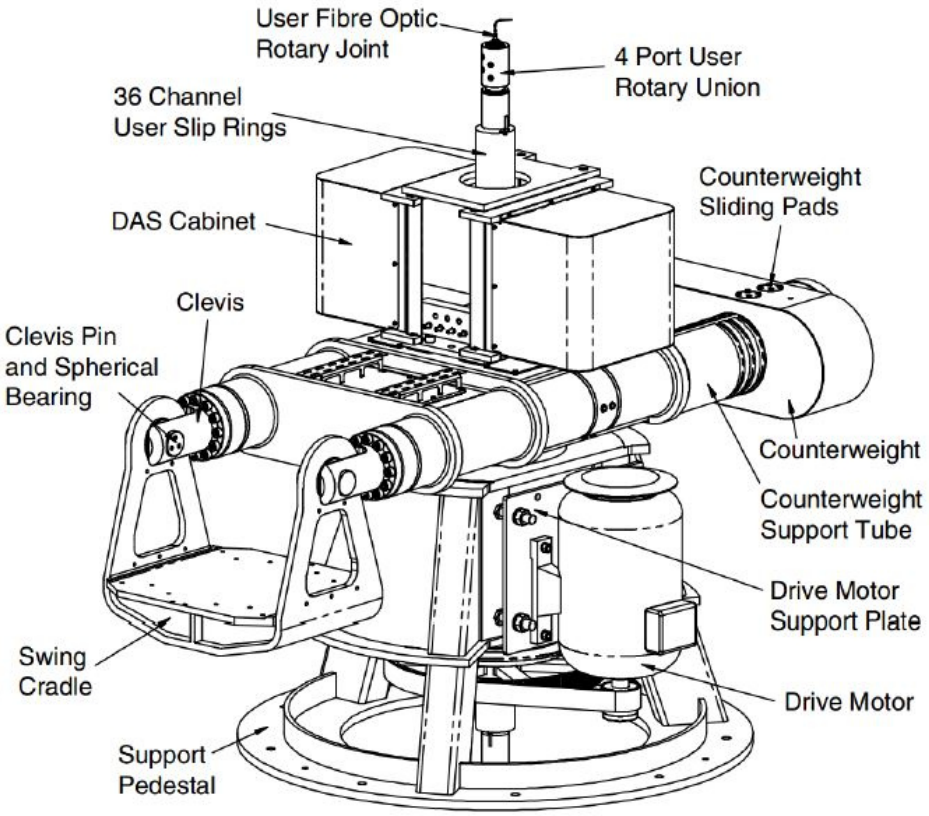

Figure 3.10. Schematic of the NCG geotechnical centrifuge; after (Ellis et al., 2006)

Based on the physical relationships and dimensional analyses, the scale factors for quasi-static models relevant to common geotechnical applications of centrifuge modelling can be derived as listed in Table 3.6

Table 3.6. Scale factors for centrifuge modelling of quasi-static problems

Quantity	Metric unit	Scaling factor (prototype /model)
Gravity /Acceleration	m/s^2	$1/N$
Density	kg/m^3	1
Unit weight	N^1/m^3	$1/N$
Length /Displacement	m	N
Area	m^2	N^2
Volume	m^3	N^3
Stiffness	N/m^2	1
Stress / Pressure	N/m^2	1
Strain	-	1
Force	N	N^2
Velocity	m/s	1

3.2.2 Numerical simulation (Monotonic/static loading)

In order to generalise the observed behaviour of the small scale experiments and to estimate the bearing capacity of winged suction caisson foundations in sandy soils, a three-dimensional (3D) finite element (FE) model was developed using the commercial software ABAQUS. Initially, the model was validated against the experimental results in the laboratory before it was extended to field scale caissons.

FE analysis was adopted to model the 3D geometry of the conventional and winged suction caisson foundations and the appropriate soil–foundation interaction. Figure 3.11 shows a schematic of the problem in the FE model. The FE models were generated in the rectangular shape of soil body. An FE domain with dimensions $9D \times 4.5D \times 4D$ (length, width and height, respectively) was used to avoid boundary effects. To model the sand behaviour, a Drucker-Prager material model assuming a soil having elastic-perfectly plastic behaviour and following an associated flow rule (the dilatancy angle ψ equal to the friction angle ϕ') was used, with material parameters of β' and d. Terms β' and d represent parameters of the material model which can be calculated indirectly using parameters of the Mohr-Coulomb model derived from Ciampi (1997).

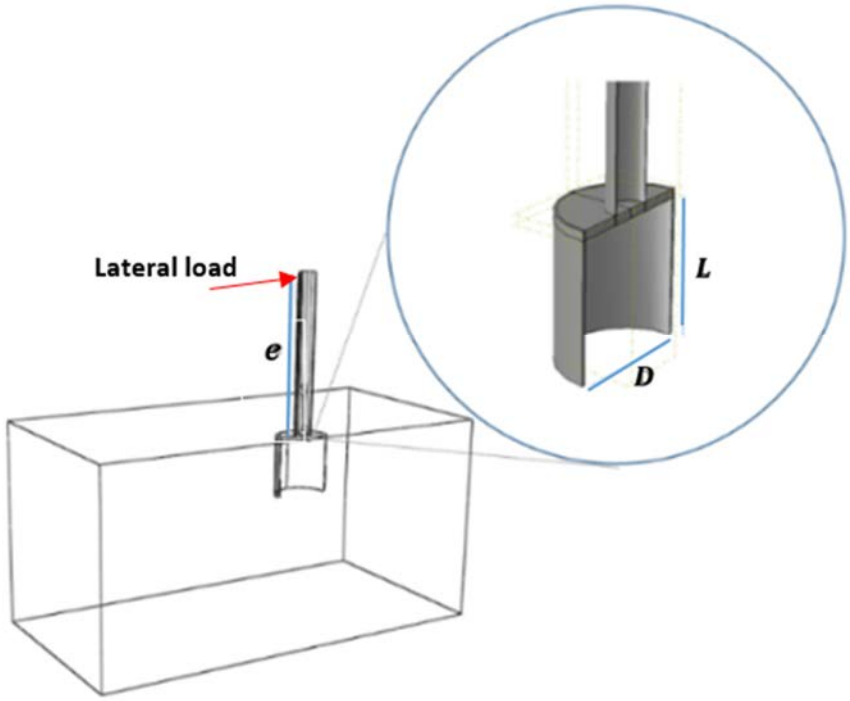

Figure 3.11. Schematic of model: direction of lateral load applied to the models, L, caisson length; D , caisson diameter; e, eccentricity

For three-dimensional problems, the Mohr-Coulomb parameters can be converted to create a Drucker-Prager surface that circumscribes (using the minus signs) or inscribes (using the plus signs) the Mohr-Coulomb surface (Ciampi, 1997):

$$\tan\beta' = \frac{6\sin\phi'}{3 \pm \sin\phi'} \quad 3.3$$

$$d = \frac{6c' \cos\phi'}{3 \pm \sin\phi'} \quad 3.4$$

Taking advantage of the symmetrical nature of the problem, only half of the problem was modelled. Figure 3.12a and Figure 3.12b show a semi-cylindrical section through a diametrical plane of the conventional (simple) and winged caisson foundations with $L/D = 1.0$, respectively. In the regions near the caisson–soil interface, a relatively fine mesh was used and it becomes coarser further away. In the FE analyses, the foundations were modelled as "wished in place", assuming that installation effects have a negligible impact on the bearing capacity. The initial stress in the soil prior to loading of the model foundation was generated considering a lateral earth pressure coefficient $K_0 = 1 - sin\phi'$ (Jaky, 1944).

To simulate the overturning behaviour of the caisson, a force-controlled FE model was created and careful attention was paid to modelling the interaction of the caisson elements with the surrounding soil. A 'Contact pair' interface captures the nonlinear behaviour in the soil-caisson interface. In the radial direction, a "allow separation" contact behaviour is assumed. The 'Small Sliding' tracking approach in ABAQUS was employed for the contact of the two bodies of soil and the caisson. This type of interaction is used to simulate the contact between two deformable bodies or a deformable body and a rigid body in 3D assuming that even if the two bodies undergo large motions, there is relatively little sliding of one surface along the other (Mardfekri et al., 2013). The soil and the caisson were modelled using the C3D8R solid

homogeneous elements available in ABAQUS/Standard element library, which are 8-noded linear brick elements with reduced integration and hourglass control (an option for reduced-integration elements in ABAQUS/Standard). The reason for choosing this type of element is that an acceptable accuracy with less time can be obtained. For standard elements, the reduced integration in ABAQUS/standard generally leads to more accurate results compared with the full integration (Haji, 2017). There are two possible problems, including Shear locking and hourglassing that may occur in an FE analysis and result in inaccurate numerical predictions. Shear locking occurs when an element becomes overly stiff in bending which leads to the generation of shear deformations instead of bending deformations. This problem is mainly caused by fully integrated elements. Hence, elements with reduced integration have been used to avoid hourglassing. Linear elements with reduced integration may experience deformations without creating strains; this phenomenon is called hourglassing which involves deformations with a zero-energy mode. Since coarse meshing can be a source of hourglassing, fine meshing was adopted to avoid the occurrence of hourglassing in the elements.

The caisson outer surface is chosen as a 'master surface' and the soil surface in contact with the skirt of the caisson as a 'slave surface'. The frictional force between these surfaces is dependent on a coefficient of friction μ (Abdel-Rahman and Achmus, 2011). In the numerical simulations presented here the friction coefficient was calculated using $\tan(\delta)$, where δ is interface friction angle and assumed with the well-known assumption of δ=2/3ϕ' (Foglia et al., 2016). The buckets were considered as linear elastic materials (E=200 GPa). Young's modulus of sand (E_s) is a function of mean effective stress σ'_m, and can be expressed as $E_s = KP_a(\sigma'_m/P_a)^f$ (Janbu 1963), where K and f are soil parameters; and P_a is atmospheric pressure. However, in this thesis, a constant value was considered for the sand.

The stress level in the soil during the small scale tests performed within the 1-g experiments is very small. Elasticity modulus of the sand in 1-g tests (Redhill 110) can be calculated based on the formula proposed by Seed and Idriss (1970). For the linear analyses the soil is assumed to have a Young's modulus E_s =8000-10000 kPa for the loose sand in the FE models. The E_s= 33 MPa was used for the sand used in centrifuge (HST95), which is estimated according to the equation proposed by Al-Defae et al. (2013):

$$E_s = 25Dr + 20.22\ (MPa) \qquad 3.5$$

In order to initiate the numerical simulation according to the assumption of a pure frictional material (sandy soil) a very low cohesion is necessary. A value of 0.1 kPa is instead recommended in order to minimize the influence of the cohesion (Larsen, 2008b). The value of ϑ (Poisson's ratio) is assumed to be 0.29 for the soil used in the laboratory. The geometry and loads are symmetric with respect to the centre of the geometry. For calculating overturning capacity of the caissons, only half of the load (because of the symmetry), equal to lateral load bearing capacity of caissons obtained from the experiments was applied. The loads obtained from centrifuge tests were considered into full-scale results in the FE analysis using the appropriate scaling factors (N^2).

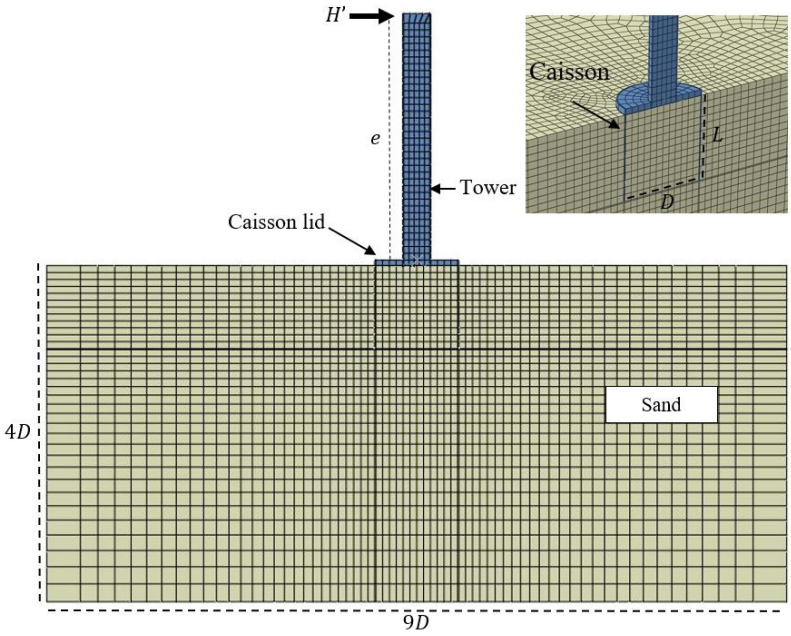

(a)

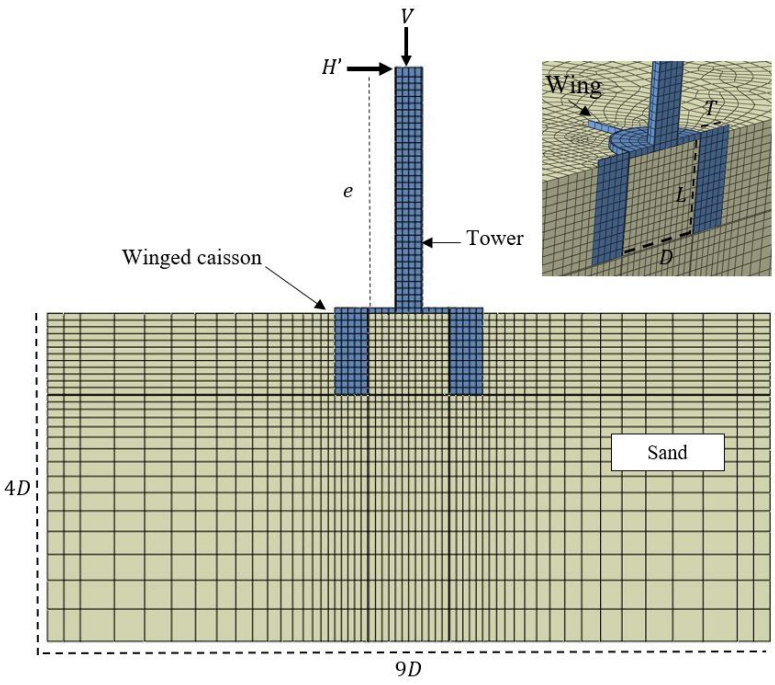

(b)

Figure 3.12. Finite element model of the a) conventional and b) winged caissons used to analyse the laterally loaded behaviour

3.2.3 Analytical solution for the horizontal capacity estimation of the conventional and winged caisson foundations

In this thesis a simple strategy to derive an analytical solution to the lateral-load resistance of the suction caisson foundations is discussed. The strategy is based on the Rankin theory method. In order to assess the validity of the proposed strategy, a series of laboratory tests and numerical simulations, using three-dimensional FEM, under monotonic loading conditions were carried out.

The proposed equation was calibrated based on the physical test results via a series of 1 g small-scale laboratory (University of Birmingham) and a centrifuge test were carried out in the Nottingham centre for Geomechanics (NCG).

Two embedment length to caisson diameter ratios (L/D) of 0.5, and 1.0 under 1-g conditions, and a centrifuge test performed on a model with an L/D ratio of 1.0 were chosen to validate the analytical model (Table 3.7).

Table 3.7. Details of the model test used for analytical method

Test ID	Length (L) mm	Diameter (D) mm	Relative density (Dr %)	Test condition
CSC2	37.5	75	25	*1-g*
CSC1	75	75	25,50	*1-g*
G1	73	75	50	Centrifuge

A simple model based on force equilibrium was used as a way of giving insight and understanding of the soil-foundation interaction problem. The proposed analytical method determines ultimate limit state (ULS) of suction caisson foundation. Rankine's theory for lateral earth pressures in active and passive conditions were used in the analyses. The presented relationships are simple, easy to use, and do not require tedious calculations. Figure 3.13 depicts

the external forces applied to a caisson at the load rotation point (RP) as well as lateral earth pressures and the reacting internal stresses. In order to calculate the earth pressure it is assumed that the caisson walls rotating around RP as visualized in Figure 3.13. The location of RP has been validated via FE method and Particle Image Velocimetry (PIV) technique. The results of FE model are presented in section 4.5, however the results from PIV are placed in Appendix B as this has not been defined as an objective in this research.

All the external forces (i.e. the weight of the caisson and the attachments, external vertical load, and lateral load), and the weight of soil encompassed by the compartment inside the caisson foundation, acting on the foundation were considered in the free body diagram (Figure 3.13).

Soil pressure distributions along the skirt were simplified based on the theoretical assumptions and FE results (Figure 3.13).

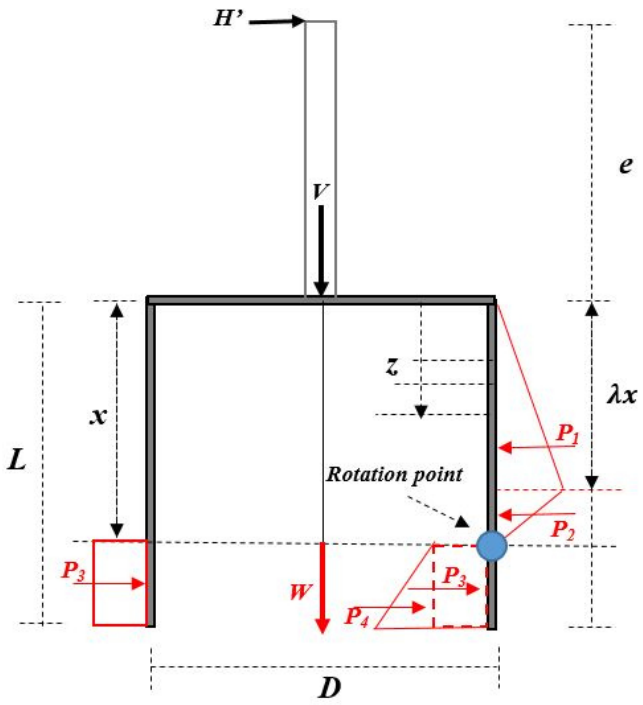

Figure 3.13. Assumed the rotation point (RP) and free body diagram i.e. external loads, weights, and earth pressure distribution along the rigid caisson shaft under lateral load

3.2.4 Experimental investigation (cyclic loading)

Generally, foundations are designed to operate under normal service conditions during the design life of an OWT (typically 20 – 30 years) (Topham and McMillan, 2017). The OWTs might be subjected to static and cyclic lateral load including, but not limited to: 1) structure-associated loads, 2) environmental loads (wind, wave, and current), and 3) other loads (accidental and operating loads). The system are excited by these different loading regimes with a wide range of frequencies, increasing complexity to the foundation behaviour.

In order to understand the cyclic lateral behaviour of the winged caisson foundation in drained condition, a series of physical cyclic lateral load tests with various amplitudes under constant vertical load were carried out in loose sand.

Physical model tests using modified a shaking table (for applying cyclic lateral load) in geotechnical lab were performed to evaluate the cyclic behavior of the winged caisson installed in granular sand. The modified shaking table was used to apply horizontal displacements to the caisson head. Displacements were measured using an inclinometer sensor placed on the top of the tower, and the horizontal loads (i.e. forward and backward) were measured using two load cells attached on the arm of the lever. The size of the soil container and soil preparations were similar to those used for monotonic tests. The sand remained dry, replicating a fully drained offshore condition.

For each test the following experimental procedure was adopted.

a) A sand sample was prepared using a pluviation method.

b) The model caissons were installed in dry sand by pushing rather than by suction. The pushing process was carried out very gently to avoid any major disruption to the soil density until the soil plug contacted the caisson cap. As mentioned earlier, the effect of the installation

technique (i.e. pushing and suction penetrations) on the subsequent behaviour of the single caisson is negligible (Villalobos Jara, 2006).

c) The tower was then situated between two jaws, connected to the lever arm (Figure 3.14a).

d) Using the shaking table casual software, the desired loading regime (i.e. amplitude and frequency) was specified, then enabled to apply a load to the foundation.

e) The forward and backward loads and corresponding rotation of the system were recorded throughout the two load cells and the inclinometer sensor.

f) The amplitude of the lever arm for each model was adjusted based on the maximum displacement of each model (it varies according to the model), obtained from static test corresponding to the maximum overturning capacity.

g) The test started with frequency equal to 0.1 Hz (mainly representative of wave loads) under 10 cycles. The amplitude was increased manually after completing 10 cycles. The amplitude was increased within three steps, until the maximum displacement (according to the static test) is achieved.

h) Once the test had been completed under the certain frequency (0.1 Hz) for three different amplitude, the loading was ceased.

A list of the test models that were examined under cyclic loading is provided in Table 3.8.

Table 3.8. Test models under cyclic loading

Model	Length (L) mm	Aspect ratio (L/D)	Wing width (T)	Wing height (h) mm	Relative density (Dr %)	Type of study
CSC1	75	1.0	-	-	23-25	Exp.
CSC2	37.5	0.5	-	-	23-25	Exp.
WSC3	75	1.0	(0.4D)	75	23-25	Exp.
WSC6	37.5	0.5	(0.4D)	37.5	23-25	Exp.

Exp.: Experimental

All of the experiments were performed at 1-g condition using two reference model caissons of the conventional caisson foundation with $L/D = 1.0$ and the winged caisson with wing width $T = 0.4D$. The novel loading system developed for model caisson studies (Figure 3.14) were employed to apply cyclic lateral load of sinusoidal waveform shape to near the head (top) of scaled suction caisson installed in dry loose sand bed. To avoid rocking motion, a vertical load (450 gr) was applied on the caisson cap. The experimental setup is illustrated in Figure 3.14. Therefore, the monotonic test was repeated for two models (CSC1 and CSC2) with additional vertical load (450 gr) in order to identify the maximum overturning capacity and the corresponding rotation. There is always some boundary wall effect on the test results using physical modelling in laboratory (Bhattacharya et al., 2013). Previous studies found that the boundary effect becomes negligible at a distance of $5D$ (where D is the diameter of the foundation) from the centre of the foundation (Bhattacharya et al., 2013; Nanda et al., 2017). In this study, the test tank dimension was chosen such that boundary effects are minimized (~$7.5D$).

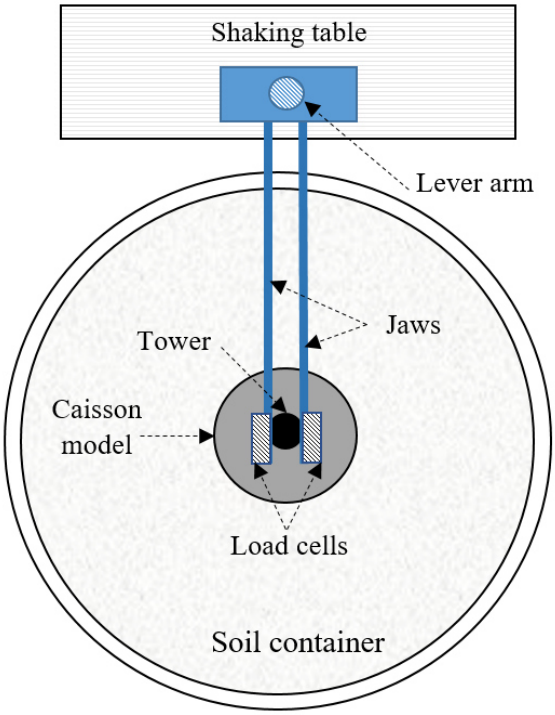

(a)

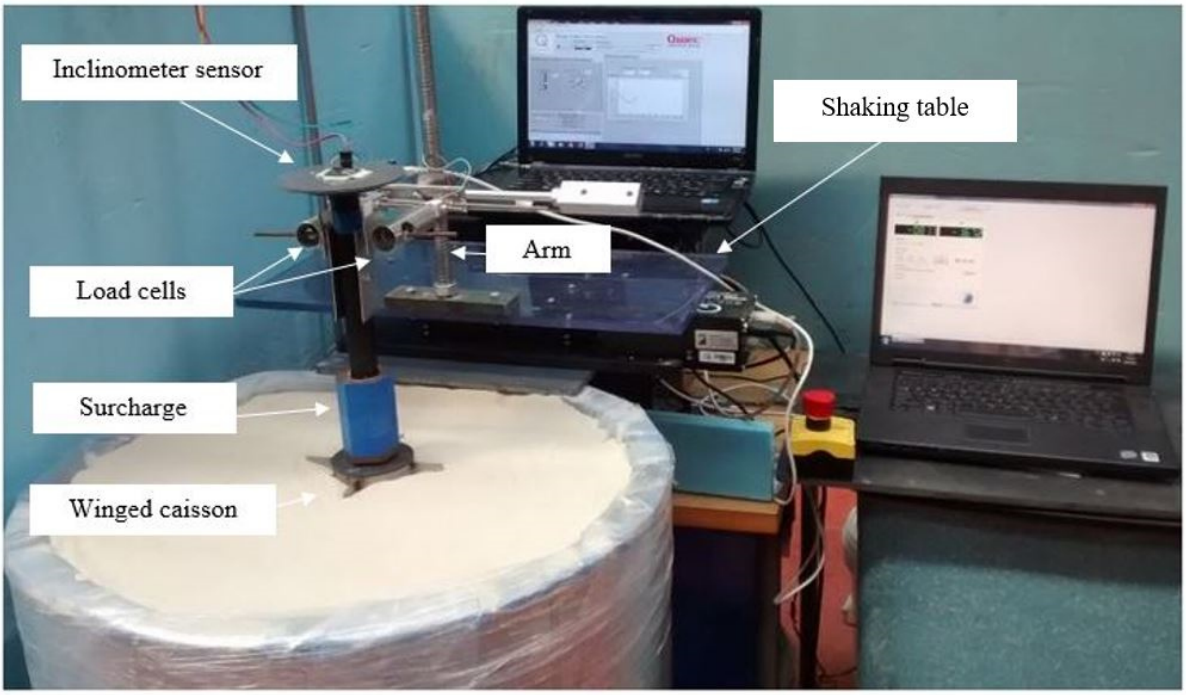

(b)

Figure 3.14. Cyclic loading system; a) Plan view, b) Photograph of the experimental setup

The cyclic loading characteristics applied on the foundation system must be uniquely defined. In the following, load levels are referred to in terms of the applied moment M. The corresponding horizontal force follows from $H = M/e$. Two independent parameters are defined to characterise the applied sinusoidal loading:

$$\xi_b = \frac{M_{max}}{M_s} \quad 3.6$$

$$\xi_c = \frac{M_{min}}{M_{max}} \quad 3.7$$

in which M_s refers to the static (monotonic) moment capacity of the caisson, and M_{min} and M_{max} are the minimum and maximum in a load cycle.

The size of the cyclic loading is measured by the ratio ξ_b, normalised with respect to the static (monotonic) moment capacity ($0 < \xi_b < 1$). The ratio $\xi_c \in [-1;\ 1]$ quantifies the characteristics of the cyclic load, where ξ_c = 1 for a static test, 0 for a one-way loading test and -1 for a two way loading test.

A two-way loading system (ξc = -1) with ξb = 0.9 was selected in this study to evaluate the cyclic response of the winged caisson foundations. ξb value of 0.9 represents designed angular rotation of the foundation which is limited to 0.25 degree (Peire et al., 2009).

3.3 Hybrid tripod caisson foundation

In this section, the methodology that was used to assess the monotonic response of an innovative proposed tripod foundation in sand is discussed. The proposed hybrid foundation consists of three single bucket foundations combined with three large circular mats attached to each bucket foundation. The general concept is shown in Figure 3.15. In the conventional tripod

bucket foundation, the bearing capacity is provided by three rigidly connected bucket foundations, while in this proposed hybrid foundation, the resistance is offered by a combination of the buckets and the circular mats. In the proposed hybrid foundation the circular mats are in complete contact with the soil surface providing greater resistance against the overturning moments. Reinforcing bracing between the caissons' lid and the tower, which is usually used in the tripod foundations (see the conceptual idea for the full-scale foundation in Figure 3.15b), were omitted in the models for simplifications (see simplified model in Figure 3.15a).

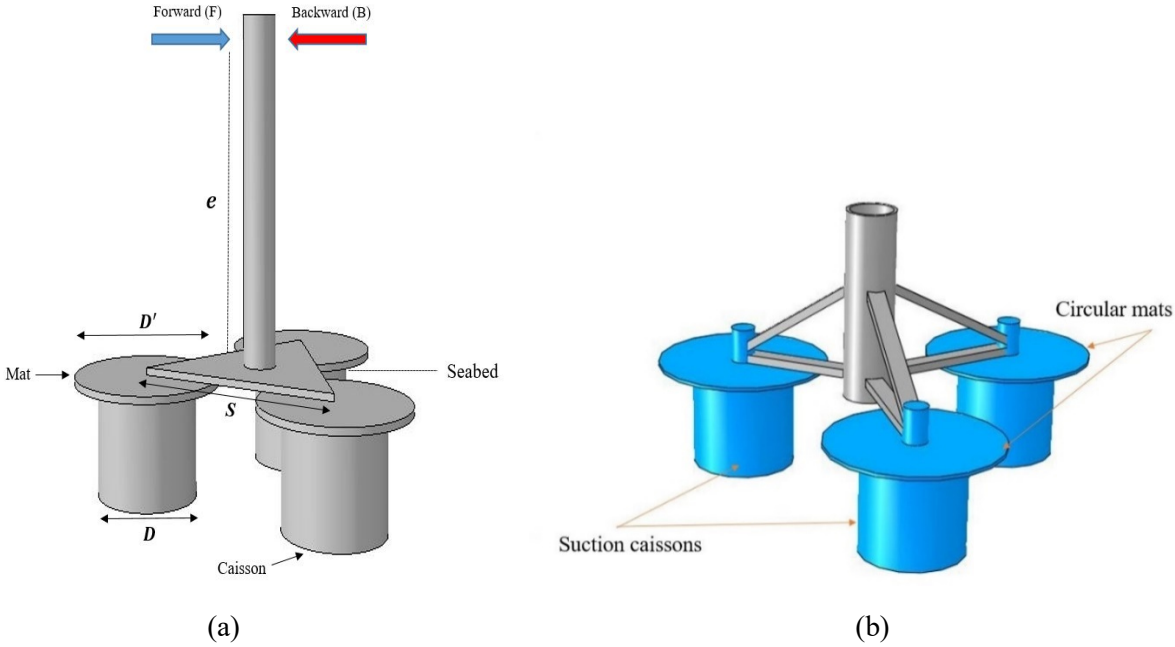

Figure 3.15. Schematic of the hybrid three suction bucket and mat foundation. The key dimensions and loading condition are also shown: a) the simplified model used in the simulations, b) the conceptual idea for the full-scale foundation

The experiments were conducted at small-scale under 1-g condition. Different bucket spacing (S) and loading directions (backward and forward) were evaluated on the basis of overturning resistance of the conventional and hybrid tripod bucket foundations. We refer to the loadings as forward and backward with respect to the loading direction, i.e. backward used

where the loading direction is towards a single bucket of a tripod foundation and the other two buckets are being rotated out of the seabed (Figure 3.15a).

Numerical analyses of the experiments were conducted for both the conventional and hybrid tripod bucket models using the finite-element (FE) method software, ABAQUS. The FE models were used to examine the behaviour of the proposed hybrid system in a tripod foundation under overturning moments. The effect of the circular mat diameter was also investigated using the validated FE model on the overturning resistance of the hybrid tripod bucket foundation.

3.3.1 Experimental investigation

3.3.1.1 Materials and model preparation

The prototype was scaled down to 1/100, and a bucket embedment depth ratio (L/D) of 1 and a skirt width to bucket diameter ratio (t/D) = 0.02, were considered. The distance between the buckets is expressed by the spacing ratio S/D, where S is the axial distance between the circular buckets and D is their diameter (Figure 3.15). Experiments were performed using various normalised spacing, S/D, ranging from 1.13 to 3.13.

The three conventional buckets with the external diameter (D) and embedment depth (L) of 75 mm were connected with an adjustable plate. The caisson specimens were fabricated from a smooth stainless steel tube with a wall thickness (t) of 1.2 mm. The adjustable mechanism consisted of an equilateral triangular plastic plate (200 mm long and 5 mm thick) with three linear holes in each angle and attached on the top of the circular mats. The three buckets were connected to the adjustable mechanism by nuts and bolts. By adjusting the distance between the buckets, three different configurations could be created (more details are provided in section 3.3.1.2). Three circular mats with a diameter of 120 mm, made of plastic,

were used to replace the conventional suction bucket caps and help to create the hybrid tripod foundation (Figure 3.16).

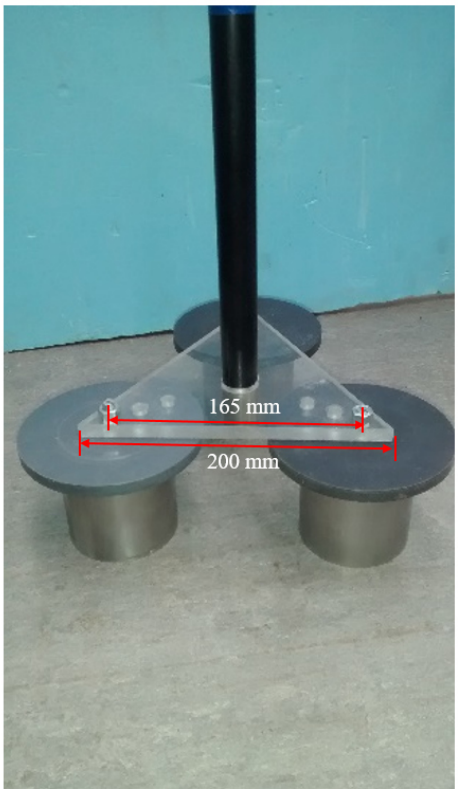

Figure 3.16. Hybrid foundation model used in the experiments, with D'=120 mm and S=165 mm

The horizontal load was applied to an extension rod (tower with 230 mm tall) that was rigidly connected to the top of the centre of the base (triangular plate). The circular mats and the towers made of plastic to reduce the effects of additional weight affecting the bearing capacity.

Tests were conducted in a strong cylindrical container. The container had an inner diameter of 550 mm, with a thickness of 30 mm and a height of 600 mm, and was filled with dry Redhill 110 silica sand. A 100 mm thick layer of gravel was placed uniformly at the base of the tank to provide a stiff layer underneath the sand layer. A homogenous sandbed and reproducible density was maintained throughout the test. The sand layer was prepared using

similar method as described for the winged caissons (same tank as used for previous tests), to achieve the targeted density (Dr =23-25%). The model buckets were installed in the dry sand by pushing rather than by suction. The pushing process was carried out very gently to avoid any major disruption to the soil density.

The models were installed into the soil at a rate of 0.1 mm/s until the lid made complete contact with the top of the sand. The tests were carried out under drained soil conditions to explore the drained response of the model foundation with a loading rate of 0.1mm/s. The properties of the Redhill 110 silica sand used in this study (Table 3.2) were obtained from the study conducted by Kelly et al.(2004) and Villalobos et al. (2005; 2006).

3.3.1.2 Test procedure

For all the models, to create a moment, M, a horizontal load H' was applied using an electric actuator at the height of 230 mm above the cap of the tripod bucket. An eccentricity ratio (i.e. $M/(H'D)$) equal to ~2.9 was used in this study, which corresponds to tall wind turbine towers (>100 m). A load cell was attached to the actuator to measure the applied force. The rotation of the foundation was recorded using an inclinometer sensor placed on the top of the tower (as shown in Figure 3.17a, b).

Figure 3.17c shows the plan view of the experimental set up and the loading system. As illustrated, the foundations were placed in the middle of the test container.

All the information related to the models and tests are summarised in Table 3.9; in this table the conventional tripod bucket foundations and the hybrid tripod bucket foundations are denoted C and H, respectively.

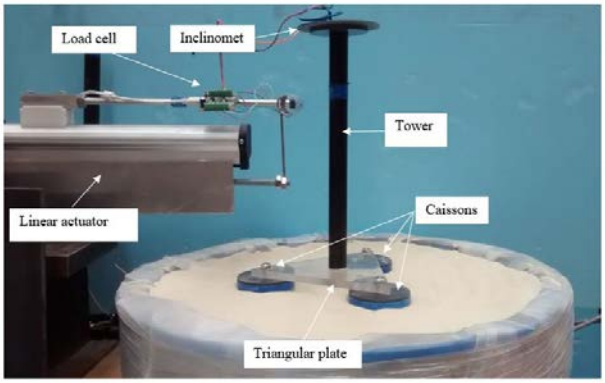

(a)

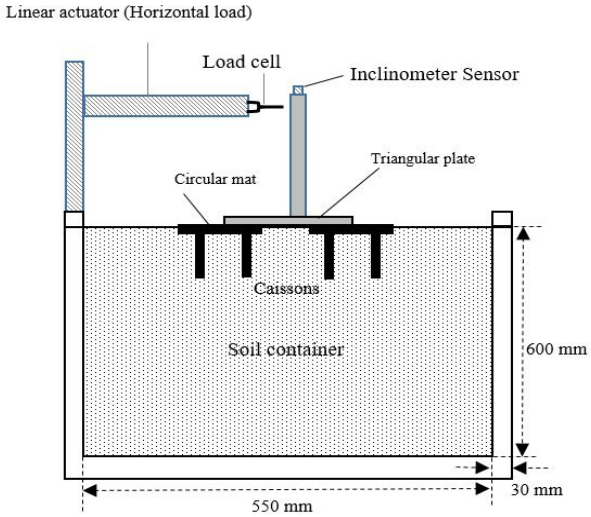

(b)

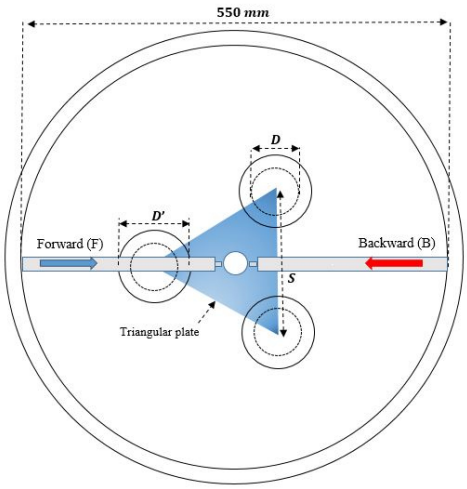

(c)

Figure 3.17. Testing system with loading actuator and tripod model (a) a photo of the experimental setup; (b) schematic side view of the experiment; (c) schematic plan view of the experiment

Table 3.9. Summary of the physical tests and numerical model analyses

Test ID	S (mm)	Loading direction Forward (F)/ Backward (B) **	Circular mat diameter (mm) D'	Exp./FEM***
C1*	95	F	-	Exp./FEM
C2*	95	B	-	Exp./FEM
C3*	130	F	-	Exp./FEM
C4*	130	B	-	Exp./FEM
C5*	165	F	-	Exp./FEM
C6*	165	B	-	Exp./FEM
C7	200	F	-	FEM
C8	200	B	-	FEM
C9	235	F	-	FEM
C10	235	B	-	FEM
H1*	130	F	120	Exp./FEM
H2*	130	B	120	Exp./FEM
H3*	165	F	120	Exp./FEM
H4*	165	B	120	Exp./FEM
H5	200	F	120	FEM
H6	200	B	120	FEM
H7	235	F	100	FEM
H8	235	B	100	FEM
H9	235	F	120	FEM
H10	235	B	120	FEM
H11	235	F	142.5	FEM
H12	235	B	142.5	FEM
H13	235	F	180	FEM
H14	235	B	180	FEM

*Reference tests
**F=Forward (single)
B=Backward (dual)
*** Exp.= Experiment
FEM= Finite element method

3.3.2 Numerical simulation

To estimate the bearing capacity of the hybrid tripod bucket foundations in sandy soils, three-dimensional (3D) finite element (FE) models were developed using the commercial software ABAQUS; to reduce the computation time, only a half of the foundation and the ground were modelled taking advantage of the symmetry within the problem.

FE analysis was adopted to model the 3D geometry of the conventional and hybrid tripod bucket foundations, and the appropriate soil–foundation interaction. Figure 3.18a and Figure 3.18b show a schematic of the conventional and hybrid tripod bucket foundation problem in the FE model, respectively. To model the sand behaviour, a Drucker-Prager material model was used with material parameters of β' =44.5 and d =135. Terms β' and d represent parameters of the material model which can be calculated indirectly using parameters of the Mohr-Coulomb model derived from Ciampi (1997).

The mesh dimensions were varied depending on the bucket diameter and spacing. A relatively fine mesh was used around the bucket and the mats, and becoming coarser further away from the bucket. Section 4.1.2.1 (Page92) is devoted to sensitivity analysis. In the FE analyses, the foundations were modelled as “wished in place”, assuming that installation effects had a negligible impact on the bearing capacity. The initial soil condition prior to loading of the model foundation was generated considering a lateral earth pressure coefficient $K_0 = 1 - \sin\phi'$ (Jaky, 1944).

To simulate the overturning behaviour of the tripod foundation, a load-controlled FE model was created. A 'Contact pair’ interface captures the nonlinear behaviour in the soil-bucket and soil-mat interfaces. In the radial direction, “allow separation” contact behaviour is assumed. The ‘Small Sliding’ tracking approach in ABAQUS was employed for the contact of the bodies of soil, mat and the bucket. This type of interaction is used to simulate contact

between two deformable bodies or a deformable body and a rigid body in 3D. The soil, mats and the caissons were modelled using the C3D8R solid homogeneous elements available in ABAQUS/Standard element library, which are 8-noded linear brick elements with reduced integration and hourglass control (an option for reduced-integration elements in ABAQUS/Standard).

The bucket and the mat surface were chosen as the 'master surface' and the soil surface in contact with the skirt of the bucket and the mat as the 'slave surface'. The frictional force between these surfaces is dependent on a coefficient of friction μ (Abdel-Rahman and Achmus, 2011). In the numerical simulations presented here the friction coefficient was calculated using $\tan(\delta)$, where δ is interface friction angle and assumed to be $2/3\phi'$ (Ahmed et al., 2015). The mats and the buckets were considered as linear elastic materials (E=200 GPa) (Abdelkader, 2015). In this study, a constant value was considered for the sand. Elasticity modulus of the sand (Redhill 110) is calculated based on the formula proposed by Seed and Idriss (1970).

Based on the results of the FE analyses, the moment-rotation curves ($M-\theta$) of the foundations are plotted to obtain the ultimate overturning capacity. The curves are inherently nonlinear being controlled by the "elastic" stiffness at small rotations and the moment capacity of the foundation at larger rotations. The ultimate moment capacity of the foundation has been defined as the moment corresponding to the yield point. To define the yield point, the method described by Villalobos (2006) was used. In this method, straight lines were fitted to the initial stiff elastic section and the plastic section, as shown in Figure 3.19. A horizontal line is then drawn from the intersection point of the two fitted lines to the load-rotation angle curve. This line will be extended until it cuts the moment-rotation curve, the intersection between the horizontal line and the curve was defined as the ultimate moment, denoted as M_u.

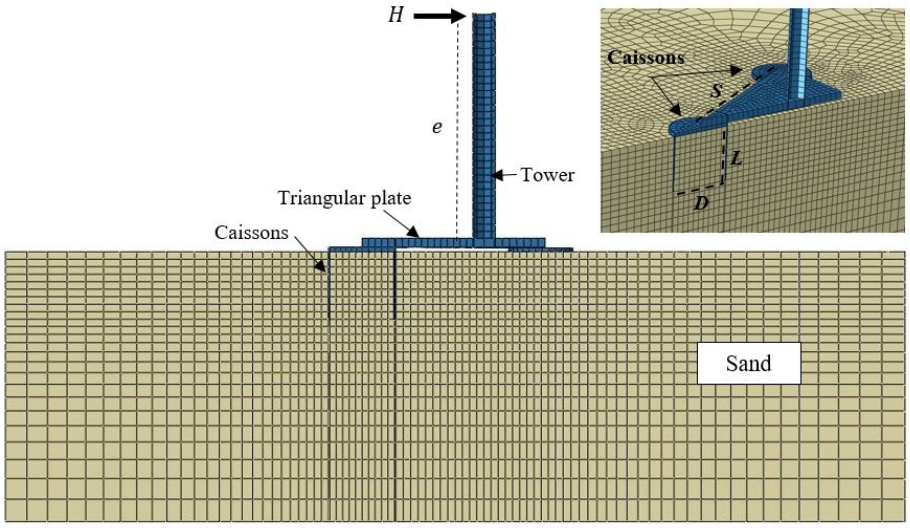

(a)

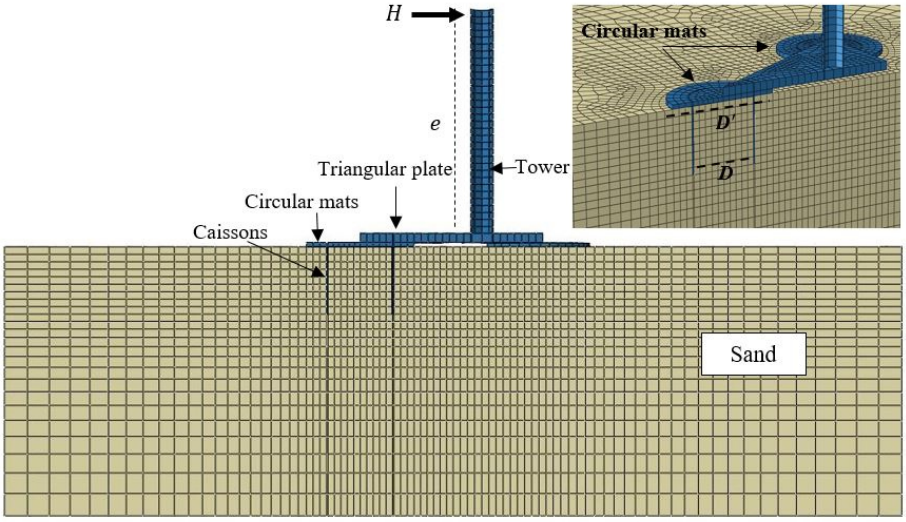

(b)

Figure 3.18. Finite element model of the a) conventional and b) hybrid tripod bucket foundations used to analyse the laterally loading behaviour.

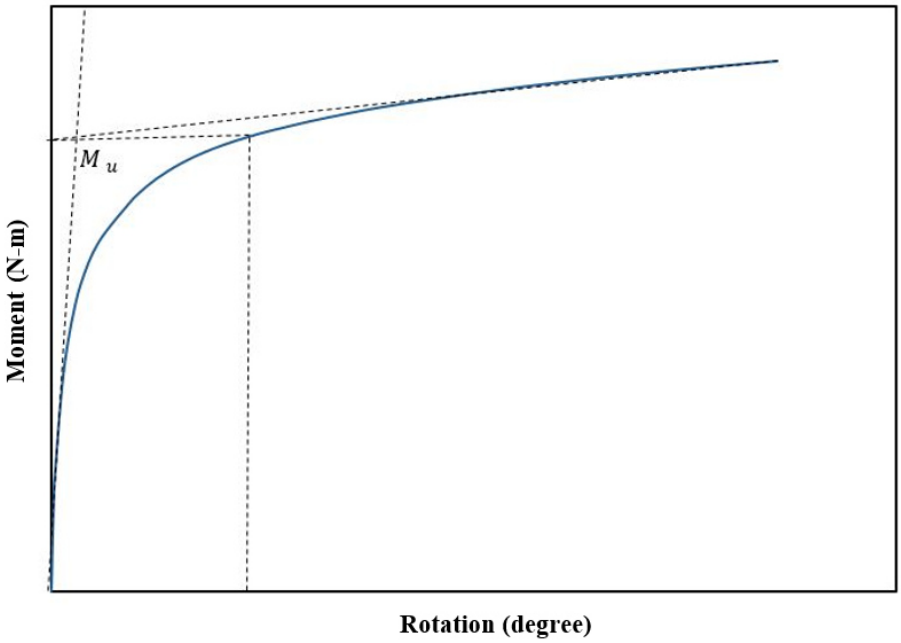

Figure 3.19. Tangent intersection method for determining the yield point and hence the ultimate bearing capacity of the foundation (M_u)

Chapter 4

4. WINGED SUCTION CAISSON (RESULTS)

This chapter presents the results of the monotonic and cyclic responses of the conventional and 'winged suction caisson' foundations based on the experimental test series and the numerical analyses, as discussed in the previous chapters.

The results of this chapter have been published by the author in a conference paper and journal paper:

Koohyar Faizi, Asaad Faramarzi, Samir Dirar, David N Chapman. "Finite Element Modelling of the Performance of Hybrid Foundation Systems for Offshore Wind Turbines". SEG-2018, DOI: 10.1007/978-3-319-99670-7_61.

Koohyar Faizi, Asaad Faramarzi, Samir Dirar, David Chapman. "Monotonic and Cyclic Lateral Load Tests on Monopod Winged Caisson Foundations in Sand". Proceedings of the Institution of Civil Engineers – Geotechnical Engineering. Doi.org/10.1680/jgeen.19.00056.

4.1 Overturning moment

4.1.1 Experimental results

The results of the model experiments embedded in loose (Dr =23-25%) and medium (Dr =48-50%) sands, under monotonic overturning moment, are presented in this section. The remaining experiments will be presented later in section 4.1.3 when parametric studies are presented.

Monotonic lateral loading experiments were carried out to examine the response of a caisson foundation under low vertical loads (equal to self-weight of the caisson). A moment

was determined by the force measured from the load cell multiplied by the eccentricity from the top of the foundation (e = 220 mm). The corresponding rotation of the foundation (θ) is recorded simultaneously using an inclinometer sensor. At this stage, only the self-weight of the foundation (3.2 N) has been considered as a vertical load (V), which is very small compared with the ultimate vertical capacity(V_u). Cases with a very high horizontal load eccentricity (moment over monotonic horizontal force M/H') and very low V/V_u are considered as pure moment loading (Kourkoulis et al., 2014). Hence, the model caissons here were examined under pure moment loading (in the absence of H and V) in order to investigate the effect of wings on the ultimate overturning capacity. Figure 4.1 shows a typical moment-rotation data collected from the experiments (dashed line).

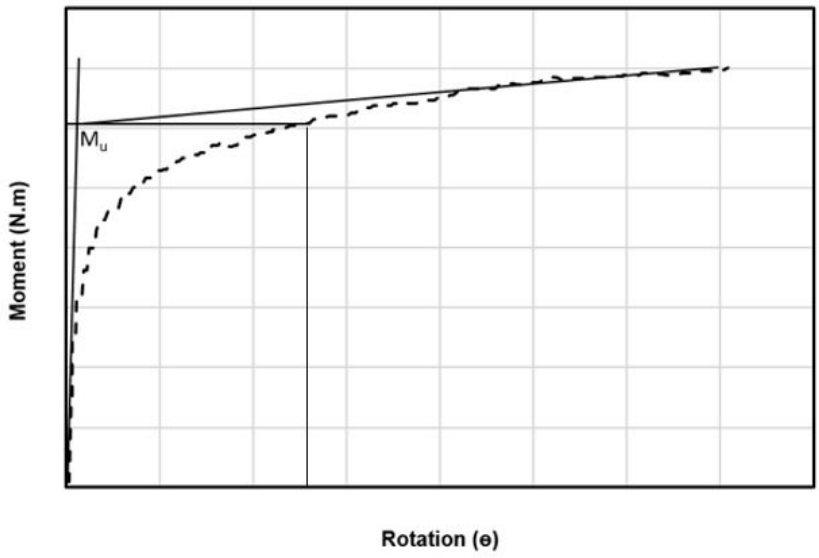

Figure 4.1. Tangent intersection method for determining bearing capacity

To interpret the moment-rotation response it is essential to focus on the initial loading curve (Byrne et al., 2003a). The response is initially stiff before yielding occurs (yield point), and a much softer response follows. The yield point is assumed as the ultimate bearing capacity M_u for the model foundations. The yield point is determined using tangent intersection method

(Mansur and Kaufman, 1958), as shown in Figure 4.1. Using this method, two tangential lines are drawn along the initial and later portions of the load-displacement curve, and the load corresponding to the intersection point of these two lines is taken as the bearing capacity. The zone between yield point and the ultimate point is known as transition zone.

In order to draw conclusions that are independent from certain dimension and force values, the results are presented in a normalised format. A series of non-dimensional parameters proposed by Houlsby et al. (2005) were used to normalise all the results. For similar values of dimensionless bearing capacity factor in sand, the loads at failure would be proportional to the unit weight of the soil (γ) and to $(\frac{D}{2})^3$, where D is diameter of the caisson. Therefore, all the moment-rotation curves in this study were plotted as $\frac{4M}{\pi D^4 \gamma}$ against $\theta(\frac{P_a}{D\gamma})^{0.5}$, where P_a is atmospheric pressure (used as a reference pressure). Further description of these normalisation procedures is available in Houlsby et al. (2005). The normalized moment-rotation ($M-\theta$) curves for the conventional and proposed models with different wing widths installed in loose sand are presented in Figure 4.2. The results from the experiments indicated that the width of the four wings used in the proposed foundation has a significant impact on the overturning capacity improvement. The test results showed that the overturning capacity of the suction caisson was increased by approximately 24%, 44%, and 68% for winged caisson with width size (T) range 20%, 30%, and 40%, respectively.

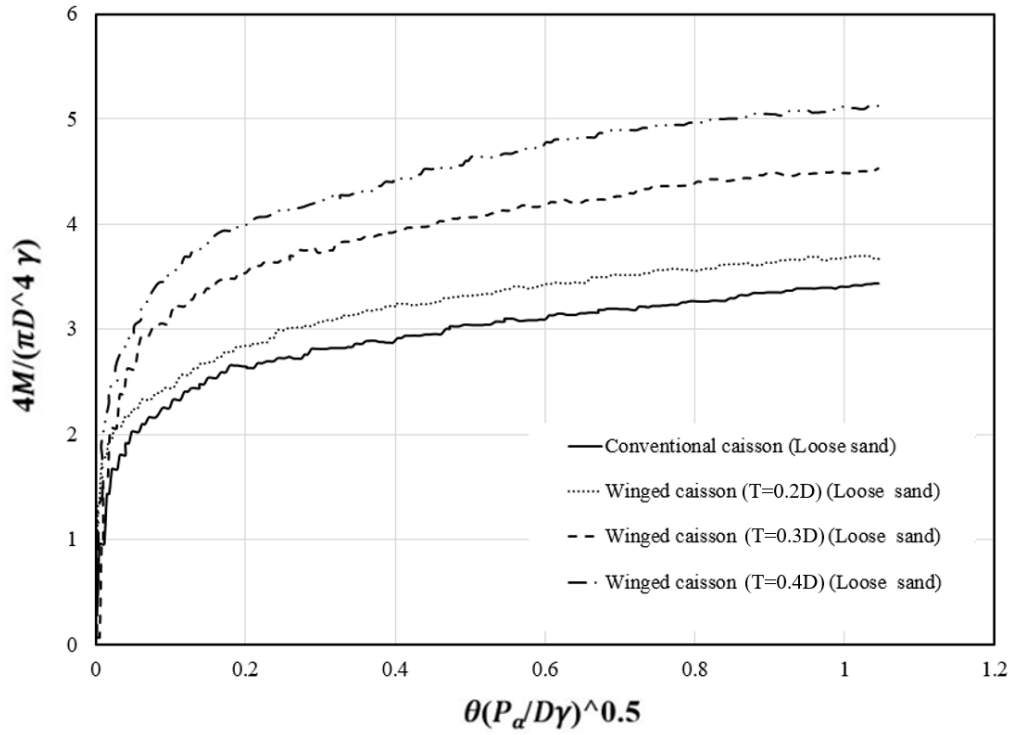

Figure 4.2. Moment-rotation curves from the experimental test for conventional and winged caissons in loose sand *(Dr*=23-25%*)* with an aspect ratio ($\frac{L}{D} = 1.0$)

4.1.1.1 The impact of soil density

To develop a better understanding of the behaviour of winged caisson under overturning moments in sand with different relative densities, four experiments were selected to be carried out in medium sand ($Dr = 48 - 50\%$). The normalized curves for the models in medium sand are provided in Figure 4.3. Generally, the bearing capacity increases by increasing the relative density of the sand and this is evident when we compare Figure 4.3 to Figure 4.2. This occurs because of increase in both the soil shear resistance and caisson surface and sand interface friction. The soil resistance to the lateral movement of the foundations depends on two factors: (1) frontal normal stress and (2) side friction (Briaud et al., 1983; Smith, 1987). As the two factors increased by increasing soil density, due to the bigger internal friction angle (ϕ'), the

strength and stiffness of the surrounding soil and thereby the overturning resistance of the caissons are expected to be higher for the models in sand with higher relative density.

However, it is worth noting that adding wing to the caissons results in a slightly better overturning capacity for the loose sand. Variations of the capacity improvement with sand relative densities are shown in Figure 4.4. In a winged caisson with $L/D = 1.0$, when wing width equals 40% of the caisson's diameter ($T = 0.4D$), the ultimate overturning capacity increased by about 68%, and 62% for relative densities of 23-25% and 48-50%, respectively.

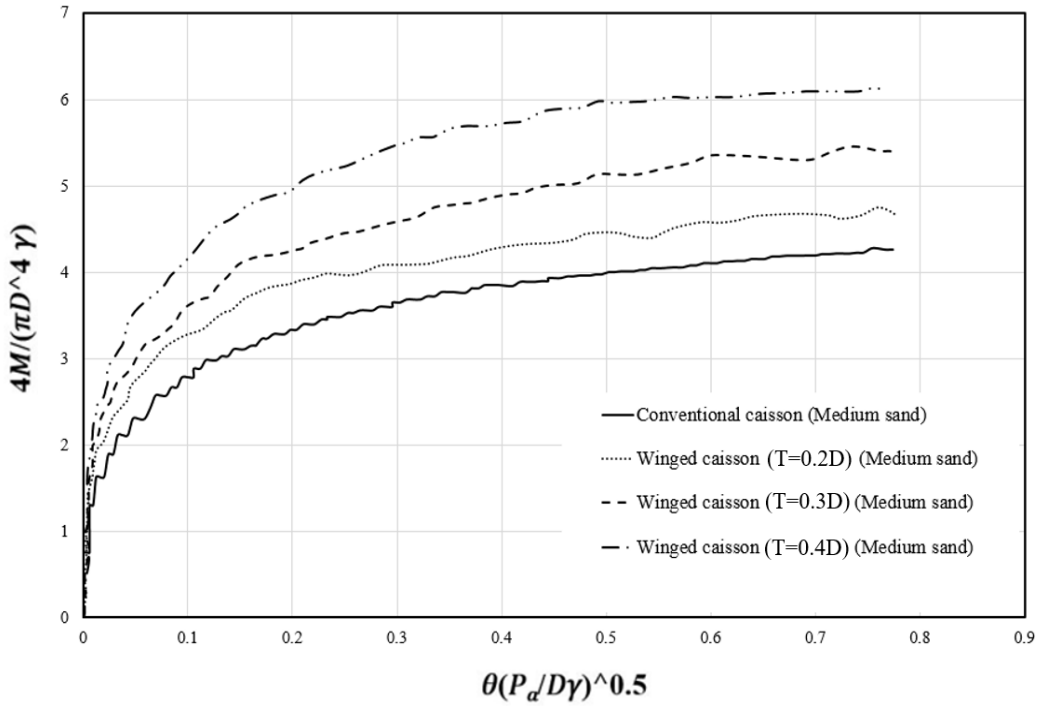

Figure 4.3. Moment-rotation curves from the experimental test for conventional and winged caissons in medium sand (Dr =48-50%) with an aspect ratio ($\frac{L}{D} = 1.0$)

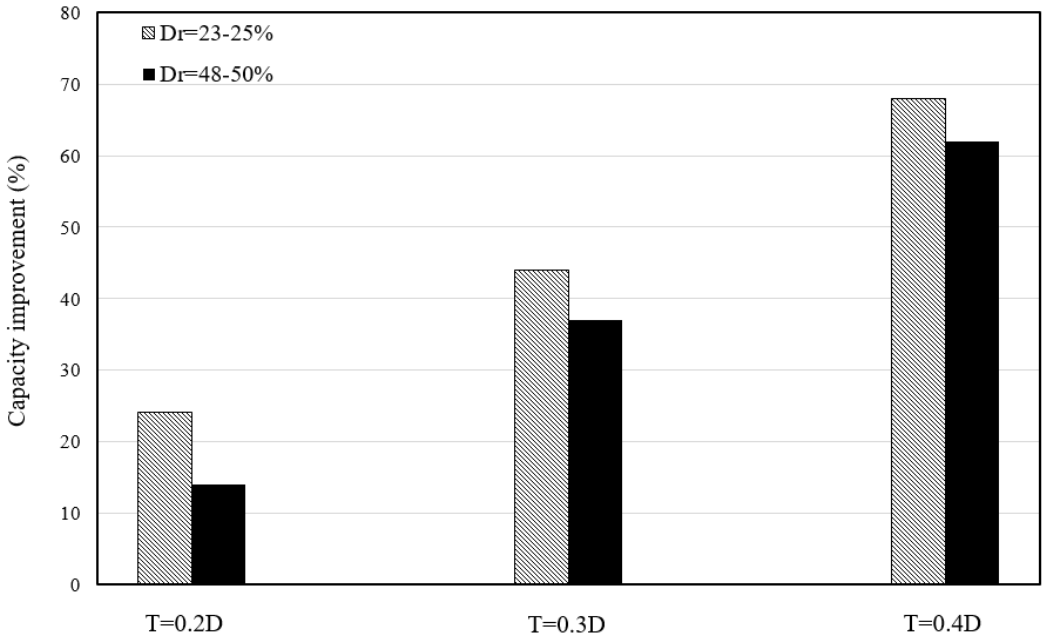

Figure 4.4. Capacity improvement versus relative densities for wringed caissons

In general, the overturning capacity of the suction caisson foundations depends on the earth pressure distributions along the caisson wall (Zhang et al., 2016b). Therefore, including wings along the length of the caisson provides additional passive soil resistance in front of the caisson foundation. As expected, the lateral response of the winged caisson increases by increasing wing size as well. This can be also attributed to the increased passive area of soil resistance by adding wing width(T).

4.1.2 Numerical results (winged caissons)

In this section the numerical analysis that was used to model the conventional and winged caisson foundations used in the 1-g experiments for the loose sand is presented. The size of the model foundations and the soil properties in the finite element models were the same as the experimental specimens. Figure 4.5 shows the geometry of half of a caisson model that was used in the FE analysis to simulate the 1:70 scale model tests. The model foundations and

the towers were assumed to be rigid. As shown in Figure 4.5, the lateral load is acting at a distance (e) of 220 mm above the model surface as a lateral point load as in the experiments. Figure 4.5a and Figure 4.5b show the plastic strains and displacements respectively around the caisson. From these graphs it is evident that the maximum deformation occurs in vicinity of the caisson wall and near the surface. The plastic shear strains start from the tip and develop near the caisson head at small rotations (e.g., $\theta < 1.5°$). In addition, significant plastic shear strains develop in the left side of the caissons (behind) with rotation, resulting in active failure of the soil. Figure 4.5c demonstrates the counters of plastic shear strains and displacement for the winged caisson with a width of $0.4D$ (WSC3). A similar pattern, i.e. maximum deformation at top surface, can be observed for the winged caisson.

The moment-rotation curves obtained from the numerical analysis were compared with the experiment results. Figure 4.6 shows the results for the conventional and winged caissons. The numerical results are in good agreement with the experimental moment-rotation results. The difference between the ultimate overturning capacity obtained from experimental results and numerical analyses varies from 2% to 9%. The comparison showed that the finite element model can capture the overall behaviour of the caisson with relatively high precision. As expected, the FE model shows that the overturning capacity increases by increasing wing width size.

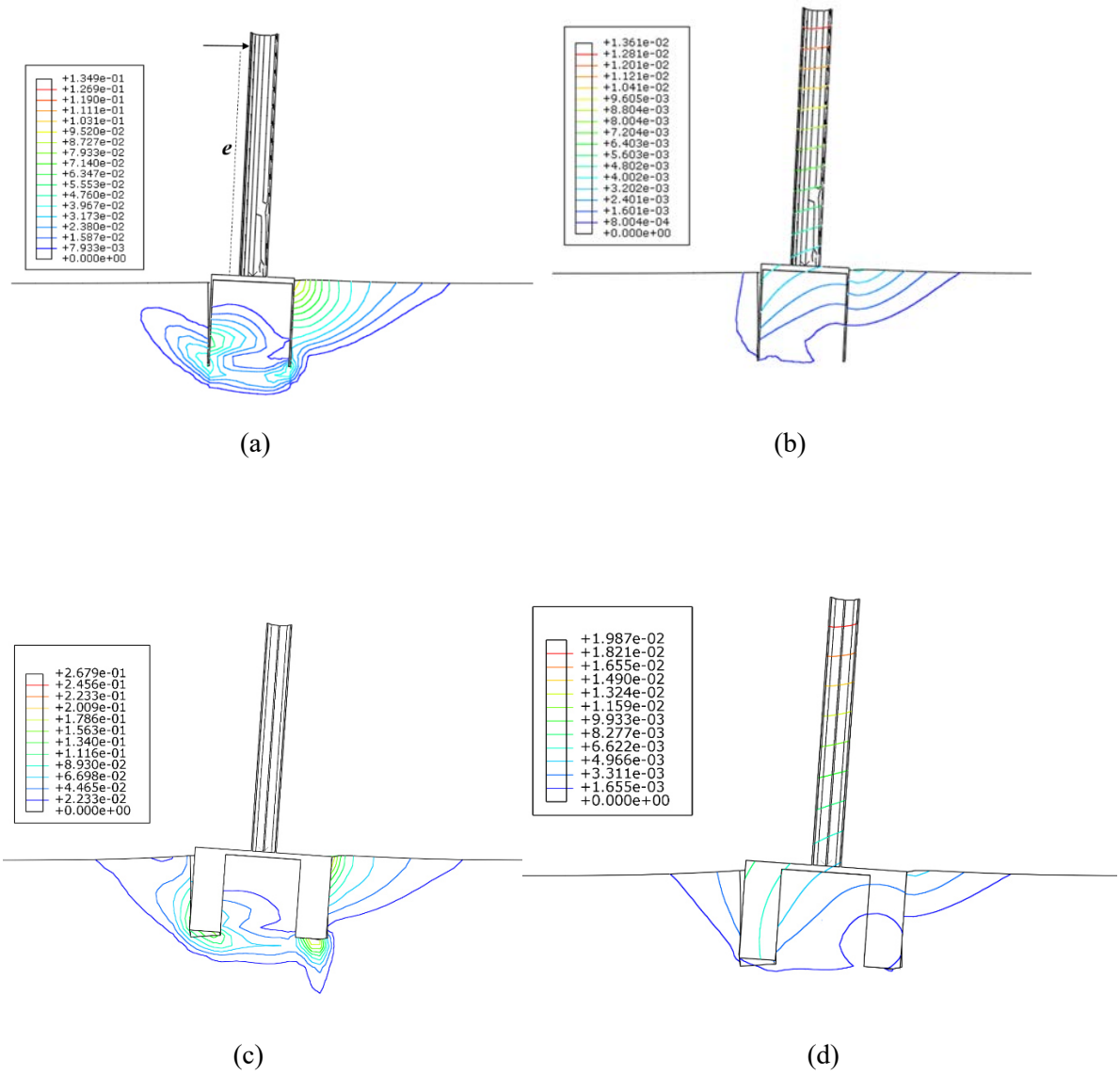

Figure 4.5. The geometry of half of a caisson model in FEM; (a) distribution of plastic strain for CSC1, (b) visualisation of counters of displacement for CSC1, (c) distribution of plastic strain for WSC3, (d) visualisation of counters of displacement for WSC3, under horizontal loading ($\theta < 1.5^o$).

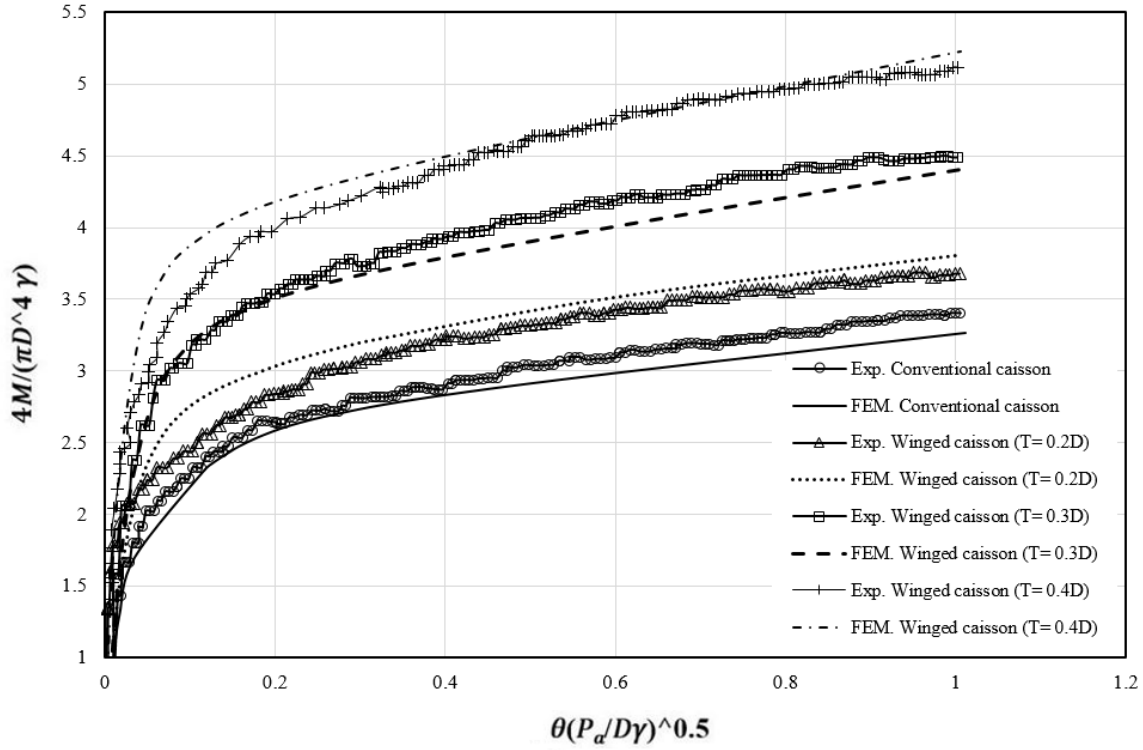

Figure 4.6. Comparison of the numerical analysis and experimental results for conventional and winged caissons

4.1.2.1 Sensitivity analysis

A sensitivity analysis is the study of how uncertainty in model and allows for the inputs soil properties and structural characteristics to quantify the relative importance of each input variable to model outputs. It also can be used as an aid to validate some of the assumptions. This section gives a brief overview of the sensitivity analysis of some of the major variables which might have an influence on both the accuracy and the computational run-time of the monotonic-response modelling.

Mesh and FE domain sizes:

As with many forms of numerical modelling, the mesh size affect the results and the run-time in FE analysis considerably. From a convergence study with the conventional caisson foundation (i.e. $L/D = 1.0$) it can be seen from Figure 4.7 that the mesh containing 17633 and

34975 elements gives a good approximation to the experimental results compared with 10961 elements. However, the model with 17633 elements gives a quicker computational run-time compared with the soil model with 34975 elements. As it is shown that a relatively fine mesh (5-8 mm) used around the caisson is a good approximation to the experimental results used for validation, whereas the coarser mesh densities (i.e. 12 mm) serve to over predict. This mesh is used in this research for simulations on the conventional and winged caisson models were shown in Chapter 3.

The minimum and maximum mesh sizes of the soil are provided as:

Mesh containing 10961: Min size 12 mm and Max size 20 mm

Mesh containing 17633: Min size 8 mm and Max size 20 mm

Mesh containing 34975: Min size 5 mm and Max size 20 mm

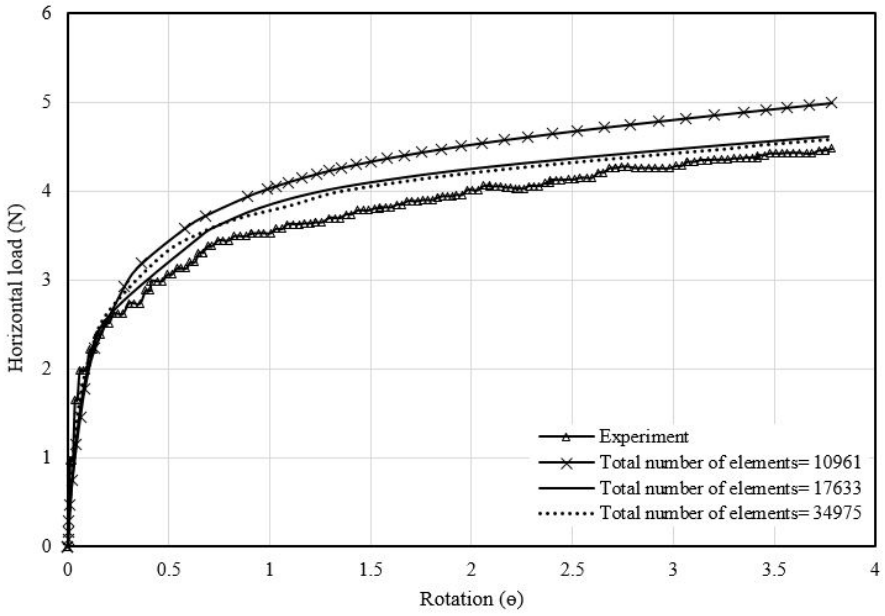

Figure 4.7. Results from lateral response study of the conventional suction caisson foundation with $L/D = 1.0$, with different mesh coarseness

FE domains with a size of $8D \times 4D \times 4D$ and $10D \times 5D \times 5D$ were used to assess the impact of the boundary size on the results. The simulations are found not to be sensitive with respect to the boundary sizes used to model the caisson foundation (Figure 4.8).

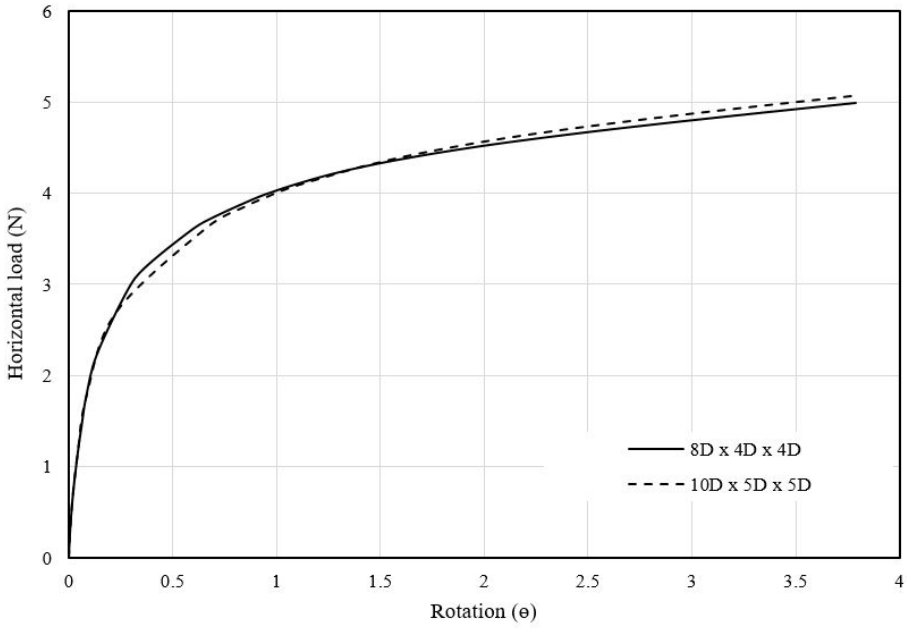

Figure 4.8. Results from lateral response study of the conventional suction caisson foundation with $L/D = 1.0$ two different boundary size

Comparison of two constitutive models:

There are many Geotechnical constitutive models in ABAQUS software. Mohr-Coulomb model (M-C) and Dracker-Prager model (D-P) are the most widely used in geotechnical engineering because their relative parameters are easy to obtain. Two constitutive models adopted in this study are M-C model and D-P model considering the viability of getting parameters easily.

The Drucker–Prager yield surface is a cone in the stress space by smoothing approximation to the Mohr–Coulomb criterion, which is an irregular hexagonal pyramid (Figure 4.9).

Two common ways can be used to approximate the surfaces. By matching the Drucker-Prager yield surface with the inner and outer apices of the Mohr-Coulomb criterion (Figure

4.9), the conversion relation of material parameters between the two surfaces can be expressed as where ± in the Eq.3.3 and Eq.3.4 corresponds to the inner and outer Drucker–Prager surfaces, respectively.

The Mohr–Coulomb and Drucker–Prager parameters are basically obtained from triaxial compression tests results, i.e. $\sigma_1 > \sigma_2 = \sigma_3$, where σ_1 is major principal effective stress, σ_2 is intermediate principal effective stress, and σ_3 is minor principal effective stress (Alejano and Bobet, 2012).

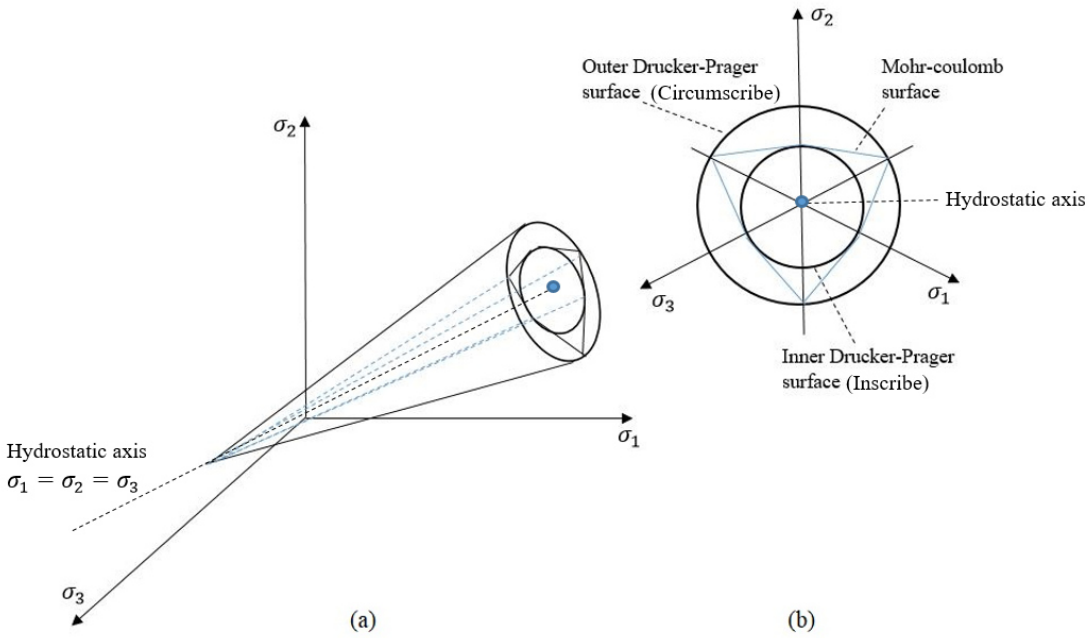

Figure 4.9. The yield surfaces of the Mohr–Coulomb and Drucker–Prager models on (a) the principle effective stress space and (b) on the deviatoric plane

In order to obtain reliable values and avoid convergence problem, a D-P model was assigned for all models in this research study. The M-C model failed to display a complete load-rotation trend due to convergence problem and was omitted from the analysis (see Figure 4.10).

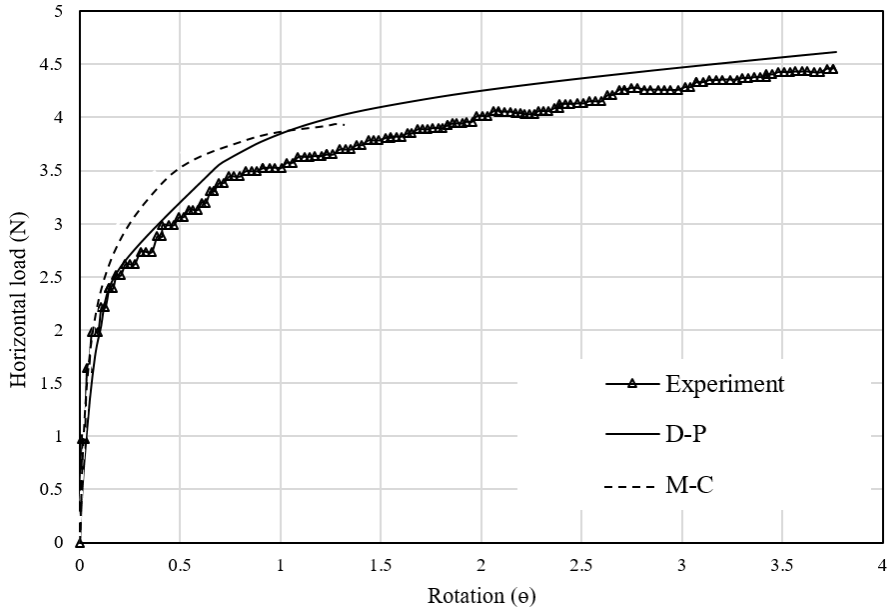

Figure 4.10. Comparison of horizontal response for the convention suction caisson with M-C and D-P soil models

The behaviour of Redhill 110 sand in a triaxial test condition, based on two constitutive models of Drucker-Prager (D-P) and Mohr-Coulomb (M-C) models, was examined through FE method. A typical consolidated drained (CD) triaxial test involves confining a cylindrical soil with 50mm in diameter and 50mm in height was simulated. The triaxial tests were simulated using axisymmetric elements in the finite element software ABAQUS. The parameters used in the simulations are given in Table 3.2.

The top elements in the FE model were loaded with an initial hydrostatic pressure maintained as a constant load on the outer radial edge. The analysis was driven by applying displacements at the top edge of the elements. The initial confining pressure in these tests was set at 210 kPa and the tests were run at the initial void ratio e_0 = 0.92 (corresponding to the Redhill sand with Dr =23-25%). Figure 4.11a and Figure 4.11b show the deviator stress versus axial strain for the models under tension and compression, respectively. The deviation stress-axial strain curve, by D-P criterion with inscribes assumption is very close to M-C criterion for the model under tension load. While, the deviation stress-axial strain curve obtained from D-P

criterion with circumscribes assumption matches well with the M-C criterion for the model under tension load.

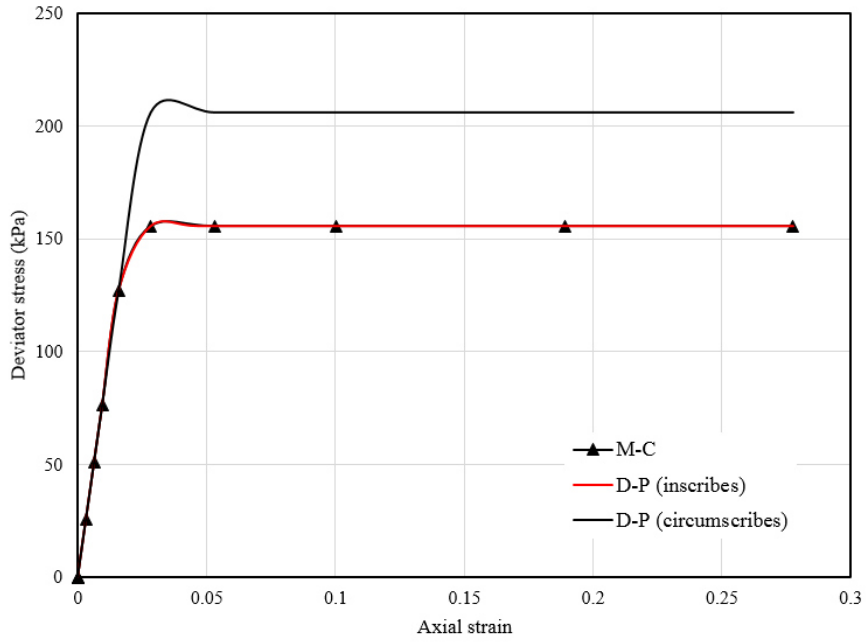

(a)

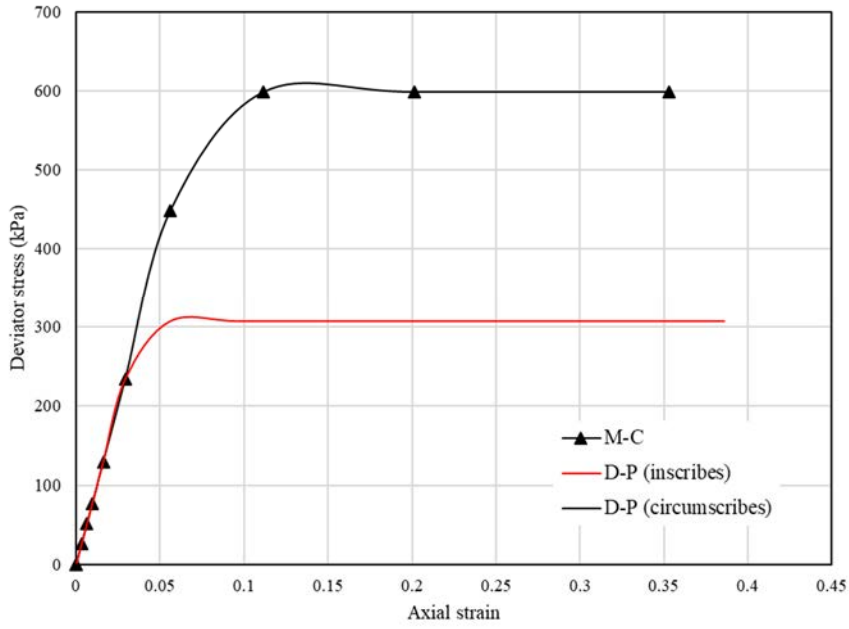

(b)

Figure 4.11. Comparison of a triaxial test result for the cylindrical sample with M-C and D-P soil models a) under tension, b) under compression

According to the FE triaxle results, it can be concluded that, in the design of caisson foundation, the tensile behavior of soils becomes a predominant factor when external forces cause bending moments. Hence, to assess the tensile failure behavior of soil, the failure criterion of sand must be determined based on tensile loading conditions.

4.1.3 Parametric study

The overturning moment capacity of suction caisson foundation depends on soil properties, caisson embedded length and the type of loading (Kourkoulis et al., 2014; Villalobos et al., 2004; Byrne et al., 2003a). The influence of the caisson aspect ratio, the shape of the wings, number of wings, and load's orientation are discussed in the following sections.

4.1.3.1 The impact of aspect ratios

Two additional experiments were conducted to investigate the effect of wings on the bearing capacity of caisson with different aspect ratios (i.e. $L/D = 0.5$ and 1.5). These ratios of embedment depth to diameter (L/D) were chosen ranges based on common ratios for relatively light structures (Olson and Gilbert, 2004).

The loading condition used for aspect ratios of 0.5 and 1.5 was adapted from the test conducted for the aspect ratio of 1.0. The effects of wing width on the overturning capacity of the caisson with different aspect ratios are shown in Figure 4.12a, Figure 4.12b and Figure 4.12c. From the figures, it can be observed that the ultimate moment capacity increases with the increase of width size and the aspect ratio of the caisson. Figure 4.12a and Figure 4.12c include validation of finite element of two conventional caissons (CSC2 and CSC3) and two winged caissons (WSC6 and WSC9). The trends clearly demonstrate good agreement between experimental and numerical analysis. It is obvious that the overturning moment increased

significantly when the wings were used. The capacity values in the transition zone (specified area in the figures between elastic and plastic section) obtained for the caisson with $L/D = 1.5$ using the FEA was lower with a difference of up to 40%. This can be attributed to the difference between the theoretical model of the tower, which assumes a fully rigid body, and the actual stiffness of the tower. This difference will become more pronounced as the L/D ratio increases.

As expected all caissons with wings provided a considerably higher resistance compared with those of the reference caissons. It is obvious that the overturning capacity of suction caisson strongly depends on the caisson length. A comparison of the results (Figure 4.13) showed that the overturning capacity increases with increasing caisson length. For longer caissons, the passive resistance is mobilised on a larger area of the foundation which lead to higher overturning moments.

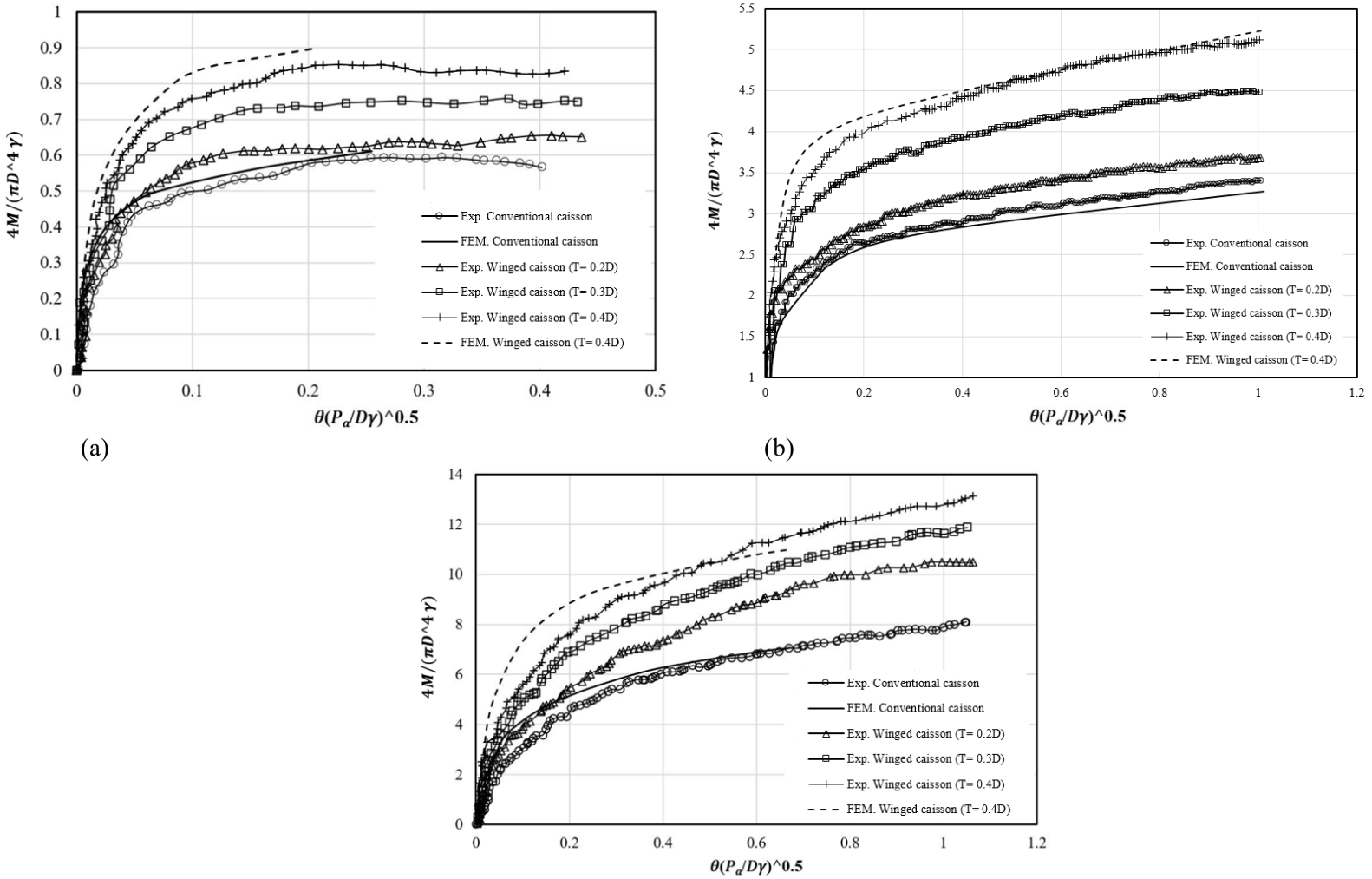

Figure 4.12. Moment-rotation curves from the experimental tests for conventional and winged caissons in loose sand with aspect ratios of (a) $L/D = 0.5$ (b) $L/D = 1.0$ (c) $L/D = 1.5$; results of numerical models of two experiments for each graph have been presented for comparison

When wing width equals 40% of the caisson's diameter ($T = 0.4D$), the ultimate overturning bearing capacity increased by approximately 54%, 68%, and 75% for suction caissons with aspect ratios of 0.5, 1.0 and 1.5, respectively (see Figure 4.14). The dotted lines of best fit show the general trends of the percentage improvement with respect to T. The percentage improvement is defined as the ratio between the capacity outputs of conventional foundation to the maximum that could be produced by a winged foundation. From Figure 4.14 it can be observed that the effect of adding wings for lower L/D ratios follows an exponential growth while this is more of a linear for higher L/D values. This can be justified based on the failure behaviour of the shallow caissons compared to the deep caissons which have an overturning failure behaviour (Byrne and Houlsby, 2004).

The failure mechanism for the caissons with aspect ratios of $\frac{L}{D} = 0.5, 1.0$ and 1.5 were also examined in the present study through three-dimensional finite element analysis and the failure modes are demonstrated in Figure 4.15. In ABAQUS, PEMAG refers to the plastic strain magnitude. The plastic strain magnitude, PEMAG is defined as $\sqrt{\left(\frac{2}{3}\right)\varepsilon^{pl}:\varepsilon^{pl}}$, where ε^{pl}=plastic strain and the symbol (:) denotes a scalar product operation (Song, 2012). As can be seen from the figure, under pure horizontal loading the failure mechanism activates more rotation and less sliding.

Previous studies reported that the type of mechanism or mode of failure depends directly on the aspect ratio of the caisson (Kennedy et al., 2015; Celestino et al., 2019). From Figure 4.15a, caisson with short aspect ratio (L/D=0.5) develop passive wedges along the caisson shaft; this type of failure is denoted as short-caisson mechanism (Celestino et al., 2019). Similar failure mechanism was observed for the caissons with slightly larger aspect ratios (L/D=1.0 and 1.5) but the wedges do not extend to the base of the caisson (Figure 4.15b and Figure 4.15c).

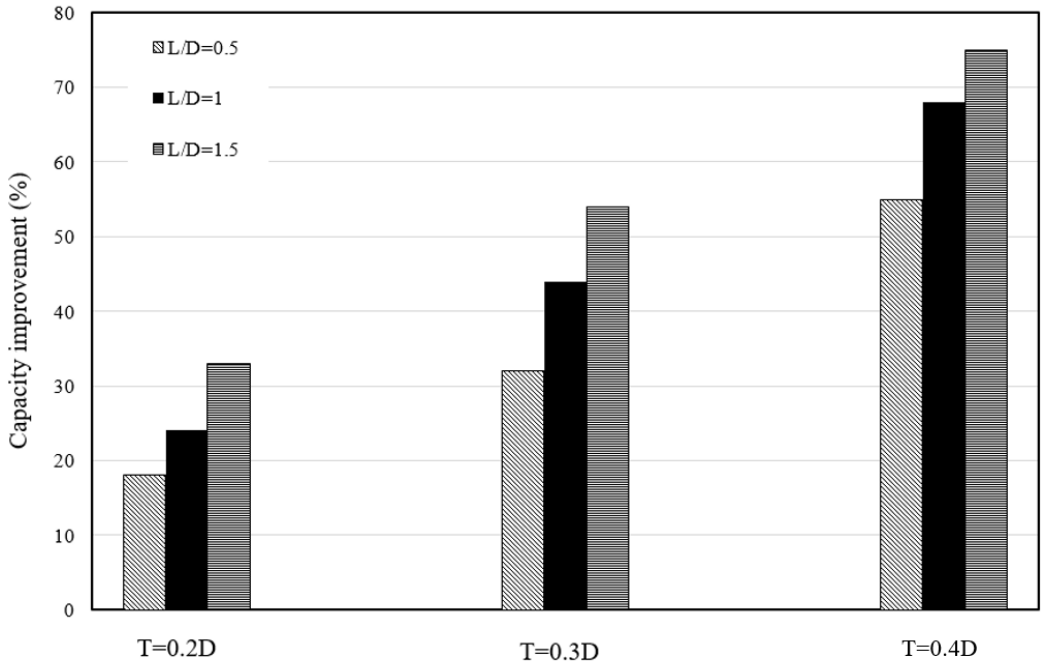

Figure 4.13. Capacity improvement versus aspect ratios for winged caissons

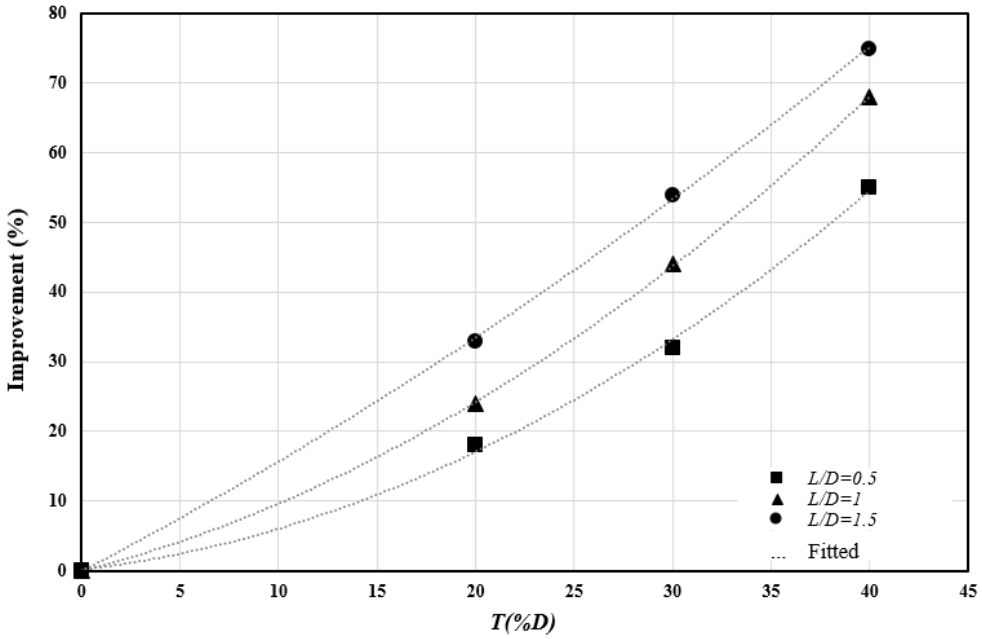

Figure 4.14. Wing efficiency for suction caissons with different aspect ratios

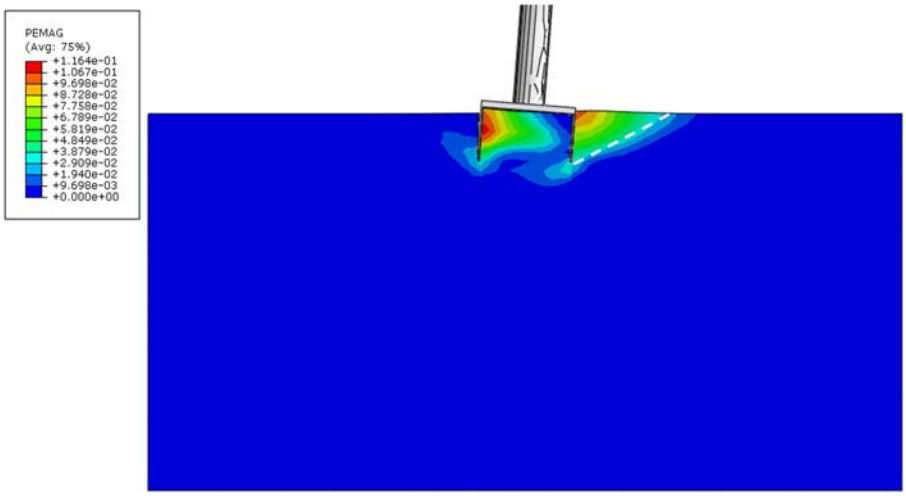

(a)

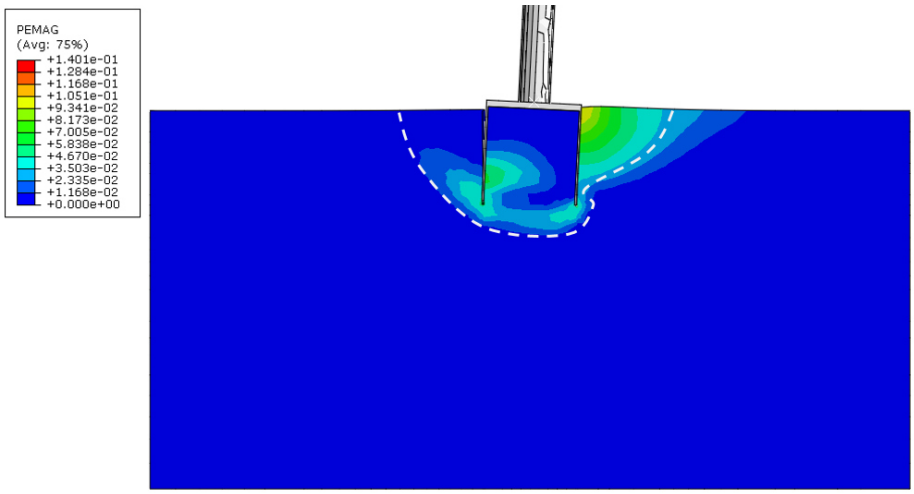

(b)

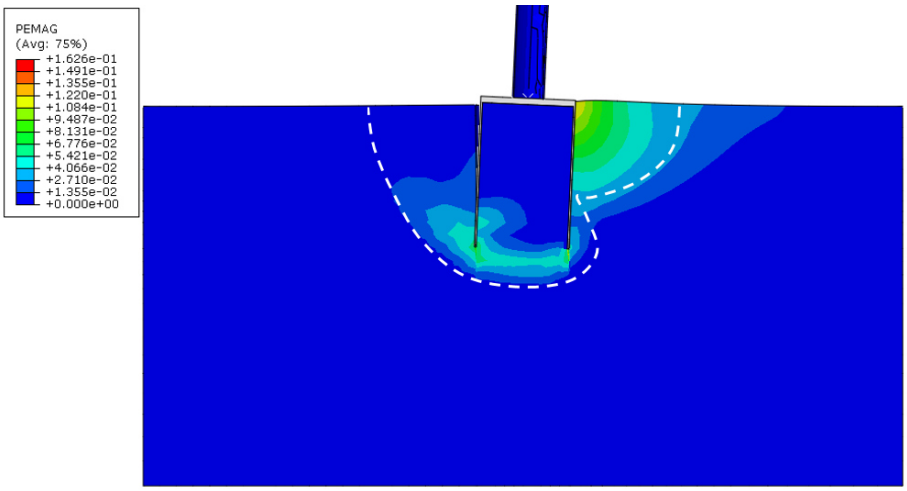

(c)

Figure 4.15. Failure mechanism under moment load for caissons with: a) CSC2 ($\frac{L}{D} = 0.5$), b) CSC1 ($\frac{L}{D} = 1.0$), c) CSC3 ($\frac{L}{D} = 1.5$)

In order to evaluate the failure mode and lateral soil pressure along the winged caisson wall, distribution of horizontal compressive stresses surrounding the winged caisson with $0.4D$ of WSC9 is shown in Figure 4.16. The result shows the variation of the stress distribution along the caisson length with respect to the applied overturning moments. Compressive stress develops on the right (outside) of the caisson up to approximately $0.8L$ and on the left side (again, outside) near the bottom of the caisson. Due to the distribution of lateral soil pressure, particularly near the tip of caisson, the wing efficiency is significantly affected by soil-wing interaction. The interaction between the wing and soil in relation to depth can be interpreted with variation of soil density. As interaction between the winged caisson and surrounding soil increased with depth, due to the increase of soil density in higher depths (Mitchell et al., 1972), the effectiveness of wing on the overturning capacity is expected to be higher for longer caissons.

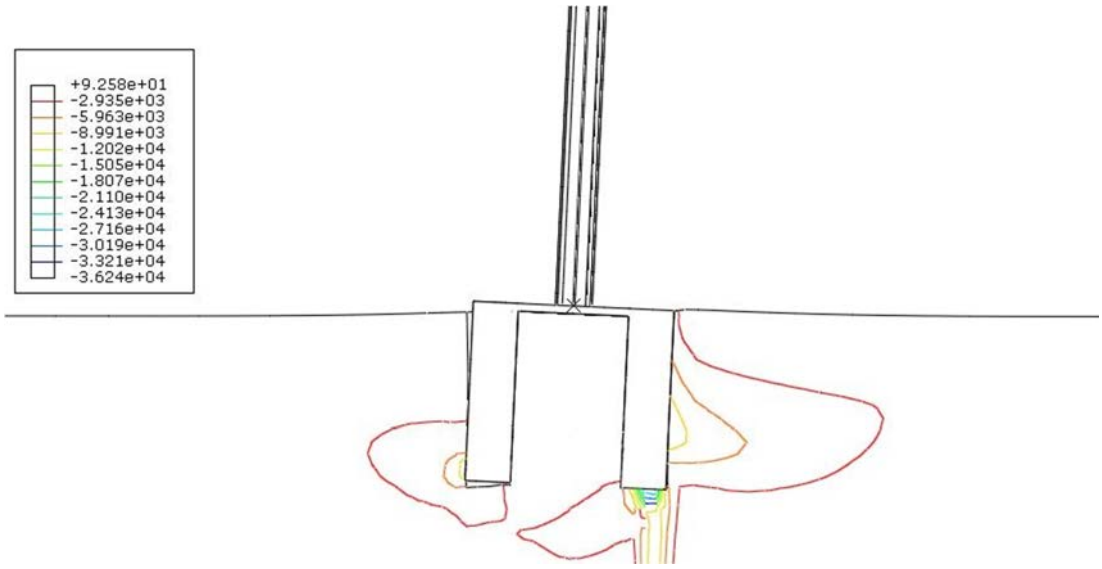

Figure 4.16. Horizontal stress (N/m^2) in soil at ultimate state in the plane of symmetry for WSC9

Based on the results from experimental and numerical models, it can be observed that the overturning moment capacity of winged suction caisson foundation depends on soil

properties, caisson embedded length and the wing size. Therefore, the wing efficiency (λ') can be determined based on the ratio of ultimate overturning capacity of winged caisson foundation over ultimate overturning capacity of conventional caisson foundation ($\lambda' = \frac{M_u^{WSC}}{M_u^{CSC}}$) where M_u^{WSC} is the ultimate overturning capacity of winged caisson foundation and M_u^{CSC} is the ultimate overturning capacity of conventional caisson foundation.

4.1.3.2 Effect of wing height on the capacity improvement

A parametric study was conducted using the FE analysis to investigate the optimum design of the wings. In particular, numerical studies were carried out to study the effects of wing height on the ultimate bearing capacity of the winged caisson. This was investigated by varying the height of the wings with respect to the embedment depth for one of the caissons with a constant wing width of $0.4D$. The variation of wing height used for the winged caissons is shown in Figure 4.17. The moment-rotation curves for winged caissons (WSC3, i.e. $L/D = 1.0$) installed in loose sand, are presented in Figure 4.18. The results clearly indicate that the wing efficiency depends on the height of the wings. The maximum efficiency is obtained by using the full height wing, and the efficiency drops by almost 50% using smaller heights. It is worth noting that, the capacity improvement is not significantly different between wing heights of 0.5 and 0.75 of the full height. This can be attributed to the influenced area of soil surrounding the suction caisson foundation under overturning moment, which distributes along the caisson wall. As a wedge failure mechanism occurs for a suction caisson with aspect ratio of 1.0 under overturning moment, the whole length of the caisson involves into the overturning capacity. A similar behaviour may not necessarily be observed for the winged caisson under combined loadings due to the complex nature of the failure mechanism.

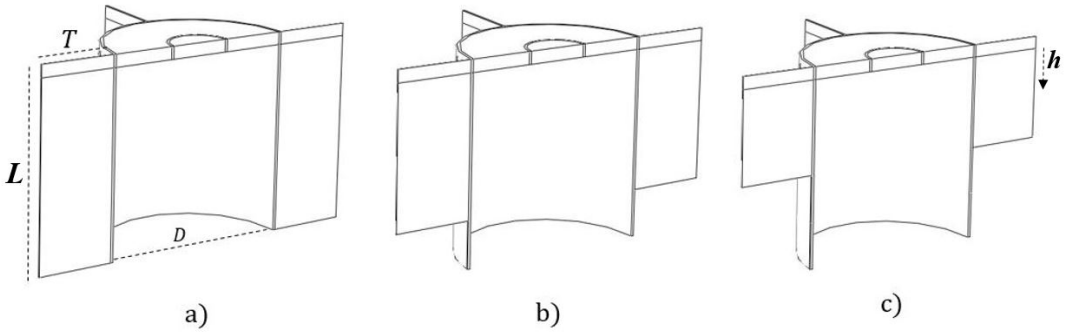

Figure 4.17. Schematic of half a winged caisson showing the parameters used to define the winged caissons with different heights of wing a) h=L, b) h =0.75L and c) h =0.5L

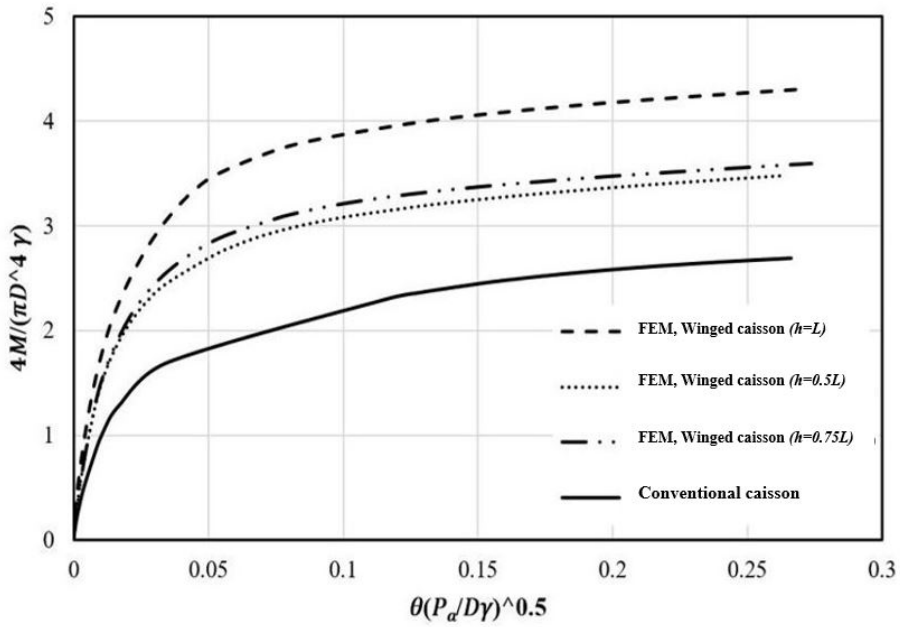

Figure 4.18. Moment-rotation curves from the numerical analyses for winged caissons in loose sand with an aspect ratio $L/D = 1.0$

4.1.3.3 Effect of wing shape on the capacity improvement

Different wing shapes were investigated for a suction caisson with aspect ratio of 1.0. The variation of wing shape used for winged caisson is shown in Figure 4.19. In the proposed wing geometries, h represents wing height, T is the ratio of wing width to the caisson diameter ($\%D$), and t' is the smaller base (the top) in trapezium shape of the wing (see Figure 4.19f)

which was considered 50% of T. The moment-rotation curves for winged caisson modeled in sand, with width of $0.4D$ and various height are presented in Figure 4.20. The results clearly indicates that the wings efficiency depends on its height. As it was observed in the previous section, the maximum efficiency obtained by full height of the wings, and the efficiency drops by almost 50% using half the height of the wing. The capacity enhancement provided by triangular shape is almost similar to those obtained by rectangular wing with half a height. The capacity improvement is not significantly altered by changing the position of the half rectangular wing (top half (c) and bottom half (d) Figure 4.19).

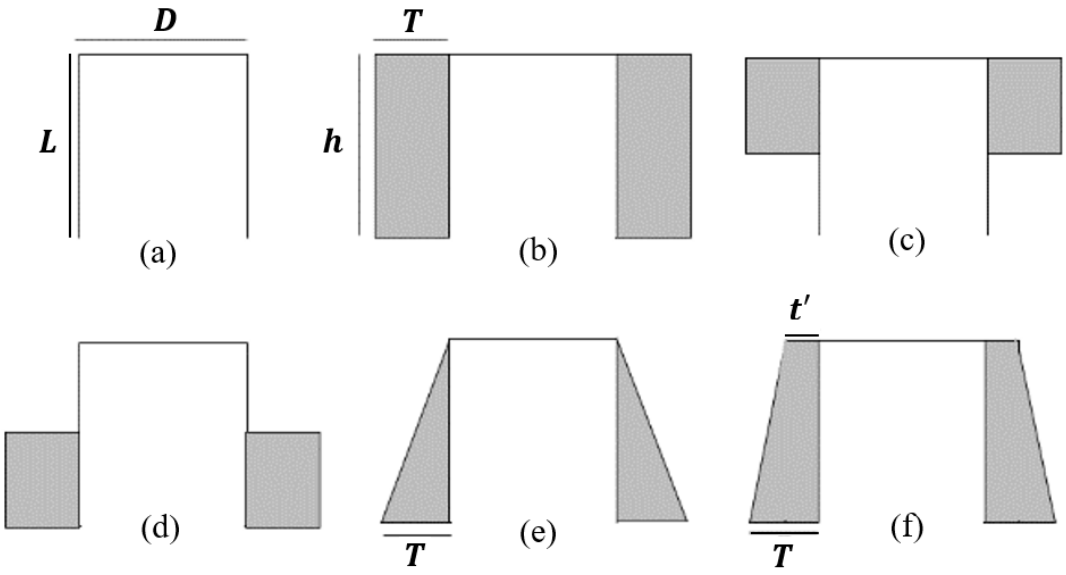

Figure 4.19. Schematic dimension of winged caisson with different height and shape

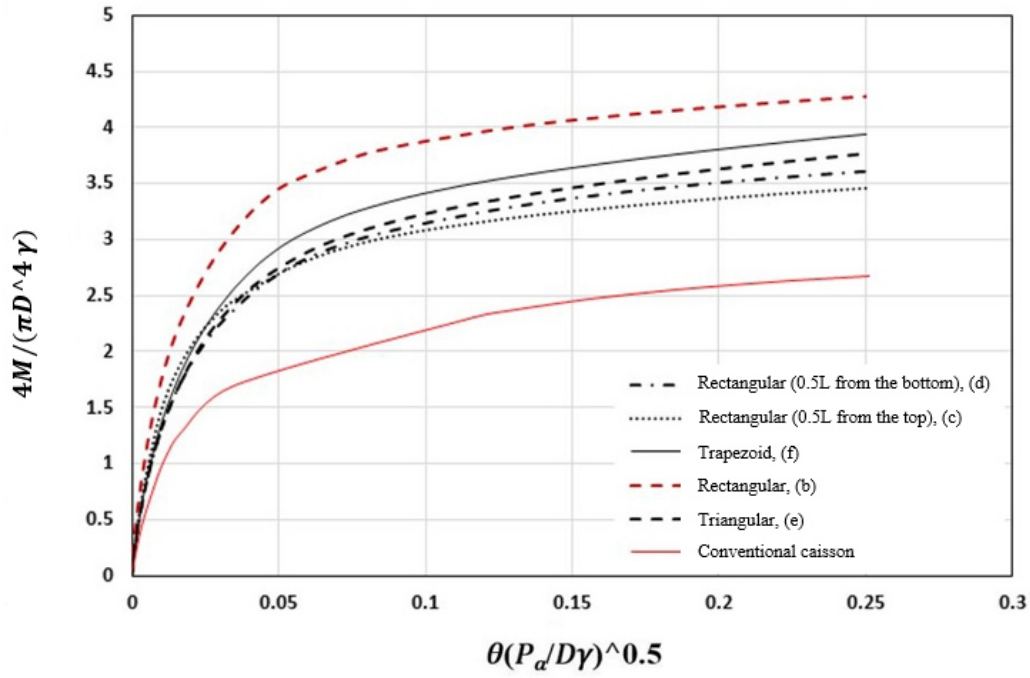

Figure 4.20. Moment-rotation curves from numerical modelling for winged caissons

4.1.3.4 The impact of load's orientation and number of wings

A series of FE models were conducted in order to investigate the effect of lateral load's orientation on the overturning capacity of the winged caissons in dry loose sand. Two scenarios were considered i) four wings at 90 degrees intervals and ii) three wings at 120 degrees intervals within the case of four wings, $L/D = 1.0$ was considered and loading was applied both perpendicular and diagonal to the wings. The soil deformations (at surface) for the winged caisson under perpendicular and diagonal loads are showed in Figure 4.21a and b, respectively. Figure 4.22 shows the effect of changing lateral load's orientation on the winged caisson with $T = 0.4D$. As can be seen from Figure 4.22, the overturning capacity of the winged caisson is not significantly altered by changing the orientation of the lateral load (< 4%).

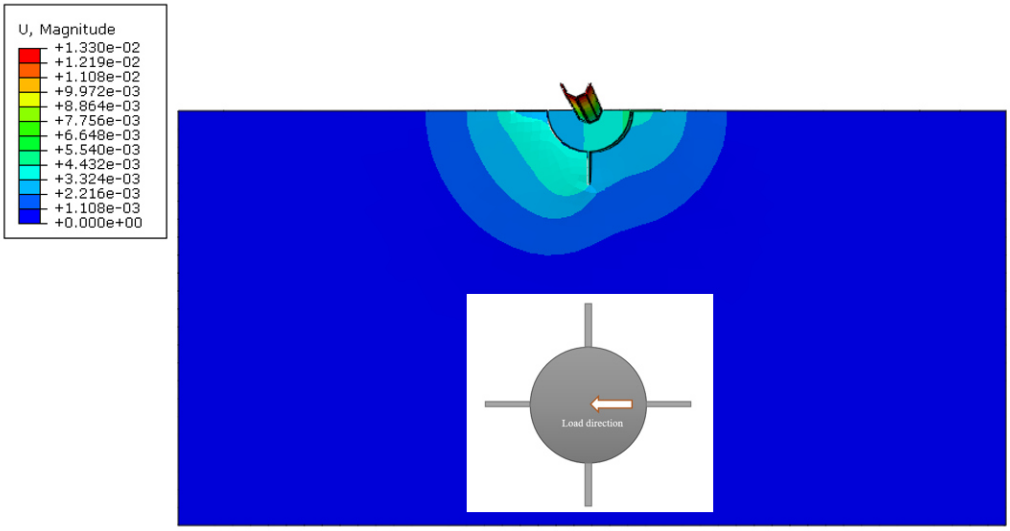

(a)

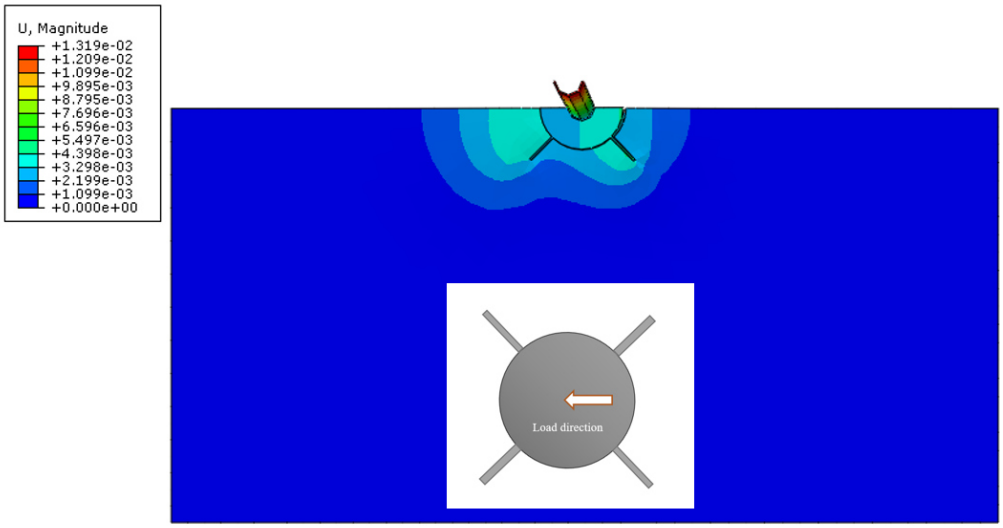

(b)

Figure 4.21. Plan view of the total displacement (m) in winged caisson with $L/D = 1.0$ and $T = 0.4D$ from the FEM results, (a) Perpendicular load, (b) Diagonal load

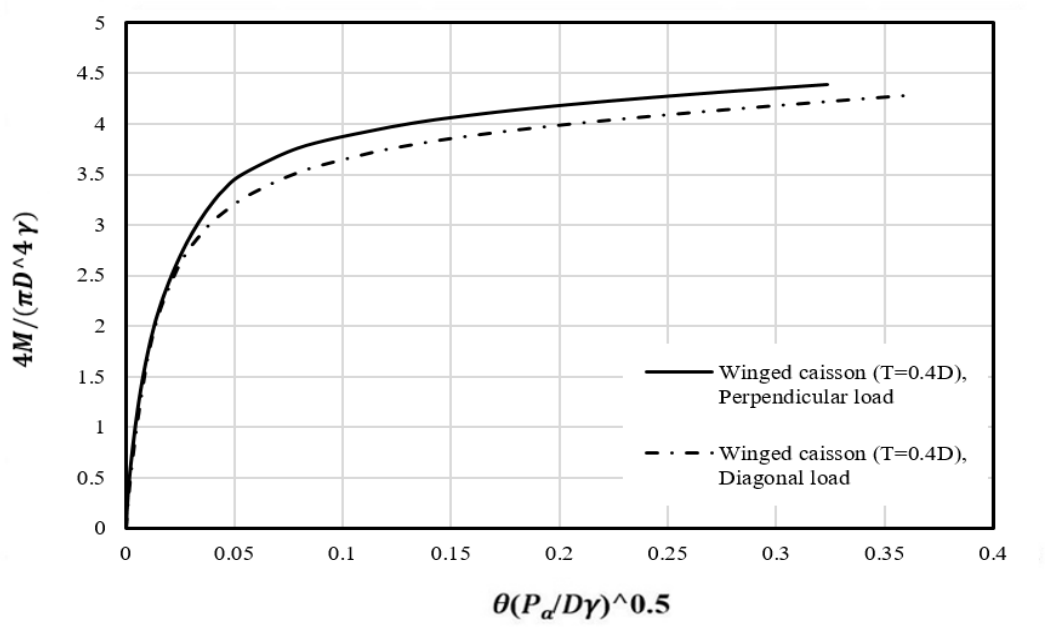

Figure 4.22. Moment-rotation curves from numerical modelling for winged caissons under different load's orientation

In the case of three wings, again, a caisson with $L/D = 1.0$ was considered. Two different loading conditions were considered L1, and L2. L1 represents load orientation along the wings, while L2 represents diagonal load (See Figure 4.23). Figure 4.23 shows the variation of total displacement around the winged caisson reinforced with three wings in loose sand, under two load's orientations of L1 and L2. From Figure 4.24, it can be observed that four wings provides 10% higher overturning capacity, compared with a caisson with three wings.

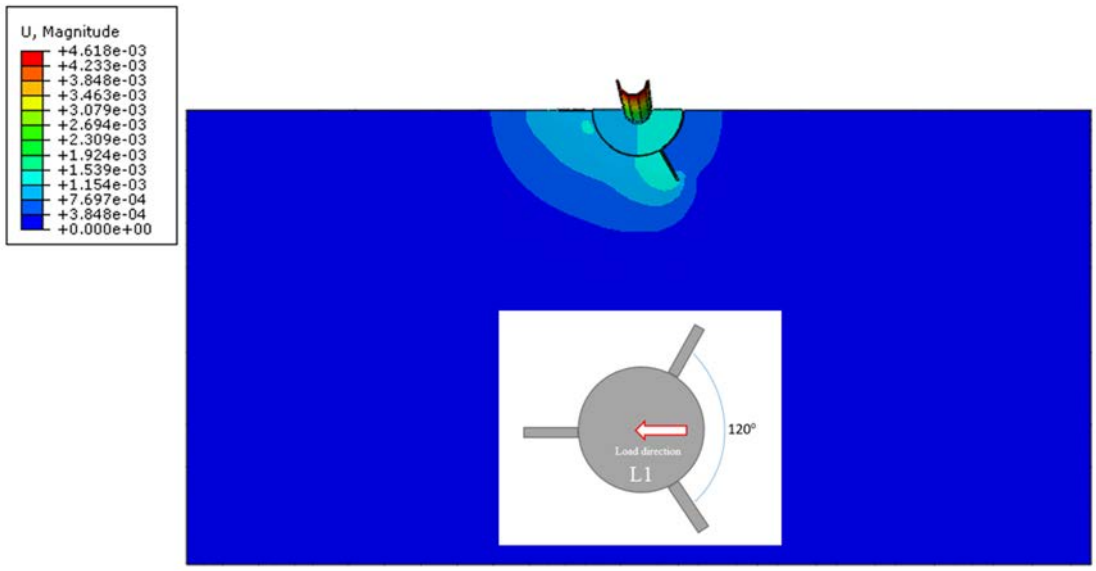

(a)

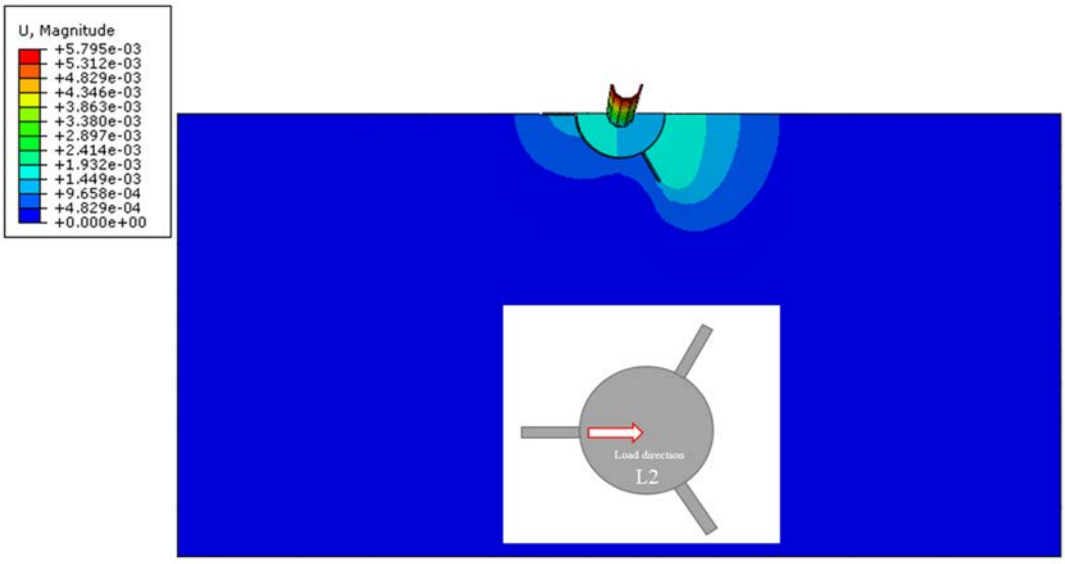

(b)

Figure 4.23. Plan view of the total displacement (m) in winged caisson with $L/D = 1.0$ and $T = 0.4D$, reinforced with three wings, from the FEM results, (a) L1, (b) L2

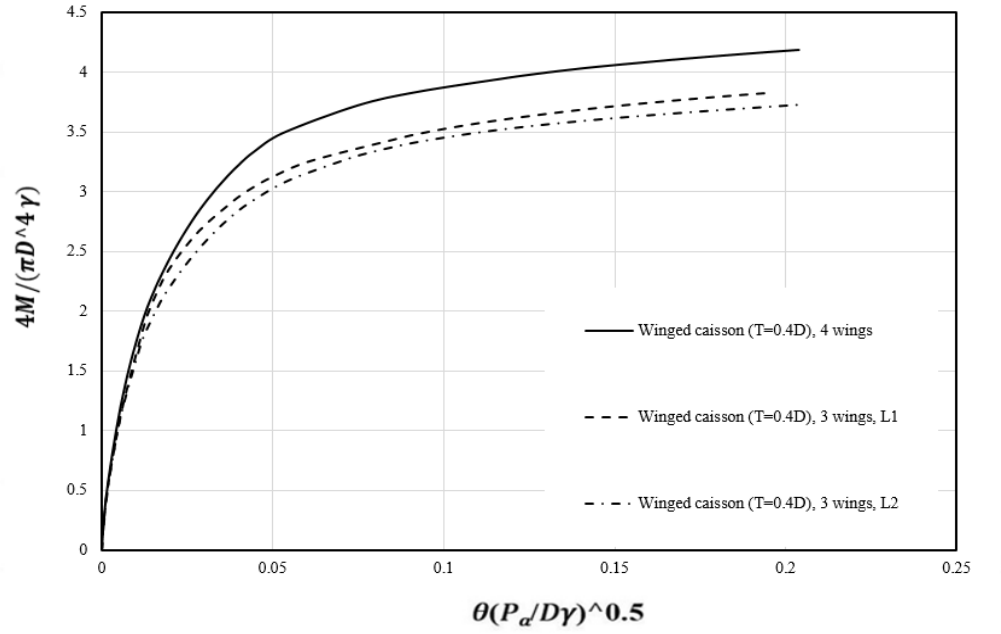

Figure 4.24. Moment-rotation curves from numerical modelling for winged caissons with three and four wings

4.2 The impact of combined loading

Foundations of wind turbines are subjected to a combined loading arising from the vertical (self-weight) forces (V), the lateral loads (H) and the overturning (M) moments induced by environmental forces (i.e. wind and wave action), which can act at any loading height above the seabed. Therefore, the behaviour of shallow foundations under combined loading ($H-V-M$) is of significant importance, particularly to offshore geotechnical engineers. This section investigates the impact of combined loading on the capacity of the proposed winged caisson foundations. To examine the combined capacities, results of FE simulations were normalised such that the impact of specific geometries can be overlooked.

To examine the combined loading capacity of the winged caisson, the lateral loading, with eccentricity (e) 220 mm above the caisson lid, was increased gradually to a maximum point whilst a horizontal load, with an eccentricity (e') of 100 mm, applied to the foundation

was kept constant. The eccentricity for the constant horizontal load was unavoidable during the laboratory experiments, as there was no access to the top of the foundation (see Figure 3.1).

The ultimate capacity values for the conventional caisson models derived from the experimental tests under combined Moment-Vertical-Horizontal ($M-V-H$) loads were compared with those of the FE models. The normalised values are presented in Table 4.1. Comparing the results shows a small difference between the experimental and FE values, particularly for the experiments where the $H/(\gamma D^3)$=0 (<8%). In addition, the combined loading capacities obtained from the FE analysis for conventional (CSC1, conventional caisson with $T = 0.4D,\ L/D = 1.0$) and winged caisson model (WSC3, winged caisson, $T = 0.4D$, $L/D = 1.0$) are shown in Figure 4.25, and Figure 4.26, respectively. As a way to view the data in the $(M/D, H)$ plane, the lines of best fit (dotted lines) through these data points were plotted in order to represent the yield capacities corresponding to the constant vertical loads.

Due to the relatively small vertical loads imposed on the OWTs compared with the horizontal loading (Byrne and Houlsby, 2006), the design of OWT foundations is governed by the horizontal loading and the overturning moments (Bransby and Randolph, 1998). Hence, 'low' values of vertical loads (compared with V_u) were selected to evaluate the combined loading capacities.

The ratio of $V/\gamma' D^3$ varies from 0.01 to 0.5 for the wind turbine problem (Byrne et al., 2003b). The ratio of $V/\gamma' D^3 < 0.44$ and > 0.57 relate to a lightly loaded foundation and a more heavily ballasted foundation and demonstrate the potential improvement in capacity from ballasting (Zhu et al., 2012).

The effect of the vertical load on the capacities for conventional and winged caisson are presented in the Figure 4.25 and Figure 4.26. The graphs show that the influence of the vertical load (V) on the bearing capacity is significant both for conventional and the winged caissons;

this finding was also reported by Byrne et al. (2002). According to the analysis presented herein, it can be concluded that the ultimate moment bearing capacities of the conventional suction caisson and the winged caisson increase with increasing vertical load. Therefore, in practice, the mechanical performance of the winged caisson can be enhanced by increasing the foundation weight, for example, using ballast tanks on the foundation surface. This is also in agreement with the findings of Byrne (2000).

Table 4.1. Comparison between the normalised ultimate capacity values from the FEM and the experimental values

$H/(\gamma' D^3)$	0		0.34		0.52		0.86		$V/(\gamma' D^3)$
	Exp.	**Num.**	**Exp.**	**Num.**	**Exp.**	**Num.**	**Exp.**	**Num.**	
$M/(\gamma' D^4)$	2.34	2.21	1.41	1.48	1.09	1.20	0.37	0.41	**0**
	2.44	2.30	1.52	1.65	1.20	1.31	0.49	0.51	**0.44**
	2.59	2.39	1.65	1.80	1.29	1.44	0.64	0.66	**0.79**
	2.64	2.52	1.82	1.94	1.47	1.60	0.74	0.82	**1.49**

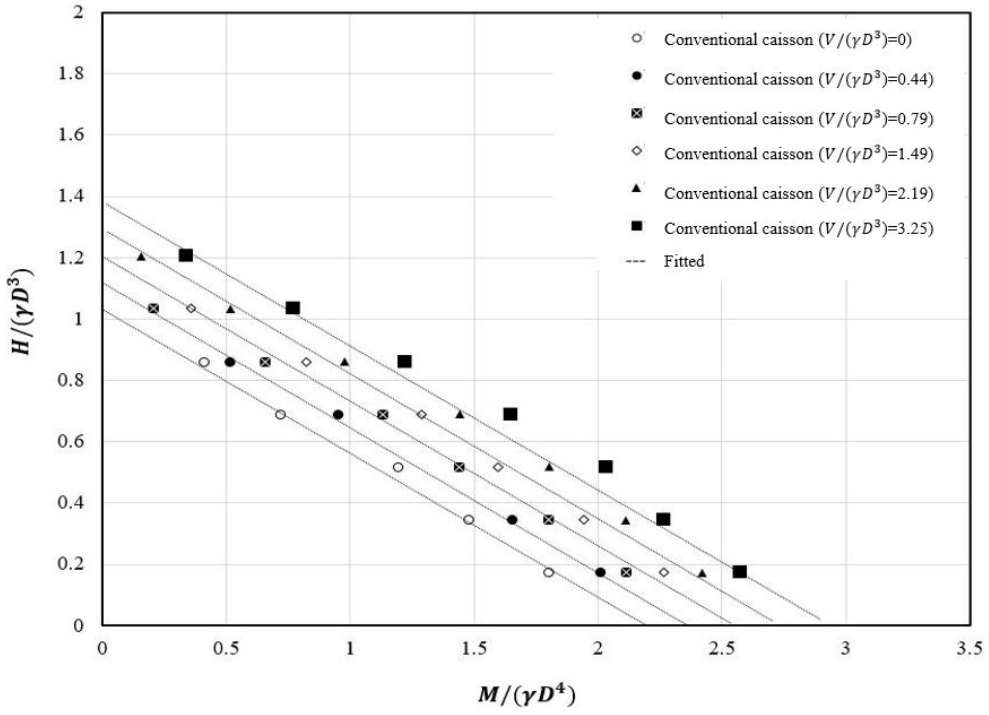

Figure 4.25. $H-M$ combined loading capacity for various normalised vertical loads (V/ γD3) for a conventional caisson (CSC1) obtained from FEM

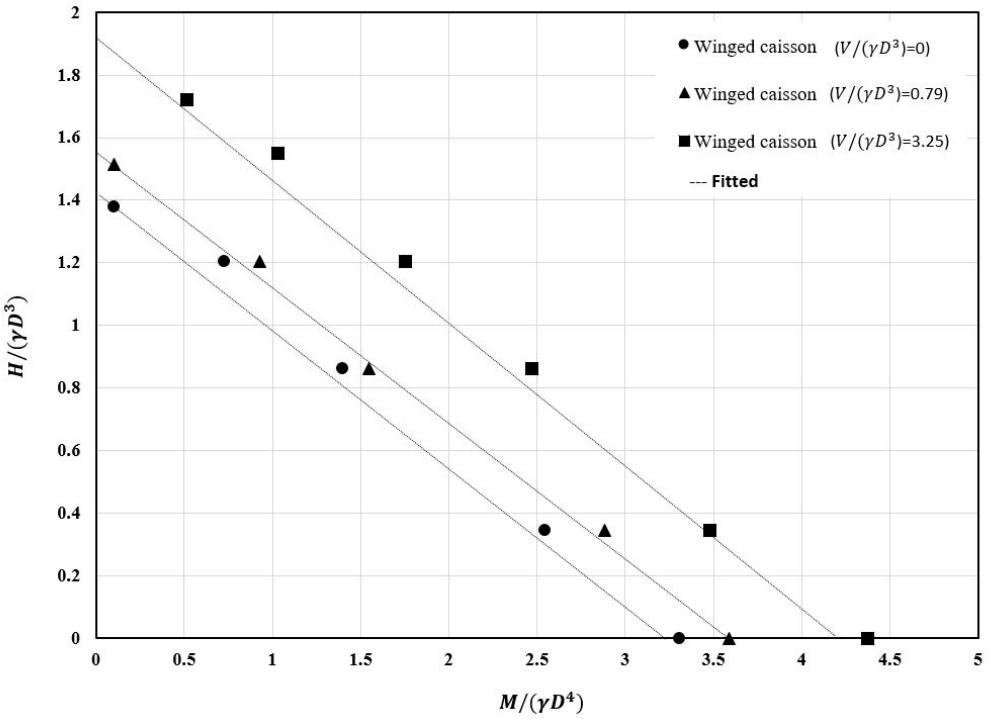

Figure 4.26. $H-M$ combined loading capacity for various normalised vertical loads (V/ γD^3) for a winged caisson (WSC3) obtained from FEM

Two lines were drawn using data from Figure 4.25, and Figure 4.26 obtained on a 45° line to show the impact of adding wings on vertical load and capacity of the caisson (Figure 4.27). The lines show change in capacity versus vertical loads. It can be seen that for a required capacity (M_R), lower values of vertical loads e.g. $V_1 < V_2$ can be used to ensure stability of the foundation using the winged caisson.

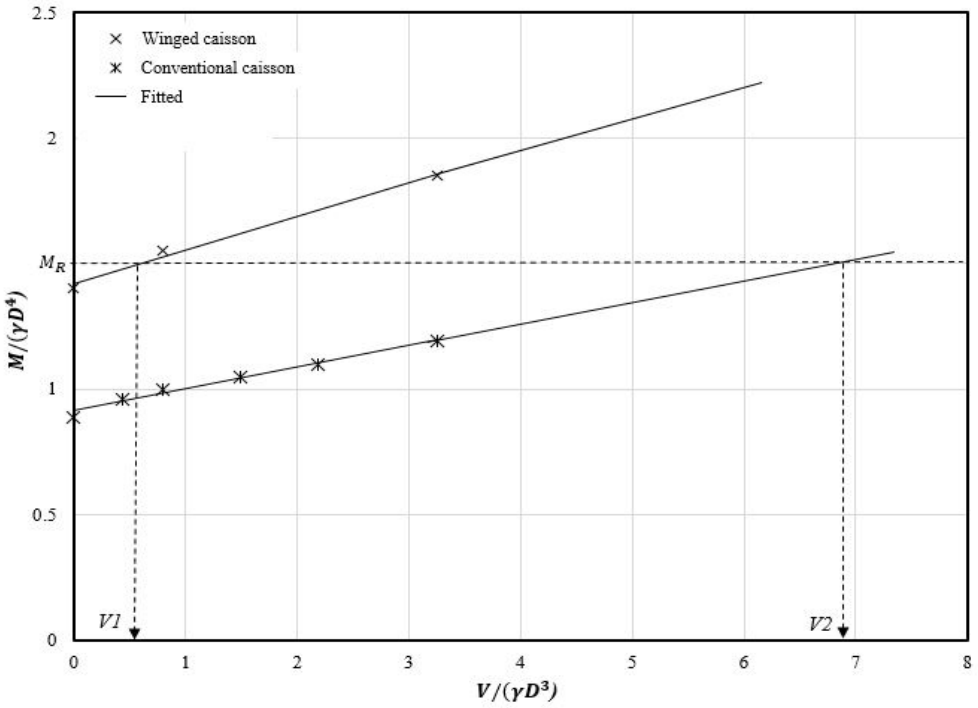

Figure 4.27. $M - V$ for conventional and winged caisson

Combined loading ($V - M - H$) condition on caissons will increase interaction effects due to the generation of simultaneous mobilization of passive earth pressure caused by lateral loads and caisson wall friction caused by vertical loads; this behaviour is also observed by Achmus and Thieken (2010) for a pile foundation in non-cohesive soil.

4.3 Centrifuge modelling

To understand the large-scale behaviour of the proposed winged caissons, a series of centrifuge tests were conducted to study their behaviour in field conditions. Although, previously in section 4.1 the FE models was validates against 1-g testing condition, however, to ensure the accuracy of the FE modelling at true stress conditions (increased value of gravity), validation against the centrifuge tests were carried out.

The normalized moment-rotation ($M - \theta$) curves for the simple and proposed models with wing width of $T = 0.4D$ installed in HST95 sand with $Dr = 50\%$ are presented in Figure 4.28. The results from the experiments indicated that the overturning capacity of the suction caisson is increased by approximately 75% for the winged caisson.

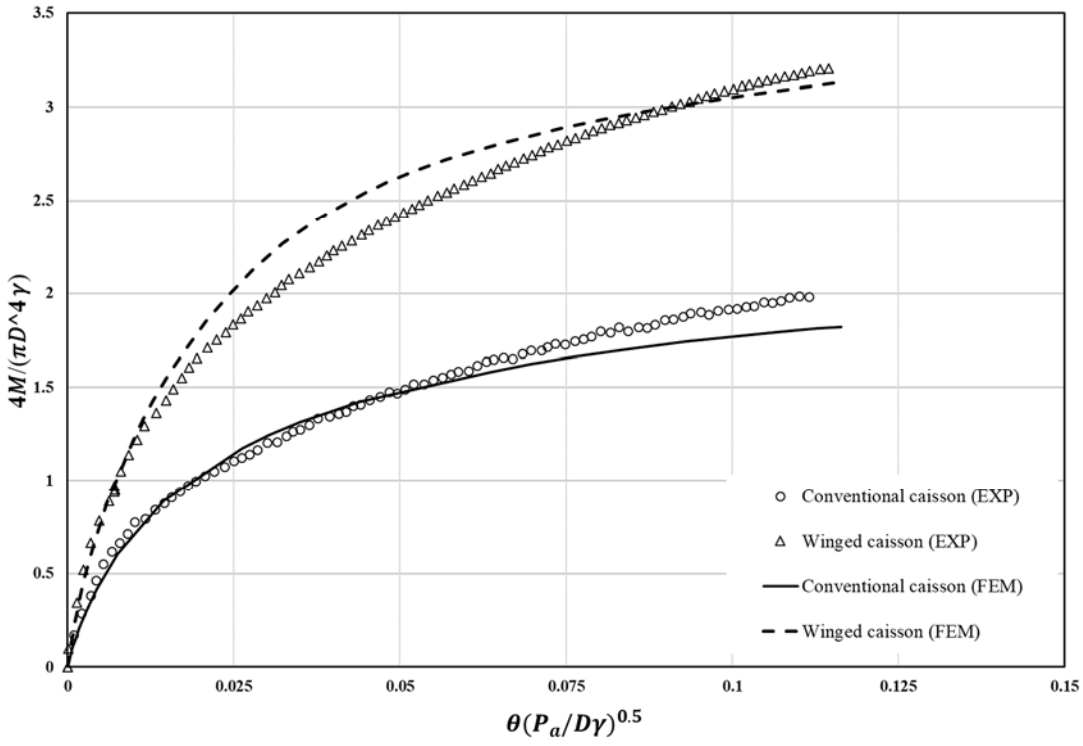

Figure 4.28. Normalised Moment-rotation curves for the simple and winged caissons, centrifuge test

Maximum allowable rotation at foundation head after installation has been restricted by some codes and standards (Bhattacharya, 2014b; Lombardi et al., 2013; Wang et al., 2018b). For instance, DnV code set a limit of 0.25 degrees in the tilt of at nacelle level. The angular rotation of the foundation was limited to 0.25 degree in the design of the gravity base foundations at Thornton Bank of the United Kingdom (Peire et al., 2009). In China, the design code FD003 (2007) specifies the angular rotation of the foundation to be less than 0.17 degree for OWTs with hub heights equal to 100 m. In the German standard, 0.5 degree is considered as the control value of the angular rotation of OWTs (Kuo et al., 2009).

According to the above mentioned values (0.17-0.5 degree), a maximum allowable rotation of 0.3 degrees was chosen in this thesis (corresponding to a normalised ratio up to $\theta(\frac{P_a}{D\gamma})^{0.5} = .006$ in Figure 4.28) to derive the maximum overturning bearing capacities for the conventional and winged foundations with $T = 0.4D$ using the results of the FE methods. The normalized allowable capacities for the conventional and winged caissons are 0.5 and 0.83, respectively.

4.4 Large-Scale numerical modelling

4.4.1 Validation of finite element modelling against large-scale field trials

To understand the large-scale behaviour of the proposed winged caissons, a series of FE models were developed to study their behaviour in field conditions. Although, previously in section 4.1 and 4.3 the FE models against 1-g and centrifuge testing conditions was validated, however, to ensure the accuracy of our FE modelling, validation against two large-scale field trials available from literature were carried out.

Of the available data in literature, two field tests were chosen to validate our FE models. The field tests were originally reported by Houlsby and Byrne (2000) and Houlsby et al. (2005) at the Sandy Haven and Frederikshavn test sites, respectively. The parameters used in the FEM simulations are given in Table 4.2. Both sites comprised of predominantly sandy soil. In the FE, the loading was simulated as drained to replicate the site condition. A constant value was considered for the sand.

The suction caisson at the Sandy Haven site had a diameter of 4 m and a skirt length of 2.5 m, and it was installed in medium to dense sand. The horizontal load test was then conducted at a loading point height of 14.5 m above the ground surface. The suction caisson tested at the Frederikshavn site, which had a diameter of 2 m and a skirt length of 2 m, was installed in dense sand. The foundation was subjected to horizontal loading at a height of 17.4 m above the ground surface under a constant vertical load of 37.3 kN. Figure 4.29a, and Figure 4.29b show that load-displacement curves obtained from the FE analysis agreed well with those measured in the field tests and the centrifuge test.

Table 4.2. Detailed reference studies for validation of FEM modelling

Case study	Diameter (D)	Length (L)	Load eccentricity (e)	Aspect ratio (L/D)	Effective unit weight (γ')	Internal friction angle $(\emptyset')$
Frederikshavn (Houlsby and Byrne, 2000)	2m	2m	17.4m	1.0	9	37-38
Sandy Haven (Houlsby et al., 2005)	4m	2.5m	14.5m	0.625	8.5	34

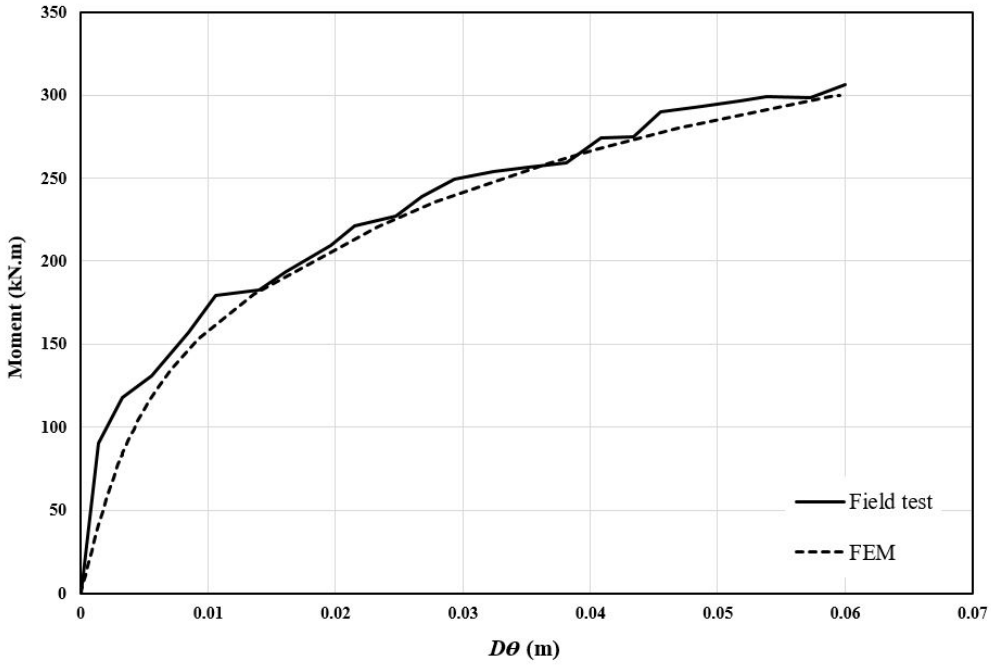

(a)

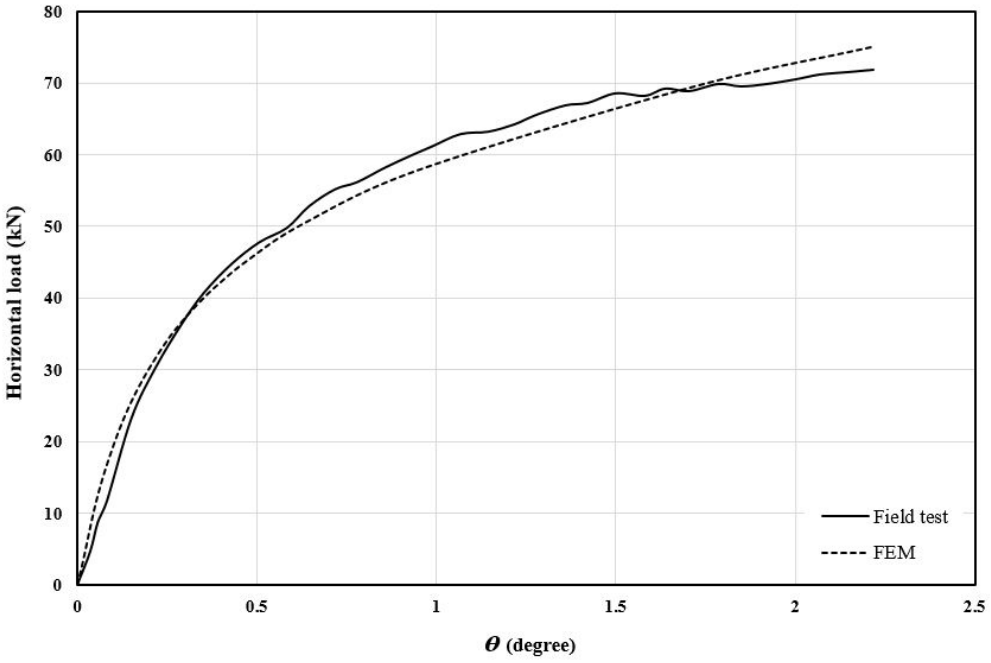

(b)

Figure 4.29. Comparison of the numerical modelling and the field test results a) Frederikshavn, b) Sandy haven

4.4.2 FE modelling of large-scale WCF

The validated FE model was subsequently used to predict the overturning capacity of a hypothetical full-size winged caisson foundation ($L/D = 1.0$), with 4 wings each with a width of 0.8 m ($0.4D$). The soil parameters and loading condition were adopted from Houlsby et al. (2005a). Three different wing sizes were modelled and the improvement in overturning moment for each was recorded. The results are shown in Figure 4.30 (filled-in triangular symbols). It is evident from these results that the overturning capacity will significantly depends on the wing size. For comparison, the improvement in overturning capacity for 1-g models are presented on the same graph (filled-in circle symbols).The soil characteristics for the two models (i.e. 1-g and large-scale) are different, but the same embedment ratio was considered in both studies. Nevertheless, similar trend in improvement of overturning capacity can be observed.

Based on the results from experiments and numerical analysis, a polynomial expression was proposed for models with $L/D = 1$, that correlates the improvement in bearing capacity and the wing width dimension (T) (see Figure 4.30).

$$y = 0.025T^2 + 0.65T \qquad 4.1$$

In the proposed equation (Eq.4.1), y represents the capacity improvement, and T is the wing width ($\%D$). The divergence at the end of the graph is due to the different soil stress conditions. As surface area of the caisson in contact with surrounding soil increases by increasing wing size, the effects of soil characteristic on the wing efficiency will change.

From the above, the test models and the FE studies indicate the benefits of using wings to enhance the overall capacity of suction caisson foundations. Despite the involvement of scale effects, this project provides a useful basis for future research using full-scale models, leading

to an increased understanding of real winged caisson behaviour under overturning and combined loads.

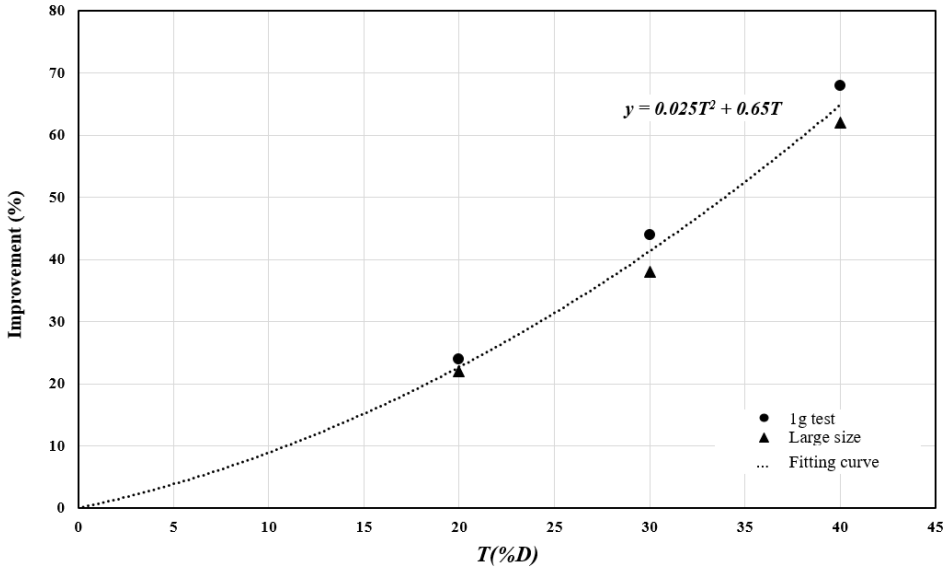

Figure 4.30. Capacity improvement with constant wing width for a suction caisson foundation

Analytical solution:

4.4.3 Conventional suction caisson

In this research a simple strategy to derive an analytical solution to the lateral-load resistance of the suction caisson foundations is discussed. The strategy is based on the Rankin theory method. In order to assess the validity of the proposed strategy, a series of laboratory tests and numerical simulations, using three-dimensional FEM, under monotonic loading conditions were carried out. The results were also compared with existing analytical solutions proposed by other researchers (i.e. Byrne and Houlsby (2003a); and Villalobos (2006)).

The proposed equation was calibrated based on the physical test results via a series of 1-g small-scale laboratory and a centrifuge test were carried out in the Nottingham centre for

Geomechanics (NCG). The FE method was used to observe the location of rotational point and stress distribution along the caisson at failure. The proposed analytical solution was also validated against published studies and field tests.

The location of rotation point (RP) at ultimate load was confirmed by FEM (Figure 4.31). From the FEM results, the centre of rotation of the caisson foundation at failure is located below the foundation level as the point along the vertical axis of the caisson 0.8 of the skirt length. As the horizontal load increased, the RP began to move toward right hand and stop at right exterior side close to the skirt in the ultimate load.

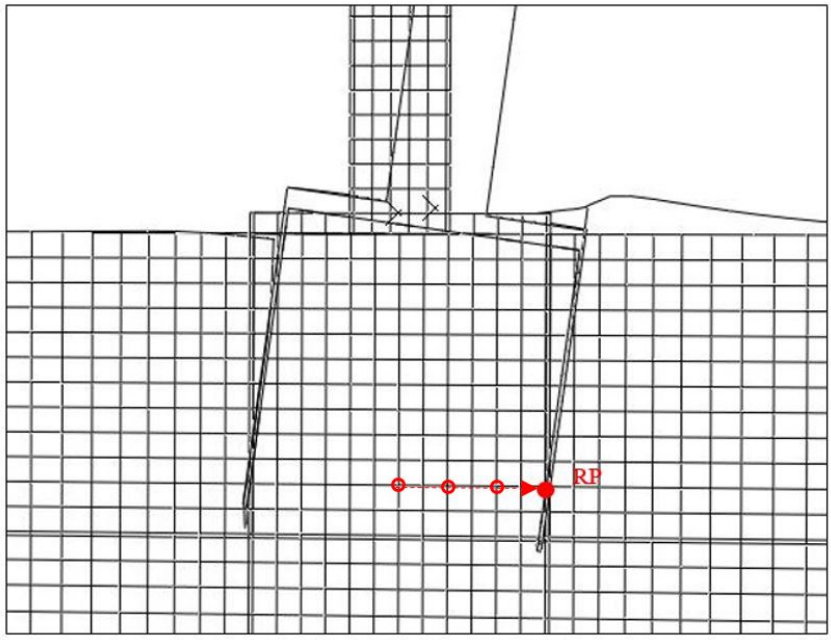

Figure 4.31. Location of RP of the caisson with $L/D = 1.0$ obtained by FE analysis ($\theta < 2^o$).

When calculating bearing capacity of the caisson foundation a rotation point (RP) located on the line at $0.8L$ depth of the caisson is considered. The vertical, horizontal and moment equilibrium must be ensured. Variation of lateral earth pressure ($S11$) on the caisson wall corresponding to the ultimate lateral load for the suction caisson in sand (Dr =50%)

obtained from FEM is shown in Figure 4.32. The variation of $S11$ on the exterior wall (right side) before and after failure is shown in Figure 4.33.

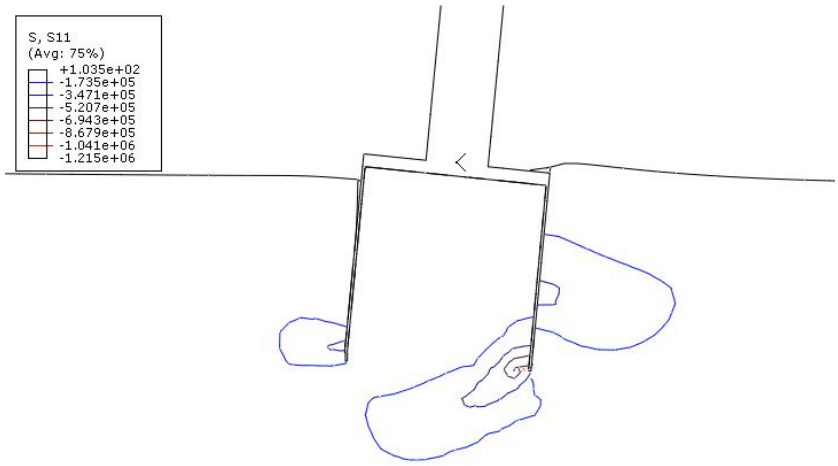

Figure 4.32. Stress distribution in soil at ultimate state in the plane of symmetry for a suction caisson with $L/D = 1$, FE analysis

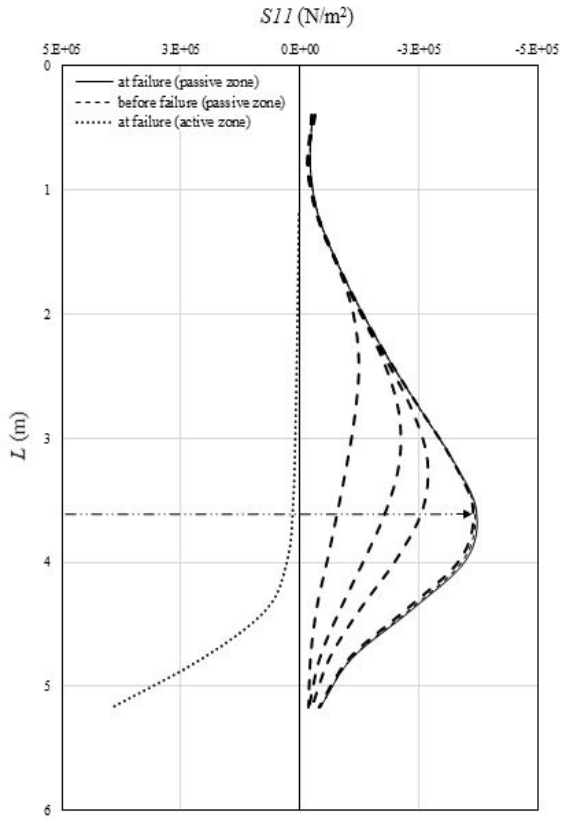

Figure 4.33. Soil pressure distribution over the outer skirt (left and right side) for a suction caisson with $L/D = 1.0$, as obtained from the FE analysis

Based on the results obtained from FEM, the lateral soil pressure, in the passive zone increases with depth up to $0.85x$ (where x=the distance to the point of rotation). The pressure then decreases linearly until it reduces to zero at depth of x. Below x, the net soil pressure is in the opposite direction and increases linearly from zero at depth x, to a maximum at the tip of the caisson. The soil pressure at the caisson tip is 1.8 times the soil pressure at $0.8x$ depth. On the other side (active zone), the soil pressure is almost equal to the maximum pressure in the passive zone. To simplify the lateral earth pressure distribution, an equivalent soil pressure in the left hand side was considered in the right side (Figure 3.13).

Usually, caisson foundations have large diameter, and the weight of the soil inside the caisson has a significant effect on their stability under lateral loading. Therefore, in this study the weight of the soil was considered to develop the formula. Zhu assumed that 80% of the enclosed soil plug moves with the caisson and subsequently does not interact with the caisson (Zhu et al., 2014). The end bearing stresses around the caisson tip are not included in the total stresses. Similar to former studies, caisson skirt has been considered rigid under lateral loading (Lombardi et al., 2017). End bearing stresses around the caisson tip are neglected in this study.

In the estimate of lateral bearing capacity of suction caissons, the earth pressure distributions along the caisson wall can be used. On the other hand, it has been proved that suction caissons can be considered to be rigid under lateral loading. Therefore, theories of investigating the earth pressure mobilization, which are principally used for the laterally loaded rigid pile, can be used to explore the earth pressure distribution over the caisson foundations (Kumar and Rao, 2010).

The proposed model in this study is fundamentally influenced by the angle of internal friction ϕ', total soil unit weight γ', caisson diameter D, and caisson length L. To develop the

formula to predict lateral capacity of caissons, the work by Prasad and Chari (1999), to describe pressure at an arbitrary depth, is used as follows:

$$P_z = sf(\phi')\gamma' z \qquad 4.2$$

In equation (4.2) γ' is the unit weight of the soil and P_z represents the peak soil passive pressure at depth z below the ground level. The shape factor s is extracted from Prasad and Chari (1999) and was adopted for this study. The function $f(\phi')$ represents Rankine's passive earth pressure coefficient (K_p). If $Log(\frac{P_z}{\gamma z})$ is plotted against $\tan\phi'$, it can be seen that the relationship is linear as shown in Figure 3.13. The straight line relation is given by:

$$Log\left(\frac{P_z}{\gamma z}\right) = (\alpha \tan\phi' + \beta) \qquad 4.3$$

Equation (4.3) can be re-arranged based on earth pressure as a function of the depth at the maximum earth pressure (λx):

$$P_z = 10^{(\alpha \tan\phi' + \beta)}\gamma'\lambda x \qquad 4.4$$

where α and β are coefficients obtained from Figure 4.34. A series of finite element models were conducted for various L/D ratios of 0.5, 1.0 and 1.5 and the results were used to generate the necessary data to determine the coefficients. The values are 1.3 and 0.3 for α and β respectively.

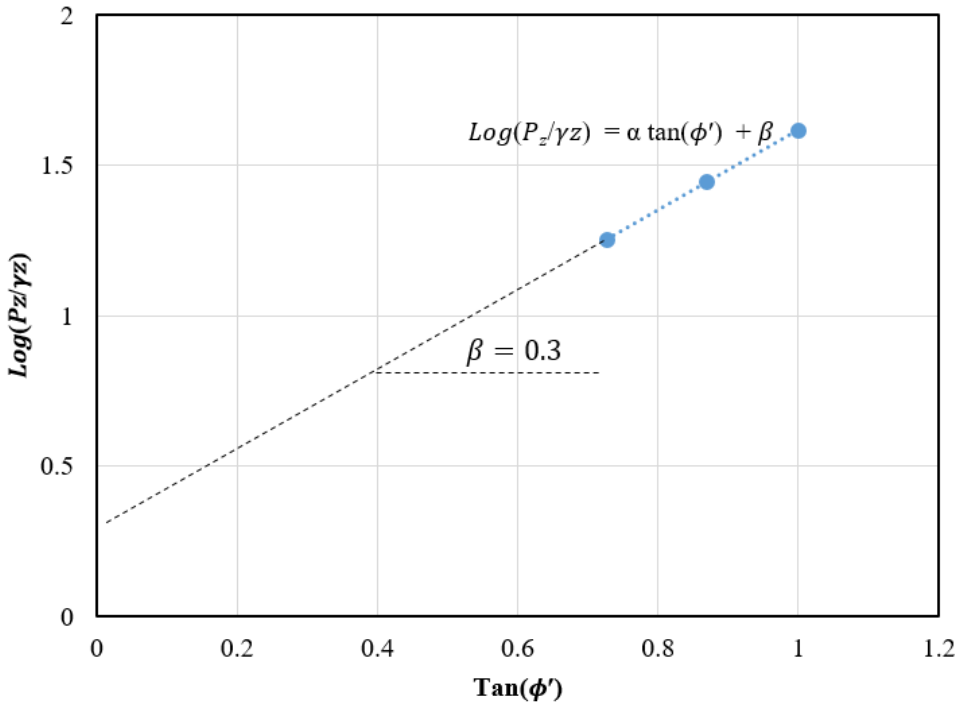

Figure 4.34. Variation of $Log(\frac{P_z}{\gamma z})$ with $tan\,\phi'$

The ultimate bearing capacity of the rigid caisson can be obtained based on moment equilibrium. If the moment of all forces is taken about the point of rotation in Figure 3.13, the maximum lateral load can be obtained as:

$$H'_{max}(kN) = \frac{1}{e+x}\left[\left(P_1 x\left(1-\frac{2}{3}\lambda\right) + P_2\frac{2}{3}x(1-\lambda) + 2P_3\left(\frac{L-x}{2}\right) + \frac{2}{3}P_4(L-x)\right)D + W'\frac{D}{2} + V\frac{D}{2}\right] \quad 4.5$$

where:

$$W' = W_s\left(\frac{2}{3}\text{of buoyant weight of the soil plug inside the caisson}\right) + W_t(\text{ buoyant weight of the tower}) + W_c(\text{buoyant weight of the caisson}) \quad 4.6$$

$$P_1 = \frac{1}{2}P_z\,\lambda x \quad 4.7$$

$$P_2 = \frac{1}{2}P_z x - P_1 \quad 4.8$$

$$P_3 = P_z(L - x) \quad (4.9)$$

$$P_4 = 0.4P_3 \quad (4.10)$$

where $x = \omega L$ and λ is a coefficient as shown in Figure 3.13.

The coefficient of 0.4 in Eq. (4.10) is extracted from the results of finite element simulations which has been shown in Figure 4.32. Using results of the experimental and numerical models, the ultimate lateral load can be considered as 80% of the maximum capacity $H'_u = 0.8H'_{max}$.

The yield point is determined using tangent intersection method (Mansur and Kaufman, 1958), as shown in Figure 4.35. Using this method, the yield capacity is defined as the intersection of two tangential lines along the initial and later portions of the moment-rotation curve.

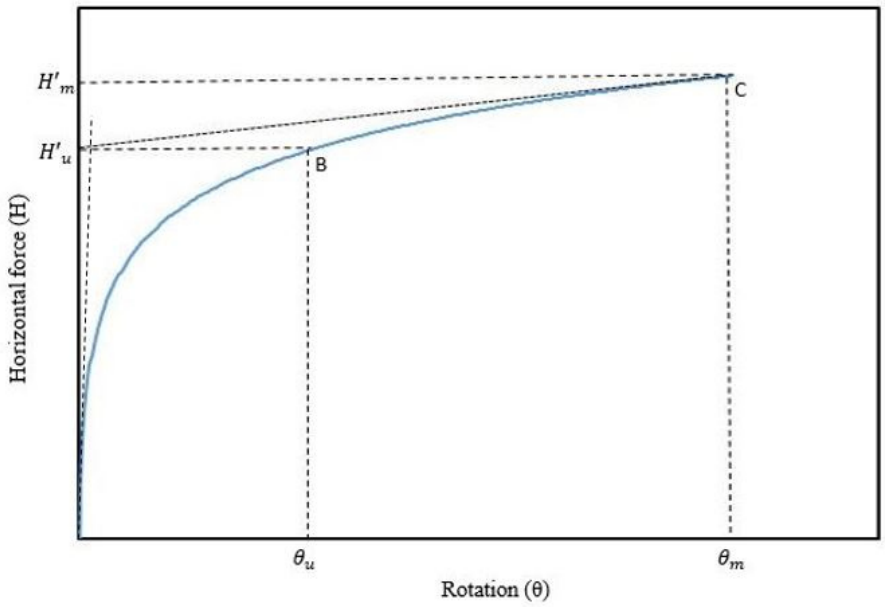

Figure 4.35. Tangent method for determining bearing capacity

The proposed method was verified using the experiments and the values were compared with other existing methods. Different models with various aspect ratio of $L/D = 0.5$ and 1.0 and different densities of $Dr = 20 - 25\%$ and $48 - 50\%$ were tested in the laboratory under lateral loading. The soil and test conditions with the observed and estimated values are shown in Table 4.3. For the caissons with $\frac{L}{D} < 1.0$, the formula proposed by Byrne and Houlsby (2003a) was used to make a comparison, whilst for the caisson with $L/D = 0.5$, Eq. (2.2) ,proposed by Villalobos (2006), was used. As can be concluded from Table 4.3, the proposed method can provide a good estimation of lateral load capacity for the caissons with varies embedment depths in different sand densities.

Most existing solutions in the literature were only validated for a particular type of loading and aspect ratio, whereas the proposed method can be easily applied to obtain an accurate response for general loading systems and for a variety of aspect ratios. From the experiment data, the load-rotation curves of two caissons with $L/D \sim 1.0$, under two stress conditions i.e. 1-g and centrifuge are presented in Figure 4.36 and Figure 4.37.

The calculations that were used to identify H'_u are graphically shown in Figure 4.36 and Figure 4.37 for two of the tests, CSC1 with Dr=50% and G1, respectively.

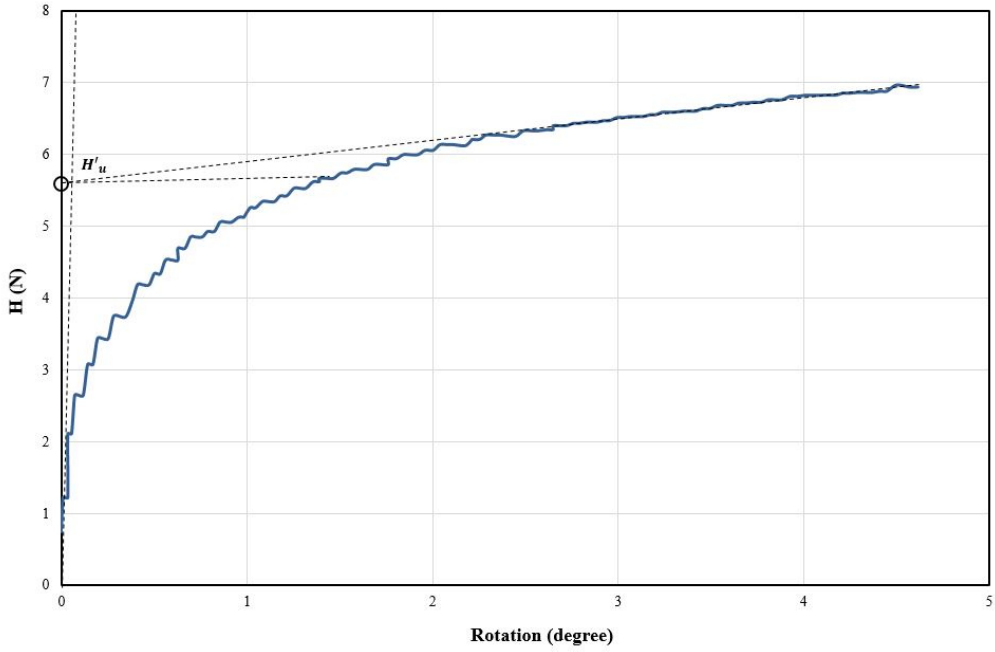

Figure 4.36. Load-rotation curve for model CSC1 with $Dr = 50\%$

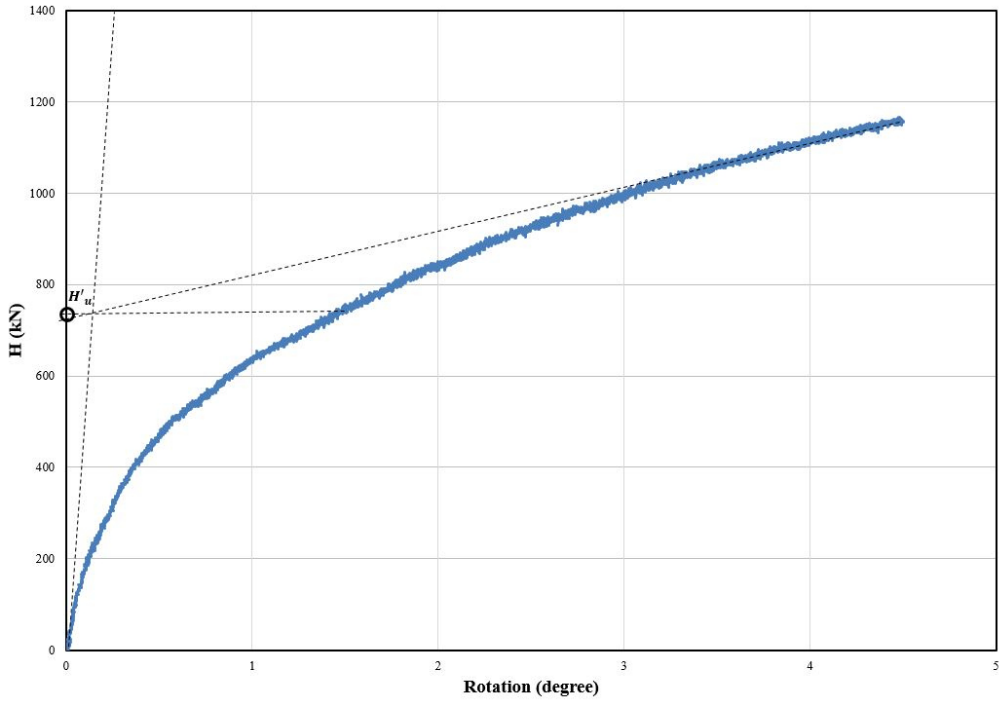

Figure 4.37. Load-rotation curve for model G1

Table 4.3. Comparison of observed and predicted capacities (H'_u) of the experiments

Test ID	Testing condition	Observed capacity (N)	Proposed method (N)	Byrne and Houlsby (2003a) (N)	Villalobos (2006) (N)
CSC2	$\phi' = 36^0$ $\gamma' = 13.7\ \text{kN/m}^3$ $D = 75\ \text{mm}$ $L = 37.5\ \text{mm}$ $V = 0$ $e = 0.220\ \text{m}$	0.85	0.78	1.5	0.6
CSC1	$\phi' = 36^0$ $\gamma' = 13.7\ \text{kN/m}^3$ $D = 75\ \text{mm}$ $L = 75\ \text{mm}$ $V = 0$ $e = 0.220\ \text{m}$	3.7	3.3	3.02	2.3
CSC1	$\phi' = 43^0$ $\gamma' = 14.43\ \text{kN/m}^3$ $D = 75\ \text{mm}$ $L = 75\ \text{mm}$ $V = 0$ $e = 0.220\ \text{m}$	5.5	5.6	3.2	3.35
G1	$\phi' = 32^0$ $\gamma' = 15.73\ \text{kN/m}^3$ $D = 5.25\ \text{m}$ $L = 5.1\ \text{m}$ $V = 0$ $e = 14.84\ \text{m}$	780000	820000	1180000	710000

4.4.3.1 Comparison of ultimate capacities:

Field and laboratory data from published literature were used to validate the proposed method. A summary of the results with soil properties were tabulated in Table 4.4. Of the available data in literature, two field tests were chosen to validate the proposed equations. The field tests were originally reported by Houlsby and Byrne (2000) and Houlsby et al. (2005) at

the Sandy Haven and Frederikshavn test sites, respectively. The parameters were used in the analytical solution are given in Table 4.4. Both sites comprised of predominantly sandy soil.

The measured ultimate capacities for two field tests were obtained from the moment rotation curves (using tangent method, which was described in Figure 4.35). The observed ultimate capacities were 57283 N and 13342 N and the estimated capacities using the proposed method are 62000 N and 16000 N for the caissons at the Sandy Haven and Frederikshavn sites, respectively. The capacities were estimated by using Villalobos (2006) is 62000 N and using Byrne and Houlsby (2003) is 147000 N for the caissons at the Sandy Haven and Frederikshavn sites, respectively.

Foglia et al. (2011, 2015) carried out six tests with a 300 mm diameter caisson foundation with embedment ratio (L/D) equal to 1.0 in sand with high relative density ($Dr >$ 0.8). The observed ultimate capacity for selected test, with no applied overburden pressure, was obtained from the moment rotation curve. The observed ultimate capacity was 382 N and the predicted capacity using the proposed method is 343 N. The predicted capacity using Byrne and Houlsby (2003a) and Villalobos (2006) is 331 N and 340, respectively.

A series of monotonic loading tests were carried out by Zhu et al. (2011a) to determine the capacity of the caisson foundation in loose sand with relative density of 20%. The observed ultimate capacity, obtained from the moment-rotation curve for the test with vertical load $V/(\gamma' D^3) = 0.19$, was 10 N and the predicted capacity using the proposed method is 17 N whilst those of Byrne and Houlsby (2003a) and Villalobos (2006) are 44 N and 16 N, respectively. Large-scale experiment was also conducted by the same authors (Zhu et al., 2012) for model caisson with L/D equal to 0.5 in silt. The observed capacity was 1871 N and the values were predicted using Eqs. 2.1, 2.2 and 4.5 are 5800 N, 2500 N and 1900 N, respectively.

Zhang et al. (2010) conducted a centrifuge test to investigate the static bearing capacity of a caisson foundation with 72 mm height and 62 mm diameter in silt sand. The static vertical load equal to 320 N was applied on the caisson foundation. The observed capacity of the caisson subjected to static lateral loads was 65 N and the predicted capacity using the proposed method is 56 N.

It may be seen that the computations using the proposed method predict the ultimate capacities with good accuracy.

Table 4.4. Comparison of observed and predicted capacities (H'_u)

Reference	Testing condition	Observed capacity (N)	present method (N)	Byrne and Houlsby (2003a) (N)	Villalobos (2006) (N)
Sandy Haven (2000)	$\phi' = 34^0$ $\gamma' = 8.5\ \text{kN/m}^3$ $D = 4\ \text{m}$ $L = 2.5\ \text{m}$ $V = 0$ $e = 14.5\ \text{m}$	57283	62000	147000	62000
Frederikshaven (2005a)	$\phi' = 37^0$ $\gamma' = 9\ \text{kN/m}^3$ $D = 2\ \text{m}$ $L = 2\ \text{m}$ $V = 37.3\ \text{kN}$ $e = 17.4\ \text{m}$	13342	16000	14900	10132
Foglia et al. (2011a)	$\phi' = 38.8^0$ $\gamma' = 10.25\ \text{kN/m}^3$ $D = 0.3\ \text{m}$ $L = 0.3\ \text{m}$ $V = 0$ $e = 0.330\ \text{m}$	382	343	331	340
Zhu et al. (2011a)	$\phi' = 35^0$ $\gamma' = 9.02\ \text{kN/m}^3$ $D = 1\ \text{m}$ $L = 0.5\ \text{m}$ $V = 0$ $e = 1\ \text{m}$	1871	1900	5800	2500
Zhu et al. (2012)	$\phi' = 35^0$ $\gamma' = 13.2\ \text{kN/m}^3$ $D = 0.2\ \text{m}$ $L = 0.1\ \text{m}$ $V = 20\ \text{N}$ $e = 0.375\ \text{m}$	10	17	44	16
Zhang et al. (2010)	$\phi' = 35^0$ $\gamma' = 7.84\ \text{kN/m}^3$ $D = 0.6\ \text{m}$ $L = 0.72\ \text{m}$ $V = 320\ \text{N}$ $e = 0.080\ \text{m}$	65	56	59	-

4.4.3.2 Effects of vertical loads on the horizontal response of caissons

From Eq. (4.5) it is evident that the horizontal load capacity of the caisson foundation depends on the vertical load applied on the caisson. Therefore, an equation can be extracted from Eq. (4.5) to express the maximum horizontal capacity as follows:

$$H'_{max}(kN) = H'_0 \frac{D}{2(e+x)} V \tag{4.11}$$

where H'_0 is the maximum horizontal capacity without vertical loading as:

$$H'_0(kN) = \frac{1}{e+x}\left[\left(P_1 x\left(1-\frac{2}{3}\lambda\right) + P_2\frac{2}{3}x(1-\lambda) + 2P_3\left(\frac{L-x}{2}\right) + \frac{2}{3}P_4(L-x)\right)D + W'\frac{D}{2}\right] \tag{4.12}$$

To identify the impact of the vertical load on the horizontal load capacity of a caisson foundation, data from model CSC1 (Table 3.7) with a relative density of 25% have been used.

The ultimate capacity values for caisson model CSC1derived from the Eq. (4.5) for various load eccentricities of 0, 1, 2, and 3 were plotted versus the vertical load. The normalized values are presented in Figure 4.38. According to the analysis presented here, and as expected, the ultimate horizontal bearing capacity of the suction caisson increases with increasing vertical load. It is worth mentioning that, increased vertical load on site could be achieved through ballast (Byrne and Houlsby, 2003a). However, the effect does not show a similar trend line for different load eccentricity ($\frac{M}{H'_u D}$). The contribution of vertical loading to the horizontal load capacity is more pronounced for the loading with lower eccentricity ($e \sim 0$).

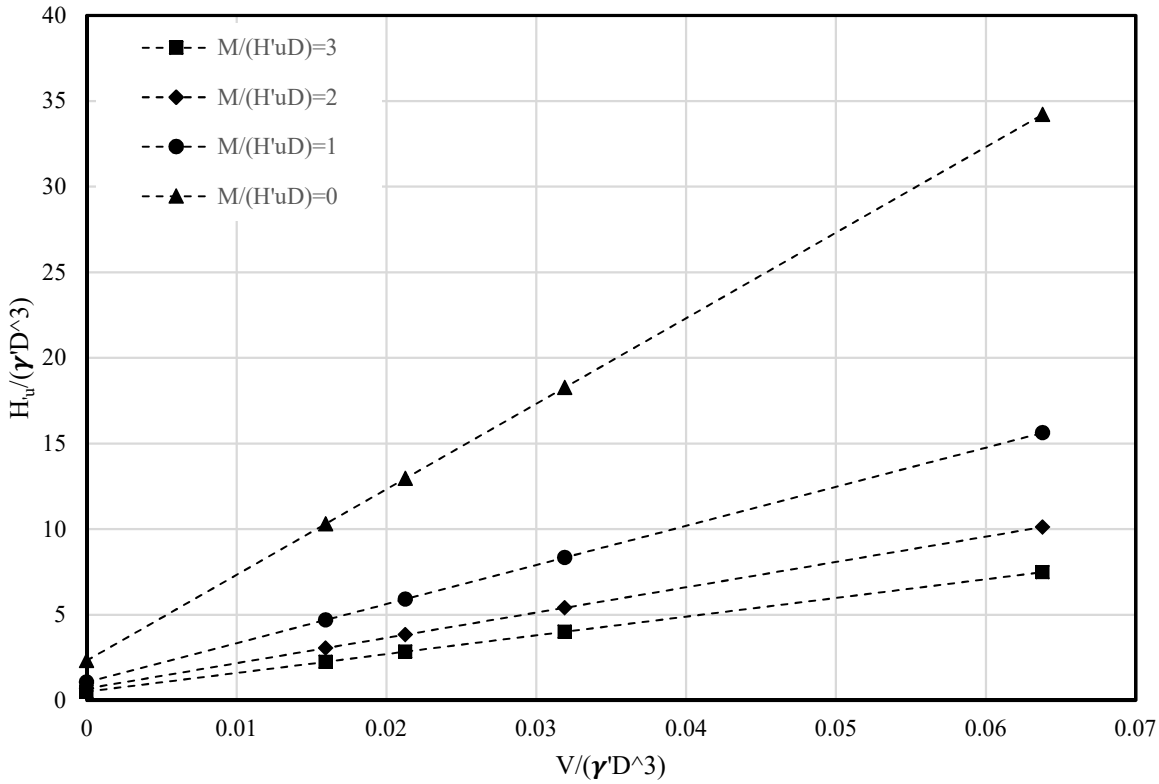

Figure 4.38. H–V with various load eccentricity for the caisson with $L/D = 1.0$

From the results presented previously, the benefits of using the proposed equation in the current study to predict the capacity of suction caisson foundations in sandy soil with the assumption of drained conditions are evident. It should also be noted that the predictions made using the method of Byrne and Houlsby (2003a) was developed for $\frac{L}{D} < 1.0$ and provides satisfactory results for this ratio. On the other hand, the equation proposed by Villalobos (2006) is good where no vertical load is applied on the caisson. However, the advantage of the present method is that it can provide very good estimations for both different vertical loading and geometrical ratios.

From Table 4.3 and Table 4.4, it can be seen that the results of the proposed model in this study agrees closely (in most cases the errors is <20%) with those of the experiments. On the other hand, model by Villalobos (2006) provides poor estimation of lateral bearing capacity,

especially where the value of vertical load is significantly higher than self-weight of the foundations. Byrne and Houlsby (2003a) predicts the lateral bearing capacity with acceptable accuracy for those scenarios that L/D ratio is <1.0. The predictions of their models diverges from the experimental results for other ratios of L/D.

4.4.3.3 The effect of combined loading on yield points

This part concentrates on the shape of yield envelopes for combined vertical and horizontal ($V - H'$) loading of caissons with aspect ratio of 1.0. The ultimate capacity of the foundation under combined loading is expressed graphically using yield envelopes. The size of the empirical expression for yield surface is controlled by the vertical capacity, defined by V. Therefore, to plot the yield envelope, the maximum vertical capacity should be estimated.

In early studies, the vertical bearing capacities of suction caisson foundations were determined (Larsen, 2008a; Ibsen et al., 2012; Byrne and Houlsby, 2003a), which some of them are generally recommended for the installation process (Senders, 2009; Houlsby and Byrne, 2005b; Ibsen et al., 2012; Larsen, 2008a). The proposed methods are basically in CPT based methods and beta-methods, based respectively on cone resistance and $\beta'' = Ktan\delta$ (Manzotti et al., 2014). For example Houlsby and Byrne (2005b), developed an equation which is based on the stress distribution on caisson tip, therefore these are suitable only for the installation process since in installation measurements is not well defined where the lid makes contact with soil (Manzotti et al., 2014).

Byrne et al. (2003a) investigated the vertical bearing capacity of circular surface footings and bucket foundations in dry sand and embedment ratios of the bucket foundation varying from 0 to 2. The Houlsby and Byrne (2005b) method takes into account the bearing

capacity factors recommended for the installation process, they obtained a new fit for the peak capacity, which captured the measured peak capacities well.

Ibsen et al. (2012) developed a new theoretical relationship of the bearing capacity introducing the reduced friction angle for the analysis of the small-scale laboratory results. The reduced friction angle is determined by back-analysis of the results of bearing capacity tests for bucket foundations and the general bearing capacity formula.

The vertical bearing capacity of a bucket foundation located in saturated sand was investigated by Larsen (2008a). The bucket foundation is assumed to behave similar to an embedded circular foundation, in case of vertical loading. Thus the soil trapped within the bucket is expected to behave as or nearly as a rigid cluster. The soil within the bucket foundation is during vertical loading constrained laterally by the skirt, preventing the soil from large deformations due to the high stiffness of dense sand. The vertical bearing capacity is, in this case, given as the sum of two contributions: 1) the bearing capacity at the base of the embedded foundation and 2) the friction between the outside of the bucket skirt and the surrounding soil. The vertical bearing capacity of a bucket foundation located in saturated sand is predicted by the formula which is based on the work by Terzaghi (1943) and on the principle of superposition which results in a conservative estimate of the bearing capacity suggested by Hansen (1975).

The bearing capacity factors recommended in the formula, and c_i values obtained from the study conducted by Barari (2016).

$$V = \gamma' \frac{D}{2} N_\gamma \left(\frac{\pi D^2}{4}\right) + q' N_q \left(\frac{\pi D^2}{4}\right) + \left(\frac{\pi D \gamma' L^2}{2}\right)(K tan\delta) \quad 4.13$$

$$N_\gamma = c_1 . \left[\left(N_q - 1\right) cos\, \phi'\right]^{c_2} \quad 4.14$$

$$N_q = c_3 . e^{c_4 . \pi . tan\, \phi'} tan^2\left(45 + \frac{\phi'}{2}\right) \quad 4.15$$

To develop the yield envelope, the ultimate vertical capacity obtained from the formula proposed by Larsen (2008a) is used in this study.

The effect of the vertical load on the expansion of the yield envelope for caisson with $L/D = 1$ is presented in the Figure 4.39. The graph shows that the influence of the vertical load (V) on the bearing capacity is significant for a suction caisson foundation; this finding was also reported by Byrne et al. (2002). The foundation behaviour within this surface is assumed to be elastic; and the elasto-plastic behaviour only occurs once the load point reaches the yield surface, which is similar to that presented by Byrne et al. (2003a). According to the analysis presented herein, it can be concluded that the ultimate moment bearing capacity of the suction caisson increases with increasing vertical load.

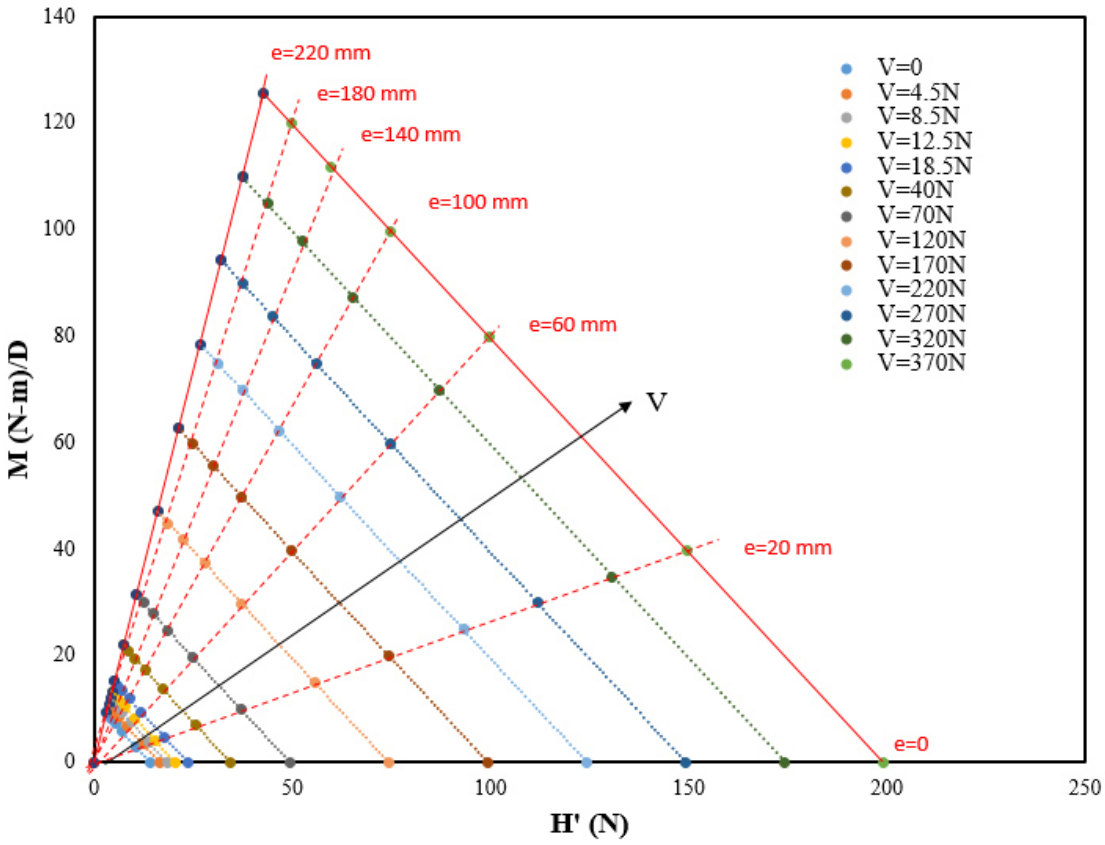

Figure 4.39. Yield points plotted in $M{:}H'$ space with various V for the caisson with $L/D = 1.0$

4.4.4 A formula to estimate ultimate overturning capacity of winged caisson:

An equation has been developed in the current study to estimate the ultimate overturning capacity of the winged foundations in cohesionless soil based on a theoretical formula proposed by Villalobos (2006). Villalobos (2006) proposed equation (4.16) to estimate ultimate moment capacity of conventional caisson foundations.

$$M = \frac{\mathrm{D}\gamma' K}{3}(L^3 - 2{z_m}^3) + F_h L + f(F_v)(\frac{D}{2}) \quad 4.16$$

where D is the caisson diameter, K the difference between the passive and active lateral earth pressure coefficients i.e. $K = K_p - K_A$, e is the force eccentricity, z_m is the depth to the point of rotation and

$$f(F_v) = \frac{(K_A + K_P)[(L - z_m)^2 + {z_m}^2]}{LK(2z_m - L)} F_v \quad 4.17$$

$$F_h = \sigma_v' \tan\phi' \pi D^2 / 4 \quad 4.18$$

$$F_v = D\gamma' L \tan\delta \, K(2z_m - L) \quad 4.19$$

where σ_v' is vertical effective stress, and K_P and K_A are the Rankine passive and active lateral earth pressure coefficients.

In the present study, the impact of adding wings have been considered by replacing the D term with F, where F is a coefficient determined from the laboratory experiments and is equal to $D + 2T$ for caissons with an aspect ratio of 1.0.

Therefore, the formula to estimate the ultimate overturning capacity for a winged caisson is defined by equation (4.20).

$$M = \frac{\mathrm{F}\gamma' K}{3}(L^3 - 2{z_m}^3) + F_h L + f(F_v)(\frac{D}{2}) \quad 4.20$$

where, $F_h = \sigma_v' \tan\phi' \pi F^2 / 4$

As shown previously in section 4.1.3.4, the overturning capacity of the winged caisson is not significantly altered by changing the orientation of the lateral load. Hence, the formula (Eq. 4.20) can be considered for the winged caisson subjected to either the perpendicular load or diagonal load.

To validate the formula, the normalised ultimate capacity of the winged caisson models with $L/D = 1.0$ was estimated using equation (4.20) to $(\frac{4M}{\pi D^4 \gamma}) = 3.2$ and $(\frac{4M}{\pi D^4 \gamma}) = 2.5$ for model testing at 1-g and centrifuge, respectively.

4.5 Cyclic loading

The results obtained from the cyclic experiments of conventional and winged suction caissons are discussed in this section.

It is easily inferred that for large turbines (~8 MW) sited in deeper waters, the wave loads will be highly dynamic and may control the design. The frequency of the loading in offshore conditions can vary during the lifetime of a foundation and typically lie within the range of 0.05–0.2 Hz (Nanda et al., 2017). For the present investigation, load frequencies of 0.1 Hz was investigated. Similar value for the frequency was considered in the study by Zhu et al.(2012). In offshore practice, frequency effects for dry sand seem to be negligible in loading frequencies below 1 Hz (Haigh, 2013).

The results obtained from the cyclic experiments on conventional and winged suction caissons are discussed in this section. In the present investigation, a load frequency of 0.1 Hz (mainly representative of wave loads) was investigated. The cyclic response of the foundations using moment–rotation curves were investigated in this project. These responses have a backbone curve and a set of unloading-reloading rules (hysteretic loops) which can represent

the total stress behaviour of the soil. Generally, the shape of the backbone curve is determined by the maximum secant shear modulus. The inclination of the loop represents stiffness of the soil, which can be described at any point during the loading process by the tangent shear modulus (G_t), or secant shear modulus (G_s) which are shown schematically in Figure 4.40.

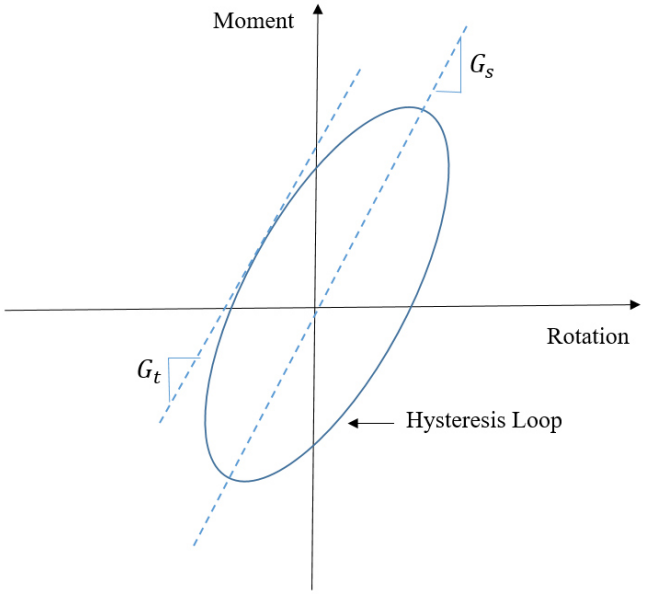

Figure 4.40. Schematic of typical hysteresis loop generated by cyclic loading

The moment–rotation curves ($M - \theta$) for conventional and winged caisson foundations with aspect ratios of $L/D = 0.5$ and 1.0 are shown in Figure 4.41 and Figure 4.42. In these tests packets of 10 cycles were applied to the caisson with 3 different amplitudes. The prescribed displacement amplitude increases with load amplitude, leading to expansion of the hysteresis. The unload–reload parts of the curve in lower amplitude are much stiffer than those obtained for the higher amplitudes. As the tests were basically displacement controlled, the load changed very rapidly at points of high stiffness.

As expected the caissons with wings provided a considerably higher cyclic resistance compared to the conventional caissons for the caissons. From the Figure 4.41a and Figure 4.41b, it can be observed that the cyclic capacity of the foundation (with $L/D = 0.5$) increases by

approximately 40% by using wings with $T = 0.4D$. The 50% capacity improvement offered by the winged caisson with $L/D = 1.0$ is compared with the conventional caisson under cyclic loading (Figure 4.42a and Figure 4.42b).

As reported in former studies, the bearing capacity under cyclic loading may be higher or lower than the bearing capacity for monotonic loading, depending on the cyclic degradation, density of soil and large cyclic and any permanent displacements that may develop (Andresen et al., 2010).

The sand surrounding an offshore foundation under quasi-static cyclic lateral load can show the progressive sand densification (Cuéllar et al., 2012). The results of the tests in this study showed a capacity increase of approximately 33% for all models under cyclic loading compared with the monotonic loading condition (Figure 4.41 and Figure 4.42) due to the sand densification. Both samples (i.e. conventional and winged caissons) showed overall contracting interface behaviour during cyclic loading with loose sand showing contraction followed by considerable densifying at each level cyclic loading. The same behaviour for a pile foundation installed in cohesionless soil of very loose densities is also observed by Rasmussen et al. (2013).

The experiments showed that specimens exhibited a slight shakedown apparent in the load at low amplitudes of displacement, with a slight stiffening occurring over several cycles of the same amplitude. The $M - \theta$ response during each set of cycles appears to approach a steady state at the end of the set. When displacement during cyclic loading reduces as the number of cycle increases, this phenomenon is known as ‘shakedown’ (Kelly et al., 2006).

From figures (Figure 4.41 and Figure 4.42), it is clear that the stiffness of the response at the low strain levels is high compared with the stiffness at larger strain amplitudes. Equally, the response of the foundation is hysteretic in that unloading stiffness (in both forms of secant and tangent shear modules) is initially high and reduces by increasing strain. In addition, the

widening of the hysteresis loops changes with strain amplitude. Comparing Figure 4.42a and Figure 5.4, it is clear that there is an increase in the stiffness of the response provided by the winged capacity with $L/D = 1$. The test results show that the secant stiffness of the foundation using winged caisson with $L/D = 1$ and $T = 0.4D$, under the cyclic loading, was increased by approximately 28%, 40%, and 50% in horizontal strains of $0.012D$, $0.038D$, and $0.077D$, respectively (Figure 4.43).

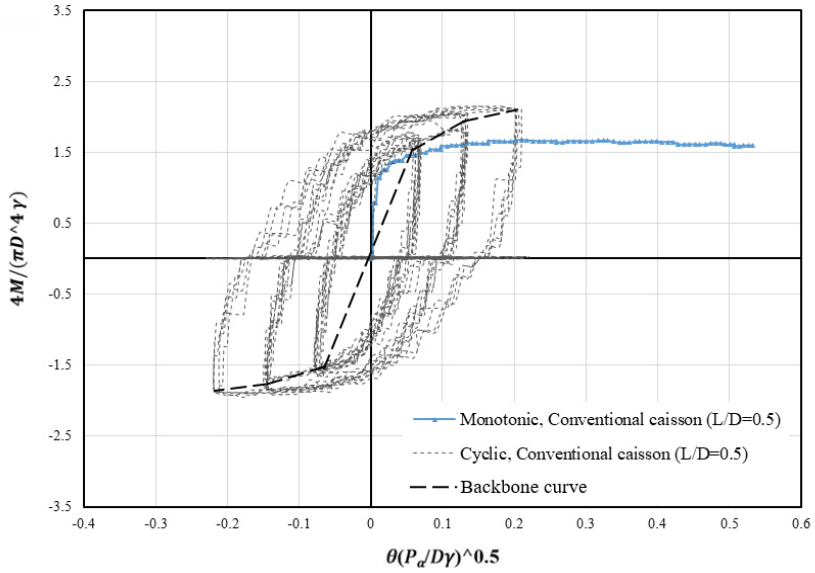

(a)

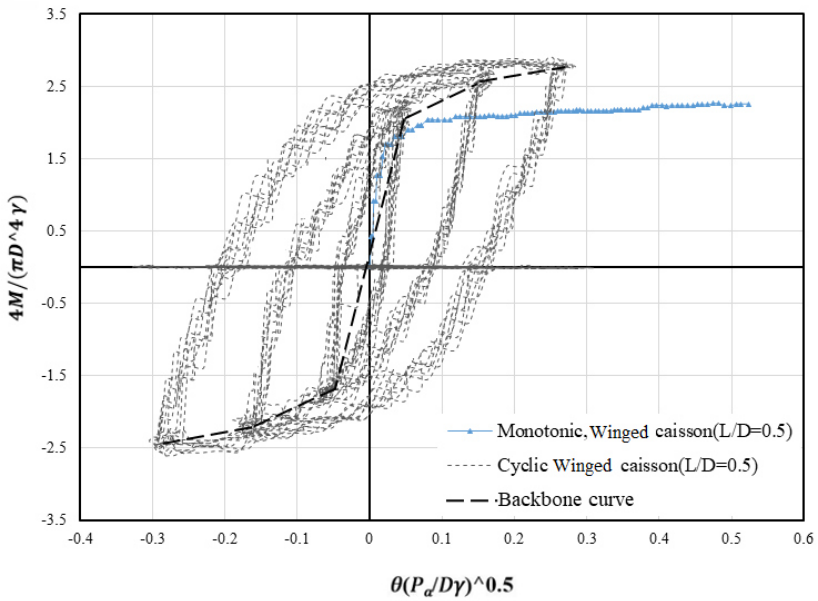

(b)

Figure 4.41. Comparison of cyclic and monotonic responses of the foundations in loose sand with an aspect ratio of $L/D = 0.5$ for (a) Conventional caisson and (b) winged caisson

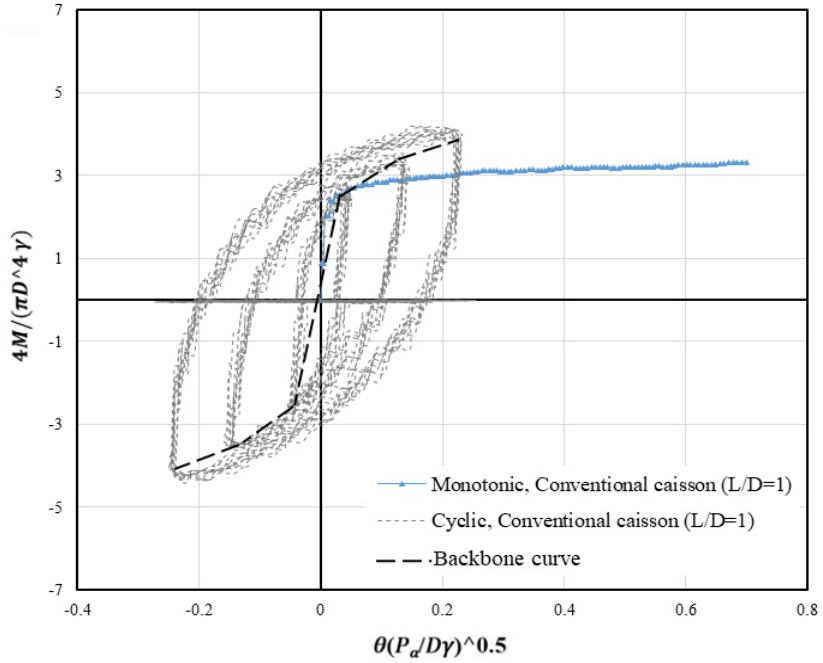

(a)

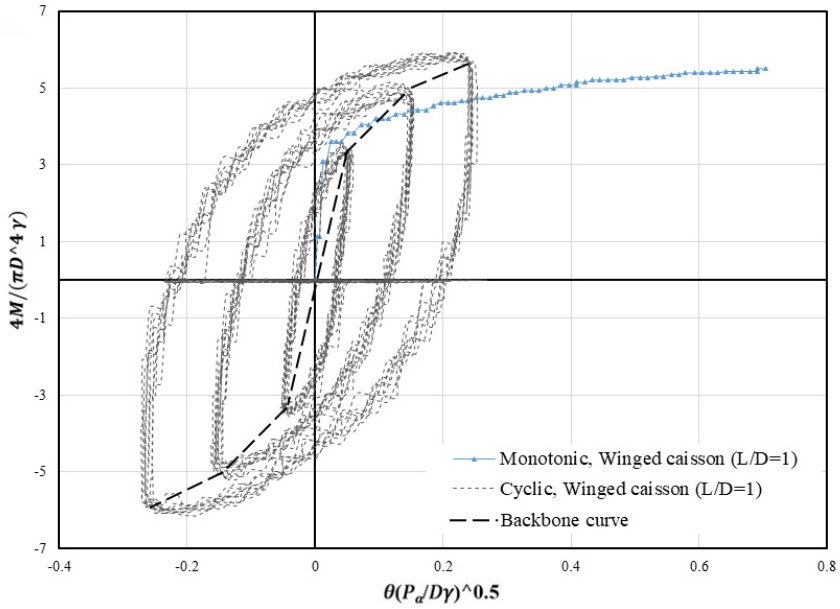

(b)

Figure 4.42. Comparison of cyclic and monotonic responses of the foundations in loose sand with an aspect ratio of $L/D = 1.0$ for (a) a conventional caisson and (b) a winged caisson

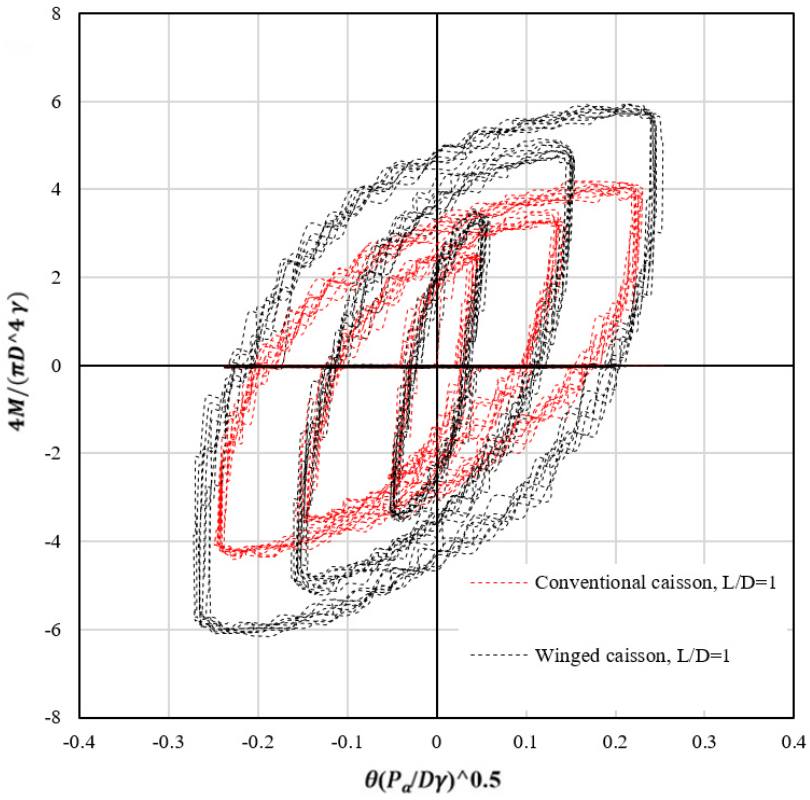

Figure 4.43. Comparison of cyclic response of the conventional and winged caisson in loose sand with an aspect ratio of $L/D = 1.0$

Although the lateral response of winged caissons under monotonic loading was examined via FE method in the previous sections, the numerical simulation of the lateral response of the foundations in sand under cyclic loading with the conventional constitutive models is not an easy task. According to the experiments, the initial stiffness of the soil mass surrounding the model caissons was gradually changes due to the cyclic loading. Hence, a unique constitutive model should be developed in order to simulate the actual behaviour of the winged caisson in loose sand under cyclic loading.

Chapter 5

5. HYBRID TRIPOD SUCTION CAISSON (RESULTS)

This chapter presents the results of the monotonic responses of the conventional and hybrid tripod caisson foundations based on the experimental test series and the numerical analyses, as discussed in the previous chapters, to examine the behaviour of the tripod hybrid foundation with different circular mats sizes and bucket spacing under pure overturning moment.

The results of this chapter have been published by the author in a journal paper: Koohyar Faizi, Asaad Faramarzi, Samir Dirar, David Chapman. Investigating the monotonic behaviour of hybrid tripod suction bucket foundations for offshore wind towers in sand. Applied Ocean Research, Volume 89, August 2019, Pages 176-187.

5.1 Overturning moment

The experiments on the conventional foundations in the C1-C6 series (as listed in Table 3.9) were conducted under identical test conditions, including soil density, bucket aspect ratio (L/D=1.0) and type of loading, although bucket spacing (S) was varied from 90 mm to 165mm (see Table 3.9). The experiments H1-H4 were carried out on the hybrid tripod bucket foundations with circular mats of diameter 1.6 times larger than the bucket diameter (D'=120 mm) in the same sequence and under the same experimental conditions as the C1-C6 experiments. The remaining models in Table 3.9 (i.e. C7-C10, and H5-H14) refer to FE models that were created to identify the effect of different spacing and different mat size beyond those used in the experiments. All the experiments assigned odd numbers within the test IDs (e.g. C1,

C3, H1, H3) are for models subjected to a forward loading direction, while the even numbers (e.g. C2, C4, H2, H4) are for the models loaded in the backward direction.

The tripod foundation resists the overturning moment with the reaction generated in the windward and leeward bucket foundations acting in tension and compression, respectively (Byrne and Houlsby, 2003b; Senders, 2009). Based on the deformation mechanisms, observed in Figure 5.1, the overturning moment is resisted by a combination of tension and compression on the windward and leeward in both conventional and hybrid tripod foundations.

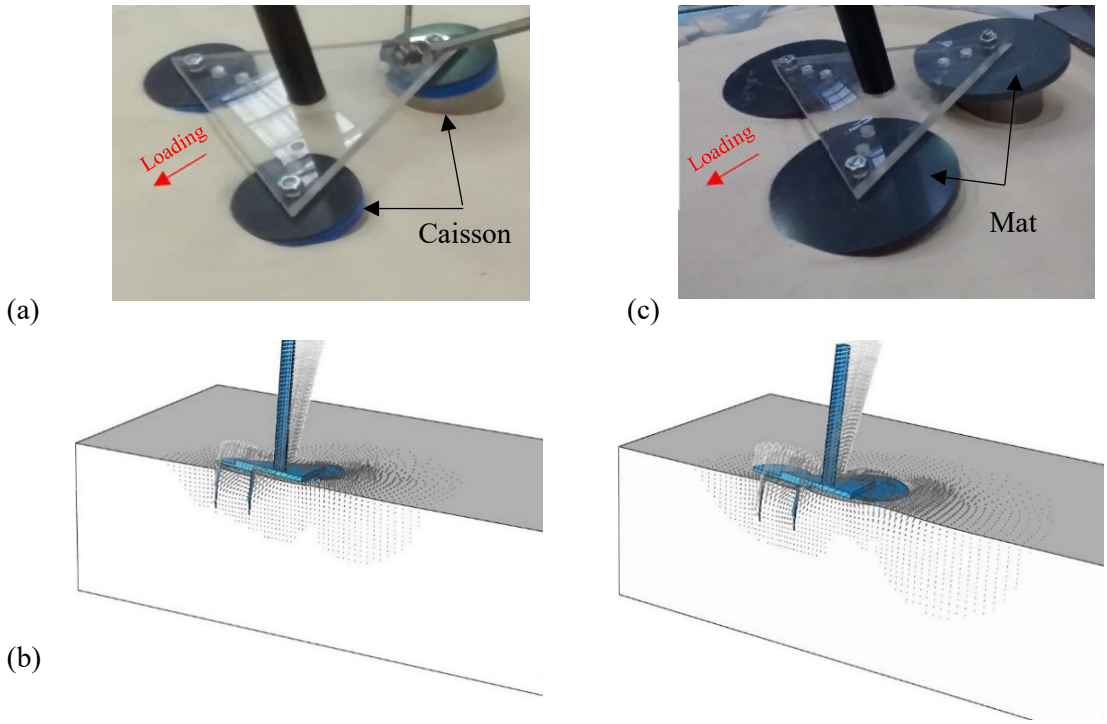

Figure 5.1. Failure mechanism due to an overturning moment in the forward direction, (a) EXP conventional foundation, (b) FEM conventional foundation, (c) EXP hybrid foundation, (d) FEM hybrid foundation

5.2 The effect of bucket spacing and loading direction on the capacity of conventional foundation (FEM and Exp. Modelling)

Initially, the impact of the bucket spacing on the overturning moment capacity of the conventional and hybrid tripod bucket foundations are examined. The experiments were performed by applying a monotonic horizontal load at the top of the tower, with an eccentricity from the top of the foundations (e = 230 mm). This load was applied until failure was reached. The numerical and experimental results have been compared based on the direction of the load and bucket spacing of both the conventional and hybrid tripod foundations. The comparison demonstrated that the numerical simulations provide very close results (<10% average error) to the experimental data (Figure 5.2-Figure 5.4).

As can be seen in Figure 5.2-Figure 5.4, the bearing capacity of the conventional tripod, due to an overturning moment, is higher when the foundations are subjected to the backward loading direction, i.e. the foundation with S=95 mm maintained an almost 18% higher capacity under backward loading compared with the experiments loaded in the forward direction (Figure 5.2).

The horizontal resistance of a tripod depends on the loading direction due to the asymmetry of the foundations (Kim et al., 2014). Previous studies have revealed that the capacity of tripod systems is primarily governed by the pull-out capacity of the windward bucket (Senders, 2009; Kim et al., 2014). It should also be noted, however, that the capacity of single suction buckets under pull-out is lower than in compression (Nabipour and Matin Nikoo, 2015). Hence, the number of windward buckets in the tripod foundation could control the overall capacity. Accordingly, the two windward buckets provide a higher capacity compared with the scenario where two buckets are in compression. Therefore, the most critical loading condition for tripods is when the horizontal loading is imposed in the forward direction (F), i.e. where one bucket of the tripod resists pull-out load, as shown in Figure 5.1. This observation for conventional tripod foundations is similar to that reported by Kim et al. (2014).

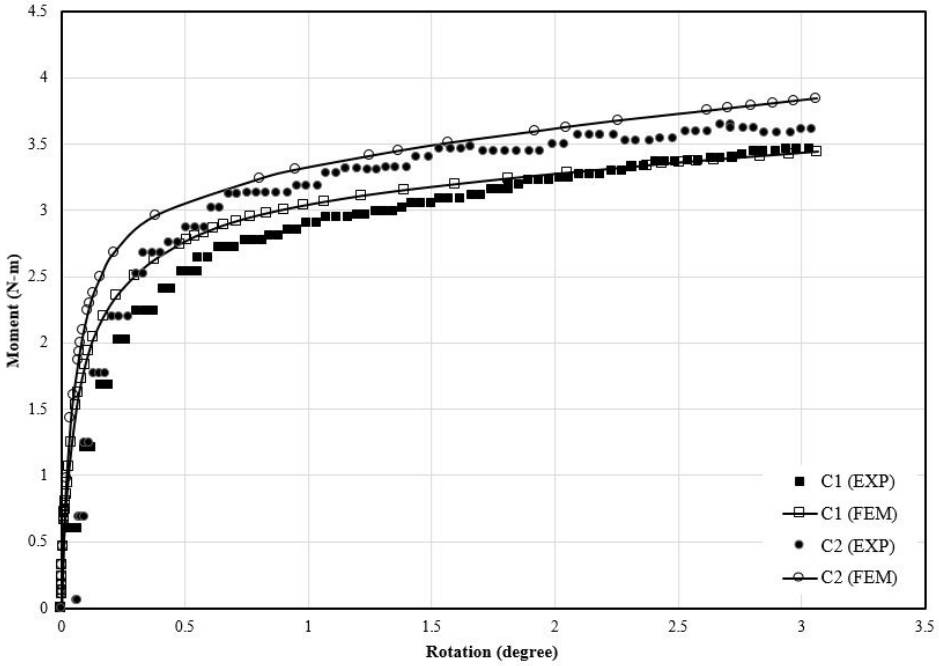

Figure 5.2. Moment-rotation plot for the conventional foundation system with a spacing dimension of 95 mm (EXP and FEM)

5.3 The effect of the hybrid system on the capacity improvement of tripod bucket foundations

The impact of using a hybrid system on the overturning capacity of a tripod bucket foundation is presented by means of a series of laboratory tests and numerical modelling. Comparing Figure 5.3 and Figure 5.4, it is clear that there is a significant increase in the overturning capacity provided by the hybrid tripod foundation. The test results show that the overturning capacity of the tripod bucket foundation, under the forward loading direction, was increased by approximately 47% and 45%, for bucket spacing of 130 mm and 165 mm, respectively (Figure 5.3 and Figure 5.4). For the same spacing, the ultimate overturning bearing capacity increased by approximately 43% and 38%, for the models under the backward loading direction.

Based on the results, it is evident that attaching circular mats can provide additional resistance compared to the original tripod foundation. The contact surfaces between the circular

mats and the seabed and the development of bearing stress beneath the mats provides a larger restoring moment to withstand the rotation. Moreover, the circular mats induce additional vertical stresses in the soil beneath the foundation, thereby helping to increase the shear resistance of the soil and further resisting rotation.

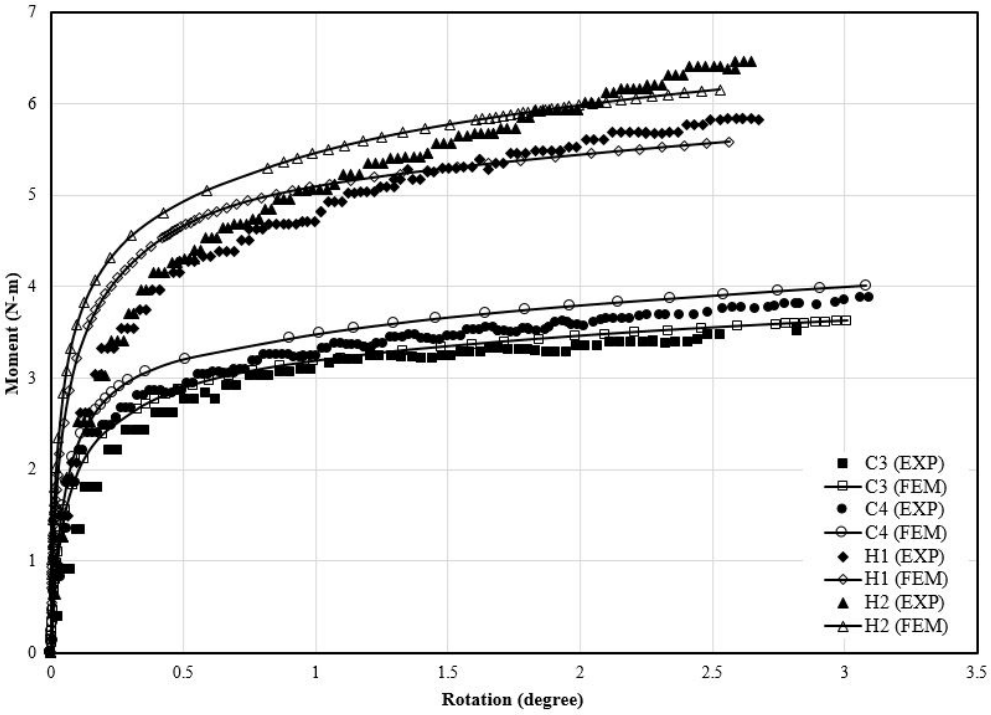

Figure 5.3. Moment-rotation plot for conventional and hybrid foundation systems with a bucket spacing of 130 mm (EXP and FEM)

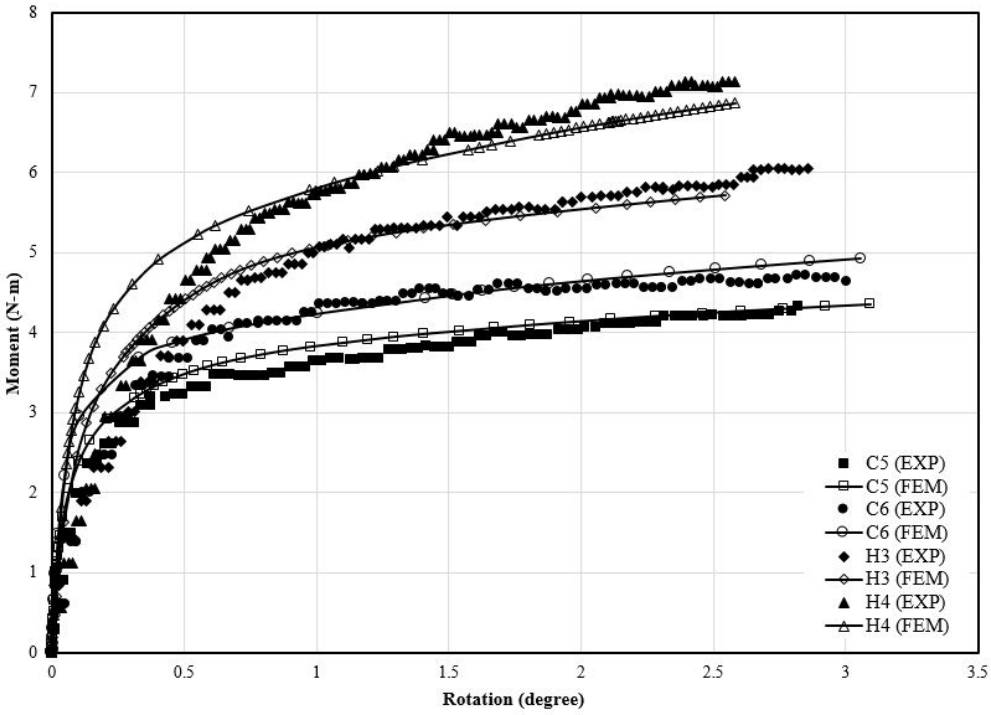

Figure 5.4. Moment-rotation plot for conventional and hybrid foundation systems with a bucket spacing of 165 mm (EXP and FEM)

5.4 The effect of bucket spacing size and mat diameter on the improvement of capacity of hybrid system (FEM)

The results from the three-dimensional finite element analyses (FEM) for the two tripod foundation models (with and without circular mats) are presented in Figure 5.5-Figure 5.7 in terms of the moment and rotation with varying circular mat diameters and bucket spacing.

A series of numerical models (C7, C8, H5 and H6) were performed in which the mat diameter was kept the same as those used in the previous models ($D' = 120\,mm$) while the bucket spacing was changed to $S = 200$ mm in order to evaluate the effect of higher spacing on the overturning moment resistance of the conventional and hybrid tripod foundations.

The moment-rotation ($M - \theta$) curves for the conventional and hybrid tripod models with diameter $D' = 120\,mm$ and spacing S = 200 mm installed in loose sand with relative density of Dr =23% are presented in Figure 5.5. The results from the FEM indicated that the

mats used in the proposed foundation have a significant impact on improving the overturning capacity. The mat aids the resisting force against the external load by extending the contact area. The results also showed that the overturning capacity of the tripod bucket foundation was increased by approximately 53%, and 47% for the hybrid bucket foundation, under F and B load conditions.

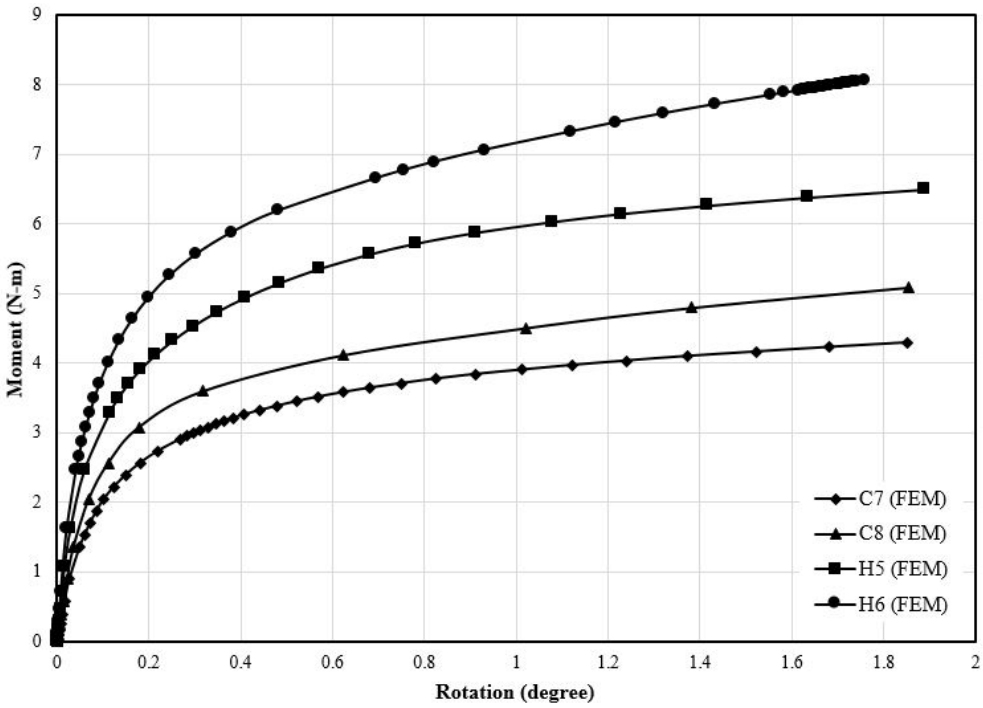

Figure 5.5. Comparison of the moment-rotation plots for conventional and hybrid foundations with a bucket spacing of 200 mm (FEM)

A FEM was also developed to investigate the effects of the mat diameter to improve the capacity of the hybrid tripod bucket foundations. The models C9, C10, H7, H8, H11, H12, H13 and H14 were selected with mat sizes both smaller and larger than those used in the reference models ($D' = 120\,mm$). When $\frac{S}{D}$ equals 3.13, the ultimate overturning bearing capacity increased by approximately 18%, 36% and 80% for hybrid tripod models under a backward loading system with mat diameter ratios ($\frac{D'}{D}$) equal to 1.3, 1.9 and 2.4, respectively (see Figure 5.6). However, it is worth noting that combining circular mats with the buckets results in a

slightly better overturning capacity under forward loading compared with backward loading. When $\frac{S}{D}$ equals 3.13, the ultimate overturning capacity increased by approximately 25%, 50%, and 100% for hybrid tripod models with mat diameter ratios ($\frac{D'}{D}$) of approximately 1.3, 1.9, and 2.4, respectively (Figure 5.7). Given the most unstable loading scenario is when the horizontal loading is imposed in the forward direction (F) (Kim et al., 2014), two circular mats attached to the two buckets at the leeward side provides higher resistance against overturning moments. This resistance corresponds to the larger contact surface areas between the circular mats, attached to the leeward buckets, and the seabed during the loading. In the forward direction, only the mat attached to the bucket at the leeward resists the horizontal load because the two other mats on the windward side are lifted from the soil surface when the whole foundation is rotating.

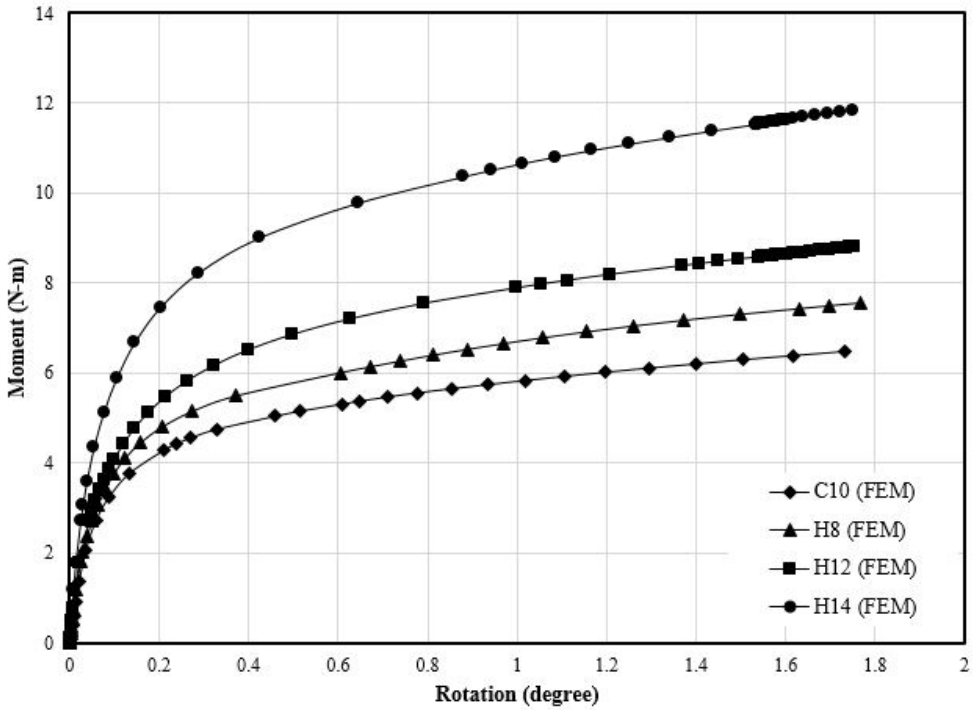

Figure 5.6. Comparison of the moment-rotation plots for conventional and hybrid foundations with a bucket spacing of 235 mm and varying circular mat sizes, due to a backward loading direction (FEM)

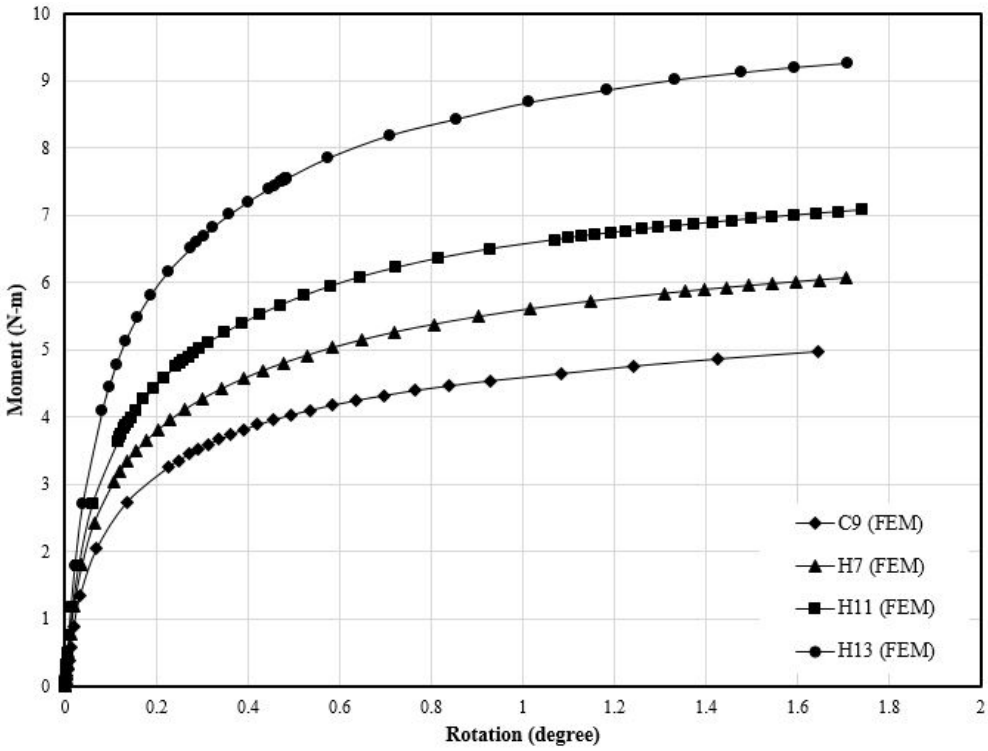

Figure 5.7. Comparison of the moment-rotation plots for conventional and hybrid foundations with a bucket spacing of 235 mm and varying circular mat sizes, due to a forward loading direction (FEM)

Figure 5.8 illustrates the variation in M_u with the normalized footing spacing S/D for the conventional (C1, C2, C3, C4, C5, C7, C8, C9, and C10) and hybrid tripod (H1, H2, H3, H4, H5, H6, H9, and H10) foundations under the forward and backward loading directions. The hybrid models are enhanced with the circular mat diameter of 120 mm. As expected, M_u increases significantly as S/D increases, which is due to the increase in the lever arm length with an increase in S/D. The bearing capacity of tripod bucket foundations is influenced by the spacing between the buckets because of their mutual interaction (Tran and Kim, 2017).

In general, the interactions in a hybrid tripod bucket foundation can be classified into two categories: the interaction between buckets (bucket–soil–bucket) and the interaction between mat and bucket (mat–soil–bucket). A close spacing between individual caissons in a tripod caisson results in overlapping stress zones.

Due to the larger surface area between the soil and the circular mats in the hybrid foundation, relatively large stress zones occur along the contact interface when the foundation system is subjected to an overturning moment. For hybrid tripod foundations, the overlap of the stress zones are even larger due to the presence of the mats. The intensity of the stresses will be affected by the centre-to-centre spacing of the buckets (Figure 5.9). In ABAQUS, PEMAG refers to the plastic strain magnitude. The plastic strain magnitude, PEMAG is defined as $\sqrt{\left(\frac{2}{3}\right)\varepsilon^{pl}:\varepsilon^{pl}}$, where ε^{pl}=plastic strain and the symbol (:) denotes a scalar product operation (Song, 2012).

Therefore, it can be concluded that the divergences in Figure 5.8 are due to the different overlapping stress zones, which can influence the capacity of the foundations.

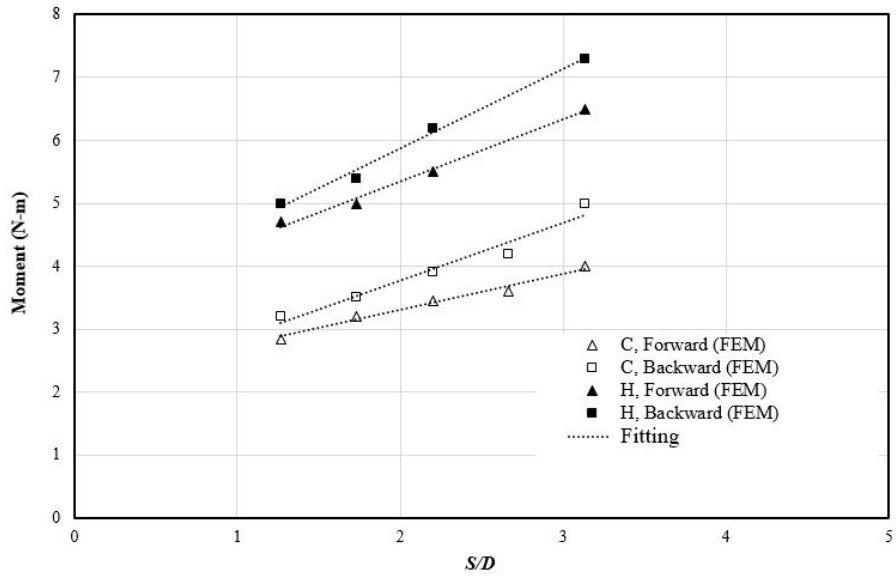

Figure 5.8. Variation of M_u with S/D for loading directions F and B (FEM)

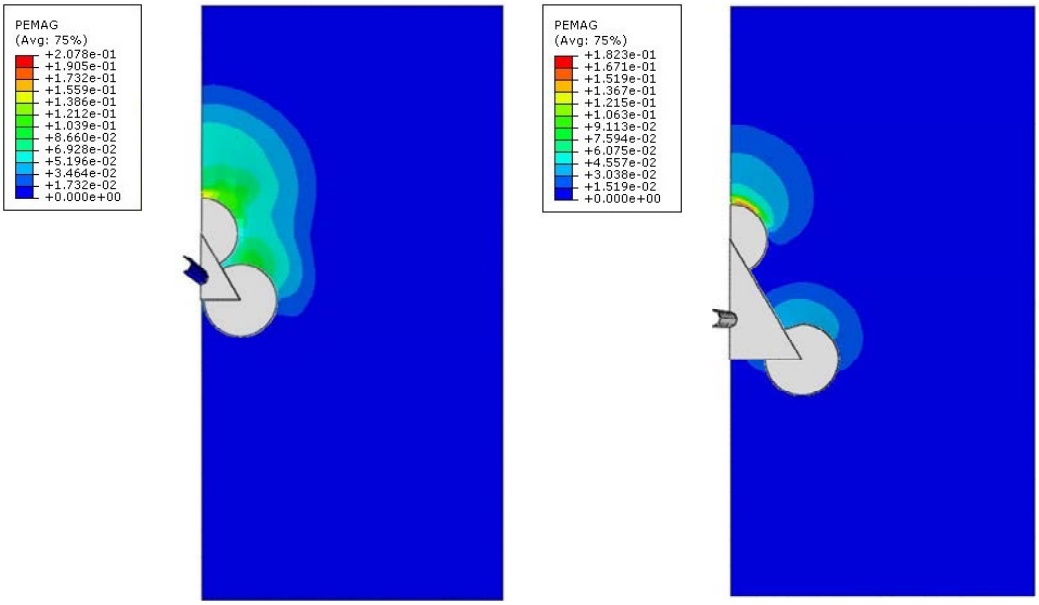

(a) (b)

Figure 5.9. Plan view of the shear zone formation in hybrid tripod foundations from the FEM results, (a) H2, (b) H10

Three caisson models of conventional model, hybrid models with $D' = 100\,mm$ and $D' = 142.5\,mm$ were examined under forward and backward loading in terms of stress distribution along the skirts and circular mats utilising FE method (Figure 5.10).

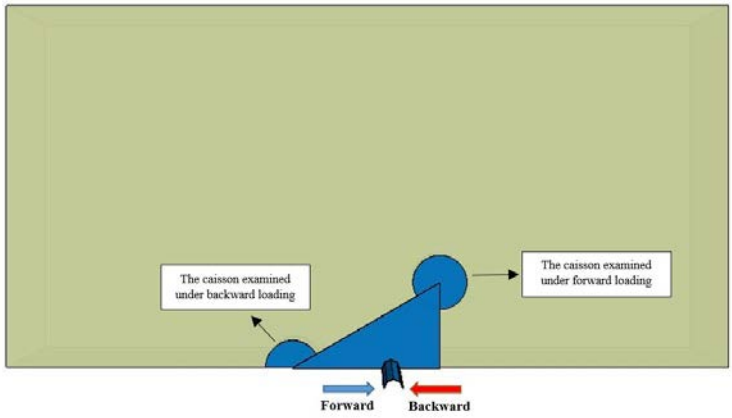

(a)

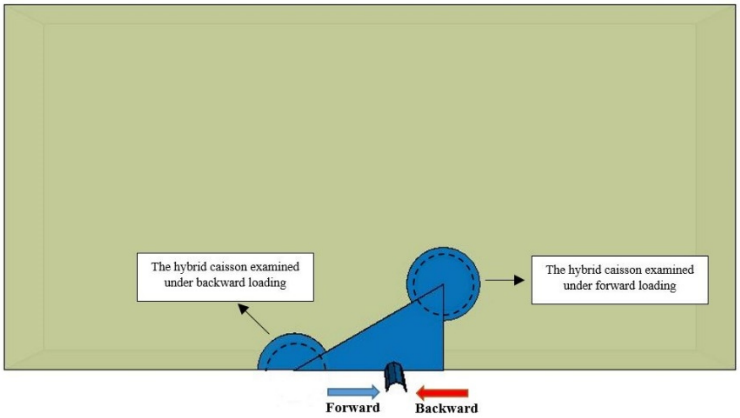

(b)

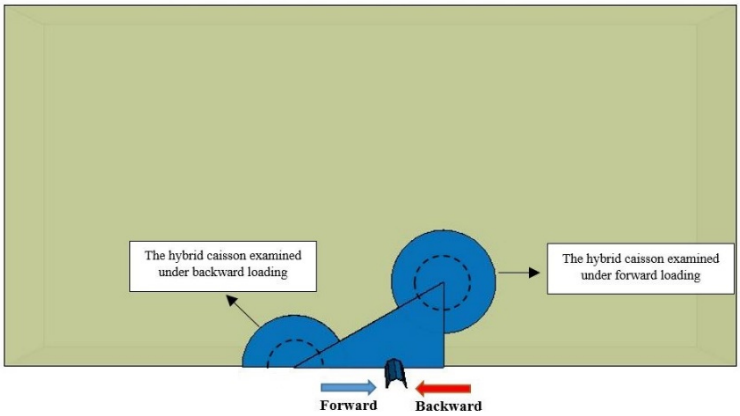

(c)

Figure 5.10. Plan view of the FE models; a) C9, C10; b) H7, H8; c) H11, H12

Contour of the 'Mid principal stress' distributions along the skirts and circular mats for the models of C9, H7, and H11 under forward loading are shown in Figure 5.11. The stress distribution for the model of C10, H8, and H12 under backward loading are also shown in

Figure 5.12. As can be seen from the figures (Figure 5.11 and Figure 5.12), the contribution of circular mat into the capacity during lateral loading increases by increasing the mat sizes.

Max Principal stress = *Max* (σ_1, σ_2, σ_3)

Min Principal stress = *Min* (σ_1, σ_2, σ_3)

Mid Principal Stress = *A-Max-Min*

$A = \sigma_1 + \sigma_2 + \sigma_3$

The maximum local stress occurred at the skirt tip for the simple tripod caisson in both direction i.e. forward and backward (Figure 5.11a and Figure 5.12a). However, the maximum stress point moves from the skirt tip (inside) toward the edge of the circular mat in the hybrid caisson foundations with larger circular mat (Figures Figure 5.11c and Figure 5.12c).

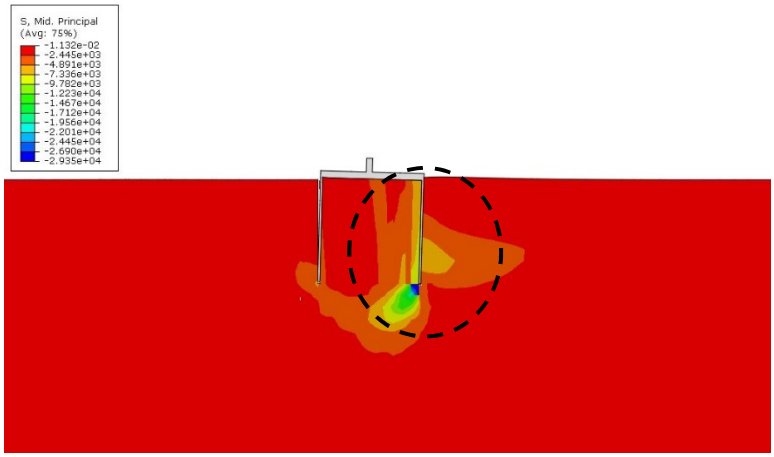

(a)

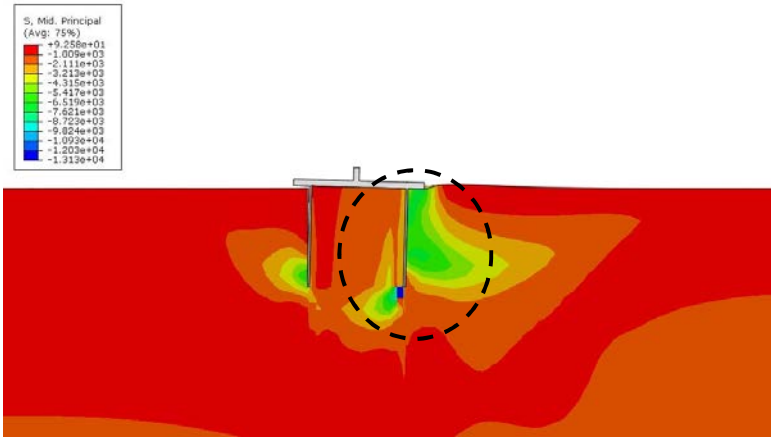

(b)

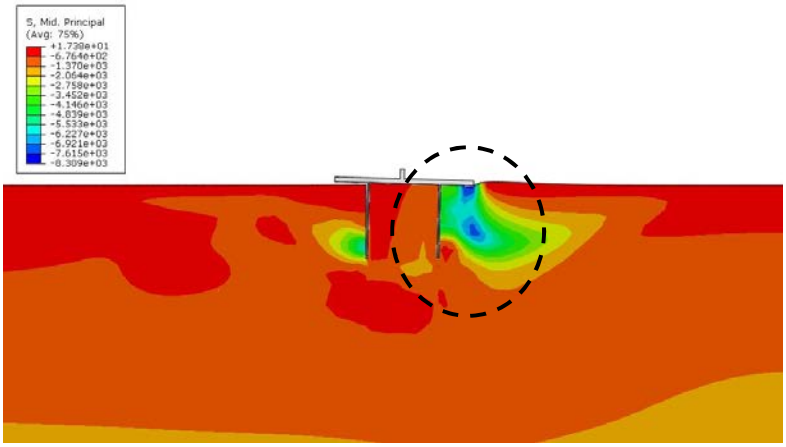

(c)

Figure 5.11. Stress distribution (N/m^2) for the caissons under the forward loading, at rotation degree of 2.5; a) C9, b) H7, c) H11

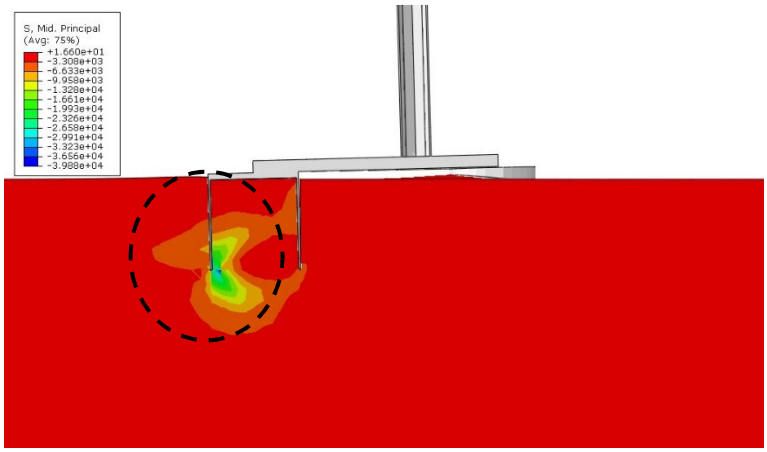

(a)

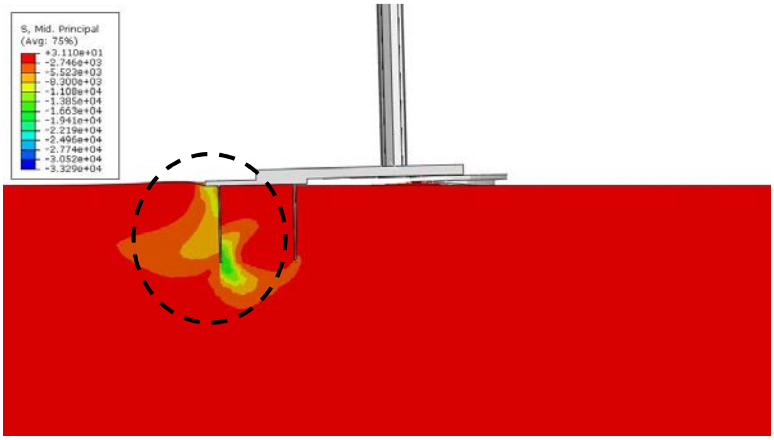

(b)

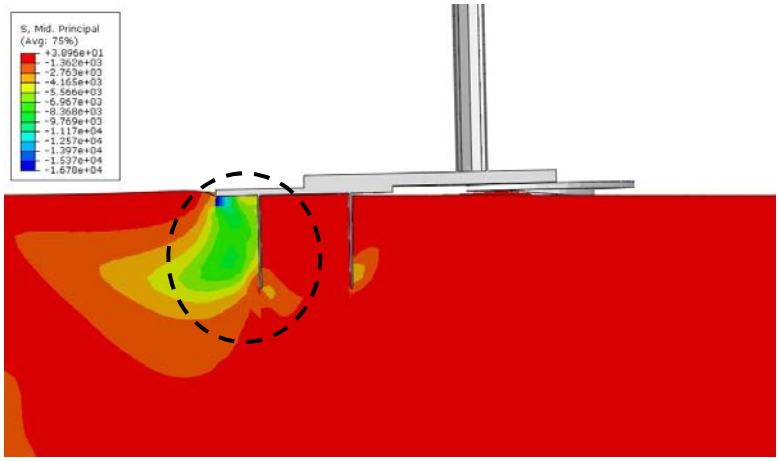

(c)

Figure 5.12. Stress distribution (N/m^2) for the caissons under the backward loading, at rotation degree of 2.5; a) C10, b) H8, c) H12

5.4.1 FE modelling of large-scale hybrid tripod foundation

The validated FE model was subsequently used to predict the overturning capacity of a hypothetical full-size tripod foundation ($L/D = 1.0$), with three caissons of diameter 2 m, circular mats of diameter 1.9 times larger than the bucket diameter (D'=3.8 m) and spacing S = 6.3 m under a constant vertical load of 37.3 kN. The soil parameters and loading condition were adopted from Houlsby et al. (2005a). Conventional and hybrid tripod foundations were modelled and the improvement in overturning moment under forward and backward loading conditions were recorded. Assuming the maximum allowable tilting angle of the foundation must be smaller than 0.25 degree (Bhattacharya, 2014b; Wang et al., 2018b), the results are presented in terms of maximum allowable tile at foundation head (Figure 5.13).

Based on the results from numerical analysis, the allowable overturning bearing capacity for the foundation with mat diameter ratios ($\frac{D'}{D}$) equal to 1.9, increased by approximately 27%, and 30% under a forward and backward loading systems, respectively (see Figure 5.13).

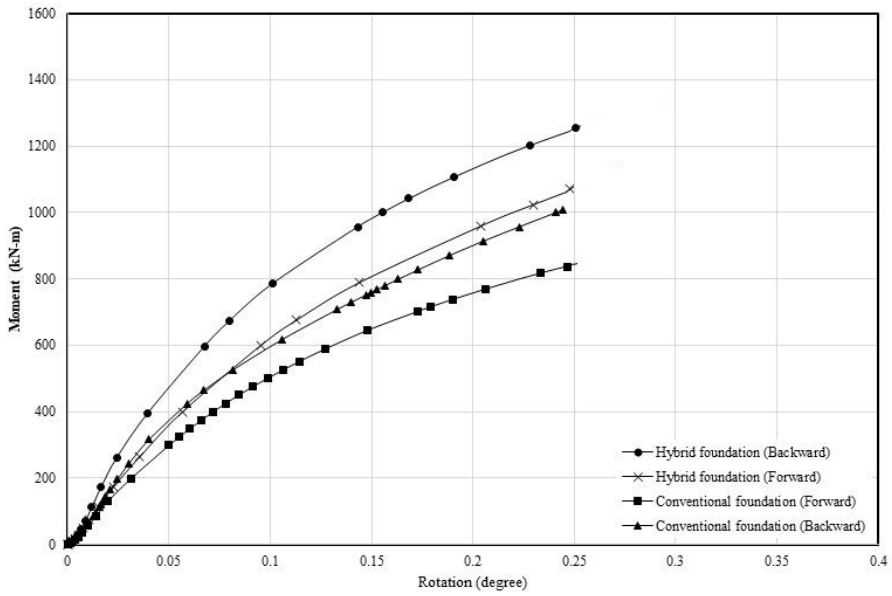

Figure 5.13. Comparison of the moment-rotation plots for the conventional and hybrid foundations with a bucket spacing of 6.3 m and circular mat size of 3.8 m, due to a forward and backward loading direction (FEM)

It is clear from the experiments and the FEM studies that there are benefits of using circular mats in combination with buckets to enhance the overall capacity of tripod suction bucket foundations. Manufacturing and installation of a conventional tripod foundation (with large diameter), and often with large spacing between individual caissons, is usually involves high costs; the hybrid tripod foundation can provide cost effective solution for offshore wind turbines.

Waves and currents can cause erosion in areas with sandy seabed around a fixed structure, a phenomena called scour (Stuyts et al., 2013). Local scour around the OWTs foundations can significantly reduce the bearing capacity. Scour is more important for caisson foundations, since they are relatively shallow, than for piles. There are, however, also several methods to minimise scour around the foundation such as rock-dumping (Houlsby et al., 2005). As scour can occur very rapidly, the self-protection is a beneficial. Therefore, the circular mat foundation attached to the caissons can be used at the three caissons of the tripod foundation ensure that the caissons protect from the scour.

Furthermore, circular mats can provide a base for applying surcharges in a tripod system. The surcharges acting on the circular mats can improve the performance of the hybrid tripod foundation. Similar advantage has been proposed in the footing-pile foundation (Anastasopoulos and Theofilou, 2016).

5.4.2 Mesh sizes

As with many forms of numerical modelling, the mesh size may affect the results and the run-time in FE analysis. A certain level of refinement produces a suitable mesh resulting acceptable results for most simulations. However, it is always good practice to perform a mesh convergence study, where we simulate the same problem with a finer mesh and compare the

results. We can have confidence that our model is producing a mathematically accurate solution if the two meshes give essentially the same result.

The number of elements in the FEM models was varied from 41330 to 61863for the models of simple and hybrid tripod modes. From a convergence study with the tripod caissons (model H2) the mesh containing elements gives a good approximation to the experimental results compared with 10961 elements.

Two different meshes were used for the model H2 in ABAQUS to assess the sensitivity of the results to mesh refinement: a coarse mesh with 25947 elements, and fine mesh with 41330 elements. Both have similar results in prediction of Moment-rotation curve.

This mesh was used in this research for simulations on the conventional and winged caisson models are shown in Chapter 3.

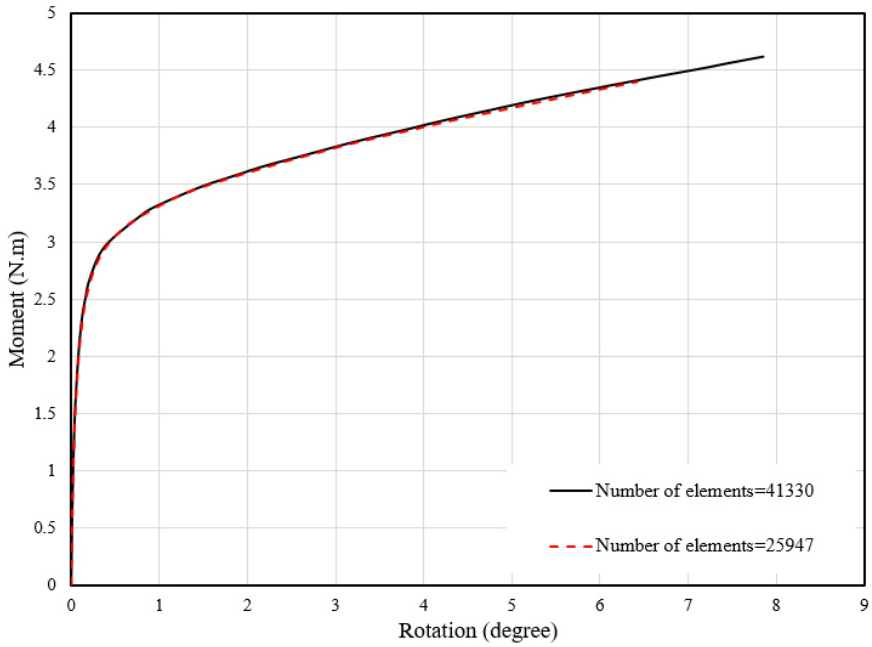

Figure 5.14. Results from overturning moment study of the simple tripod suction caisson foundation H2, with different mesh coarseness

Chapter 6

6. CONCLUSIONS AND RECOMMENDATIONS FOR FURTHER RESEARCH

6.1 Conclusions

In this thesis, numerical and experimental investigations have been carried out to evaluate the overturning capacity and performance of innovative foundation systems for offshore wind turbines, namely the 'winged suction caisson' foundation and the 'tripod hybrid bucket' foundation. The test models and the FE studies indicate the benefits of using wings to enhance the overall overturning capacity of monopod suction caisson foundations. The hybrid system proposed for the tripod caisson foundation is capable of increasing the serviceability and capacity requirements. Hence, the original Aim of this research to evaluate the performance of these innovative foundation systems was achieved. This is demonstrated in more detail in the remainder of this section.

Despite the advantages of suction caissons, such as simpler manufacturing and transportation, easier installation and removal, lower foundation cost compared with other conventional foundations (e.g. pile foundations) conventional suction caisson foundations may not provide the overturning capacity required for the new generation of OWTs.

To help overcome this issue, a novel hybrid caisson foundation, i.e. a winged caisson foundation, was proposed in the present study with the intention to improve overturning capacity of caisson foundations typically used for OWTs. The behaviour of winged caissons subjected to an overturning moment, horizontal cyclic loading, and combined loads in drained sand with different densities was investigated using 1-g experimental studies, centrifuge tests

and three-dimensional nonlinear FE analyses. The results obtained from the experimental and numerical studies were used to validate the FE modelling and to assess the suitability and possible benefits of using winged caisson foundations at large-scale.

Furthermore, a method based on force equilibrium analysis to predict the ultimate horizontal capacity of the conventional suction caisson in sand was also proposed. The proposed theoretical solution assumes simplified earth pressure distributions on the caisson. An equation was also developed in the current study to estimate the ultimate moment capacity of winged foundations with full length wings in cohesionless soil, based on a theoretical formula proposed by Villalobos (2006) for a conventional caisson foundation, and calibrated based on the results of centrifuge tests.

Based on the experimental, numerical and analytical results, the following key conclusions can be drawn:

- Suction caissons combined with four wings provide considerably higher overturning capacity under monotonic loading conditions compared with a reference (conventional) caisson (between 15–75% depending on the size of the wings).
- The monotonic overturning capacity improvement depends greatly on the width of the wings and this is enhanced by increasing the width as a ratio of the caisson diameter ($\%D$). Wings are very effective in improving the ultimate overturning capacity of the suction caisson embedded in loose sand ($Dr = 23 - 25\%$), while in medium sand ($Dr = 48 - 50\%$), the wings results in a relatively smaller amount of improvement on the overturning moment. The recorded enhancement in capacity due to the wing attachments ($T = 0.2D - 0.4D$) is approximately 24–68% for loose sand, whilst for the medium dense sand this ranges from 15 to 62%.

- For different aspect ratios of suction caisson (L/D), the wing efficiency increases with an increase in wing width. This increase varies from a linear to exponential relationship depending on the embedment ratio (L/D) of the caisson. Overall, the embedment ratio (L/D) has a relatively minor influence on the wing efficiency. An approximate range of capacity improvement due to the wing attachments ($T = 0.4D$) used for suction caisson foundations with aspect ratios of 0.5, 1.0 and 1.5 are 54%, 68%, and 75%, respectively.
- The overturning capacity improvement depends significantly on the full height of the wings, which is at its maximum when extended to the tip. The improvement drops by about 50% when the wing height is 0.75 of the length of the caisson.
- The results of FE modelling showed that, the allowable overturning bearing capacity for the winged foundation with T equal to 40% of D, increased by approximately 66%.
- It is always encouraged to consider more than two wings to resist lateral loads, as the lateral load may act in any direction in practice. The results of FE modelling showed that, winged caisson, reinforced with four wings, provide higher overturning capacity in loose sand, compared with three wings (10%). However, load's orientation has a minor impact on the monotonic overturning capacity of the caisson for both winged caissons with three and four wings (< 4%).
- The impact of the combined loading ($V - H - M$) on the capacity of the conventional and winged caissons were investigated. Under a combined loading regime, the capacity of the foundations increases with increasing vertical load.
- The cyclic overturning capacity increases by approximately 33% for the models under cyclic loading compared with the monotonic loading condition. The cyclic capacity

of the conventional and winged caissons installed in loose sand increases gradually with increasing the number of cycles and amplitude.

- Wings are very effective in improving the ultimate cyclic overturning capacity of the suction caisson embedded in loose sand. A significant increase in overturning capacity due to the wing attachments ($T = 0.4D$) was observed in loose sand under cyclic loading. This was approximately 40% and 50% for caissons with aspect ratios of $\frac{L}{D} = 0.5$ and 1.0, respectively.
- The experimental results show that the secant stiffness of the foundation using winged caisson with $T = 0.4D$, under the cyclic loading, was increased by approximately 28%, 40%, and 50% in horizontal strains of $0.012D$, $0.038D$, and $0.077D$, respectively.
- The FE analyses agreed well with those measured in the 1-g experimental and the centrifuge tests.
- Based on the proposed analytical solution, the variation in peak pressure distribution along the length of caisson can be idealized as a linear increase up to 0.8x (where x=the distance to the point of rotation) in the passive zone. The pressure then decreases linearly until it reduces to zero at depth of x. Below x, the net soil pressure is in the opposite direction and increases linearly from zero at depth x, to a maximum at the tip of the caisson.
- The results using the proposed analytical solution showed that the proposed method can predict the ultimate overturning capacity of suction caisson foundation in sand more accurately than the conventional analytical method (error < 20%).
- The effectiveness of the vertical load on the horizontal load capacity of the caisson foundation was identified by means of an analytical equation. The analysis showed

that there was a substantial increase in horizontal load capacity with an increase in the vertical load (V) for a suction caisson foundation embedded in cohesionless soil. Increasing the vertical load is very effective in increasing the ultimate horizontal load capacity of the suction caisson if the eccentricity of the horizontal load is equal or close to zero.

For offshore wind farms located on sandy soil seabeds and in shallow water, single footing foundations have the potential advantage of quicker and simpler construction. In deep water, foundations such as the tripod foundation are more popular. However, using a tripod foundation with large buckets and a big bucket spacing may not be cost effective. Therefore, a novel hybrid tripod bucket foundation has been proposed in the present study with the intention of improving the overturning capacity of bucket foundations typically designed for offshore wind turbines. The behaviour of conventional and 'hybrid tripod bucket' foundations subjected to an overturning moment with different bucket spacing and circular mat sizes has been investigated using 1-g experimental studies and three-dimensional nonlinear FEM analyses in dry loose sand under drained condition.

The results obtained from the experimental and numerical studies were compared to validate the FEM and to assess the suitability and possible benefits of using hybrid tripod bucket foundations. Based on the results, the following key conclusions can be drawn:

- Tripod foundations combined with three circular mats provides considerably higher overturning capacity compared with a conventional tripod foundation (between 25–100% depending on the diameter of the circular mats and the spacing of the buckets).
- The overturning capacity of the conventional and the hybrid tripod bucket foundations is influenced by the loading direction, where higher capacity is usually achieved under

backward loading, i.e. where the loading direction is towards a single bucket of a tripod foundation and the other two buckets are being rotated out of the seabed.

- The overturning capacity of the conventional and the hybrid tripod bucket foundations depends greatly on the centre-to-centre distance between the buckets and the direction of the load. In general, the overturning capacity increases as the bucket spacing increases.
- The contribution of the circular mat to the capacity is more pronounced by increasing the mat size.

Despite the issue of scale effects, this study provides a useful basis for future research using centrifuge or full-scale models, leading to an increased understanding of real winged caisson and hybrid tripod bucket foundations behaviour under overturning and combined loads.

6.2 Recommendations for further research

Based on the knowledge and experience gained from the research presented in this thesis, the following directions for future work are suggested.

The overturning capacity of the winged caisson was investigated in sand with relative densities (Dr) of 23-25% and 48-50%. However, suction caissons may be installed in a sand with higher relative density, e.g. 90%. Further experiments are necessary to describe the complete influence of the relative density on the overturning capacity of the winged caissons.

As the stress-strain behaviour of sandy soil is complicated and will depend on a number of factors including the initial soil conditions (e.g. density, moisture content, grading, plasticity) and the type and rate of loading, it would be useful to examine the cyclic responses of the winged caissons and hybrid tripod foundations via FE method with the view to developing a

suitable constitutive model. Currently, the available models are unable to cope with all these conditions.

In the FE simulations, the foundations were assumed ‘wished in place’, where the stress and density state after the installation process was not included in the analysis. However, in order to accurately capture the stress and strain conditions, the installation stage should be incorporated into the analysis.

In the present study, drained conditions have been assumed for the experiments, however the models should also be examined under partially drained or undrained conditions. Suction caissons may be installed in a variety of soils, therefore the effectiveness of wings and circular mats in the proposed foundations installed in different soil types should also be investigated. Further studies are also necessary in order to include the installation process of the winged caisson foundations and the factors that may influence the process.

Foundations of offshore wind turbines experience cyclic lateral loading which varies in amplitude and frequency. Understanding and predicting the proposed response of the foundations to various cyclic lateral loading is necessary for optimised the design, as it can lead to permanent foundation rotation and the evolution of the foundation’s dynamic response. In addition, this loading is multidirectional in nature because cyclic loading induced by wind and waves offshore are not necessarily coincident. Hence, further investigations are needed to examine the proposed foundations under various biaxial cyclic loading.

The research efforts in this thesis were directed toward developing novel foundations systems for OWT designs, however the structural aspects of the proposed foundations were neglected. Future research should address potential structural issues associated with the proposed foundations, as these are often more pronounced at full-scale.

References

ABDEL-RAHMAN, K. & ACHMUS, M. Behavior of foundation piles for offshore wind energy plants under axial cyclic loading. Proceedings of Simulia Customer Conference, 2011.

ABDELKADER, A. M. R. 2015. Investigation of Hybrid Foundation System for Offshore Wind Turbine.

ACHMUS, M., AKDAG, C. & THIEKEN, K. 2013. Load-bearing behavior of suction bucket foundations in sand. *Applied Ocean Research,* 43**,** 157-165.

ACHMUS, M. & THIEKEN, K. 2010. On the behavior of piles in non-cohesive soil under combined horizontal and vertical loading. *Acta Geotechnica,* 5**,** 199-210.

AHMADI, M. & GHAZAVI, M. Effect of Skirt Geometry Variation on Uplift Capacity of Skirted Foundation. The Twenty-second International Offshore and Polar Engineering Conference, 2012. International Society of Offshore and Polar Engineers.

AHMED, S. S., HAWLADER, B. & ROY, K. Finite Element Modeling of Large Diameter Monopiles in Dense Sand for Offshore Wind Turbine Foundations. ASME 2015 34th International Conference on Ocean, Offshore and Arctic Engineering, 2015. American Society of Mechanical Engineers, V001T10A009-V001T10A009.

AHMED, S. S. & HAWLADER, B. C. 2015. Numerical analysis of inclined uplift capacity of suction caisson in sand. *International Journal of Offshore and Polar Engineering,* 25**,** 145-155.

AL-DEFAE, A., CAUCIS, K. & KNAPPETT, J. J. G. 2013. Aftershocks and the whole-life seismic performance of granular slopes. 63**,** 1230.

ALEJANO, L. R. & BOBET, A. 2012. Drucker–prager criterion. *The ISRM Suggested Methods for Rock Characterization, Testing and Monitoring: 2007-2014.* Springer.

ANASTASOPOULOS, D. L., CHALKIAS, A., IAKOVIDOU, N. & XANTHOS, T. 2016. Effect of cardiac pacing on sleep-related breathing disorders: a systematic review. *Heart Fail Rev,* 21**,** 579-90.

ANASTASOPOULOS, I. & THEOFILOU, M. 2016. Hybrid foundation for offshore wind turbines: Environmental and seismic loading. *Soil Dynamics and Earthquake Engineering,* 80**,** 192-209.

ANDRESEN, L., PETTER JOSTAD, H. & ANDERSEN, K. H. 2010. Finite element analyses applied in design of foundations and anchors for offshore structures. *International Journal of Geomechanics,* 11**,** 417-430.

API, R. 2011. 2GEO Geotechnical and foundation design considerations. *American Petroleum Institute, Washington, DC, USA, page120*.

ARROYO, M., ABADIAS, D., ALCOVERRO, J. & GENS, A. 2013. Shallow foundations for offshore wind towers. *Proc. 18th ICSMGE*.

ARSHAD, M. & O'KELLY, B. C. 2013a. Offshore wind-turbine structures: a review. *Proceedings of the Institution of Civil Engineers-Energy,* 166**,** 139-152.

ARSHAD, M. & O'KELLY, B. C. J. P. O. T. I. O. C. E.-E. 2013b. Offshore wind-turbine structures: a review. 166**,** 139-152.

ARSHI, S. 2016. *Physical and numerical modelling of hybrid monopiled-footing foundation systems.* University of Brighton.

BAGHERI, P., SON, S. W. & KIM, J. M. 2017. Investigation of the load-bearing capacity of suction caissons used for offshore wind turbines. *Applied Ocean Research,* 67**,** 148-161.

BAKMAR, C. L., AHLE, K., NIELSEN, S. A. & IBSEN, L. B. The Monopod Bucket Foundation: recent experiences and challenges ahead. The European Offshore Wind Conference & Exhibition, 2009. European Offshore Wind Conference 2009.

BANG, S., JONES, K., CHO, Y. & KWAG, D. J. D. J.-T. J. O. T. D. F. I. 2009. Suction Piles and Suction Anchors for Offshore Structures. 3**,** 3-13.

BANG, S., JONES, K., KIM, K., KIM, Y. & CHO, Y. 2011. Inclined loading capacity of suction piles in sand. *Ocean Engineering,* 38**,** 915-924.

BARARI, A., IBSEN, L. B., TAGHAVI GHALESARI, A. & LARSEN, K. A. 2016. Embedment effects on vertical bearing capacity of offshore bucket foundations on cohesionless soil. *International Journal of Geomechanics,* 17**,** 04016110.
BASSI, S., BOWEN, A., FANKHAUSER, S. J. G. R. I. O. C. C. & ENVIRONMENT POLICY BRIEF, L. 2012. The case for and against onshore wind energy in the UK.
BENTO, N., FONTES, M. J. R. & REVIEWS, S. E. 2019. Emergence of floating offshore wind energy: Technology and industry. 99**,** 66-82.
BHATTACHARYA, S. 2014a. Challenges in design of foundations for offshore wind turbines. *Engineering & Technology Reference,* 1.
BHATTACHARYA, S. 2014b. Challenges in design of foundations for offshore wind turbines. *Engineering & Technology Reference,* 1**,** 1-9.
BHATTACHARYA, S., NIKITAS, N., GARNSEY, J., ALEXANDER, N., COX, J., LOMBARDI, D., WOOD, D. M., NASH, D. F. J. S. D. & ENGINEERING, E. 2013. Observed dynamic soil–structure interaction in scale testing of offshore wind turbine foundations. 54**,** 47-60.
BIENEN, B., GAUDIN, C., CASSIDY, M. J., RAUSCH, L., PURWANA, O. A. & KRISDANI, H. 2012. Numerical modelling of a hybrid skirted foundation under combined loading. *Computers and Geotechnics,* 45**,** 127-139.
BOONYONG, S., PARK, K. C. & KIM, I. C. 2015. Analytical Parametric Study on Pullout Capacity of Embedded Suction Anchors. *Journal of Korean Society of Coastal and Ocean Engineers,* 27**,** 182-189.
BRANSBY, M. & RANDOLPH, M. 1998. Combined loading of skirted foundations. *Géotechnique,* 48**,** 637-655.
BRIAUD, J. L., SMITH, T. & MEYER, B. Using the pressuremeter curve to design laterally loaded piles. Offshore Technology Conference, 1983. Offshore Technology Conference.
BUTTERFIELD, S., MUSIAL, W., JONKMAN, J. & SCLAVOUNOS, P. 2007. Engineering challenges for floating offshore wind turbines. National Renewable Energy Laboratory (NREL), Golden, CO.
BYRNE, B. & HOULSBY, G. 2003a. Foundations for offshore wind turbines. *Philosophical Transactions of the Royal Society of London A: Mathematical, Physical and Engineering Sciences,* 361**,** 2909-2930.
BYRNE, B. & HOULSBY, G. 2003b. Foundations for offshore wind turbines. *Philosophical Transactions: Mathematical, Physical and Engineering Sciences***,** 2909-2930.
BYRNE, B. & HOULSBY, G. Assessing novel foundation options for offshore wind turbines. World maritime technology conference, 2006. London:[sn].
BYRNE, B. & HOULSBY, G. 2015. Helical piles: an innovative foundation design option for offshore wind turbines. *Phil. Trans. R. Soc. A,* 373**,** 20140081.
BYRNE, B., HOULSBY, G., MARTIN, C. & FISH, P. 2002. Suction caisson foundations for offshore wind turbines. *Wind Engineering,* 26**,** 145-155.
BYRNE, B., MCADAM, R., BURD, H., HOULSBY, G., MARTIN, C., ZDRAVKOVIC, L., TABORDA, D., POTTS, D., JARDINE, R. & SIDERI, M. New design methods for large diameter piles under lateral loading for offshore wind applications. 3rd International Symposium on Frontiers in Offshore Geotechnics (ISFOG 2015), Oslo, Norway, June, 2015. 10-12.
BYRNE, B., VILLALOBOS, F., HOULSBY, G. & MARTIN, C. Laboratory testing of shallow skirted foundations in sand. Proc. British Geotechnical Association Int. Conf. on Foundations, Dundee, 2, 2003a. 161-173.
BYRNE, B., VILLALOBOS, F., HOULSBY, G. & MARTIN, C. Laboratory testing of shallow skirted foundations in sand. Proc. Int. Conf. on Foundations, 2003b. 161-173.
BYRNE, B. W. 2000. *Investigations of suction caissons in dense sand.* University of Oxford Oxford, UK.
BYRNE, B. W. & HOULSBY, G. T. 2004. Experimental investigations of the response of suction caissons to transient combined loading. *Journal of geotechnical and geoenvironmental engineering,* 130**,** 240-253.

BYRNE, B. W., HOULSBY, G. T. J. J. O. G. & ENGINEERING, G. 2004. Experimental investigations of the response of suction caissons to transient combined loading. 130**,** 240-253.
CELESTINO, V.-M., JORGE, S.-M., ALFONSO, S.-S., CARLOS, G.-N. & GILBERTO, O.-R. 2019. Numerical evaluation of the combined capacity of suction caissons of subsea systems for deep water hydrocarbon exploitation Evaluación numérica de la capacidad de carga combinada de pilotes de succión de sistemas submarinos para explotación de hidrocarburos en aguas profundas. *IngenIería InvestIgacIón y tecnología,* 20**,** 1-10.
CHATZIVASILEIOU, G. 2014. Installation of suction caissons in layered sand: Assessment of geotechnical aspects.
CHENG, N., GAUDIN, C., CASSIDY, M. & BIENEN, B. Centrifuge study of the combined bearing capacity of a hybrid foundation system. ICPMG2014–Physical Modelling in Geotechnics: Proceedings of the 8th International Conference on Physical Modelling in Geotechnics, 2014. CRC Press, Boca Raton, FL, USA, 487-492.
CIAMPI, V. 1997. MA Crisfield, Non-linear Finite Element Analysis of Solids and Structures. *Meccanica,* 32**,** 586-587.
COLLIAT, J.-L., BOISARD, P., GRAMET, J.-C. & SPARREVIK, P. Design and installation of suction anchor piles at a soft clay site in the Gulf of Guinea. Offshore Technology Conference, 1996. Offshore Technology Conference.
COTTER, O. 2010. *Installation of suction caisson foundations for offshore renewable energy structures.* Oxford University.
CUÉLLAR, P. 2011. Pile foundations for offshore wind turbines: Numerical and experimental investigations on the behaviour under short-term and long-term cyclic loading.
CUÉLLAR, P., GEORGI, S., BAEßLER, M. & RÜCKER, W. J. G. M. 2012. On the quasi-static granular convective flow and sand densification around pile foundations under cyclic lateral loading. 14**,** 11-25.
DEB, T. K. & SINGH, B. 2018. Response and capacity of monopod caisson foundation under eccentric lateral loads. *Marine Georesources & Geotechnology,* 36**,** 452-464.
DIMMOCK, P., CLUKEY, E., RANDOLPH, M., MURFF, D. & GAUDIN, C. 2013. Hybrid subsea foundations for subsea equipment. *Journal of Geotechnical and Geoenvironmental Engineering,* 139**,** 2182-2192.
DING, H., LI, Z., LIAN, J., ZHANG, P. & HUANG, X. 2012. Soil reinforcement experiment inside large-scale bucket foundation in muddy soil. *Transactions of Tianjin University,* 18**,** 168-172.
DNV-OS-C502 2010. Offshore Concrete Structures - Rules and standards.
DNV 1992. DNV Classification Note 30.4: Foundations.
DNV 2013. DNV-OS-J101 - Rules and standards.
DNV, G. 2004a. DNV-OS-J101–Design of offshore wind turbine structures. *DNV GL*.
DNV, G. 2016. Support structures for wind turbines. *Standard DNV GL-ST-0126*.
DNV, O. S. D.-O. 2004b. J101: Design of Offshore Wind Turbine Structures. *Det Norske Veritas*.
DTI 2007. STUDY OF THE COSTS OF OFFSHORE WIND GENERATION. *A Report to the Renewables.*
DUAN, N. 2016. *Mechanical characteristics of monopile foundation in sand for offshore wind turbine.* UCL (University College London).
DÜHRKOP, J., GRABE, J., BIENEN, B., WHITE, D. & RANDOLPH, M. Centrifuge experiments on laterally loaded piles with wings. Vol. 2, Proceedings of International Conference on Physical Modelling in Geotechnics (ICPMG), 2010. 919-924.
DÜHRKOP, J. & GRABE, J. R. Design of laterally loaded piles with bulge. Proceedings of 28th International Conference on Ocean, Offshore and Artic Engineering. electronically published under No. OMAE2009-79087, 2009.
EL-MARASSI, M. 2011. Investigation of hybrid monopile-footing foundation systems subjected to combined loading.
EMREN, V., HUVAJ, N. & TUNCAY, K. 2017. Three-Dimensional Finite Element Modeling for Spudcan Penetration into a Clayey Seabed. *Geotechnical Frontiers 2017.*

ESTEBAN, M., COUÑAGO, B., LÓPEZ-GUTIÉRREZ, J., NEGRO, V. & VELLISCO, F. 2015. Gravity based support structures for offshore wind turbine generators: Review of the installation process. *Ocean Engineering,* 110**,** 281-291.
EUROPE 2018a. Annual combined onshoreand offshore wind energy statistics. Wind Europe.
EUROPE, W. 2017. The European offshore wind industry—Key trends and statistics 2016. *Wind Europe: Brussels, Belgium***,** 37.
EUROPE, W. 2018b. Offshore Wind in Europe–Key trends and statistics 2017. *Via Internet (10.10. 2018)< https://windeurope. org/wp-content/uploads/files/about-wind/statistics/WindEurope-Annual-Offshore-Statistics-2017. pdf.*
FAIZI, K., ARMAGHANI, D. J., SOHAEI, H., RASHID, A. S. A. & NAZIR, R. 2015. Deformation model of sand around short piles under pullout test. *Measurement,* 63**,** 110-119.
FD-003 2007. Design regulations on subgrade and foundation for wind turbine generator system.
FISCHER, T. 2011. Executive Summary–UpWind Project. WP4: Offshore Foundations and Support Structures. See http://www. upwind. eu/pdf/WP4_Executive_Summary_Final. pdf .
FOGLIA, A. 2011a. *Behaviour of Bucket Foundations under Horizontal Load in Dense Sand.*
FOGLIA, A. 2011b. Behaviour of Monopod Bucket Foundations Under Horizontal Load in Dense Sand.
FOGLIA, A., GOTTARDI, G., GOVONI, L. & IBSEN, L. B. J. A. O. R. 2015. Modelling the drained response of bucket foundations for offshore wind turbines under general monotonic and cyclic loading. 52**,** 80-91.
FOGLIA, A., KOHLMEIER, M. & WEFER, M. 2016. Physical modeling and numerical analyses of vibro-driven piles with evaluation of their applicability for offshore wind turbine support structures. *Proc nord geotech meet*.
FRANKE, E. & MUTH, G. 1985. SCALE EFFECT IN 1G-MODEL TESTS ON HORIZONTALLY LOADED PILES. PROCEEDINGS OF THE ELEVENTH INTERNATIONAL CONFERENCE ON SOIL MECHANICS AND FOUNDATION ENGINEERING, SAN FRANCISCO, 12-16 AUGUST 1985. *Publication of: Balkema (AA)*.
FU, D., BIENEN, B., GAUDIN, C. & CASSIDY, M. 2014. Undrained capacity of a hybrid subsea skirted mat with caissons under combined loading. *Canadian Geotechnical Journal,* 51**,** 934-949.
FUGRO CONSULTANTS, I. 2016. Effects of Cyclic Loading on Suction Bucket Foundations for Offshore Wind Turbines. FUGRO CONSULTANTS, INC.
GAUDIN, C., MOHR, H., CASSIDY, M. J., BIENEN, B. & PURWANA, O. A. Centrifuge experiments of a hybrid foundation under combined loading. The Twenty-first International Offshore and Polar Engineering Conference, 2011. International Society of Offshore and Polar Engineers.
GONZÁLEZ, J. Z. 2017. *Suction Bucket lid plate design and welding automation.* MasterThesis Project, Aalborg University.
GOURVENEC, S. & JENSEN, K. 2009. Effect of embedment and spacing of cojoined skirted foundation systems on undrained limit states under general loading. *International Journal of Geomechanics,* 9**,** 267-279.
GREEN, R. & VASILAKOS, N. J. E. P. 2011. The economics of offshore wind. 39**,** 496-502.
GWEC 2019. GLOBAL WIND REPORT 2018. GWEC.
HAIGH, S. 2013. Foundations for offshore wind turbines. *ICPMG2014? Physical Modelling in Geotechnics***,** 153-159.
HAJI, T. K. 2017. *Evaluating the effects of tunnel construction on buildings.* University of Nottingham.
HARIRECHE, O., MEHRAVAR, M. & ALANI, A. M. 2013. Suction caisson installation in sand with isotropic permeability varying with depth. *Applied Ocean Research,* 43**,** 256-263.
HETTLER, A. 1981. *Verschiebung Starrer und Elastischer GriindungskOrper in Sand bei Monotoner und Zyklischer Belastung.* Ver" oentlichungen des hastitutes Rir Bodenmechanik und Felsmechanik der Universitait Fridericiana in Karlsruhe, Deutsch-land.

HOSSAIN, M., ZHENG, J. & HUSTON, A. 2015. Effect of spudcan geometry on penetration and extraction resistance in clay. *Géotechnique,* 65**,** 147-154.
HOSSAIN, M. S. & RANDOLPH, M. F. 2009. New mechanism-based design approach for spudcan foundations on single layer clay. *Journal of Geotechnical and Geoenvironmental Engineering,* 135**,** 1264-1274.
HOULSBY, G. 2016. Interactions in offshore foundation design.
HOULSBY, G. & BYRNE, B. 2004. Calculation procedures for installation of suction caissons. *Report No. OUEL2268/04, University of Oxford*.
HOULSBY, G. T. & BYRNE, B. W. 2000. Suction caisson foundations for offshore wind turbines and anemometer masts. *Wind engineering,* 24**,** 249-255.
HOULSBY, G. T. & BYRNE, B. W. 2005a. Design procedures for installation of suction caissons in clay and other materials. *Proceedings of the Institution of Civil Engineers-Geotechnical Engineering,* 158**,** 75-82.
HOULSBY, G. T. & BYRNE, B. W. 2005b. Design procedures for installation of suction caissons in sand. *Proceedings of the Institution of Civil Engineers-Geotechnical Engineering,* 158**,** 135-144.
HOULSBY, G. T., IBSEN, L. B. & BYRNE, B. W. 2005. Suction caissons for wind turbines. *Frontiers in Offshore Geotechnics: ISFOG, Perth, WA, Australia***,** 75-93.
HOULSBY, G. T. A. B., B.W. 2000. Suction caisson foundations for offshore wind turbines and anemometer masts *Journal of Wind Energy* 24**,** 249-255.

IBSEN, L. B., BARARI, A. & LARSEN, K. A. 2012. Modified vertical bearing capacity for circular foundations in sand using reduced friction angle. *Ocean Engineering,* 47**,** 1-6.
ICE 2010. IEC-Design Requirements for Offshore Wind Turbines. *Wind Turbines- Part 3:*.
IRENA 2018. Offshore wind investment, policies and job creation. Halifax, Canada.
ISO-19901-4:2016(EN) 2016. Petroleum and natural gas industries — Specific requirements for offshore structures — Part 4: Geotechnical and foundation design considerations.
JAKY, I. 1944. The coefficient of earth pressure at rest. *Journal Soc. of Hungarian Architects and Engineers***,** 355-358.
JENSEN, K., PETERSEN, S. & PEDERSEN, R. European offshore wind engineering–past, present and future. Proceedings of the Institution of Civil Engineers-Civil Engineering, 2018. Thomas Telford Ltd, 1-30.
JIN, S., YANG, Y. & ZHANG, Y. 2014. Bucket group effect of the composite multi-bucket structure. *Journal of Marine Science and Application,* 13**,** 62-66.
KÅBERGER, T. J. G. E. I. 2018. Progress of renewable electricity replacing fossil fuels. 1**,** 48-52.
KELLY, R., BYRNE, B., HOULSBY, G. & MARTIN, C. Tensile loading of model caisson foundations for structures on sand. The Fourteenth International Offshore and Polar Engineering Conference, 2004. International Society of Offshore and Polar Engineers.
KELLY, R., HOULSBY, G. T. & BYRNE, B. 2006. Transient vertical loading of model suction caissons in a pressure chamber. *Géotechnique,* 56**,** 665-675.
KENNEDY, J., OLIPHANT, J., MACONOCHIE, A., STUYTS, B. & CATHIE, D. Suction anchor geotechnical design practice: A case study. Frontiers in Offshore Geotechnics III: Proceedings of the 3rd International Symposium on Frontiers in Offshore Geotechnics (ISFOG 2015), 2015. Taylor & Francis Books Ltd, 283-288.
KIM, D.-J., CHOO, Y. W., KIM, J.-H., KIM, S. & KIM, D.-S. 2014. Investigation of monotonic and cyclic behavior of tripod suction bucket foundations for offshore wind towers using centrifuge modeling. *Journal of Geotechnical and Geoenvironmental Engineering,* 140**,** 04014008.
KIM, D.-J., CHOO, Y. W., LEE, J.-S., KIM, D.-S., JEE, S.-H., CHOI, J., LEE, M.-S. & PARK, Y.-H. Numerical Analysis of Cluster and Monopod Suction Bucket Foundation. ASME 2013 32nd International Conference on Ocean, Offshore and Arctic Engineering, 2013. American Society of Mechanical Engineers, V006T10A022-V006T10A022.
KIM, D., CHOO, Y. W., PARK, J. H. & KWAK, K. 2016a. Review of offshore monopile design for wind turbine towers. *Japanese Geotechnical Society Special Publication,* 4**,** 158-162.

KIM, J. H., KIM, S., KIM, D. S., YOUN, J. U., KIM, D. J. & JEE, S. H. 2016b. Bearing capacity of hybrid suction foundation on sand with loading direction via centrifuge model test. *Japanese Geotechnical Society Special Publication,* 2**,** 1339-1342.
KIM, S.-R. 2014. Evaluation of combined horizontal-moment bearing capacities of tripod bucket foundations in undrained clay. *Ocean Engineering,* 85**,** 100-109.
KIM, S.-R. & OH, M. 2014. Group effect on bearing capacities of tripod bucket foundations in undrained clay. *Ocean Engineering,* 79**,** 1-9.
KIM, S. R. 2012. Evaluation of vertical and horizontal bearing capacities of bucket foundations in clay. *Ocean Engineering,* 52**,** 75-82.
KOPP, D. R. 2010. *Foundations for an offshore wind turbine.* MSc Thesis, Massachusetts Institute of Technology.
KOURKOULIS, R., LEKKAKIS, P., GELAGOTI, F. & KAYNIA, A. 2014. Suction caisson foundations for offshore wind turbines subjected to wave and earthquake loading: effect of soil-foundation interface. *Géotechnique,* 64**,** 171.
KUHN, M. R. 2005. Scaling in granular materials. *Powders and grains,* 1**,** 115-122.
KUMAR, N. D. & RAO, S. N. 2010. Earth pressures on caissons in marine clay under lateral loads—A laboratory study. *Applied Ocean Research,* 32**,** 58-70.
KUO, Y., ACHMUS, M. & ABDEL-RAHMAN, K. 2009. Estimation of lateral deformation of monopile foundations by use of cyclic triaxial tests. *Chin. J. Geotech. Eng,* 31**,** 1729-1734.
LARSEN, K. A. 2008a. Static behaviour of bucket foundations. *DCE Thesis, Department of Civil Engineering, Aalborg University, Denmark*.
LARSEN, K. A. J. D. T., DEPARTMENT OF CIVIL ENGINEERING, AALBORG UNIVERSITY, DENMARK 2008b. Static behaviour of bucket foundations.
LARSEN, P. Suction anchors as an anchoring system for floating, offshore constructions. Offshore Technology Conference, 1989. Offshore Technology Conference.
LEBLANC, C., HOULSBY, G. & BYRNE, B. 2010. Response of stiff piles in sand to long-term cyclic lateral loading. *Geotechnique,* 60**,** 79-90.
LEHANE, B., PEDRAM, B., DOHERTY, J. & POWRIE, W. 2014. Improved performance of monopiles when combined with footings for tower foundations in sand. *Journal of Geotechnical and Geoenvironmental Engineering,* 140**,** 04014027.
LEHANE, B., POWRIE, W. & DOHERTY, J. Centrifuge model tests on piled footings in clay for offshore wind turbines. Proceedings of International Conference in Physical Modelling in Geotechnics, ICPMG2010. Rotterdam: Balkema, 2010.
LI, D., FENG, L. & ZHANG, Y. 2014. Model tests of modified suction caissons in marine sand under monotonic lateral combined loading. *Applied Ocean Research,* 48**,** 137-147.
LI, D., ZHANG, Y., FENG, L. & GAO, Y. 2015. Capacity of modified suction caissons in marine sand under static horizontal loading. *Ocean Engineering,* 102**,** 1-16.
LIANG, T., KNAPPETT, J. & DUCKETT, N. J. G. 2015. Modelling the seismic performance of rooted slopes from individual root–soil interaction to global slope behaviour. 65**,** 995-1009.
LOMBARDI, D., BHATTACHARYA, S. & NIKITAS, G. 2017. Physical Modeling of Offshore Wind Turbine Model for Prediction of Prototype Response. *Wind Energy Engineering.* Elsevier.
LOMBARDI, D., BHATTACHARYA, S. & WOOD, D. M. 2013. Dynamic soil–structure interaction of monopile supported wind turbines in cohesive soil. *Soil Dynamics and Earthquake Engineering,* 49**,** 165-180.
LOMBARDI, D., COX, J. A. & BHATTACHARYA, S. 2011. Long-term performance of offshore wind turbines supported on monopiles and suction caissons.
LORC. 2013. *LORC, Lindoe Offshore Renewables Center* [Online]. [Accessed].
LUND, H. 2014. *Renewable energy systems: a smart energy systems approach to the choice and modeling of 100% renewable solutions*, Academic Press.
MALHOTRA, S. 2010. Design and construction considerations for offshore wind turbine foundations in North America. *GeoFlorida 2010: Advances in Analysis, Modeling & Design.*

MALHOTRA, S. 2011. Selection, design and construction of offshore wind turbine foundations. *Wind turbines.* IntechOpen.
MANA, D. S., GOURVENEC, S. & MARTIN, C. M. 2012. Critical skirt spacing for shallow foundations under general loading. *Journal of geotechnical and geoenvironmental engineering,* 139**,** 1554-1566.
MANSUR, C. I. & KAUFMAN, R. I. 1958. Pile tests, low-sill structure, Old River, Louisiana. *Transactions of the American Society of Civil Engineers,* 123**,** 715-743.
MANZOTTI, E., IBSEN, L. & VAITKUNAITE, E. 2014. Present knowledge about Laboratory Testing of Axial Loading on Suction Caissons.
MARDFEKRI, M., GARDONI, P. & ROESSET, J. M. J. J. O. E. 2013. Modeling laterally loaded single piles accounting for nonlinear soil-pile interactions. 2013.
MEHRAVAR, M., HARIRECHE, O. & FARAMARZI, A. 2016. Evaluation of undrained failure envelopes of caisson foundations under combined loading. *Applied Ocean Research,* 59**,** 129-137.
MEHRAVAR, M., HARIRECHE, O., FARAMARZI, A. & ALANI, A. M. 2017. Modelling the variation of suction pressure during caisson installation in sand using FLAC3D. *Ships and Offshore Structures,* 12**,** 893-899.
MITCHELL, J., HOUSTON, W., SCOTT, R., COSTES, N., CARRIER III, W. & BROMWELL, L. Mechanical properties of lunar soil: Density, porosity, cohesion and angle of internal friction. Lunar and Planetary Science Conference Proceedings, 1972. 3235.
MUSIAL, W., BEITER, P., SCHWABE, P., TIAN, T., STEHLY, T., SPITSEN, P., ROBERTSON, A. & GEVORGIAN, V. 2017. 2016 Offshore Wind Technologies Market Report. National Renewable Energy Laboratory (NREL), Golden, CO (United States).
MUSIAL, W., BUTTERFIELD, S. & RAM, B. 2006. Energy from offshore wind. National Renewable Energy Lab.(NREL), Golden, CO (United States).
NA, S., JANG, I., OH, M. & KWON, O. Numerical simulation of pullout behavior of embedded suction anchors in clay. Proceedings of the 7th International Conference on Asian and Pacific Coasts. Bali: Hasanuddin University Press, 2013. 860-865.
NABIPOUR, M. & MATIN NIKOO, H. 2015. An Investigation into the Pull-out Failure Mechanisms of Suction Caissons. *International Journal of Maritime Technology,* 4**,** 21-35.
NANDA, S., ARTHUR, I., SIVAKUMAR, V., DONOHUE, S., BRADSHAW, A., KELTAI, R., GAVIN, K., MACKINNON, P., RANKIN, B. & GLYNN, D. J. P. O. T. I. O. C. E.-G. E. 2017. Monopiles subjected to uni-and multi-lateral cyclic loading. 170**,** 246-258.
NASR, A. M. 2013. Experimental and theoretical studies of laterally loaded finned piles in sand. *Canadian Geotechnical Journal,* 51**,** 381-393.
NG, C. W. J. J. O. Z. U. S. A. 2014. The state-of-the-art centrifuge modelling of geotechnical problems at HKUST. 15**,** 1-21.
NGUYEN-SY, L. 2005. *The theoretical modelling of circular shallow foundation for offshore wind turbines.* DPhil, University of Oxford.
NIKITAS, G., BHATTACHARYA, S., VIMALAN, N., DEMIRCI, H. E., NIKITAS, N. & KUMAR, P. 2019. Wind power: A sustainable way to limit climate change. *Managing Global Warming.* Elsevier.
OGUNJUYIGBE, A., AYODELE, T. & BAMGBOJE, O. J. F. I. E. 2017. Optimal placement of wind turbines within a wind farm considering multi-directional wind speed using two-stage genetic algorithm. 1-16.
OLSON, R. E. & GILBERT, R. B. 2004. Suction Caissons: Model Tests. *Comprehensive Status Report: Nov*.
OVESEN, N. The use of physical models in design. Proceedings of the 7th European Conference on Soil Mechanics and Foundation Engineering, Brighton, 1979. 319-323.
OWUSU, P. A. & ASUMADU-SARKODIE, S. 2016. A review of renewable energy sources, sustainability issues and climate change mitigation. *Cogent Engineering,* 3**,** 1167990.
PEIRE, K., NONNEMAN, H. & BOSSCHEM, E. J. T. E. A. 2009. Gravity base foundations for the thornton bank offshore wind farm. 115**,** 19-29.

PENG, J.-R., ROUAINIA, M. & CLARKE, B. 2010. Finite element analysis of laterally loaded fin piles. *Computers & structures,* 88**,** 1239-1247.
PRASAD, Y. V. & CHARI, T. 1999. Lateral capacity of model rigid piles in cohesionless soils. *Soils and Foundations,* 39**,** 21-29.
RASCH, C. 2016. Modelling of cyclic soil degradation: Development of a cyclic accumulation model and the application to a gravity based foundation.
RASMUSSEN, K. L., HANSEN, M., WOLF, T. K., IBSEN, L. B. & ROESEN, H. R. 2013. A Literature Study on the Effects of Cyclic Lateral Loading of Monopiles in Cohesionless Soils. *Department of Civil Engineering, Aalborg University, DCE Technical Memorandum*.
SEED, H. B. A. I., I.M. 1970. Soil moduli and damping factors for dynamic response analysis. *Report No. UCB/EERC-70/10. University of California, Berkeley*.
SENDERS, M. 2009. *Suction caissons in sand as tripod foundations for offshore wind turbines*, University of Western Australia.
SHARP, E., DODDS, P., BARRETT, M. & SPATARU, C. J. R. E. 2015. Evaluating the accuracy of CFSR reanalysis hourly wind speed forecasts for the UK, using in situ measurements and geographical information. 77**,** 527-538.
SMITH, T. D. 1987. Pile horizontal soil modulus values. *Journal of Geotechnical Engineering,* 113**,** 1040-1044.
SNELL, R. O. & WISCH, D. J. ISO 19900 series: offshore structures standards. Offshore Technology Conference, 2008. Offshore Technology Conference.
SONG, A. 2012. *Deformation analysis of sand specimens using 3 D digital image correlation for the calibration of an elasto-plastic model*.
STERGIOU, T., TERZIS, D. & GEORGIADIS, K. 2015. Undrained bearing capacity of tripod skirted foundations under eccentric loading. *geotechnik,* 38**,** 17-27.
STUYTS, B., CATHIE, D. & XIE, Y. Scour assessment and measurements for pile-supported wind turbine foundations. ASME 2013 32nd International Conference on Ocean, Offshore and Arctic Engineering, 2013. American Society of Mechanical Engineers, V006T10A025-V006T10A025.
SUDAGAR, J., LIAN, J. & SHA, W. 2013. Electroless nickel, alloy, composite and nano coatings–A critical review. *Journal of Alloys and Compounds,* 571**,** 183-204.
SUKUMARAN, B., MCCARRON, W., JEANJEAN, P. & ABOUSEEDA, H. 1999. Efficient finite element techniques for limit analysis of suction caissons under lateral loads. *Computers and Geotechnics,* 24**,** 89-107.
SVANØ, G. & TJELTA, T. I. 1996. Skirted spud-cans—Extending operational depth and improving performance. *Marine structures,* 9**,** 129-148.
SWIFT, G. 2008. Geotechnical Design of an Offshore Gravity Base Structure.
TERZAGHI, K. 1943. Theoretical soil mechanics. John Wiley & Sons, New York. *Theoretical soil mechanics. John Wiley & Sons, New York.*, -.
THOMSON, R. C. & HARRISON, G. P. 2015. Life cycle costs and carbon emissions of offshore wind power. Citeseer.
TOPHAM, E. & MCMILLAN, D. 2017. Sustainable decommissioning of an offshore wind farm. *Renewable energy,* 102**,** 470-480.
TRAN, M. N., RANDOLPH, M. F. & AIREY, D. W. 2007. Installation of suction caissons in sand with silt layers. *Journal of Geotechnical and Geoenvironmental Engineering,* 133**,** 1183-1191.
TRAN, N. X. & KIM, S.-R. 2017. Evaluation of horizontal and moment bearing capacities of tripod bucket foundations in sand. *Ocean Engineering,* 140**,** 209-221.
UESUGI, M. & KISHIDA, H. 1986. Frictional resistance at yield between dry sand and mild steel. *Soils and foundations,* 26**,** 139-149.
VERDURE, L., GARNIER, J. & LEVACHER, D. 2003. Lateral cyclic loading of single piles in sand. *International journal of physical modelling in geotechnics,* 3**,** 17-28.
VERITAS, D. N. 2004. Design of Offshore Wind Turbine Structure. *Offshore Standard DNV-OS-J101*.

VERITAS, D. N. 2013. Design of floating wind turbine structures. *Offshore Standard DNV-OS-J103,* 5.
VILLALOBOS, F. A. 2006. *Model testing of foundations for offshore wind turbines.* University of Oxford.
VILLALOBOS, F. A., BYRNE, B. W. & HOULSBY, G. T. Moment loading of caissons installed in saturated sand. Proceedings of international symposium on frontiers in Geotechnics, ISFOG. University of Western, 2005. 411-16.
VILLALOBOS, F. A., HOULSBY, G. T. & BYRNE, B. W. Suction caisson foundations for offshore wind turbines. Proc. 5th Chilean Conference of Geotechnics (Congreso Chileno de Geotecnia), Santiago, 2004. 24-26.
VILLALOBOS J, F. 2006. *Model testing of foundations for offshore wind turbines.* University of Oxford.
VILLALOBOS JARA, F. A. 2006. *Model testing of foundations for offshore wind turbines.* University of Oxford.
VILLALOBOS.F 2007. Bearing Capacity of Skirted Foundations in Sand. *In VI Congreso Chileno de Geotecnia, Valparaiso.*
VULPE, C., BIENEN, B. & GAUDIN, C. 2013. Predicting the undrained capacity of skirted spudcans under combined loading. *Ocean Engineering,* 74**,** 178-188.
WANG, H., WANG, L. & HONG, Y. Centrifuge Study on the Lateral Loaded Response of the Monopod and Tripod Bucket Foundations in Sand. Vietnam Symposium on Advances in Offshore Engineering, 2018a. Springer, 428-433.
WANG, L., WANG, H., ZHU, B. & HONG, Y. 2018b. Comparison of monotonic and cyclic lateral response between monopod and tripod bucket foundations in medium dense sand. *Ocean Engineering,* 155**,** 88-105.
WANG, X., YANG, X. & ZENG, X. 2017. Lateral response of improved suction bucket foundation for offshore wind turbine in centrifuge modelling. *Ocean Engineering,* 141**,** 295-307.
WANG, X., ZENG, X., LI, J., YANG, X. & WANG, H. 2018c. A review on recent advancements of substructures for offshore wind turbines. *Energy Conversion and Management,* 158**,** 103-119.
WANG, X., ZENG, X., YANG, X. & LI, J. 2018d. Feasibility study of offshore wind turbines with hybrid monopile foundation based on centrifuge modeling. *Applied Energy,* 209**,** 127-139.
WATERS, L. B., MUELLER, C. V., HELLEN, P. C. & HURST, G. Design and Construction of Gravity Based Structure and Modularized LNG Tanks for the Adriatic LNG Terminal. International conference on liquefied natural gas, 2007.
WELSCHEN, Y. 2015. Suction bucket buckling: Buckling behaviour of suction buckets during installation in layered soils.
WESTGATE, Z. J. & DEJONG, J. T. 2005. Geotechnical considerations for offshore wind turbines. *Report for MTC OTC Project*.
YANG, X., ZENG, X. & WANG, X. J. I. J. O. G. 2018. Lateral-Moment Loading Capacity and Bearing Behavior of Suction Bucket Foundations for Offshore Wind Turbines in Sand. 18**,** 04018152.
YU, L.-Q., WANG, L.-Z., GUO, Z., BHATTACHARYA, S., NIKITAS, G., LI, L.-L., XING, Y.-L. J. T. & LETTERS, A. M. 2015. Long-term dynamic behavior of monopile supported offshore wind turbines in sand. 5**,** 80-84.
ZHANG, J., CHEN, Z. & LI, F. 2010. Three dimensional limit analysis of suction bucket foundations. *Ocean Engineering,* 37**,** 790-799.
ZHANG, P., DING, H., ZHAI, S. & XIONG, K. 2013. Test on muddy soil reinforcement by negative pressure and electro-osmosis inside cover-bearing-type bucket foundation for offshore wind turbines. *Transactions of Tianjin University,* 19**,** 10-16.
ZHANG, P., ZHANG, Z., LIU, Y. & DING, H. 2016a. Experimental Study on Installation of Composite Bucket Foundations for Offshore Wind Turbines in Silty Sand. *Journal of Offshore Mechanics and Arctic Engineering,* 138**,** 061901.
ZHANG, Y., LI, D. & GAO, Y. 2016b. Earth pressures on modified suction caisson in saturated sand under monotonic lateral loading. *Journal of Renewable and Sustainable Energy,* 8**,** 053312.

ZHANG, Y., LI, D., GAO, Y. J. J. O. R. & ENERGY, S. 2016c. Earth pressures on modified suction caisson in saturated sand under monotonic lateral loading. 8**,** 053312.
ZHU, B., BYRNE, B. & HOULSBY, G. 2012. Long-term lateral cyclic response of suction caisson foundations in sand. *Journal of Geotechnical and Geoenvironmental Engineering,* 139**,** 73-83.
ZHU, B., KONG, D.-Q., CHEN, R.-P., KONG, L.-G. & CHEN, Y.-M. 2011a. Installation and lateral loading tests of suction caissons in silt. *Canadian Geotechnical Journal,* 48**,** 1070-1084.
ZHU, B., KONG, D.-Q., CHEN, R.-P., KONG, L.-G. & CHEN, Y.-M. J. C. G. J. 2011b. Installation and lateral loading tests of suction caissons in silt. 48**,** 1070-1084.
ZHU, B., ZHANG, W.-L., YING, P.-P. & CHEN, Y.-M. 2014. Deflection-based bearing capacity of suction caisson foundations of offshore wind turbines. *Journal of Geotechnical and Geoenvironmental Engineering,* 140**,** 04014013.

APPENDICES

APPENDIX A

A. A list and a brief description of the equipment used in the experiments

The following equipment was used to perform the experiments (Figure A.1):

- The linear electric actuator with specification provided in Table A.1, with an electronic board (Speed Controller) were used to apply force on the system are shown in Figure A.1c.
- The DC Speed Controller for Actuators will allow you to control the speed of the actuator by turning a knob. This is achieved through increasing or decreasing the voltage that is going to the unit Figure A.1b.
- The inclinometer of LCP-45 – Dual Axis Inclinometer Sensor ±45°, was used in this experiment which is manufactured and calibrated in the UK factory of Level Developments Ltd. The general specification of the product is provided in Table A.2.
- A Micro Load Cell (0-5kg) - CZL635 with specification provided in Table A.3 was used to measure the forces (Figure A.1a). A simple formula, suggested by the company, was used to calibrate the load cell, as below:

To convert the measured mv/V output from the load cell to the measured force:

Measured Force = A * Measured mV/V + B (offset)

This load cell has a rated output of 1.0±0.15mv/v which corresponds to the sensor's capacity of 5kg. To find A we use

Capacity = A * Rated Output A = Capacity / Rated Output A = 5 / 1.0 A = 5

- Phidgets PhidgetBridge Wheatstone Bridge sensor interface, manufactured by RobotShop Inc., was connected to the load cell in order to acquire data. The Flow Botics App for Phidgets Wheatstone Bridge Sensor Interface (provided by RobotShop Inc.) was used to interface with

the Phidgets Wheatstone Bridge Sensor Interface board and read its load cell inputs (Figure A.1b).

Table A.1. Specifications of the linear actuator

Input voltage:	24V DC / 12V DC
Maximum Load:	6000N (Push) / 4000N (Pull)
Maximum Current (DC):	6 A @ 12 V and 3 A @ 24 V
Maximum Speed (No Load):	33.3 mm/s
Maximum Speed (Full Load):	2.9 mm/s @ 6000N
Stroke:	100 mm to 1600 mm
Duty Cycle:	10% or 2 minute continuous operation in a 20 minute cycle
Noise Level:	Less than 53dB
Adjustable limit switches	

Table A.2. Product specification of LCP-45 – Dual Axis Inclinometer Sensor

Parameter	Value	Unit
Number of Axis:	2	-
Range	±45	°
Resolution	0.1	°
Accuracy at 20°C	0.5	°
Output Type	RS232	-
Output Format	38.4, 8,1,n	-
Technology	MEMS	-
Maximum Zero Bias Error	±0.2	°
Uncompensated Temp Error	0.01	° / °C
Maximum Mechanical Shock	3000 (0.5ms), 10000 (0.1MS)	G
Frequency Response	1Hz	Hz

Table A.3. Product specification of Micro Load Cell (0-5kg) - CZL635

Mechanical	
Housing Material	Aluminum Alloy
Load Cell Type	Strain Gauge
Capacity	5kg
Dimensions	55.25x12.7x12.7mm
Mounting Holes	M5 (Screw Size)
Cable Length	550mm
Cable Size	30 AWG (0.2mm)
Cable - no. of leads	4
Electrical	
Precision	0.05%
Rated Output	1.0±0.15 mv/V
Non-Linearity	0.05% FS
Hysteresis	0.05% FS
Non-Repeatability	0.05% FS
Creep (per 30 minutes)	0.1% FS
Temperature Effect on Zero (per 10°C)	0.05% FS
Temperature Effect on Span (per 10°C)	0.05% FS
Zero Balance	±1.5% FS
Input Impedance	30±10 Ohm
Output Impedance	1000±10 Ohm
Insulation Resistance (Under 50VDC)	≥5000 MOhm
Excitation Voltage	5 VDC
Compensated Temperature Range	-10 to ~+40°C
Operating Temperature Range	-20 to ~+55°C
Safe Overload	120% Capacity
Ultimate Overload	150% Capacity

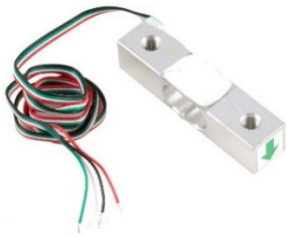

a) Micro Load Cell (0-5kg) - CZL635

b) Bridge Sensor Interface

c) 24v Linear Track Actuator Motor

d) DC Speed Controller for Actuators

Figure A.1. Equipment used in the experiments

APPENDIX B

B. Particle Image Velocimetry (PIV)

As mentioned earlier (Chapter 3), in order to derive an analytical equation for predicting lateral capacity of a caisson foundation in sand, a rotation point (RP) at ultimate load has been assumed. The location of RP has been validated via FE method and Particle Image Velocimetry (PIV) technique. The location of rotation point (RP) at ultimate load was confirmed by FEM in chapter 5. However, the results from the PIV are presented in this appendix.

From the FEM results, the centre of rotation of the caisson foundation at failure is located below the foundation level as the point along the vertical axis of the caisson 0.8 of the skirt length.

The PIV technique with half models of suction caisson foundations with two various embedment ratios $\frac{L}{D} = 0.5$, and 1 was used in this research to observe the rotation point (RP) at failure. The location of rotational point was compared with the results predicted by finite-element analysis.

The location of rotation point was confirmed by FEM (Figure B.1a, c, e) and PIV technique (Figure B.1b, d, f). PIV analysis was carried out with GeoPIV (White et al., 2003) on the selected images taken during the incremental displacement of the half-model foundation (L/D=0.5 and 1) for overturning tests. The PIV methodology is used to present the digital output as a series of velocity vectors to determine the soil failure mechanism during lateral loading (Faizi et al., 2015).

For the PIV tests, a plane strain chamber with observation window has been constructed in order to observe the soil deformation around the caisson models. A 12 mm thick Perspex window extended along the length of one side of the chamber. Half section model caissons with

L/D =0.5 and 1 were used for the PIV experiments. Along the caisson walls at the edge, a Teflon tape was placed to reduce friction between caissons and transparent sidewall. The soil type, soil preparation and experiment conditions were the same as those were described in section 2.

The greater displacement for analysis of the compression tests was adopted in order to ensure that failure had been reached in all cases. Typical images captured during the test for caissons with $L/D = 1$ and 0.5 are shown in Figure B.1c and e, respectively. From the results, the centre of rotation of the caisson foundation at failure is located below the foundation level as the point along the vertical axis of the caisson 0.8 of the skirt length. As the horizontal load increased, the rotation point began to move toward right hand and stop at right exterior side close to the skirt in the ultimate load.

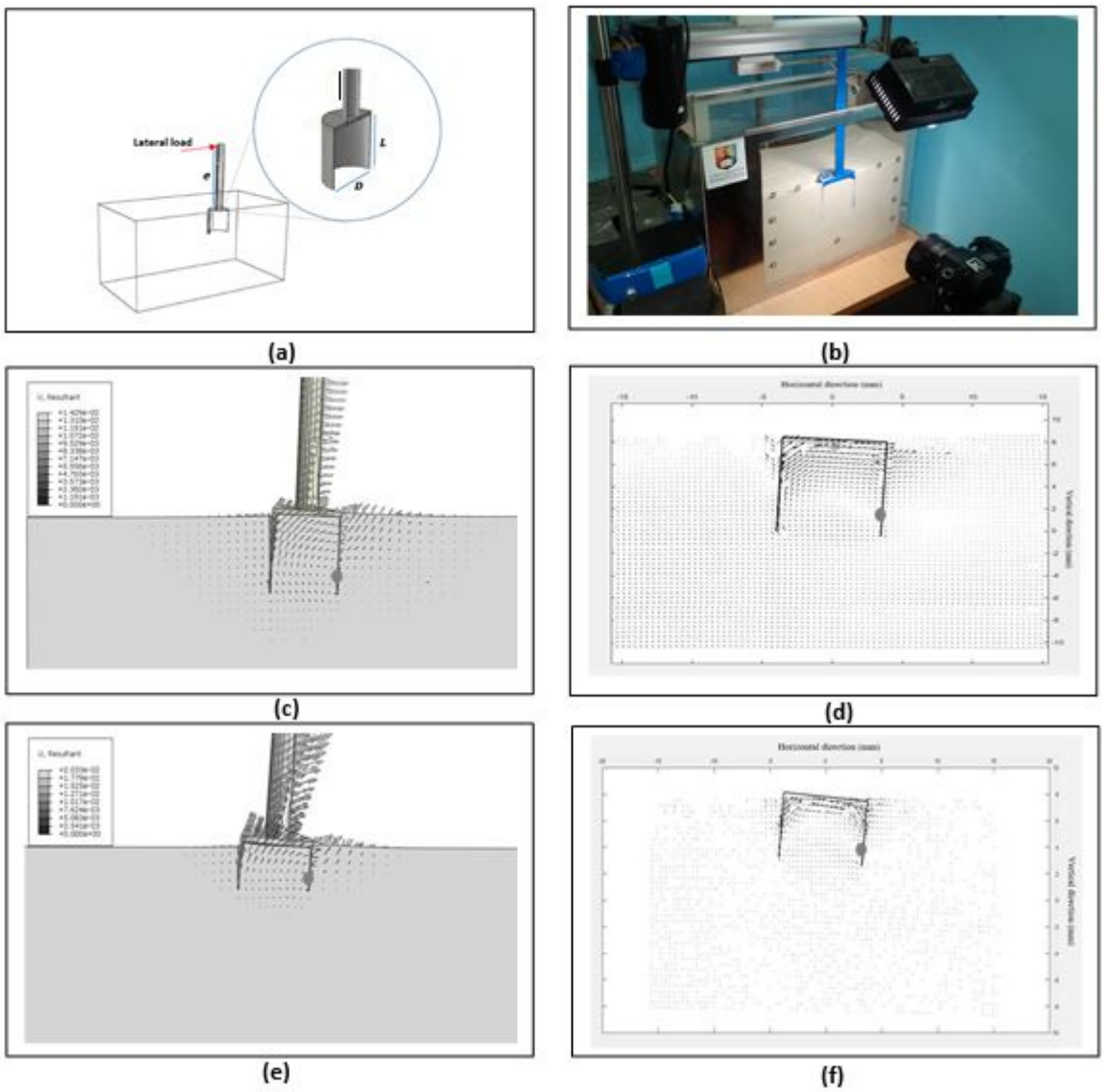

Figure B.1. (a) Schematic of model (b) PIV setup, (c) visualisation of vector of displacements for caisson with $L/D = 1$,FEM, (d) visualisation of vector of displacements for caisson with $L/D = 1$,PIV, (e) visualisation of vector of displacements for caisson with $L/D = 0.5$ „FEM, (f) visualisation of vector of displacements for caisson with $L/D = 0.5$,PIV

APPENDIX C

C. Installation of suction caisson foundations in sand

There are two aspects to the engineering design of this foundation: installation and the bearing capacity. The bearing capacity of the suction caisson foundation has been discussed comprehensively in Chapter 4 and 6.

As the sand used during all the model suction caissons used in the experiments was dry, the model caissons were installed into the prepared sand by pushing. Hence, the installation process of the novel caisson foundations (i.e. 'winged caisson' and 'hybrid caisson tripod' foundations) through suction pressure which is basically used in the field for a conventional suction caisson foundation (in a saturated condition) has been ignored in this research.

Nevertheless, a few studies about the installation of suction caisson in sand have been conducted at the beginning of this PhD. Hereby, The results obtained from laboratory tests sand numerical simulations have been presented in a conference and in an under review paper, which are provided in appendix C:

Faramarzi, Asaad; Faizi, Koohyar; Dirar, Samir; Mehravar, Moura; Harireche, Ouahid. "Modelling the seepage flow during caisson installation in a natural seabed". Conference: Proceedings of the 24th UK Conference of the Association for Computational Mechanics in Engineering, At Cardiff University, Cardiff.

.

EVALUATION OF SEEPAG FLOW DURING INSTALLATION OF SUCTION CAISSON FOUNDATION IN HOMOGENEOUS SAND AND SAND OVERLAYING INCLINED CLAY

Koohyar Faizi [1], **Asaad Faramarzi** [2]
[1,2,3] School of Engineering, University of Birmingham, UK

Samir Dirar [3], **Moura Mehravar** [4]
[4]School of Engineering and Applied Science, Aston University, UK

ABSTRACT

Suction caissons are relatively new and cost-effective foundations for offshore wind turbines (OWTs) and meteorological mast (met tower). In a permeable soil, seepage induced by suction plays an important role in the installation process by reducing caisson penetration resistance. This study aims to investigate the seepage behaviour during caisson installation in sand. The pore pressure changes within the soil around the caisson tip during installation of suction caisson foundation into a homogeneous sand layer and sand overlaying inclined clay were examined. A series of experiments was conducted to measure the suction pressure and determine the variation and distribution of excess pore water pressure (EPP) generated by suction in a homogeneous sand layer. The changes of EPP during installation in sand were compared with the finite element (FE) method. Experiments showed that, suction pressure and EPP tends to increase with depth from the mudline to the maximum penetration depth. A series of 3D FE models were also undertaken in which installation is considered through sand into an inclined clay layer to simulate the behaviour of seepage.

Keywords: OWTs; sand; seepage; suction; inclined layer; experiment; FE

NOMENCLATURE

P	Water pressure
h	Caisson penetration
γ'	Effective unit weight
K_i	Permeability of the sand inside the caisson
K_o	Permeability of the sand outside the caisson
a	Pressure factor
EPP	Excess pore pressure
r	Caisson radios
L	Caisson length
D	Caisson diameter
$\bar{S}$	Suction pressure
t	Caisson wall thickness

INTRODUCTION

Pile foundations are traditionally used in the offshore wind industry. However, Suction caissons (SC) foundations have recently been considered for use in offshore wind turbines [1]. Suction caissons (SC) are large upturned bucket structures of cylindrical shape typically made of steel. Installation of a suction caisson foundation in seabed soil is achieved by pumping out the water trapped inside a caisson which enables its penetration into the seabed after initial penetration under self-weight [2, 3]. The installation process of the foundation in permeable soils is affected by induced seepage flow which leads to a reduction in soil effective stress and hence its resistance to penetration [4]. As such, permeability of soil plays an important role in the installation process, particularly when dealing with layered soils [5].

The effect of seepage in installation has been well documented for soil profiles with a homogenous nature [3, 6, 7]. Challenges regarding to the installation process in multi layers of soil (e.g. the presence of a low-permeable layer) have been also investigated in the few previous studies [8, 9]. According to the previous studies, there are concerns during the suction caissons installation in sand underlain by a low permeability soil such as clay or silt. In such a soil profile the low permeability layer may create a hydraulic barrier in the soil and causes the installation to become very difficult or even practically impossible [10].

The proximity of clay in multilayer soil structures, can cause abrupt changes in pore pressure within the soil [2, 5, 9]. Consequently, the suction required to install the caisson could be influenced by pore pressure changes. It is therefore concluded that the soil layer configurations, (e.g. the

[1] Contact author: K.Faizi@pgr.bham.ac.uk
[2] Contact author: A.Faramarzi@bham.ac.uk

presence of a low-permeable layer), can have significant impact on the seepage mechanism and thereby the installation process.

Furthermore, natural seabed layers are not made of homogeneous materials and often positioned with degrees of inclination [5]; thus it is to be expected that the properties of the soil may vary from one side to the other. As the pore pressure parameter varies with changes of soil layer configurations, it would be useful to measure the pore pressure around the skirt tip during installation in an inclined soil profile.

During installation, the caisson may tilt because of the inclination, and consequently problem may arise [11]. Although the feasibility studies in the installation process of a suction caisson in an inclined soil profile comprising a sand layer over inclined clay has been studied experimentally [5], seepage model for this case has not been investigated numerically.

Current study has investigated the behaviour of suction caisson foundation during installation in homogeneous sand through the laboratory tests. Numerical studies, utilizing FE method, were also conducted to simulate the experiment. It also aimed to increase understanding of installation in multi layered soil including a sand over an inclined clay layer, by providing some knowledge of how inclined low impermeable layer, located below the sand, can influence the installation behaviour.

1.1 Caisson installation in homogeneous sand

Test preparation:

In this study, the suction pressure required ($\bar{S}$) for installation of a small-scale caisson model, made of aluminium with 140 mm diameter (D), 140 mm length (L) and 0.7 mm thickness (t), in sand was measured. The wall thickness to diameter ratio t/D was 0.5%. These values is comparable with typical prototype caisson dimensions used in sand, which normally have L/D of 1, and t/D in the region of 0.3 % to 0.4 %, but with internal stiffeners that increase the effective wall thickness [4].

The test apparatus consists of a cylindrical soil chamber 500 mm in diameter and 600 mm high, filled with sand to a depth of 200 mm. The saturated sand sample was prepared by filling the chamber with water. Dry sand then was pluviated into the chamber at a slow rate to avoid densification. The water depth was kept 200 mm above the sand layer to ensure the caisson, was fully submerged at the start of installation.

The caisson model was then positioned in the middle of the chamber, and protected from tilting which could only move freely in the vertical direction via a guide system. The soil sample was prepared and the surface was levelled. The installation process of the model in the lab involves two steps; (i) first allowing it to penetrate into soil under self-weight and (ii) then further penetration achieved using suction pressure (which creates a differential pressure within the caisson thereby enabling penetration).

After self-weight penetration (20mm), the installation of caisson continued up to approximately full depth (120mm) by pumping out the trapped water in the caisson cavity. In the last 20 mm penetration depth, there was less control over the installation process due to the sand heaving. Therefore, all the results presented in this study are based on the findings for penetration depth up to 120mm.

The caisson model was installed by continuously pumping water out of the caisson compartment. The caisson model was installed in the sand with constant installation rate of 0.45 m/s.

If an installation is to be undertaken in the laboratory using sand collected from the site of installation, the permeability of the model and prototype would be similar, so the same installation rate should be applied in both experiments. Seepage volume depends on both permeability and installation speed rate [5]. Therefore, the correct installation rate leads to the proper modelling of the pumped water volume. The rate of installation for field tests is recorded to be in the range of 0.1 to 2 mm/s, and the sand permeability is recorded to be 4×10^{-5} to 1.4×10^{-4} m/s [4, 5]. A constant head permeability test was conducted in the laboratory to obtain permeability of sand. The sand which was used in the laboratory (Redhill 110 sand) has a permeability of $3.8 \times 10^{-4}\,\mathrm{m/s}$ which results in appropriate laboratory installation rates of 0.1 to 0.5 mm/s [4, 5].

Instead of using an electric pump, a water head difference method was used to assist the installation of caissons in the laboratory. A water evacuation valve attached to the hose, which was left open during pushed in penetration. Flow was achieved using the water head difference between the test chamber and the hose outlet. Desirable pumping rate achieved by varying the degree of opening of the valve connected to the pipe.

The suction pressure was measured with two vertical sealed-tube piezometers attached to the top of the caisson (piezometers of 1 and 2 in Fig.1). The differential pressure or suction pressure, i.e. pressure difference between the outside and inside of the caisson, was recorded using a differential pressure in piezometers.

Piezometer attached to the caisson is added in order to obtain excess pore pressure within the sample during caisson installation (piezometer of 4 in Fig.1). The

piezometer was connected to a nozzle attached to the tip of caisson (inside the caisson). Geotextile as a filter was wrap-around the tip of the nozzle to prevent sand particles from migrating up into the tube.

To measure the pore water pressure generated during installation around the tip of caisson (inside), the difference pressure obtained by piezometer when the valve is open and fully closed for each penetration depth.

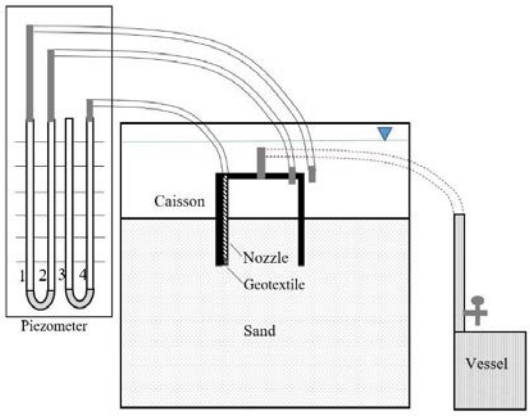

FIGURE 1. General view of the test set-up

Numerical Simulation:

In this study a series of 2D axisymmetric models have been developed using ABAQUS/Standard to simulate the seepage mechanism during the installation in homogenous sand. By investigating the development of hydraulic gradient along the inner wall, the ratio of permeability within caisson to outside caisson was identified. FE modelling was also calibrated to explore the influence of the hydraulic blockage by the inclined low impermeable layer. A 3D FE package ABAQUS model was also used for the purpose of numerical simulations of seepage during caisson installation in soil profile containing a layer of inclined clay covered with a sand layer. To minimise computational time, only a half of the domain is considered for symmetry reasons.

The model problem of a suction caisson with radius r and height L were considered in the simulation (Figure 2). Seepage flow around the caisson wall during the installation was simulated by applying the flow boundary condition on the inner soil surface with an appropriate hydraulic head. A hydraulic head on the soil surface of 200 mm was applied outside the caisson where seepage flow is downward. This number can be arbitrary, but must be sufficient to initiate the suction installation process. The head difference on the surface inside the caisson was directly related to the value of the applied suction [12]. A normalised excess pore water pressure P can be also used to simulate seepage flow by satisfying the boundary conditions: to represent suction pressure $P = -1$ inside the caisson and $P = 0$ outside the caisson [13].

The depth of caisson penetration into the seabed is denoted by h. The soil consists of homogenous sand with permeability K and effective unit weight γ'. A one-phase seepage analysis in saturated soil implemented under assumption of rigid soil skeleton, neglecting inertia effects and disregarding soil deformation, and the caisson is modelled by solid elements.

The caisson penetration at any penetration depth was considered as a self-balancing process between the total driving force, which includes the caisson submerged dead weight and the suction force acting on the caisson lid, and the soil resistance. In other words, at any wall embedment level, the total driving force is in equilibrium with the soil resistance, and the caisson will not penetrate deeper until a higher driving force is applied (through suction in this case). Therefore, it is possible to assume that the continuous caisson penetration is a combination of a series of discrete movements. This allows the process to be modelled using the finite element (FE) method. At any specific skirt embedment, the suction pressure obtained from the experiment was applied in the FE model. The seepage induced by the pressure difference (suction) at that stage is assumed to be at an instantaneous steady state. The model geometry and boundary conditions for each simulation were similar to those from the experiment.

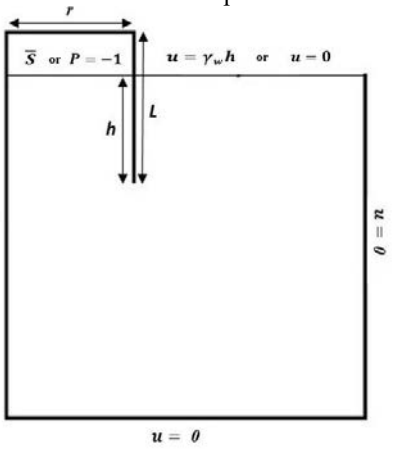

FIGURE 2. The axisymmetric geometry of suction caisson in the FE simulation

1.2 Results and discussions (caisson installation in sand):

The variation of suction pressure for the suction caisson foundation during the installation in sand is shown in Figure 3. The suction pressure was observed to increase relatively linearly with penetration depth. It should be noted that the penetration resistance, at a particular depth, is calculated as the sum of the skirt end bearing and side friction forces [5]. Therefore, increases in suction pressure can be interpreted as a result of increasing skirt tip resistance and skirt friction with embedment depth. The results are presented in a normalised form so it can be used for any size of caisson foundation, where γ' is soil unit weight and considered 10 kN/m^3 for the sand.

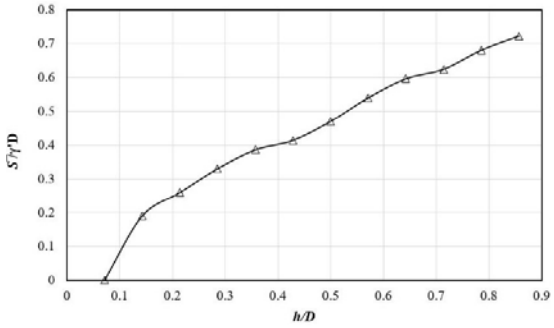

FIGURE 3. Variation of suction pressure during caisson installation in sand

A successful installation can be achieved by calculating the appropriate excess pore pressure which can influence soil resistance at the skirt tip. To obtain soil resistance acting on the caisson during caisson installation, the excess pore pressure at the skirt tip was measured in the laboratory and the results were compared with FE models. A FE analysis was performed to verify the excess pore pressure (EPP), suction pressure (S) changes and total pore pressure (TPP=S- EPP) of sand during the installation.

Comparisons between experimentally measured and calculated (FE method) of the TPP and EPP for a 140 mm diameter caisson are shown in Figures 4 and 5, respectively. The simulations were conducted first assuming a single value of sand permeability $K_i = K_o = 3.8e-4\ m/s$ (permeability measure value for the tested sand), where K_i is the permeability of the sand inside the caisson, and K_o is that of the surrounding sand. Then the seepage was simulated based on the assumption of $K_f = 1.5$ where K_f is the ratio of K_i/K_o .

It can be seen from the results that the behaviour of the measured seepage was simulated very well. The higher measured seepage values can be explained by loosening of the sand plug inside the caisson, and the resulting increase of permeability in the plug. This is illustrated in the results in Figures 4 and 5, where $K_f(K_i/K_o)$ ratios were increased to 1.5 to account for sand loosening. Therefore, better agreement was indeed obtained under assumption of $K_f = 1.5$.

The excess and total pore pressure generation due to the installation of suction caisson increases by increasing penetration depth. The excess pore pressure at the tip increases with depth because the effect of seepage is limited in depth therefore the sand drains less.

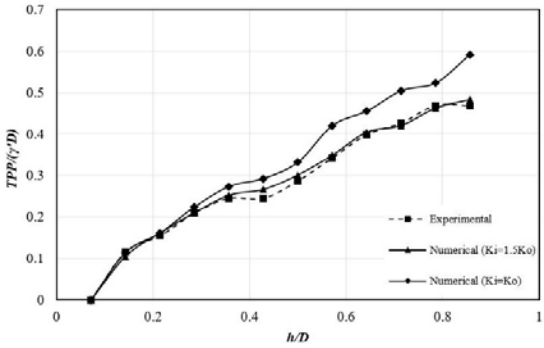

FIGURE 4. Simulated and measured dimensionless TPP in laboratory with two different assumptions of $K_f = 1$ and 1.5

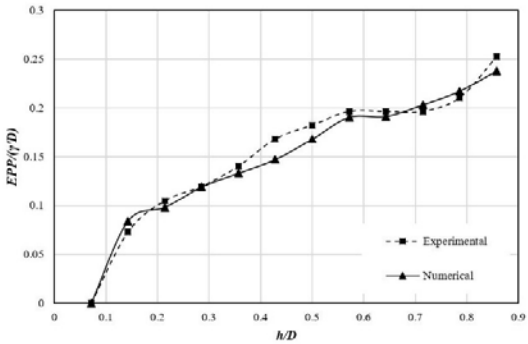

FIGURE 5. Simulated and measured dimensionless EPP in laboratory under assumption of $K_f = 1.5$

The downward seepage gradient occurred on the external caisson wall, resulting from the suction application, leads to an increase in effective stress in the soil, and hence the external skin friction. Whilst, the upward flow gradient inside the caisson reduces the soil effective stress at the caisson tip, thus reducing the tip resistance [4]. Figure 6, shows the development of excess

pore pressure with penetration depth at the skirt tip during the installation, for two penetration ratios of 0.1 and 1.

As can be seen, the hydraulic gradient at the inside skirt and at the tip is much bigger compared with the gradient at the outside skirt for higher penetration depth. Therefore, the reduction of soil resistance at the beginning of the installation is expected to be small. When the bucket penetrates deeper, less suction is required to achieve significant reduction in penetration resistance.

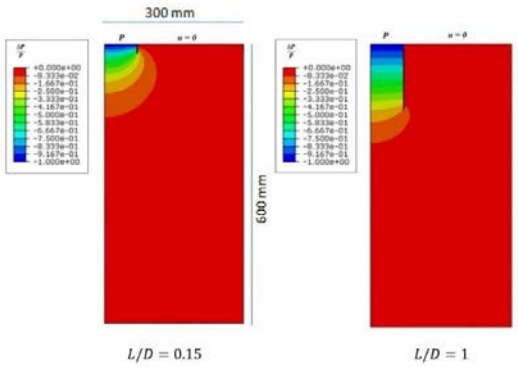

FIGURE 6. FE results of ratio between excess pore pressure and applied suction under the bucket lid for L/D=0.15, and 1

Water flows upwards inside the caisson plug, therefore flow around the tip of the caisson will reduce the skirt tip resistance. The penetration resistance (tip) is a function of the effective stress, which is affected by the change in the pore pressure, and subsequent sand loosening (if any). Hence, different changes in pore pressure and sand loosening at a specific wall depth are likely to result in different levels of soil resistance obtained. Excess pore pressure increase will decrease the effective stress in the soil, thereby decreasing the soil shearing strength (resistance).The effective vertical stresses in the soil inside the caisson can be calculated as follows [14]:

$$\sigma'_{seepage} = \left[1 - \frac{(1-a)S}{\gamma' h}\right]\sigma' \quad (1)$$

Where σ' corresponds to the case without seepage, h is penetration depth, γ' is soil unit weight, a Pore pressure factor, and S is suction pressure.

The installation suction calculations rely partly on appropriate values of the pore pressure factor (a) to produce accurate estimates [5]. Pressure factor that represents the ratio between the excess pore fluid pressure at the tip of the caisson skirt and next to the base $(0 \le a \le 1)$ [14].

In this study, the pressure factor (a) is calculated numerically, in terms of two scenarios: the ratio of excess pore fluid pressure at the tip of the caisson skirt and next to the caisson lid $(\alpha = \frac{\Delta P}{P})$, and as a ratio of the excess pore pressure (Epp) measured at the tip of skirt to the applied suction (obtained from the experiment) and is found for all penetration ratios from Eq. (2):

$$\alpha = \frac{Epp}{S} \quad (2)$$

In both scenarios, the effect of permeability variation $(K_f = 1\ and\ 1.5)$ on the pore pressure factor was also investigated. The red dots in Figure 7 show the computed α values from Eq. (2) with two assumptions of $K_f = 1\ and\ 1.5$, and the black dots are corresponding to the α values obtained from $\alpha = \frac{\Delta P}{P}$. Comparison of two methods shows almost good agreement on the distribution of pore pressure at the tip of the caisson.

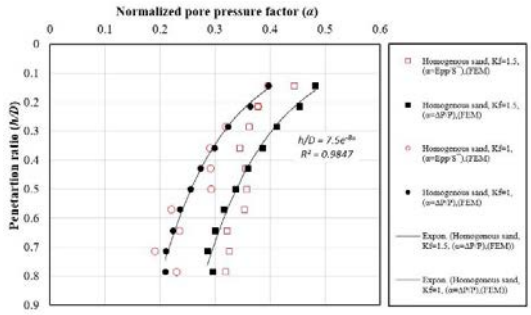

FIGURE 7. Variation of pore pressure parameter (a) with depth for caisson installation in homogeneous sand, (FE)

1.3 Caisson installation in sand over inclined clay (FE):

In practice, it is unlikely that sand will be encountered overlying a perfectly flat clay horizon [5], such as those tested in the laboratory, as the influence of geological processes move the layers. The soil profile sample comprised sand over inclined clay was considered to simulate seepage mechanism during caisson installation (Figure 8). A 3D FE developed to simulate the seepage behaviour during installation of model caissons into the certain soil layer condition, where sand is over inclined clay with the clay inclination selected at random of 8º.

A sand with uniform permeability of $3.8e10^{-4}$ m/s, and clay with permeability of $1e10^{-9}$ m/s were considered for numerical modelling. The main purpose of the FE

modelling is to indicate the difference seepage for two sides of the caisson: up and down slope of the clay, once the skirt tip approaches the highest point of the clay layer.

A series of three-dimensional finite element models are developed using ABAQUS 3D software which is dimensional numerical programme to simulate seepage for different penetration depth. Taking advantage of the symmetrical nature of the problem, only half of the whole problem is modelled (Figure 9).

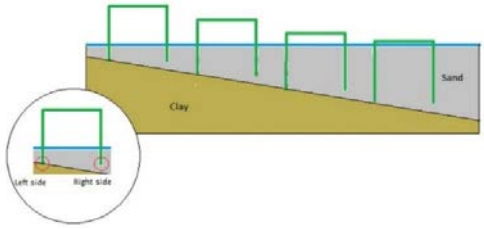

FIGURE 8. The installation process in soil profile comprising sand over inclined clay

1.4 Results and discussions (caisson installation in sand over inclined clay):

The seepage was simulated for that certain depth, once the skirt tip (left skirt) approaches the highest point of the clay layer. Therefore, the installation process is simulated based on the assumption of critical scenario for each penetration depth. Figure 9, shows the development of excess pore pressure with penetration depth at the skirt tip during the installation in sand overlaying clay, for penetration ratio of 0.43. An asymmetrical EPP distribution around the caisson wall is identified due to the presence of clay layer in left side (Figure 9).

Results of pore pressure factor plotted versus penetration ratio for homogeneous and inclined layers are shown in Figure 10. The results indicate that the inclined impermeable layer (clay) below the sand is affecting the flow in sand, and that influence is dependent on the distance to the caisson tip. At shallow depths, the pore pressure factor around the skirt tip is much higher compared to the pore pressure factor at deeper penetration depths.

As can be seen from the figure, the subsurface layer has significant influence on excess pore pressure at the bucket tip, for caisson side where the caisson tip reach to the layer with low permeability (left side). Whereas, excess pore pressure around the caisson tip for the right side is almost closed to the condition where the caisson installed in homogeneous sand. For the right side of the caisson, there is a gap between the skirt tip and the clay layer, showing that the seepage has relatively smaller impact.

As the pore pressure factors are beneficial to the installation process, therefore the discrepancy of the pore pressure factors around the caisson tip during caisson installation in inclined multilayers must be accounted for in the design calculation.

In case of an inclined clay layer below a sand layer, the pore pressure gradient at skirt tip level may become critically high, which has been reported for the installation in multilayer soil profiles [2, 5, 9], since the changed drainage conditions will affect the seepage flow pattern. That can potentially trigger a local failure or piping along the skirt at the side of the caissons which is still in the sand.

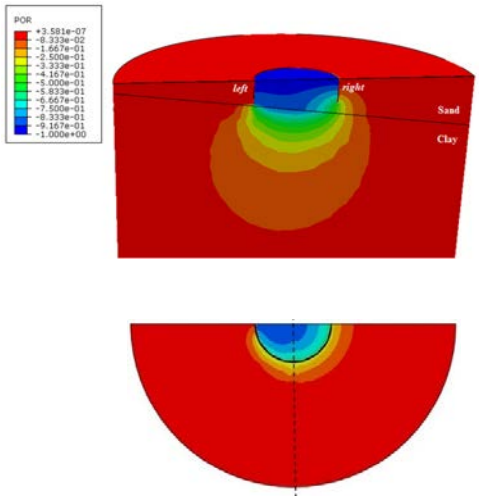

Figure 9. FE results of pressure gradient for caisson installation with h/D=0.43 in inclined layer; (a) front view of the model; (b) cross section view of the caisson tip

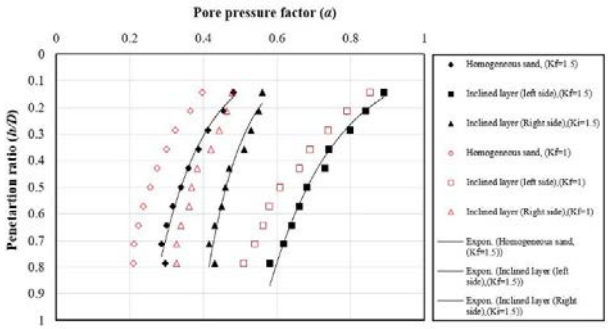

Figure 10. Comparison of pore pressure parameter (a) for caisson installation in homogeneous sand and inclined layer, (FE)

In case of an inclined clay layer, the penetration resistance may considerably increase since a seepage flow, as reported for perfectly horizontally layered profiles. Therefore, a tilt of the caisson may arise due to the asymmetric soil resistance. However, the deeper the caisson get more soil support from both end bearing and skin friction, which can compensate for the asymmetric penetration resistance.

Suction caisson foundations may be installed in a variety of soil type which could have a different impact on the installation process. Therefore, the seepage mechanism in inclined layers with different soil parameters, inclination and configuration should also be investigated. Further physical and numerical modeling studies are also necessary in order to investigate the seepage mechanism during suction caisson installation in multilayered soils with different types of layers.

1.5 Conclusions

Seepage mechanism for installation of suction caisson in homogenous sand and in sand overlaying inclined clay were investigated. The results showed that for the installation in homogeneous sand under a constant installation rate, the suction pressure increased relatively linearly with penetration depth. Based on the FE results, seepage generated by the suction influenced by the soil profiles with different permeability. Changes of pore pressure factor (a) at the caisson tip during installation of suction caisson in an inclined layered soil, was investigated. It was found that the proximity of clay in multilayer soil structures, causes the pore pressure ratios to be higher than those encountered at similar depths in homogeneous sand. The low-permeability layer hindered the generating of seepage gradients in sand, and the consequence might be that larger suction pressures required.

REFERENCES

1. Byrne, B., et al., *Suction caisson foundations for offshore wind turbines.* Wind Engineering, 2002. **26**(3): p. 145-155.
2. Faramarzi, A., et al., *MODELLING THE SEEPAGE FLOW DURING CAISSON INSTALLATION IN A NATURAL SEABED.* Proceedings of the 24th UK Conference of the Association for Computational Mechanics in Engineering, 2016(Cardiff University, Cardiff.): p. 150-153.
3. Harireche, O., M. Mehravar, and A.M. Alani, *Soil conditions and bounds to suction during the installation of caisson foundations in sand.* Ocean Engineering, 2014. **88**: p. 164-173.
4. Tran, M.N., *Installation of suction caissons in dense sand and the influence of silt and cemented layers*. 2005.
5. Cotter, O., *Installation of suction caisson foundations for offshore renewable energy structures*. 2010, Oxford University.
6. Houlsby, G., et al., *Field trials of suction caissons in sand for offshore wind turbine foundations.* 2006.
7. Mehravar, M., O. Harireche, and A. Alani, *Modelling suction caisson installation in sand using FLAC3D.* 2014.
8. Chatzivasileiou, G., *Installation of suction caissons in layered sand: Assessment of geotechnical aspects.* 2014.
9. Tran, M.N., M.F. Randolph, and D.W. Airey, *Installation of suction caissons in sand with silt layers.* Journal of Geotechnical and Geoenvironmental Engineering, 2007. **133**(10): p. 1183-1191.
10. Raines, R., O. Ugaz, and J. Garnier. *Centrifuge modelling of suction piles in clay*. in *Proc., Int. Symp. Frontiers in Offshore Geotechnics—ISFOG*. 2005. Taylor and Francis London.
11. Pinna, R., *Buckling of suction caissons.* 2003.
12. Koteras, A.K. and L.B. Ibsen, *Medium-scale Laboratory Model of Mono-bucket Foundation for Installation Tests in Sand.* Canadian Geotechnical Journal, 2018(ja).
13. Harireche, O., M. Mehravar, and A.M. Alani, *Suction caisson installation in sand with isotropic permeability varying with depth.* Applied Ocean Research, 2013. **43**: p. 256-263.
14. Villalobos.F, *Bearing Capacity of Skirted Foundations in Sand.* In VI Congreso Chileno de Geotecnia, Valparaiso., 2007.

APPENDIX D

D. Torsional capacity of the winged caisson

As mentioned earlier, the tower and foundation structures of the typical OWTs are exposed to various kinds of loads. The situation may become worse with the introduction of hyper-tall wind turbines and the increasing intensity of storms, including the possibility of hurricanes, which will impose large torsional and overturning moments on the superstructure.

A small project in form of a Master's dissertation, based on the foundation concept proposed by the current research (winged caisson), was simultaneously carried out by one of the students at the University of Birmingham. The Master's project focused on studying the behaviour of the winged caisson under torsional loading using finite element modelling. The torsional capacity of the winged caisson foundation was investigated in undrained condition. I was involved in this project however, that work was deemed beyond the scope of the current thesis, as the present study focuses mainly on the overturning capacity of the foundations under drained soil conditions. Hence, the results of the torsional capacity of the winged caisson in undrained soil has been published:

L. W. Derby, A. Faramarzi, K. Faizi, M. Mehravar, O. Harireche. "Finite element modelling of winged suction caissons in clay under uniaxial and combined loading". 2nd International Conference on Natural Hazards & Infrastructure, June 2019, Chania, GREECE.